218

GAS INSULATED TRANSMISSION LINES (GIL)

Joint Working Group
23/21/33.15

February 2003

agré

CIGRE Brochure

Gas Insulated Transmission Lines (GIL)

By WG 23/21/33-15

Working Group members contributing to the brochure:

Alain Sabot,	France (Convenor)
Andreas Schuette,	Germany (Secretary)
Abdellah Chakir,	Germany
Paul Coventry,	United Kingdom,
Fabrizio Donazzi,	Italy,
Dominique Feldmann,	France,
Brian Gregory,	United Kingdom,
Hiroyuki Hata,	Japan
Mel Hopkins,	USA
Sander Meijer,	Netherland,
Guiseppe Rizzi,	Italy,
Dave Royle,	France (formerly **Maxime Bertrand**),
Markus Vestner,	Switzerland,

and with the help of **Jacques Pernot** (France) for the mechanical chapter of the brochure.

Contents

1 Introduction

Gas-insulated transmission line (GIL) is now being actively pursued for long distance transmission. At present, experience is limited largely to transmission over short distances (typically less than 500 m). This brochure provides technical information to be of assistance in the design of circuits using GIL.

In Chapter 2, a definition and description of GIL is given, including a brief description of GIL development and a summary of the main features.

In Chapter 3, the general technical characteristics of GIL are detailed and compared to those of overhead lines and conventional cables. The interaction of a GIL with the transmission system in which it is installed are discussed especially the following issues: the load sharing with other lines, voltage and reactive compensation, sytem stability (static and transient) and short circuit levels.

In Chapter 4 the continuous and short term current ratings of directly buried GIL are discussed and sensitivity analysis to design parameters are presented. Based on modelling and experience pratical formulae are derived. In the annex A these issues are described and analyzed in depth.

In chapter 5 the insulation and overvoltage aspects of any GIL are discussed from an insulation co-ordination and long term reliability of the internal insulation point of view as well as from a bonding and grounding for permanent and transient voltages of the enclosure point of view. In the annex B these issues are more in deth analyzed and discussed.

Chapter 6, is dealing with mechanical, corrosion and installation aspects of directly buried GIL. For the mechanical aspect some simple methods for the calculation and analysis of the stress on the enclosure are recommended disregarding the mechanical aspects of the internal components. Effects of short circuit forces on the enclosure are excluded. The main aspects are the calculation of required enclosure thickness, the vertical and horizontal stability and the interaction between the soil and the enclosure. For the corrosion aspects two methods are described, the coating and the cathodic polarisation. Over-ground and tunnel installations are not dealt with because they are similar to GIS bus ducts which were first installed more than 30 years ago and have been previously studied in the Substation Study Committee 23.

In Chapter 7, environment considerations relating to GIL are discussed. The concept of environmental life cycle assessment as applied to GIL is introduced. The general environmental impacts of GIL are summarised.

In Chapter 8, the economic aspects of GIL projects are discussed and compared with overhead line and conventional cable alternatives. No firm conclusions can be drawn but the factors to be considered are summarised.

In Chapter 9, recent GIL projects and research and development programmes are described.

2 Definition and description

The IEC Technical Report IEC 61640 [1] on HV gas-insulated transmission lines is intended to be used where the provisions of the International Standard IEC 60517 [2] on gas-insulated metal enclosed switchgear are not adequate, examples of which are stated to be:

- where all or part of the HV gas-insulated transmission line is directly buried; or
- where the HV gas-insulated transmission line is located, wholly or partly, in an area accessible to the public; or
- where the HV gas-insulated transmission line is long (typically longer than or equal to 500 m).

The present document considers gas-insulated transmission lines (GIL) as follows:

- of rated voltage 72.5 kV and above
- for alternating current
- single-phase enclosed
- rigid
- installed above ground, directly buried and in tunnel
- laid horizontally, vertically and at any angle
- using pure SF_6 or a mixture of SF_6 with nitrogen as the insulating gas
- greater than 500 m in length
- located within substations and in the transmission network, for example in a mid-section of overhead line

The basic structure of GIL is similar to that of well established gas-insulated switchgear (GIS), in which the conductor at high voltage is located within an earthed conducting enclosure and the space between the two filled with a gas under pressure to provide electrical insulation [2]. The conductors are held in position by solid support insulators. The conductors of each phase may be located within separate enclosures (single-phase enclosed). Compensation for thermal expansion is provided, often by sliding contacts in the conductor and, where the enclosure is free to move (i.e. in tunnel or trough installations), by bellows as for long GIS busbars. The GIL is divided along its length into separate gas compartments.

GIL dimensions are determined by dielectric, thermal and mechanical considerations. Conductor and enclosure diameters and thicknesses and gas composition and pressure may be varied according to the application to provide an optimum solution. In many cases, dielectric considerations will be predominant in determining dimensions and the required current rating will be achieved without difficulty. For more highly rated circuits, thermal considerations may be predominant and larger dimensions will be chosen to maintain temperatures within acceptable limits.

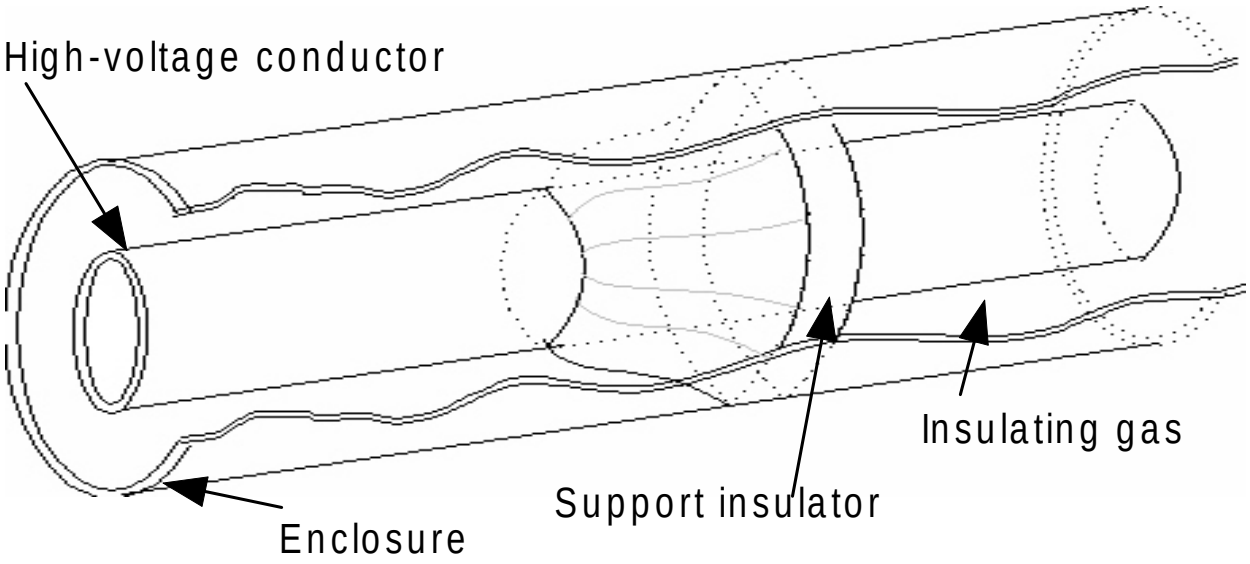

Figure 1: GIL structure

2.1 GIL development

While largely based on proven GIS technology, significant differences exist in some areas. Connections using GIS technology have been used for a number of years. These have been installed cost effectively for lengths of up to about 500 m. Up to this length, connections using GIS technology have been more economic than cables mainly because their cost has been offset by savings on the cost of cable sealing ends. The cost of long distance connections based on existing GIS technology remains prohibitive.

In contrast, GIL technology is optimised for cost-effective, site-assembled connections across long distances. For example, enclosure lengths will often be joined by welding, rather than by bolted flanges, and this is performed and inspected on-site. Typically, developments were and are pursued in the following areas:

- reduction of materials costs by optimisation of the design and materials for a given rating.
- reduction of manufacturing costs by simplification and reduction in the number of components; automation of manufacturing processes to reduce labour costs and increase production rates.
- reduction of installation costs by designing components for simple assembly so that large numbers of joints may be made on-site in a reasonable timescale; automation of assembly processes to reduce labour costs, increase production rates and allow consistent quality to be achieved.
- means of reducing civil engineering costs through simple laying and burial techniques; low cost solutions are required for the negotiation of obstacles such as roads, railways and water courses.
- cost and environmental considerations: the insulating gas will often be a mixture of nitrogen and SF_6, rather than pure SF_6, and will therefore have different dielectric properties.

GIL are intended primarily for below ground applications. Where a GIL is directly buried, corrosion protection is provided in the form of a passive corrosion resistant coating and possibly an active corrosion protection system. For long GIL, greater than 100 m in length, the enclosures are not free to expand due to soil friction and so become mechanically stressed under heating.

2.2 Special features of GIL

- Technical:
  - the overall losses are relatively low, because of large conductor cross sections;
  - no significant dielectric losses;
  - ratings of 2000MVA with a single circuit and directly buried without cooling;
  - low capacitance per unit length;
  - reactive compensation not needed even for lengths > 100 km;
  - above ground, trough/tunnel or directly buried installation is possible;
  - a GIL is immune to weather conditions: snow, ice, wind, pollution
- Environmental:
  - No visual impact;
  - Low external power frequency electromagnetic fields;
  - No audible noise;
  - No risk of fire;
  - Presence of SF_6;
- Economical:
  - cost of a GIL is greater than an equivalent overhead line.

3 General technical characteristics

The electrical characteristics of a GIL are different to those of an overhead line or a cable and will affect the way it interacts with a transmission system. The interaction of a GIL with the system will need to be studied in detail. In some cases, means of compensation may need to be considered.

3.1 GIL electrical parameters

For single-phase type GIL with the enclosures solidly bonded at both ends, each phase has series inductance and capacitance to earth. Coupling between phases is negligible due to the screening effect of the enclosures.

The resistance *R* per unit length depends on the conductor and enclosure dimensions and electrical resistivities, the skin and proximity effects and the conductor and enclosure temperatures. A method for calculating the resistance is given in [6].

The shunt conductance *G* per unit length is not significant.

Typical values for the electrical characteristics of a 400 kV GIL with a continuous thermal rating of 2000 MVA are shown in Table 1. Typical values for cables and overhead lines (OHL) having comparable ratings are shown for comparison. A frequency of 50 Hz has been assumed.

Table 1:
Electrical characteristics for 400 kV GIL, overhead lines and cables

	GIL	OHL	XLPE cable (2 per phase)
Current rating (A)	3000	3000	3000
Transmissible power (MVA)	2078	2000	2000
Resistive losses at 3000A (Wm^{-1})	180	540	166
Dielectric losses (Wm^{-1})	-	2.4	15.0
Total losses (Wm^{-1})	180	542.4	181
AC resistance ($\mu\Omega m^{-1}$)	6.7	20	6.0
Inductance (nHm^{-1})	162	892	189
Capacitance (pFm^{-1})	68.6	13	426
Characteristic impedance (Ω)	48.6	263	21.0
Natural load (MW)	3292	608	7619
Surge impedance (Ω)	48.6	263	12.0

In preparing the above table, values have been sought for GIL, cables and overhead lines having a continuous thermal rating of approximately 2000 MVA. Other geometries having equivalent continuous thermal ratings but different electrical characteristics are possible, hence the table is intended for indication only.

The overhead line characteristics correspond to a 420 kV French line with 3 x 570 mm^2 conductors per phase and two earthwires.

The values given for GIL correspond to a directly buried, single-phase GIL with conductor diameter 280 mm and enclosure inner diameter 630 mm. The enclosures are assumed to be solidly grounded. The depth of laying is 1050 mm and axial spacing between phases 1300 mm. The soil conditions are an ambient temperature of $15^{O}C$ and a thermal resistivity of 1.2 KmW^{-1}. The continuous thermal rating is determined by the maximum soil temperature, which is limited to $60^{O}C$.

The cable solution proposed for achieving the 3000 A rating, uses two cables per phase with conductor section of 2000 mm^2, without cooling. The cables were disposed in two circuits in trefoil formation. The interaxial distance of the two trefoils is 1800 mm. The soil conditions are an ambient temperature of 15^oC, a soil thermal resistivity of 1.2 KmW^{-1} and a depth of laying to the top of the cables of 1050 mm. The rating was achieved using standard practice of IEC 60287 whre the conductor temperature was 90°C and thermally stabilized backfill was used.

A solution with one cable per phase involving either a conductor section of 4000 mm^2 without cooling or a 2000 mm^2 with cooling have not been taken into consideration but are technologically feasible [3], [4].

3.2 System influence

3.2.1 Load sharing

In Table 1, the inductance of the GIL is less than that of the cable system and less than that of the overhead line by a factor of about 5.5. In a meshed transmission network, GIL may provide a parallel path to overhead lines. Due to its lower inductance, the GIL will tend to carry a greater share of the transmitted power.

The influence of GIL on load sharing can be illustrated using the well-known formula for the power flow *P* through a transmission line:

$$P = \frac{V^2}{X} \sin \delta$$

where *V* is the magnitude of the voltage, δ is the phase angle between sending and receiving ends of the line and *X* is the line reactance. This relation assumes that the resistive component of the impedance is small compared with the reactive component. The assumption is reasonable for the examples given in Table 1.

Where the power is transmitted by two lines in parallel, with reactances X_1 and X_2 respectively, the proportion of the total power transmitted by the line with reactance X_1 is

$$\frac{P_1}{P} = \frac{X_2}{X_1 + X_2}$$

Using values shown in Table 1, a circuit consisting of GIL for its entire length would carry 85% of the total power when connected in parallel with an overhead line, assuming both circuits are of equal length. A more likely scenario is where an overhead line circuit is undergrounded using GIL for part of its length. If the GIL in the above example constituted 10% of the circuit length, the proportion of the total power carried would fall to 52%. The tendency for a circuit to divert power away from other circuits is sometimes referred to as the funnel effect.

For any given application under consideration, a system study will be performed to determine the effect on power flows. A connection using GIL may have to be more highly rated than an overhead line. In some cases, means of compensation may be needed, adding to the cost of the circuit.

3.2.2 Voltage and reactive compensation

The voltage in a transmission system is affected by the electrical characteristics of its component transmission lines [6]. When a transmission line is terminated in a load equal to its characteristic impedance, the voltage at the receiving end of the line is equal to the voltage at the sending end. The power transmitted under this condition is shown as the Natural Load in Table 1. Where the power transmitted is greater than the Natural Load, the voltage at the receiving end of the transmission line will fall. Where the power transmitted is less than the Natural Load, the voltage at the receiving end of the transmission line will rise. The level of voltage fall or rise is also dependent on the length of the circuit.

The capacitive charging current of a transmission line may reduce the amount of power that can usefully be transmitted within the thermal load limit. The situation may be improved by the use of reactive compensation

In terms of reactive compensation requirements, Jouaire [8] indicates that for GIL up to roughly 100 km and for cables up to roughly 20 km no reactive compensation is actually needed.

3.2.3 System stability

3.2.3.1 Steady state stability (Dynamic stability)

Small disturbances arise frequently as a result of normal load variations and switching operations. The scale of the disturbance is such that linear approximations to the non-linear equations describing the dynamics of the power system may be used. Steady state stability concerns the ability of a power system to return to essentially the same steady state operating condition following a small disturbance. It is mainly influenced by

control systems and the characteristics of transmission lines in the power system are of less importance. The use of GIL would have no significant influence on steady state stability.

3.2.3.2 Transient stability

Large disturbances arise occasionally, for example following a network fault. Transient stability concerns the ability of a power system to attain a steady state operating condition following a large disturbance.

In Table 1, the inductance of the GIL is less than that of the cable system. The inductance of the GIL is less than that of the overhead line by a factor of about 5.5. As the inductance decreases, the synchronising torque increases, therefore increasing transient stability. The use of GIL would therefore tend to increase transient stability.

3.2.4 Short circuit (fault) levels

When a short circuit occurs in a transmission system, the current that flows is dependent on the source impedance of the system feeding the fault. The magnitude of the current that may flow when a fault occurs at a point in a transmission system is termed the fault level at that point. The fault level is an important consideration in transmission system design. A high fault level is undesirable due to the effects of heating and electromagnetic forces produced by the fault current. It is clear that the switchgear controlling the faulted circuit must be rated adequately to interrupt the fault current.

In Table 1, the inductance of the GIL is less than that of the cable system. The inductance of the GIL is less than that of the overhead line by a factor of about 5.5. The use of GIL would therefore tend to increase fault levels in a transmission system. However, the use of GIL is unlikely to be sufficiently widespread for the effect on fault levels to be significant.

In any given application under consideration, system studies will be performed to determine the effect of GIL on fault levels.

4 Current Rating

4.1 Introduction

Much published work exists on the calculation of current ratings of a) SF_6 gas insulated bus bar for in-air applications above ground and b) conventional cables for buried (laid direct) applications. However, prospective laid direct applications of GIL may differ in the following respects:

- the GIL conductor is of larger diameter and is of annular geometry
- heat transfer through the primary insulation is by convection and radiation
- the insulation may comprise a mixture of gasses, such as N_2 and SF_6
- the gas is contained within a metallic enclosure of large diameter and low electrical resistance
- the high electrical conductivity of the metallic enclosure permits it to be earthed at its ends by the method of solid bonding and, although the circulating currents are of almost the same magnitude as those in the primary conductors, the heat generation is small.
- the diameter of the metallic enclosure and the horizontal spacing between the adjacent phases is large compared to the depth of burial, thereby influencing the method of calculation of heat dissipation through the surrounding ground
- the conductor and metallic enclosure have larger cross sectional areas and higher thermal capacities; these being of benefit to short time overload ratings.

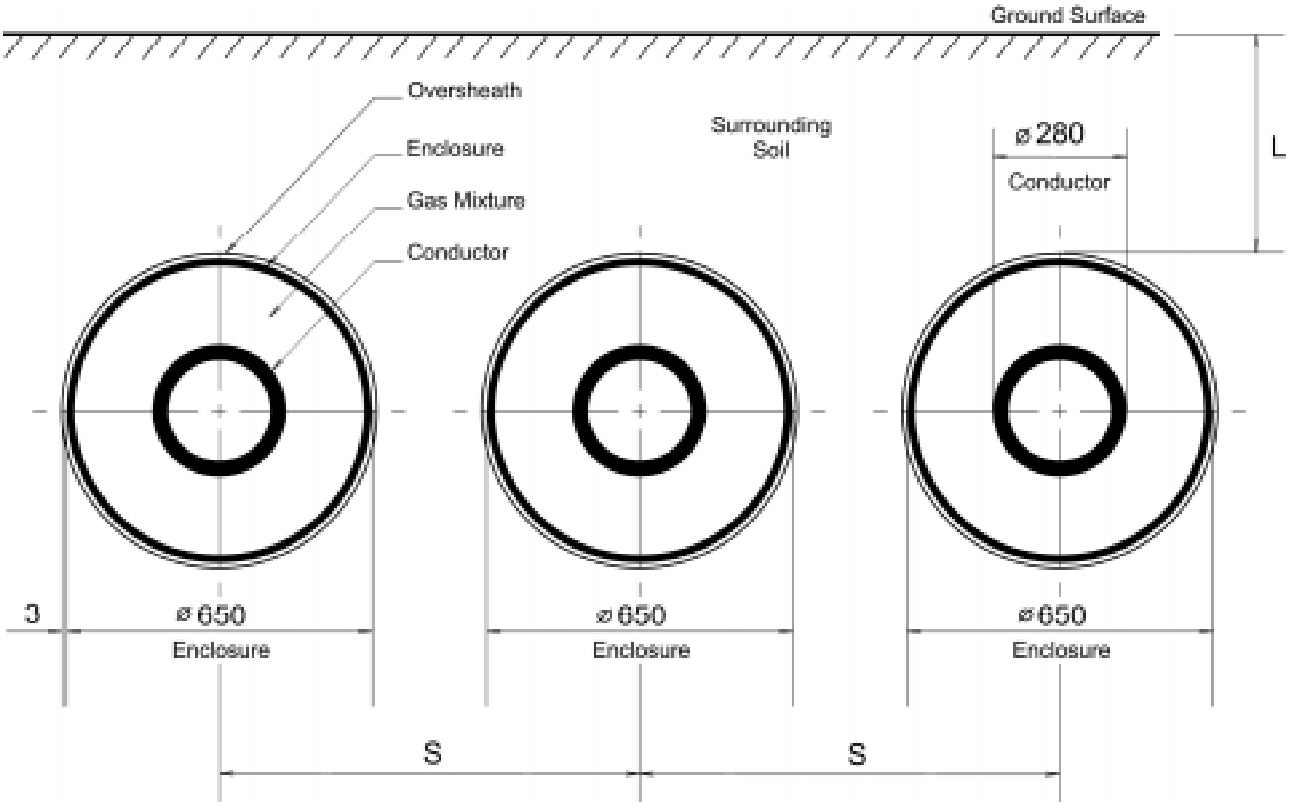

Figure 2: Cross Section of GIL Laid Direct in the Ground

A Task Force was formed to recommend methods of calculation for both the continuous and short time current ratings. The work described in Annex A of this document records the recommended calculation methods and gives sensitivity studies for laid direct, horizontal, single phase GIL. The GIL is insulated with either pure SF_6 gas or a mixture of N_2 and SF_6. A summary of the recommendations and work is given below.

4.2 Thermal Circuit

An idealised thermal model of the laid direct GIL circuit is shown in Figure 3. This model represents both continuous and short time current ratings. The reader is advised to consult Annex A, Chapters 2 and 3, which give the thermal circuits and formulae in greater detail; it should be noted that the thermal circuits for the continuous and short time ratings are different.

Heat, Wc, is generated in the conductor by I^2R conduction losses, where R is the temperature dependent ac resistance of the conductor. The heat is transferred through the insulating gas to the metallic enclosure by the parallel mechanisms of thermal radiation Tr and convection Tc, these are highly dependent on the temperatures of the conductor, θc, and enclosure, θe. Additional I^2R heat, We, is generated in the enclosure by circulating currents, these flow as a consequence of the magnetic flux linkages with the conductor current, which link to the electrical circuit formed by the three solidly bonded enclosures. The pressure containing enclosures are of large cross-sectional area and are usually fabricated from an aluminium alloy, hence their electrical resistance is low, permitting the magnitude of the circulating current to approach that of the current in the primary conductors. As with the primary conductors, the ac resistance is temperature dependent.

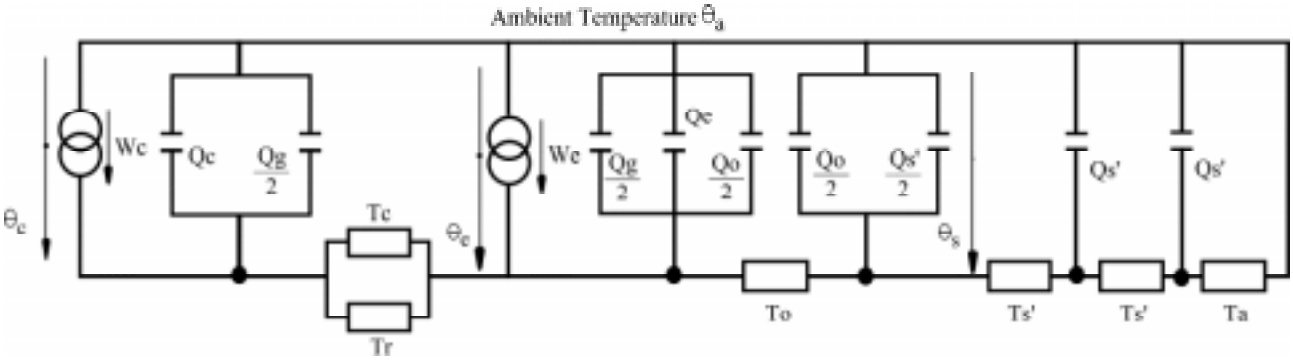

Figure 3: Diagramatic Thermal Circuit

Where:

- θc = Conductor Temperature Rise
- θe = Enclosure Temperature Rise
- θs = Soil / Oversheath Interface Temperature Rise
- θa = Ambient Temperature
- Wc = Conductor Losses (Dependent on θc+θa)
- We = Enclosure Losses (Dependent on θe+θa)
- Tc = Convective Heat Transfer Thermal Resistance (Dependent on θc and θe)
- Tr = Radiation Heat Transfer Thermal Resistance (Dependent on θc+θa and θe+θa)
- To = Thermal Resistance of Oversheath
- Ts' = Equivalent Thermal Resistance of Soil (Divided into Distributed Elements)
- Ta = Equivalent Heat Transfer Thermal Resistance to Air at Ground Surface
- Qc = Thermal Capacitance of Conductor
- Qg = Thermal Capacitance of Gas Mixture
- Qe = Thermal Capacitance of Enclosure
- Qo = Thermal Capacitance of Oversheath
- Qs' = Thermal Capacitance of Soil (Divided into Distributed Elements)

The heat generated by the combined conductor and enclosure losses (Wc + We) flows radially outwards by thermal conduction through the polymeric oversheath, To, and through the surrounding soil, Ts, to the surface of the ground where they are transferred by convection, Ta, to air at ambient temperature. The thermal resistivity of the soil is an important parameter as it may vary along the GIL route. It may also be temperature dependent as a consequence of the phenomenon of soil drying out through moisture migration. The flow of heat increases the temperature of the two adjacent GIL enclosures by mutual heating. Because the magnitude of the thermal losses in each of the three enclosures is closely similar, the temperature rise of the single phase GIL can be represented in the thermal circuit by calculating an increased external thermal resistance of the soil. The later is termed the equivalent external thermal resistance.

The diagram also shows thermal capacitors, Q, which represent the thermal capacitance of each component. Each component is divided into one or more elements which are represented by a ***π*** circuit comprising a series thermal resistance in between two parallel thermal capacitances. The thermal capacitances only need to be calculated and included for short time thermal ratings.

Conventional cables have a specified limiting design temperature (θc+θa) for the conductor and insulation and (θs+θa) for the adjacent soil. The limiting values of soil temperature may differ from country to country, these being recorded in IEC 60287; for example the maximum temperature in France is given as 60°C. In the study of GIL ratings in this document, the limiting value of soil temperature has also been taken as 60°C. It

should be noted that for conventional cables it is permissible and usual to operate above this temperature by surrounding the cables in the trench with an imported backfill exhibiting thermally stabilised properties that guarantee a value of thermal resistivity even when the soil is completely dried out.

A limiting value for the conductor and insulation temperature has not been published specifically for GIL, although a value of 90^{o}C has been published for epoxy resin insulation. Cast epoxy resin is one of the materials that may be employed for the conductor post insulators, the gas sectionalising insulators and the insulators which terminate the GIL into GIS switchgear. Temperature limits are given in IEC 60694 for the sliding connectors that join each section of conductor together, these vary according to the material of the electrical contacts.

The thermal circuit is used to calculate the magnitude of the current, I, by setting a constant design temperature limit for the conductor ($\theta c+\theta a$), or for the adjacent soil ($\theta s+\theta a$) at the interface with the enclosure. Alternatively the resulting temperatures of the conductor and soil can be calculated by setting a specified constant conductor current. The design of the GIL and of its layout in the ground is then optimised to achieve the required rating by varying such parameters as the conductor cross sectional area, the enclosure diameter and the axial spacing between the three GILs. The conductor current, ambient temperature and the depth of burial are usually specified by the Transmission Company.

The work in this document recommends formulae to calculate the thermal losses, thermal resistances and current ratings for both continuous and short time ratings. Sensitivity studies are given on the effect of varying the key parameters to act both as a guide in the selection of a GIL configuration and to illustrate the consequence of varying the design geometry and material parameters. .

4.3 Recommended Formulae for Continuous Rating

The formulae given in Annex A for the calculation of I^2R losses in the conductors and enclosures are derived from those of Arnold, these are also in use for conventional cables.

The formula for radiative heat transfer through the insulating gas is the Stefan Boltzmann expression. The heat transfer depends on the difference between the fourth powers of the conductor and enclosure temperatures and of the emmissivities of their respective surfaces.

Thermal convection is given by the Vermeer formula. This contains a convection coefficient which depends upon the type of insulating gas. An expression has been derived which permits this coefficient to be calculated for different mixtures of N_2 and SF_6 gas.

Thermal conduction through the gas mixture is of negligible proportion and is not calculated.

The thermal conduction through the concentric layer of oversheath is based upon the elementary logarithmic expression for radial thermal resistance.

The thermal conduction through the soil to the ground surface and the effect of mutual heating between the GIL phases is given by the Kennelly formula. It is important to note that the simplification given in IEC 60287 for conventional cables of taking the ground surface as an isothermal plane at ambient temperature is not acceptable for GIL. This is because the ratio of depth of burial to enclosure diameter is significantly less than the ratio of 10:1. The full Kennelly equation must be taken, in which convection at the ground surface is given by an equivalent thermal resistance, mathematically represented in the thermal circuit by an additional layer of soil.

4.4 Recommended Formulae for Short Time Current Rating

No previous method for the short time rating of GIL has been published. The method recommended in Annex A is derived from the finite differences method given in Electra 87 for conventional cables. This method was checked against a finite element software model and gave good agreement.

A mathematical expression was derived and is given in Annex A for the temperature dependent convective transfer of heat through the insulating gas. Heat transfer by radiation is taken to be immediate and so the Stefan Boltzmann expression is employed.

An iterative finite difference computation is given. The computation is terminated at an arbitrary boundary in the soil, this being determined during the calculation as the position at which a pre-set temperature increase of less than 0.1^{o}C occurs in a consecutive time step.

Mutual heating by the two adjacent GIL phases is represented by the superimposition of the temperature in the soil coincident with their axial centres. This superimposition occurs as part of the iterative process.

4.5 Guide to Numerical Modelling

The use of numerical modelling using software computer programs was studied as an alternative to the analytical mathematical methods recommended and described above.

4.5.1 Computational fluid dynamics (CFD)

This was the preferred alternative method for the continuous rating calculation, as it truly modelled convective flow patterns and heat transfer through the gas. It is therefore an independent method to the Vermeer formula. CFD has the advantage that it is ideal for modelling complex geometry in both two and three dimensions. Examples are; a) asymmetry in flow resulting from non-isothermal temperatures around the circumference of the enclosure due to GIL mutual heating and, b) three-dimensional flow in GIL inclined at an angle to the horizontal.

The case of buried GIL is an unusual modelling application for CFD, as a major part of the heat transfer is by thermal conduction through the soil in addition to convective transfer through the gas. For the continuous rating study it was necessary to develop the method to include both radiative and conductive heat transfer. At present the method does not model the transient heat flow required in short time ratings.

Further work is required to derive and publish the physical parameters required to characterise the range of N_2 and SF_6 gas mixtures and to validate the heat transfer results against experimental measurements.

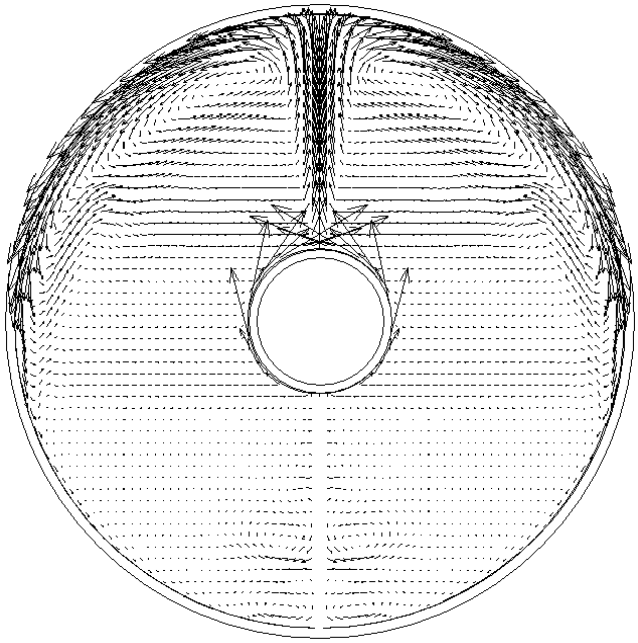

Figure 4: Computational Fluid Dynamics (CFD) Result; Vector Diagram of Velocity and Direction of Gas Convection

4.5.2 Finite element analysis (FEA)

This method has advantages in modelling heat flow by conduction through complex geometries of soil surrounding the GIL formation. However it is necessary to write a sub-routine to represent convective and radiative heat flow between the conductor and the enclosure. Convection was represented by the Vermeer formula given in Annex A; in this respect FEA is a complementary method and is not a true alternative method to the analytical mathematical methods recommended in Annex A.

A second advantage of FEA is that the transient generation of heat in the conductor and enclosure can be modelled as can the transient conduction of heat through the thermal RC network of the soil. This method provides a complementary alternative to the analytical short time rating method recommended in Annex A.

4.5.3 Modelling and computational accuracy

As with all methods of computational modelling it is strongly recommended that the method and model is validated against measurements, or proven alternative mathematical algorithms. Errors can be reduced by setting the boundaries of the soil at a sufficiently remote distance from the GIL such that a sensitivity study produces no change in the computed GIL temperatures. For this study a distance of 25m was found to be adequate. It is equally important that elements of sufficiently small size are selected such that a sensitivity study on varying their dimensions produces no significant change in the computed solution.

4.6 Continuous Rating Sensitivity Study

A representative design of GIL (Figure 2) was selected for the sensitivity study with the target of achieving a nominal continuous rating of 3000A:

- aluminium conductor 280mm OD and 13,270mm² cross-sectional area
- aluminium alloy enclosure 650mm OD
- gas mixture 90% N_2 10% SF_6
- gas pressure 0.67 MPa at 20°C
- 1.050mm depth of burial to top of GIL (installation in agricultural land)
- 1.312 mm axial spacing between GIL in flat formation (one diameter clearance between GIL)
- 1.2 Km/W soil thermal resistivity
- 15°C ambient temperature.

At 3000A the conductor temperature was calculated to be 71°C and the maximum soil temperature adjacent to the oversheath to be 65°C. A reduction in current rating to 2890A reduced the maximum soil temperature to the 60°C limit. (It should be noted that the example GIL design was not optimised to achieve 3000A at a 60°C soil temperature, an increase in axial spacing would have achieved this condition).

The sensitivity study is recorded in detail in Annex A and is summarised as follows:

At 3000A constant current, the parameter that had the largest effect on the maximum soil temperature in contact with the GIL was the diameter of the enclosure. The second most significant parameter was the thermal resistivity of the soil (Figure 5).

At 71°C conductor temperature, the parameter with the largest effect on the current rating variation was the soil thermal resistivity and the second was the enclosure diameter (Figure 6).

At 60°C maximum soil temperature, the parameter that had the largest effect on the current rating variation was the thermal resistivity of the soil and the second was the enclosure diameter (Figure 7).

Variation in the parameters controlling the convective and radiative heat transfer through the gas mixture had a negligible effect on both the current rating and operating temperatures, this is because the temperature drop between the conductor and enclosure is much smaller than that between the enclosure and the ground surface.

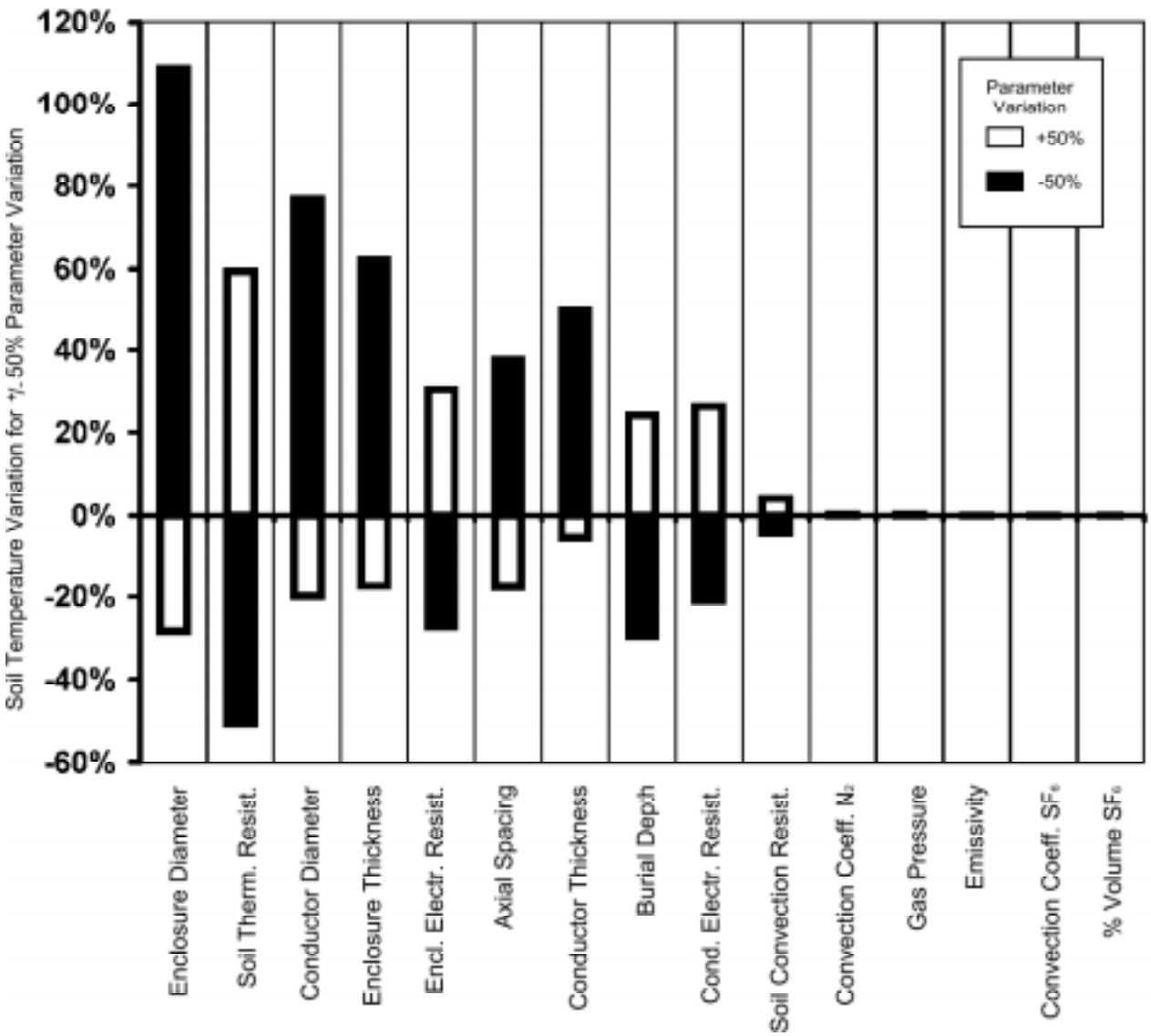

Figure 5: Effect [%] on Maximum Soil Temperature of Varying Each Parameter by +/- 50% at 3000A Rating.

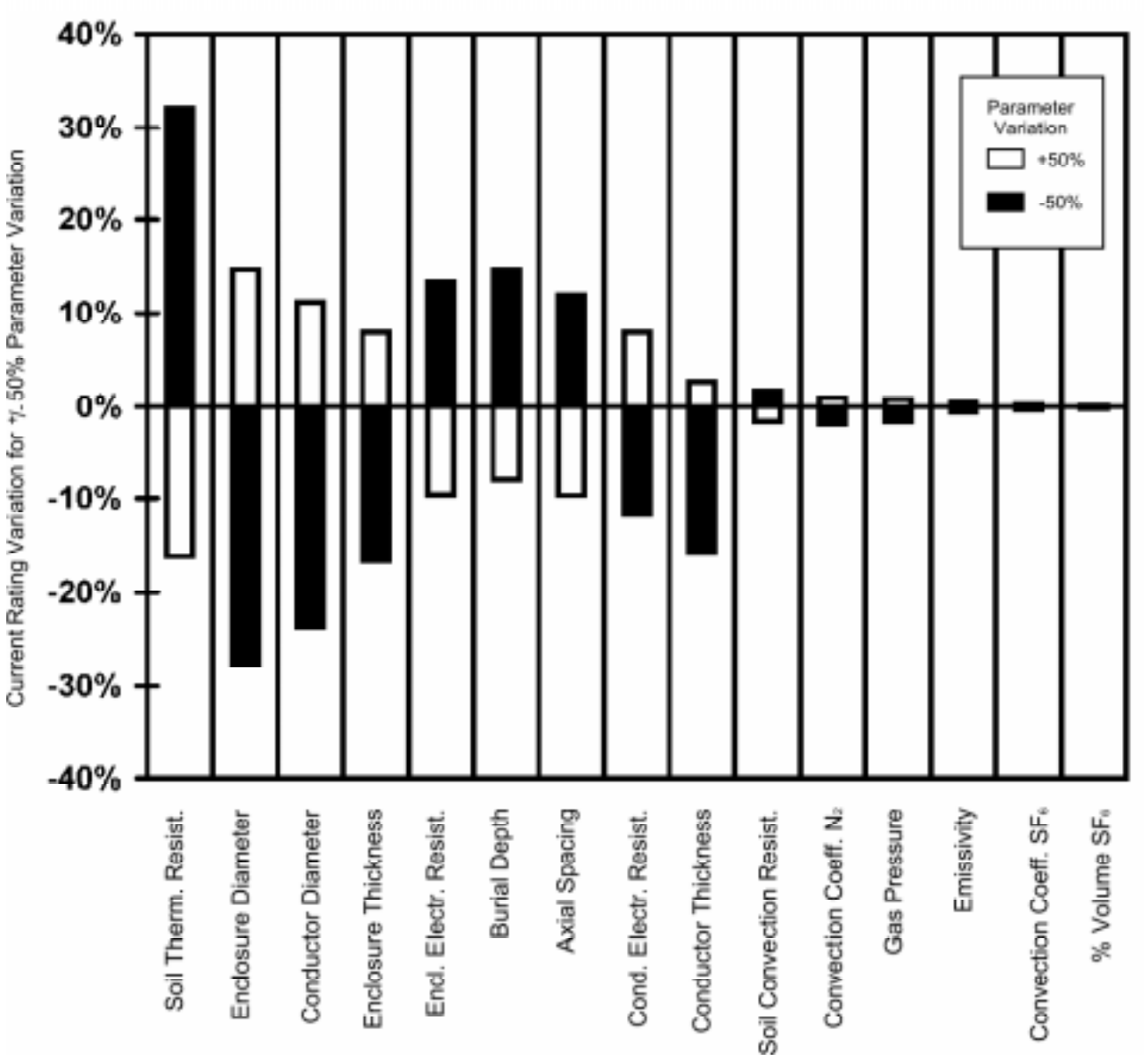

Figure 6: Effect [%] on Current Rating of Varying Each Parameter by +/- 50% at Constant Conductor Temperature (71°C)

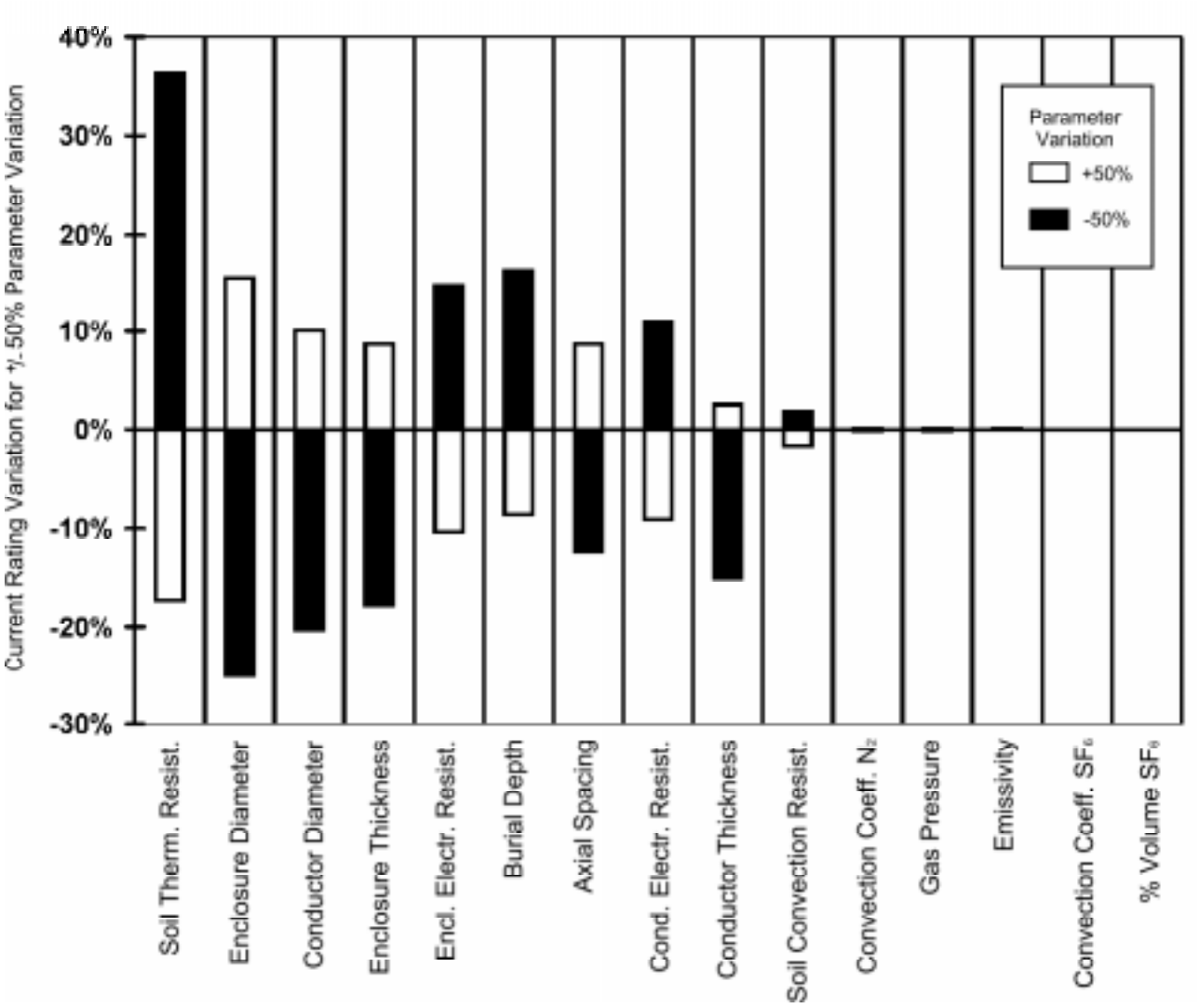

Figure 7: Effect [%] on Current Rating of Varying Each Parameter by +/- 50% at Constant Soil Temperature (60°C)

4.7 Short Time Rating Sensitivity Study

The same representative GIL dimensions were taken for the short time rating. A higher conductor short time rating temperature limit of 95°C was taken, compared to the 3000A continuous rating conductor temperature of 71°C calculated in Paragraph 4.6.

In the first example, a zero starting current was taken. In a 12 hour period it was possible to carry a current of 9840A (328% of 3000A full load), this demonstrates the high thermal capacity of GIL.

In the second example, the starting current was taken as a steady state load current of 2550A (85% of 3000A full load). In a 12 hour period it was possible to carry a current of 7290A (243% of 3000A full load). This illustrates that this particular design of GIL circuit could have taken the additional full load current from a parallel faulted circuit for a useful period of 12 hours (i.e. 185% of full load), without reaching 95°C.

The sensitivity study is recorded in detail in Annex A and is summarised as follows:

The parameter that had the most effect on a 12 hour rating period was $K_{0,}$ the gas convection coefficient. The second most significant parameter was the soil thermal resistivity.

The parameter that had the most effect on a 20 minute rating period was the specific heat of the conductor, the second was K_0, the gas convection coefficient. This shows that the heating in this short period is nearly adiabatic.

It is recommended that, because the calculated short time current ratings for GIL are of such high magnitude, a) a factor of safety be included in either the maximum conductor temperature or in the current rating to avoid the risk of overheating the conductor connectors and insulators and b) the short time rating for a particular design of GIL be validated by experimental measurement.

4.8 Future Work

The recommendations given in this document permit current ratings to be calculated for laid direct GIL in a horizontal orientation. For completeness, the following subjects are identified for future study:

- Rating of GIL inclined at an angle to the horizontal:
  - Recommend rating methods;
  - Sensitivity study on varying angle of inclination;
- Use of CFD modelling (2-D and 3-D):
  - Obtain experimental data on N_2 and SF_6 gas mixtures;
  - Validate modelling results against experimental measurements on GIL;
- Convection from large conductors (diameter greater than 160mm):
  - Study thermal results from full sized field trials, at present in progress;
  - Review the recommended formula given in Annex A for convective heat transfer;
- Conductor operating temperature:
  - Study and recommend a maximum continuous limit and a short time temperature limits for ratings;
- Moisture migration in Soil:
  - Study the mechanism of moisture migration from large diameter GIL enclosures;
  - Review the applicability to GIL of the soil temperature limits recorded in IEC 60287.

5 Insulation cordination

The insulation coordination is a key issue for reliability of components and here only the main results are summarized. All the points are dealt in depth in the annex B.

When dealing with Insulation Coordination, a few basic points should be always kept in mind:

- firstly, a Utility must know the GIL Major Failure Rate (MFR) that is acceptable and then targeted for its own grid; in this respect, it is important to derive from Return of EXperience (REX) for equipment of the same type (when possible) or similar type equipment what the achievable MFR is with the present technology and insulation level practice.
- secondly, the insulation coordination deals not only with the overvoltage aspects but should include also:
  - the insulation characteristics of the GIL insulation,
  - the relations that links the dielectric type tests, routine tests and on site tests with respect to the overvoltages in service and the self or not self restoring aspect of the GIL insulation,
  - the long term withstand at service voltage taking into account random occurrence of insulation imperfections;

In addition, the on line monitoring and diagnostic techniques are also reviewed together with the enclosure grounding and bonding for permanent and transient voltages.

5.1 Accepted (targeted) Major Failure Rate (MFR) and present REX

It is always difficult to choose an accepted MFR and the expected availability required from a link has to be evaluated. Indeed very rarely Utilities display clearly the accepted MFR.

For GIL as for insulated cables, according to two Utilities that publicly announce their target MFR for GIL, an acceptable MFR for GIL should be in the range of 0.2 to 0.3 MFailures/100km of three phase circuit per year ($0.2\text{-}0.3 \times 10^{-5}$ MF/year/meter of circuit per year). That means a Mean Time Between Failures (MTBF) of:

- 5 years for a three phase GIL circuit of 100 km
- 500 years for a three phase GIL circuit of 1 km.

This reliability aspect and the link with Insulation Coordination are intensively discussed in annex B together with the REX on a large GIL world sample together with a GIL MFR GIL derived from a larger sample of GIS (similar technology). According to these surveys the MFR to be expected from GIL with present technology and insulation practise for GIS and GIL are very close but one order of magnitude larger than the targeted ones publicly expressed in Cigré by two Utilities. Such a gap between targeted MFR and that which can be expected should be kept in mind when selecting the standard withstand voltage to be applied forthe GIL.

5.2 Insulating gas

The GIL insulating gas can be either SF_6 (as for GIS) or a gas mixture. Besides the fact that SF_6 is a very expensive gas, it is also a greenhouse gas. Therefore, gas mixtures of SF_6 and Nitrogen N_2 are suitable for reducing costs of the equipment and impact of SF_6 leakage. N_2 is the main component of air. Properties of nitrogen are that it is cheap, inert, nontoxic, nonflammable, and of course environmentally acceptable [13] and [15]. However, the dielectric strength of nitrogen is much lower than that of SF_6. For example, a mixture containing 10% SF_6 results in 85% reduction of the SF_6used and hence reduces the environmental impact of equipment leakage [10].

Because of greenhouse effect, for long GIL gas mixture seems to be preferred. From industrial, environmental and economical points of view a N_2/SF_6 (5 to 20% of SF_6) gas mixture at around 1 up to 2 MPa is the best compromise for electric withstand capability and pressure (Figure 8).

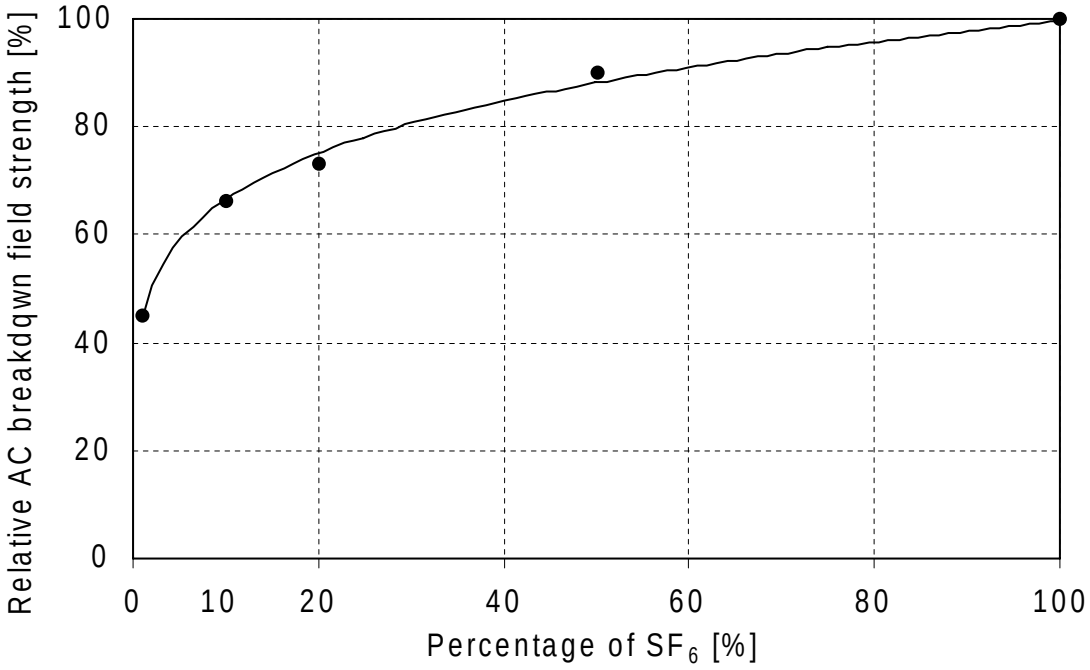

Figure 8: Relative AC breakdown field strength of SF_6-N_2 mixture to pure SF_6 as function of the SF_6 percentage.

Beside all the test conversion factors ratio between the natural withstand voltages of an equipment to the three standard test voltage waveshapes (Lightning Impulse Withstand Voltage, Switching Impulse and Power Frequency) are given for N_2/SF_6 gas mixtures of interest. Compared to pure SF_6, N_2/SF_6 gas mixtures have higher ACWL/LIWL and thus for the same chosen standard LIWV for GIL the actual PFWV is higher (roughly 10%) than PFWV of a pure SF_6 GIL design for the same LIWL. This is a positive element for long term reliability of GIL using N_2/SF_6 gas mixtures compared to the GIS and GIL of the surveys giving MFR one order of magnitude larger than the targeted ones.

Although now widely agreed, it should be repeated that the use in GIL of pure N_2 is economically and industrially impossible. Although N_2/SF_6 gas mixtures are economically and industrially feasible for insulation purposes they are not technically suited for arc interrupting application as in circuit breakers.

5.3 Overvoltages between conductor - enclosure

Due to the different applications of GIL with their parameters of the connected elements at both ends and the generation of possible voltage stresses the expected overvoltages will vary over a wide range. Calculation of the transients can show the maximum overvoltages to be expected along the GIL.

The integration of suitable overvoltage limiting devices is necessary to achieve an economic and safe system. Therefore it is necessary to consider surge arresters from the beginning of overvoltage stress evaluation. These can be metal-clad types integrated into the GIL or air-insulated types installed very close to the ends of the GIL.

For the study of overvoltages in GIL the main focus has to be pointed onto the lightning impulse voltages, because they give the highest stresses, which have to be known for dimensioning and testing.

The power-frequency overvoltages are normally low in comparison to the stresses due to fast and slow front overvoltages. However the combination of AC prestress with the transient phenomena resulting out of lightning activities has to be considered. The importance of considering this prestress is dependant on some parameters as shown below.

The continuous power-frequency voltage and the temporary overvoltages are the basis for dimensioning the overvoltage limiting devices. The characteristic of the surge arresters is necessary must be known for calculation of the transient overvoltages.

Lightning surge voltages within GIL have been illustrated in principal by [16]. Shielding failures and back flashovers have been investigated for a GIL directly connected to an overhead line. The investigations show variation of the maximum voltage amplitude along the length of the GIL (for more details see annex B).

For long GIL (above 1 km), the voltage profile of the fast front overvoltages due to lightning is not flat all along the GIL when the GIL is protected by one surge arrester at both ends (Figure 9).

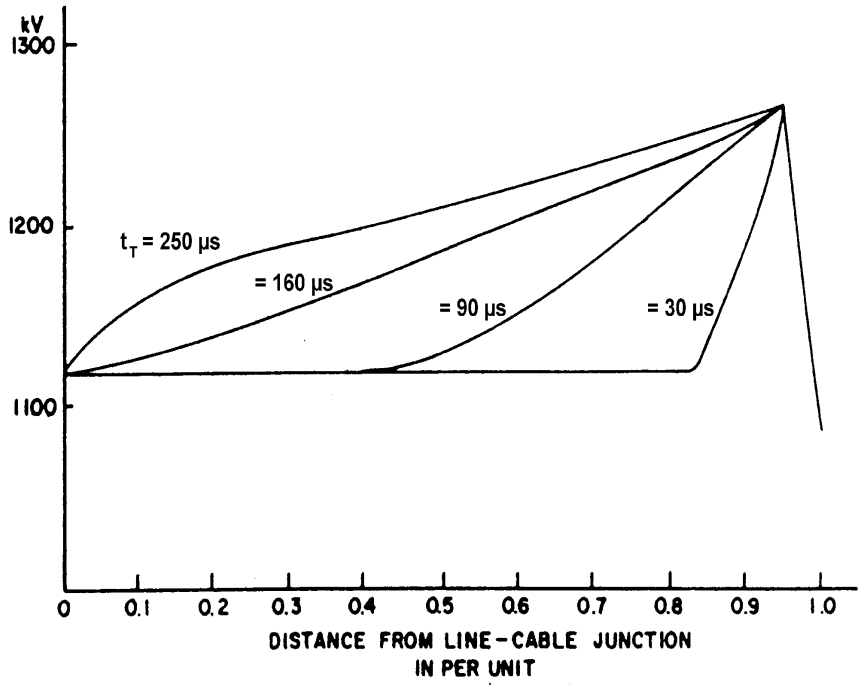

(a)

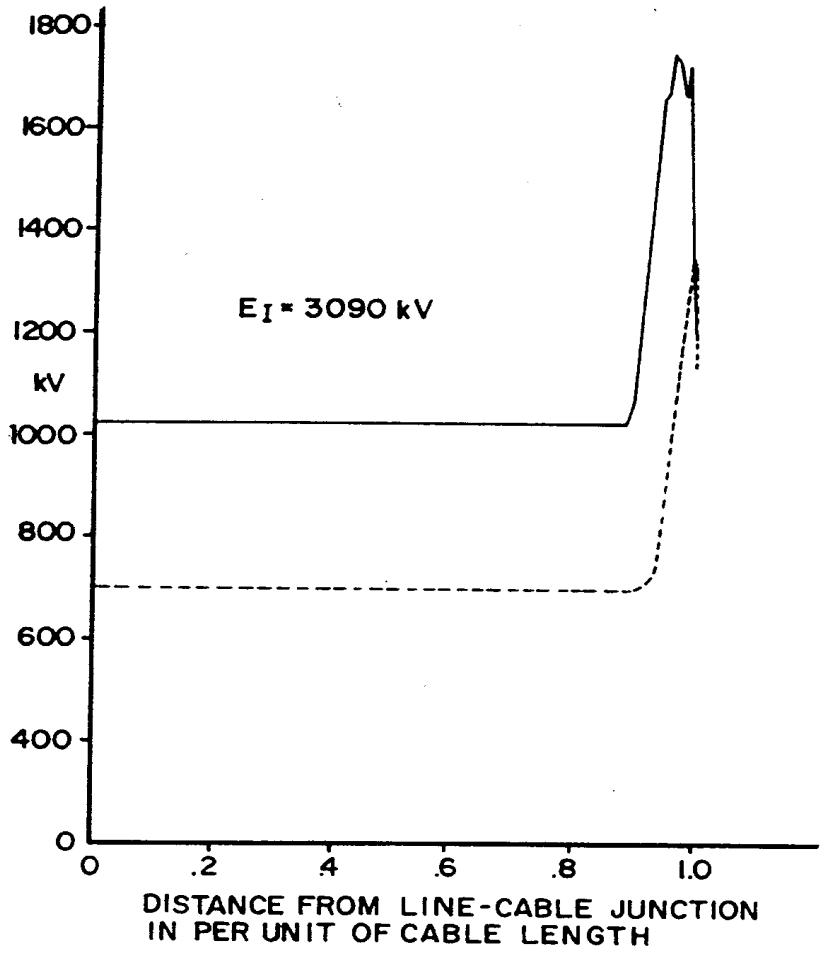

(b)

Figure 9: (a) voltage profile along a 30 km GIL resulting from shielding failure, t_T tail-time of the surge [16]
(b) voltage profile along GIL for a surge caused by back flashover at the first tower (solid line: actual profile considering struck point; dotted line: profile of struck point is ignored): this shows the reflection effect on the first tower on the amplitude of the voltage profile.

Such a peaked voltage profile for long GIL can be flattened and thus lowered by internal surge arresters located at a certain distance from the ends [19]; but one must notice that the optimum distance to the ends is not easy to assess because it depends on the incoming surge slope.

Additionally, surge arresters can be installed in parallel with the insulator chains on the closest towers to the GIL extremities [20] reducing the impact of the reflection on the first tower by reducing the probability of large amplitude overvoltages.

Thus the highest overvoltages along the GIL could be reduced to values close to the surge arrester fast front protective level. However, it must not be forgotten that in addition to the lightning overvoltage aspect, for GIL the chosen rated power frequency withstand voltage is a key parameter of the reliability of GIL [18].

For slow front overvoltage mainly such as those due to switching of the GIL-Overhead line circuit, the overvoltage profile along GIL is rather flat and very close to the surge arresters slow front protective level even for long GIL.

5.4 Insulation Withstand and Overvoltage stresses

So flattening (and thus reducing) the transient overvoltages to overvoltage levels close to the surge arresters protective levels leads to consider that the insulation is distributed all along the GIL: the withstand voltage of many similar insulations in parallel and stressed by the same voltage amplitude is lower than the withstand of only one insulation [16]. Beside when flattening the voltage profile along the GIL, the sensitivity of the GIL is higher in case of defects occurrence. So, choice of too low Lightning, Switching Impulse Withstand Level and Power Frequency Withstand Level for GIL increase the risk of Major Insulation Failure at permanent voltage when random imperfections occur during the GIL life time [18]. All the aspects of type tests, routine tests and on site test procedure and the relations that link all these on site test in relation with the self or not self restoring insulation of the GIL are discussed in depth in the annex B.

Nevertheless, according to the last GIL projects there is no reduction of Lightning Insulation Withstand Voltage requested by Utilities compared to present LIWL of GIS. But this no reduction of LIWV induces an increase of the PFW voltage for N_2/SF_6 gas mixtures GIL and consequently an improvement of their long term reliability: a positive element to reduce the gap between targeted MFR compared to the expected one.

5.5 Long term test

In addition to the type test of short GIL samples, as for insulated cables, long term tests on GIL prototypes have been performed.

The long term test aims to establish the reliability of all components and to test the on-site mounting procedure and the repair procedure.

These long term tests performed at a voltage higher than the system voltage and lasting thousands of hours are intended to represent ageing over life expected duration. So despite the possibility of applying a separarate test for each stress, the long term test is a unique opportunity to apply simultaneously with a voltage stress many of the other stresses affecting equipment life [42]: thermal due to current cycles, mechanical because of enclosure thermal expansion. Descriptions of different long term tests are given in annex B.

Once performed successfully on a GIL basic design, all GIL based on the same basic design are expected to present very similar long term behaviour.

5.6 On line insulation monitoring

This matter has been dealt with by CIGRE WG 15-03 and the part applicable to GIL has been treated in depth in the brochure to be published. Annex B reviews also quite intensively all the various diagnostic methods to apply either during on site test or for on line monitoring in service: physical sensors and signal processing to detect, locate and identify the occurring defects. Nowadays, two methods are mainly used to detect on line the presence of possible defects: UHF methods for new equipment provided with internal UHF sensors and acoustic methods for other equipment. ; Up to now, however the assessment of the actual impact of the detected defects on the GIL insulation and thus on the remaining life is indeed still a difficult matter.

5.7 Bonding and Grounding for permanent and transient voltages

The grounding of Gas Insulated Line must be adapted to the different service conditions represented by normal service, short circuit and over-voltage conditions. The disposition of the GIL (buried, in a tunnel, in a trench) and the possibility of having low voltage equipment such as densimeters, temperature sensors or partial discharge monitoring systems connected on the enclosure has to be considered when the grounding mesh is studied. The design of the grounding system must provide all the safety regarding persons and

equipment in case of potential rise: touch voltage and .step voltage must remain lower than the limit values for permanent or short circuit conditions.

The optimisation of the grounding system should be performed by calculation with a dedicated program but some basic recommendations are formulated in the annex B to avoid major troubles during operation of the GIL.

For short length GIL (less than 500 m), the GIS design rules are applicable [43]. For longer ones, the design must be done taking into account the Technical Report IEC 61640 [1].

In contrast to insulated cables, the grounding and bonding of the enclosure at short spacing does not affect the thermal rating of GIL because of the good enclosure conductivity. Thus, for safety reasons the enclosure grounding and bonding would be done for directly buried GIL every 500m to 1 km reducing the power frequency touch voltage to safe limit values and the transient overvoltage between enclosure and ground to very low values not dangerous for people or for the insulating layer over the aluminum alloy GIL enclosure. For GIL in tunnel the enclosure grounding and bonding is done for shorter length. Examples of grounding realisation are given in annex B.

6 Directly Buried GIL: Mechanical, corrosion protection and installation aspects

The objectives of this chapter are mainly to describe mechanical, corrosion and installation aspects of directly buried GIL. For the mechanical aspect some simple methods for the calculation and analysis of the stress on the enclosure are recommended disregarding the mechanical aspects of the internal components. Effects of short circuit forces on the enclosure are excluded. The main aspects are the calculation of required enclosure thickness, the vertical and horizontal stability and the interaction between the soil and the enclosure. For the corrosion aspects two methods are described, the coating and the cathodic polarisation. Over-ground and tunnel installations are not dealt with because they are similar to GIS bus ducts which were first installed more than 30 years ago and have previously studied in the substation study committee.

6.1 Mechanical aspects

6.1.1 Stresses

One of the main issues for gas insulated transmission lines is the mechanical behaviour in the soil during installation and operation. The GIL consists of 3 single phase encapsulated tubes which are directly buried in the ground. Each tube consists of an outer aluminium alloy enclosure and an inner aluminium conductor. In operation, thermal expansion and gas pressure generate the main forces acting on the enclosure. Differential expansion between the inner and outer tubes is accommodated by the use of sliding contacts already widely used in GIS. In addition, the enclosure is anchored in the soil because of the friction which leads to high mechanical loads. The enclosure is also subjected to load bearing, soil pressure and traffic loads. The GIL has to follow curvatures in vertical and horizontal directions (minimum bending radius approximately 400 m), according to the terrain. Stresses for abrupt changes (for example elbows) in direction are not dealt with in this study.

The mechanical design needs to take into account all the effects applied on the pipe listed below in general order of the importance :

- thermal expansion,
- friction between the soil and the enclosure due thermal effect,
- internal pressure,
- bending resulting from the vertical and horizontal curvatures,
- soil pressure
- traffic loads,
- water pressure (if any)
- seismic loads (if any)

6.1.1.1 Thermal expansion (thermo-mechanical stress)

The GIL is a thermal system with inner heat production by circulating of electrical current in both the conductor and the enclosure. Two mechanical states can be found in buried GIL. The centre section (anchored) is blocked solidly by friction with the soil, towards the extremities the enclosure may move unless other constraints are applied. Heating causes a mechanical stress in the anchored parts in the longitudinal direction of the enclosure. This thermomechanical stress is proportional to the thermal coefficient of the material and the temperature difference between the operating and the laying temperature.

The thermomechanical stress causes a compressive force on the pipe in the axial direction (Figure 10).

For example with a diameter of the enclosure of 650 mm and thickness of 10 mm, the stress caused by a temperature difference of 50 C is 86 N/mm^2.

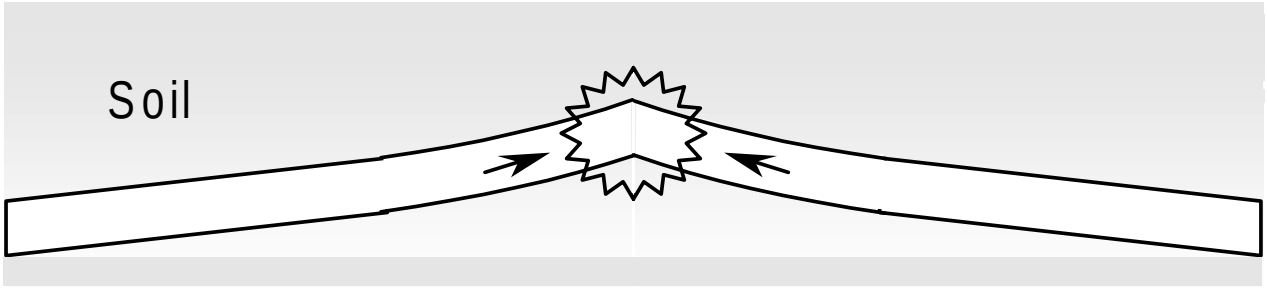

Figure 10: Schematic figure of the mechanical forces induced by thermal expansion and its possible effect in bending/elbow if not taken into account in the path and GIL design.

6.1.1.2 Internal pressure

The internal pressure induces on the enclosure 3 components of stress, hoop (tensile), axial (tensile) and radial stress (compression) (Figure 11). The main stress to be considered for the dimension of the thickness is the hoop stress. The axial stress reduces the axial stress caused by the thermo-mechanical stress.

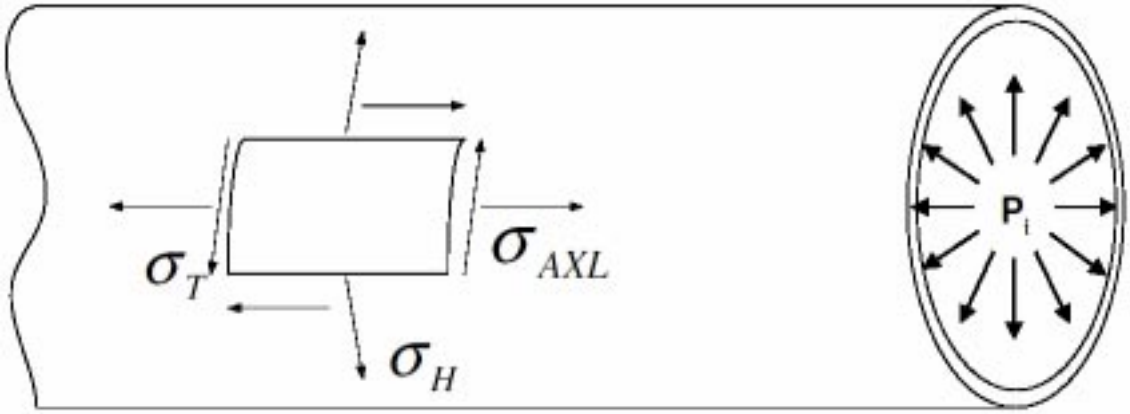

Figure 11: The hoop, axial and radial stress induced in the enclosure by the internal pression.

For example with a diameter of the enclosure of 650 mm and thickness of 10 mm, the hoop stress caused by a pressure of 7 bar is 22.7 N/mm^2 and the axial stress is 7.3 N/mm^2.

6.1.1.3 Bending

The bending stress results from the conditions of installation. It may be necessary to introduce curves in the GIL to follow the terrain. Such bending will introduce a tensile stress on the outside of the bend and a compressive stress on the internal side of the bend. These stresses are proportional to the stiffness of the enclosure and inversely proportional to the bending radius.

For example with a diameter of the enclosure of 650 mm, the maximum stress tangential to the bend caused by a bend radius of 500 m is 46.2 N/mm^2.

6.1.1.4 Soil pressure

The weight of the soil exerts a vertical pressure on the enclosure. The enclosure has a tendency to become oval and the soil reacts with a horizontal pressure on both sides. All these pressures depend on the buried depth, the soil characteristics and the conditions of the laying. There is an evolution of lateral pressure with time.

For example with a diameter of the enclosure of 650 mm, and thickness of 10 mm and burying depth of 1.5 m, the stress caused by soil pressure is 0.03 N/mm^2.

6.1.1.5 Traffic loads

It is necessary to pay attention to traffic loads which may be temporarily applied locally to the GIL.

For example with a diameter of the enclosure of 650 mm, and thickness of 10 mm and burying depth of 1.5 m, the stress due to soil and traffic loads are shown below.

Table 2

		Vertical loads (N/mm2)		Horizontal load (N/mm2)		
h (m)	P_E	P_V	Q_V	Q_H	qhsl	qhsk
1.5	0.030	0.021	0.048	0.015	0.035	0.035

The vertical and horizontal Loads depend on the soil cover h

- P_E vertical soil load acting on the pipe
- P_V vertical traffic loads acting on the pipe resulting
- Q_V vertical total load on the pipe
- Q_H lateral pressure on the pipe resulting from the soil pressure
- qhsl, qhsk lateral pressure from the pipe displacement ; l for long term, k for short term.

Lateral pressure on the pipe is the sum of Q_H and qhsl/k.

6.1.1.6 Water pressure (if any)

Where the water table is at the same level or higher than the GIL there will be an upwards vertical force applied to the enclosure (Archimedes' principle).

6.1.1.7 Seismic loads (if any)

Seismic disturbances will usually effect the internal components of the GIL in terms of vibration in which case natural frequencies have to be considered. The GIL cannot be designed to withstand the sheering effect of an earthquake.

6.1.2 Enclosure design and factors important to the continued mechanical performance of the GIL

The mechanical design of the enclosure is an iterative process starting with the minimum wall thickness due to internal pressure; after that first step, the thermo-mechanical stress and axial stability, vertical stability, analysis of all stress combined, maximum allowable stresses and thermal loading history (fatigue) have to be investgated for checking their influence on the enclosure design.

6.1.2.1 Minimum wall thickness due to the internal pressure

The first step in stress analysis is to calculate minimum wall thickness required to withstand the internal pressure. While the diameter of the enclosure is generally determined by thermal and electrical engineering, the thickness is determined by thermal and mechanical engineering in order to have operating temperatures under the thermal limit and the stress under the allowable stress. For the calculation of the minimal thickness all codes of pressure vessels and piping systems give approximately the same formula taking into account the quality of welding. The minimal thickness depends on the pressure, the diameter of the enclosure and the allowable stress of the material. The pressure must be the maximum operating pressure expected at the location on the GIL under anticipated steady state operating conditions.

6.1.2.2 Thermo-mechanical stress and axial stability

Once the minimum wall thickness has been calculated, thermo-mechanical stresses must be calculated. The second step is to examine the axial conditions as follows:

- the combination of axial stress due to internal pressure and thermo-mechanical stress results in a compressive stress which must remain lower than the allowable stress of the enclosure material;
- the axial stability which is connected to the axial stress must then be calculated for buckling. With an excessive heating of the pipe the compressive force may exceed the limits of the admissible force and produce a buckling phenomena in the pipe. The stress which produces buckling depends on the length, cross section, the moment of inertia and the E-Modulus of the material. For example, on one hand, for an unburied GIL with 100 m length and with $\Delta T=50°C$, the compressive force $F_r=1.154$ MN exceeds the critical buckling force (0.29 MN) and is therefore not stable. On the other hand, a buried GIL with a minimum cover of soil of 1 m is stable. The buried GIL of 100 m length needs a larger compressive force in the magnitude of 17 MN to pop out of the soil while the same line with $\Delta T=50$ is only under a load compressive force of 1.65 MN. The main factors influencing the axial stability are temperature difference between installation and operation, and the burying depth.

6.1.2.3 Vertical stability

The third step in the design of the GIL is to study the vertical stability depending mainly on the soil pressure and traffic loading. There are other factors which influence the vertical stability such as the internal pressure, the pressure of the water if any and the GIL weight. The determination of the normal forces and moments applied over a cross section allows to calculate the stress and deformation on the GIL. This is the main step of checking the mechanical design of the GIL in a vertical direction. These forces and moments are generated by the non-uniform pressure distribution on the cross section of the enclosure. The results of the calculation will be near to reality only if the loads, the laying conditions and the characteristics of the soil are well known.

Various National standards give methods to calculate the soil pressure, traffic loads, the combined active and passive vertical and horizontal loads acting on pipelines which may be adapted for GIL. All these loads depend on the buried depth, the soil characteristics and the conditions of laying. The vertical soil pressure and the traffic loads induce a lateral pressure resulting from the displacement of the pipe. The lateral pressure is determined by two soil states. The first corresponds to the soil conditions immediately after laying, the second to the soil conditions after years of operation.

An optimum burying depth must be found by comparing the soil pressure due to depth and the traffic load pressure. The soil pressure increases with depth, and the traffic load pressure decreases with depth. In burying the GIL at a depth of one metre there should be no problems of vertical stability.

6.1.2.4 Analysis of all stress combined

A heated pipe which is buried underground tends to expand and move. The experience from pipelines system show that only the ends move and the big part, the middle one, is anchored in the soil which is called the restraints portions. The active length, the moving part is proportional to the temperature difference and inverse proportional to the friction coefficient between the soil and the enclosure, the buried depth and the diameter of the pipe.

All types of stress previously discussed are combined in the principal stress. For that, the von Mises hypothesis can be used, but other methods can be chosen such as shear hypothesis. The calculated value must be lower than the allowable stress to have an acceptable design of the GIL.

For example using the same GIL dimensions as above, at ΔT=50 °C, the axial stress is 86 N/mm^2, von Mises with a bending vertical or horizontal with a radius of 400 m is about 93 N/mm^2. The variation of the principal stress as a function of the ΔT is shown in the diagram below (Figure 12).

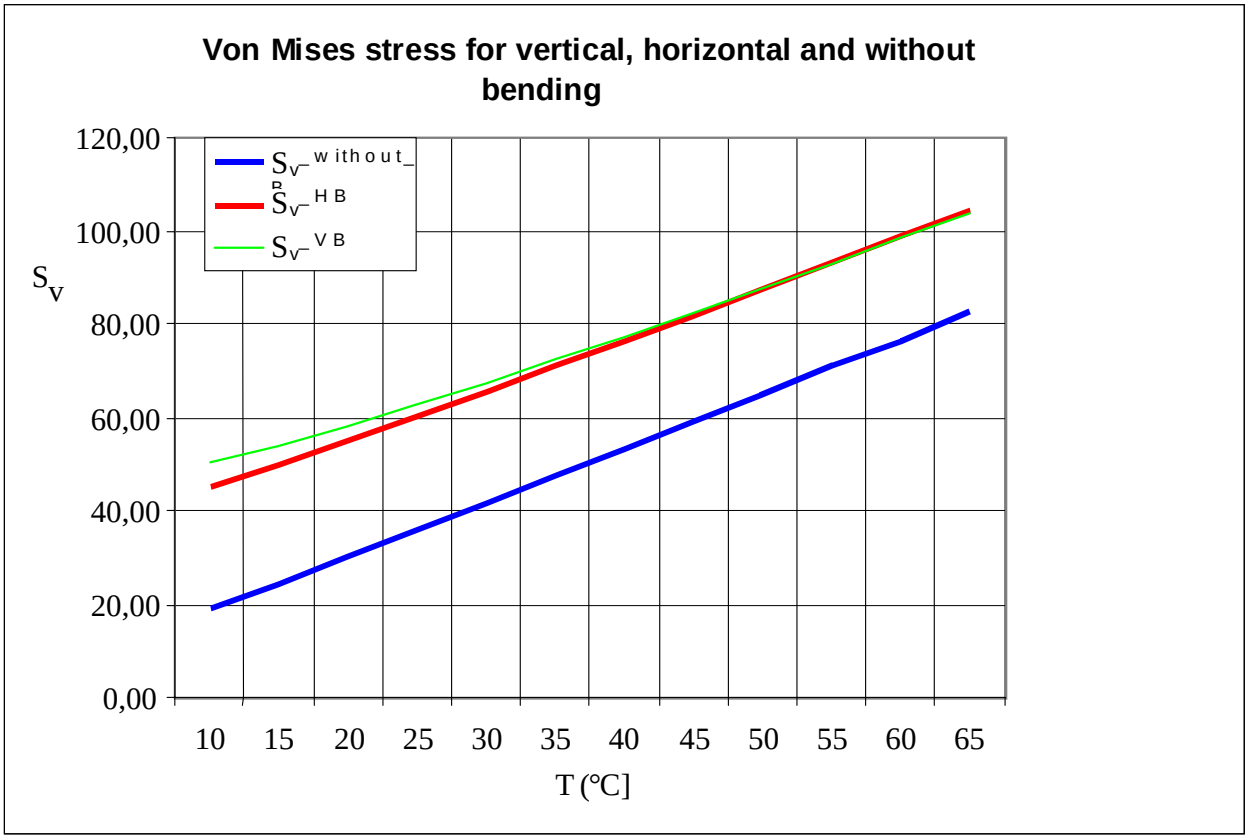

Figure 12: von Mises stress for vertical (N/mm^2)

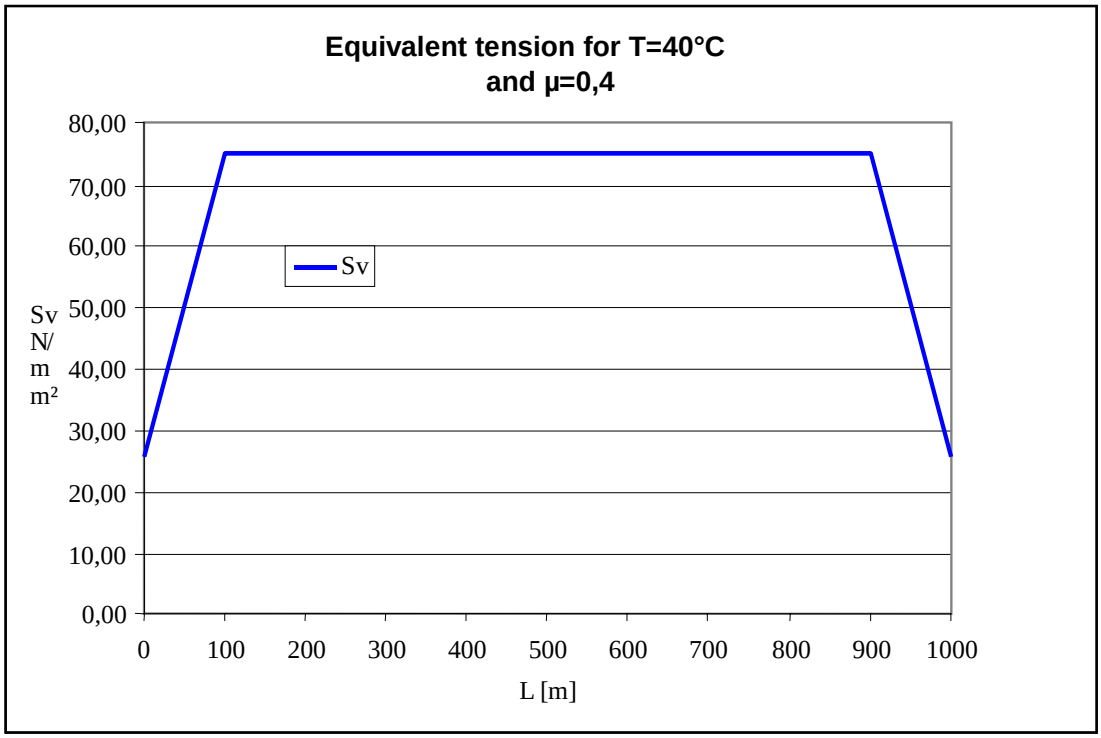

Figure 13 Principal stress for a buried GIL in case of free ends (μ the friction coefficient soil/GIL)

The Figure 13 shows the stress in the restraints portions and this is less in the moving portions (at the ends) because of the relative movement of the pipe to the soil. This decrease proportionally from the anchoring part to the free ends . In the case where the ends are blocked, the principal stress along the GIL will be constant and equal to that in the anchored part.

6.1.2.5 Maximum allowable stresses

The maximum allowable stress can be determined from the characteristics of the enclosure material chosen using the rules given in the national standards for pressure vessels and pipelines. Unfortunately none of the existing codes are applicable in full to gas insulated lines (GIL):

- pressure vessel codes such as ASME VIII, CODAP, EN 50064, ... do not take into account the specificity of buried cross-country structures,
- pipelines codes such as ANSI B31.8, CSA codes, GAZ de FRANCE CCTP, ... do not take into account the specificity of a structure carrying electricity.

CSA code Z169 for aluminium gas pipelines is the closest to the case of GIL as it is specific to buried cross-country structures made of aluminium and is served by experience in Canada where there are several kilometres of gas distribution buried aluminium pipelines. The code applies coefficients based on the behaviour of gas under explosion, which are not applicable to insulating gas mixtures. Care must be taken to apply the appropriate coefficients.

For calculation of allowable stresses and factors for changes in direction the US based, ASME standards or the European EN 50 064 1989 “Wrought aluminium and aluminium alloy enclosures for gas-filled high-voltage switchgear and controlgear” can be used.

6.1.2.6 Thermal loading history (fatigue)

For direct buried GIL the stress range becomes more important than the actual maximum stress. The enclosure may yield the first time the maximum temperature is reached. There will be significant stress relaxation as the enclosure material approaches yield and depending on how long the maximum temperature is maintained, some or all of these stresses will reappear as a tension load as the pipe cools. Thermal time constants are long for direct buried GIL. Generally the time constants exceed the normal daily current cycling for the line, so there should be only minimal changes in enclosure stresses and they should remain in the elastic range. Annual changes in load profile will produce lower changes in pipe temperature than the full delta T caused by going from no current to full rated current but may produce some plastic strain. Thus, the design consideration becomes one of fatigue rather than maximum stress. To avoid the problem of fatigue the GIL should be designed so that it remains in the elastic range.

6.2 Corrosion Protection of GIL

Efficient corrosion protection is essential to ensure design life of 40 years. Current experience with buried aluminium pipes is very limited, nevertheless the experience already gained with steel pipes can be adapted for the properties of aluminium.

Corrosion is always linked with the presence of electrical current circulation due to a potential difference. This can be due to internal unbalanced chemical elements inside a metal which create an elementary battery cell, or due to external influences such as a difference in pH between two points on a metallic surface or circulation of vagabond currents through the metal.

Buried steel pipes have been used for the transport of water, gas and oil for many years. Two main types of corrosion protection are employed, independently or together : cathodic protection and/or coatings.

Cathodic protection consists of applying a negative potential to the metal surface. This is easy for steel because a negative polarity of only -0,8 V applied to the enclosure relative to the copper reference electrode, installed in the surrounding soil, is sufficient for protection. This potential does not electrolyse the water contained in the soil excessively. This negative polarity can be achieved using a Zinc anode. As the current flowing is proportional to the enclosure surface in contact with the soil, the size and the number of Zinc anodes distributed along the length may be quite large for a long steel pipes. In order to reduce the Zinc anode size, an insulating coating must be applied around the pipe.

Steel is relatively easy to protect using only cathodic polarisation, but this is not the case for aluminium. For aluminium complete immunity from corrosion could only be assured by applying a potential of -2,0V which would highly electrolyse the water. The electrolysed water would become alkaline and would attack the aluminium. Cathodic polarisation must therefore be limited to a value between -0,8 V and -1,0 V to avoid electrolysation of the water. These values can be achieved with zinc reactive anodes or by a static generator. This is not sufficient to assure an efficient protection against corrosion. To ensure that the polarisation remains within the correct limits (-0,8 V and -1,0 V) monitoring system is required.

For aluminium enclosures therefore the main method of corrosion protection is the use of a coating on the aluminium to prevent direct contact with the surrounding soil. This protection may be complemented by the use of the cathodic protection.

The coating must withstand chemical attack and mechanical damage. This is generally achieved by using more than one layer of coating. The inner protective layer will normally be a thin layer of epoxy. This protects against attacks from acids, alkalis and various salts. This layer needs to protected mechanically, however. This mechanical protection will normally be polyethylene or polypropylene and will be quite thick. Because of the difficulty of bonding PE or PP to epoxy an intermediate layer is sometimes used. Choice of PE or PP will depend on factors such as temperature. The coating must be flexible enough to cope with thermal expansion of the GIL without sheering the bonding between layers.

The coating has an impact on the heat dissipation of the GIL because of it's high thermal resistance (3.5 mK/W). For this reason, as well as cost, the thickness of coating needs to be limited. A thickness of between 3 mm and 6 mm appears to have only a moderate effect on heating.

Concrete is highly alkaline and attacks aluminium strongly. Where the GIL is to be blocked in concrete it is necessary to thoroughly check the coating before pouring the concrete because it is difficult to repair the coating afterwards.

The GIL enclosures will be delivered to site with the coating already applied. Because the GIL is welded on site it must be possible to apply the coating over the welds on site.

Tests must be carried out to validate the coating but no standard specific for aluminium coatings exists, but the tests for coating of steels may be employed.

As the earthing circuit is generally copper, care must be taken to avoid creating a natural cell between the copper and aluminium which could lead to ionisation of the aluminium atoms. This may be achieved by separating the connection between the two metals with the use of a polarisation cell.

Due to corrosion risks it is advisable to avoid acid or alkaline soils or areas of industrial contamination. Also to be avoided are roads which are subjected to salt treatment for snow clearing during long winters. It is also advised to avoid parallel paths with dc supplied railways as these can generate vagabond currents.

No protection is necessary for the inside of the GIL as the gas mixture is not aggressive for the aluminium.

6.3 Installation of direct buried GIL

The GIL installation is quite similar to the installation of gas or oil pipes, except that the enclosures are aluminium and not steel, and an internal conductor is necessary for transmission of electricity .

The main difference is relative to the cleanliness, which must be the top priority in order to avoid the input of particles inside the tubes as much as possible. Particles and particularly metal particles may be at the origin of dielectric flashover.

The second difference is relative to the presence of a central conductor supported by spacer insulators. All the GIL components must be handled and assembled with caution in order not to damage these insulators.

The people in charge of the assembly must pay special attention to the manufacturer instructions.

Before starting any work, it is necessary to make a complete study of the soil that will be crossed. Some soils can present a danger for the GIL because of risk of corrosion and need at least deeper chemical analyses.

Compared to pipelines the GIL components must be handled with care because of the components inside and the coating on the outside.

6.3.1 GIL assembly operation

The trench is prepared in accordance with the consistency of the soil. The extracted materials are stocked in order to be used for back filling, as much as possible. The bottom of the trench is filled with sand on which the GIL will be laid down.

Junction chambers along the GIL are used to fix the GIL, to allow access for monitoring, earthing and to allow high voltage testing section by section. These vaults are prepared in appropriate positions in advance of the GIL assembly. After the GIL installation the vaults are completed. Where anchorages are needed the process is the same as for vaults.

After inspection, cleaning etc. the GIL is positioned and the sliding contacts of the conductors are carefully fitted together. The two prepared enclosure extremities are then assembled and welded and tested in accordance with local health and safety regulations.

After installation the welds must be protected from corrosion using a non conducting coating material similar to that used for the rest of the enclosure. The coating then has to be tested for porosity using a "holiday detector". Any weak points found have to be repaired.

The trench is then ready for backfilling. Where necessary for thermal reasons and/or integrity of the coating reasons because of rocky soil, the original soil directly against the GIL may be treated or simply replaced with sand. The soil is compacted around the GIL during backfilling to avoid movement later. The rest of the trench can be filled with the natural soil and progressively packed down. It may be necessary to check for damage of the coating after backfilling.

In order to minimise the electromagnetic field, the 3 GIL enclosures are linked together and earthed at each end, and in each vault. Earthing connections are made to an earth mat through a polarisation cell to avoid circulation of corrosion currents. Any cathodic polarisation system will have to be installed before backfilling and the monitoring installed in the vaults.

The SF6/nitrogen gas mixture assures the dielectric insulation withstand of the GIL and must be exempt of impurities and moisture. For this reason gas handling is very important. The accurate mixing and separation of gas mixtures is now well handled by gas suppliers.

Before being put into service the GIL willhave to be routine tested. Routine tests include weld inspection (which will have to be carried out before the corrosion protection is applied), pressure testing, leak testing and dielectric tests. These tests may be carried out during the continuous installation process depending on GIL length and other practicalities.

The control system must also be installed. Each gas compartment must be monitored for gas density, with alarms and lockout thresholds. Other fault detection systems may also be installed. A communication link will have to be installed to connect all the transducers etc. with a central control unit.

6.3.2 Buried GIL Installation History

During the 1970’s and 80’s GIL produced several direct buried GIL installations at 145 kV and 242 kV. Run lengths were usually less than a few hundred meters and all installations were equipped with active corrosion protection. These early installations were not supported by detailed mechanical calculations, however, most of the installations are still in service today. There have been 2 instances where the GIL line was dug up to correct a problem. There was no evidence of corrosion or detectable deformation of the parts examined during these repairs.

6.4 Final remarks

The mechanical stability of directly buried gas insulated transmission lines (GIL) in axial and vertical directions as well as the forces, the deformation and the stresses during operation were investigated.. The effects of the soil load, the traffic load and the inner pressure, the water pressure in the soil on the enclosure were considered

From a corrosion point of view, the behaviour of buried aluminium is very different from that of steel. It is impossible to secure cathodic protection and so it must be assured that the coating protection has no imperfections which lead to expose aluminium.

7 Environmental aspects

7.1 Environmental life cycle assessment

A standardised procedure for quantifying the environmental impact of a technology is the Environmental Life Cycle Assessment (LCA), the procedural basis for which is documented in the international standard series ISO 14040 [9].

An LCA has been outlined for the case of gas-insulated power equipment by CIGRE WG 23.02 [10]. The approach is applicable to GIL and is described in the report in a simplified manner as being performed in 5 steps as follows:

- choice of a representative functional unit of the technology
- definition of the “horizon” (frame of reference) of the study
- establishment of a life cycle inventory
- derivation of a life cycle impact assessment
- derivation of life cycle interpretation

The functional unit chosen for the assessment might be a unit length of GIL with a given rated voltage and current.

The horizon of the study includes the life cycle phases which are considered, the material production and energy generation scenarios that are assumed, the types of environmental impact that are to be assessed and the methodologies to be used.

The life cycle inventory (LCI) quantifies the relevant material and energy flows into the system and emissions and waste flows out of it. In the case of GIL, the LCI will include the materials used and the energy consumed in producing them, emissions and waste generated during production and manufacture, energy losses generated during the operational lifetime of the equipment, and energy losses and emissions associated with decommissioning and disposal or recycling.

The life cycle impact assessment (LCIA) derives quantitative environmental impacts from the LCI data.

The life cycle interpretation draws conclusions from the LCI and LCIA data.

A comparative assertion is a special type of LCA in which the environmental impacts of two systems of equivalent performance are compared. The report illustrates the basic principles of a comparative assertion for the case of SF_6 emissions from systems using pure SF_6 and a mixture of nitrogen and SF_6.

Most of the materials used in GIL are easily recyclable at end of life

7.2 General environmental aspects

A comparison of overhead lines and underground cables, with particular reference to environmental effects, has been reported by CIGRE Joint Working Group 21/22.01 [5]. Many of the arguments are applicable to GIL. The environmental impact of transmission technologies including GIL has been reported by Jouaire [8]. Factors considered in the two reports are:

- visual impact
- electromagnetic fields
  - magnetic fields
  - electrostatic fields
- depreciation of property/land values
- restrictions on land use: buildings, air traffic, land cultivation
- audible noise
- electromagnetic interference (radio interference voltage)
- effects on forests and natural environment
- risk of soil pollution

The present report will only deal with those factors where the use of GIL has a different impact to that of conventional cables.

7.3 Electromagnetic Fields

7.3.1 Electrostatic fields

The earthed, conducting enclosure of a GIL will provide complete screening against the power frequency electrostatic field of the conductor at high voltage. The screening will remain effective under transient conditions.

7.3.2 Magnetic fields

Where a GIL is of the single-phase enclosed design and the enclosures are solidly bonded at each end (which will normally be the case), enclosure currents will circulate tending to reduce the magnetic field external to the GIL. However, due to the spatial disposition of the three phases, screening is not complete.

Magnetic fields have been calculated for the overhead line, GIL and cable systems that were considered in Paragraph 3.1. RMS values of the magnetic flux density at 1 m above ground and at different distances from the central axis are shown in Table 3. The values correspond to a transmitted power of 2000 MW.

Table 3:
Magnetic flux density for 400 kV lines and 3000 A (see Table 1)

B (μT)	Distance from central axis (m)			
	0	10	20	30
Overhead line	42	36.5	21.0	10.8
GIL Flat formation	5	0.25	0	0
XLPE cable 1 per phase Flat formation	109	11	2.9	1.3
XLPE cable 2 per phase Trefoil formation	13.2	0.74	0.19	0.08

The magnetic field of the GIL was generally lower than that of the overhead line and the cable system. The magnetic field of the cable system with two cables per phase was generally lower than that of the overhead line.

Where a GIL is of the single-phase enclosed design and the enclosures are bonded in such a way that enclosure currents cannot circulate, e.g. where single point bonding is used, eddy currents will flow in the enclosures but these will provide no effective magnetic screening. The magnetic field external to the GIL will therefore be higher than in the case where the enclosures are solidly bonded. It is thought that such an arrangement will seldom be used.

The magnetic field external to the GIL may be calculated analytically using Ampère's Theorem and Biot and Savart's Law. Alternatively, the magnetic field can be calculated using a numerical method, such as the finite element method. An analysis of magnetic fields of underground cable systems has been reported by CIGRE Joint Task Force 36-01/21 [12].

7.4 Global warming

A survey of the present situation concerning the environmental implications of SF_6 used in electric power equipment is given in a paper by WG 23-02 [11]. As a consequence of its high global warming potential, SF_6 was put on the list of greenhouse gases in the Kyoto protocol in 1997. According to the study, in 1999 the share of "electric" SF_6 in man-made greenhouse gas emissions was approximately 0.1%. With the implementation of conservative SF_6 handling in the electricity industry, the share of the "electric" SF_6 emission in relation to the total greenhouse gas emissions will reduce to about 0.04% by 2010. It is concluded that "electric" SF_6 emissions, which are already now quantitatively insignificant, will become irrelevant in the future despite the ongoing installation of SF_6 insulated equipment.

Therefore when it is possible the environmental impact of SF_6 can be further reduced by reducing the quantity of it inuse . For GIL, the use of a mixture of nitrogen and SF_6 is a practical alternative to pure SF_6. A comparison of the environmental impact of emissions from a system using pure SF_6 and one using a mixture of nitrogen and SF_6 is outlined in the report by CIGRE WG 23.02 [10].

8 Overall Economic aspects

GIL is a means of transmitting electrical power at transmission voltages. It provides an alternative to cables for the undergrounding of circuits. It has comparatively high ratings and is suitable for transmission over long distances.

The comparison of overhead lines and underground cables reported by CIGRE Joint Working Group 21/.22.01 [5] commented on comparative costs. Again, many of the arguments are applicable to GIL. An economic comparison of transmission technologies including GIL is included in the report by Jouaire [8].

On the basis of capital costs of the circuit, overhead lines are the most economic means of high voltage transmission compared with cables and GIL.

The decision on whether to underground a circuit takes into account the need to transmit electricity at minimum cost and the need to minimise the effects on the environment. Undergrounding is therefore applied in situations where an overhead line would be impracticable or where amenity considerations are overwhelming. Environmental concerns and public opposition to overhead lines are influential.

The time required in which to obtain planning permission from the relevant authorities is generally less where a circuit is undergrounded. Difficulty in obtaining permission for an overhead line may lead to significant costs due to late commissioning of a project and costs associated with the legal process.

The costs associated with rights of way depend on practices adopted in different countries. The land crossed by a transmission circuit may be purchased by the utility or rented. The price of land in different locations will vary significantly.

The cost of losses over the lifetime of an installed circuit can be significant. The losses depend on the actual power transmitted and are highly variable. In the examples shown in Table 1, the losses were highest for the overhead line. The losses for the grounded GIL and cross bonded cable system with comparable rating were similar in level. For comparison with capital costs, the cost of losses incurred throughout the life of a circuit can be converted to an equivalent capital sum at the time of purchase, or capitalised to the present worth. The capital cost of losses will be specific to the particular project.

When comparing the costs of GIL with cables, it is difficult to state a clear boundary due to the large number of variables that influence the economics, many of which depend on the particular project.

To match the ratings of some overhead lines, it is sometimes necessary to use two cables per phase, thus increasing the cost per unit length of the cable option. GIL has a significantly higher rating than cable and it may be possible to match the overhead line rating with a single GIL per phase.

The design of a GIL must satisfy dielectric, thermal and mechanical requirements. If the current rating for an application is low, it does not follow that GIL dimensions may be reduced. GIL may therefore be less competitive than conventional cables at lower ratings.

GIL terminations are less expensive than cable sealing ends. The costs of reactive compensation are less for GIL than cables.

Indeed, as many of the factors that influence the costs will depend on the particular project. Each project will require careful study. As guidelines, the following items should be at least considered but the list is far to be exhaustive:

- Capital costs:
  - equipment costs - voltage and current rating, length
  - installation costs - costs of labour and materials for installation
  - cost of land
  - civil engineering - routing, direct burial/tunnel
  - cost of reactive compensation
  - cost of terminations, switchgear, protection
- Costs incurred throughout life of a project:
  - losses
  - maintenance/monitoring
  - land rental
  - spares
- Cost of decommissioning, recycling materials.

9 State of the art

9.1 Actual installations

9.1.1 Experiences/references

Significant lengths of GIL have been installed above ground and in tunnels and have been in service for years ([36] [36], [54]). However directly buried GIL has not been widely applied. Some applications are reported ([39], [40], [41]). Recent full size trials of directly buried installations have been performed and will be described below together with the last known GIL installations whatever are the laying conditions.

9.1.2 Shinmeika - Tokai GIL

Chubu Electric Power Co. Inc. has installed a 275 kV GIL in a tunnel between Shin-Nagoya Power Station and Tokai Substation, a route length of 3.25 km. The project is well documented in the literature [44], [45], [46], [47]. The GIL went into service in February 1998. It comprises two three-phase circuits with a present transmission capacity of 1300 MW, rising to 2850 MW when forced cooling is implemented.

GIL was chosen due to its being a more economic alternative than XLPE cables, for which five circuits would have been required.

Figure 14: View of the 275 kV Shinmeika - Tokai GIL.

9.1.2.1 Ratings

The GIL ratings are summarised in Table 4. The two circuits of the GIL normally carry equal current, but either can carry the rated current.

Table 4:
Shinmeika - Tokai GIL ratings

Rated voltage	275 kV
Lightning Impulse Withstand Voltage	1050 kV
Switching Impulse Withstand Voltage	N/A
AC Withstand Voltage	460 kV
Frequency	60 Hz
Rated current	6300
Short time withstand current	50 kA for 2 second

9.1.2.2 Design

Sections of the line were supplied by three manufacturers. The basic structure and performance of the line was standardised. The design is summarised in Table 5.

Table 5:
Design of Shinmeika-Tokai GIL

Outside diameter of enclosure	480 mm
Connection Method of enclosure	Welded
Total circuit length	3.25 km
Transport length	14 m
Insulating gas	SF_6
Gas Pressure at 20°C	4.4 bar abs

Development testing included a long term accelerated field test, performed at the Yokosuka Research Laboratory of CRIEPI on a full size 140 m length. A voltage of 235 kV was applied for half a year and a current of 6300 A was applied in 50 cycles of 8 hours on and 16 hours off. The test demonstrated the durability of the GIL for 50 years actual use.

The GIL was assembled from approximately 1500 factory built units of length 14m. The conductor lengths were joined by plug-in contacts and the enclosure lengths were joined by on-site welding.

The GIL is anchored by fixed supports every 56 m; aluminium bellows in the enclosure and sliding contacts in the conductor allow for thermal expansion, installation tolerances and displacement due to seismic activity. Each 56 m length constitutes a gas zone.

The enclosures are solidly bonded at both ends of the line and earthed at every support structure.

9.1.2.3 Installation

The factory-built units were joined on site within a mobile clean room. The enclosures were welded by fully automatic welding machine. Dimensional measurement and pinhole inspection were performed on all welded joints.

A pressure test was performed at 0.57 MPa (1.25 times the maximum operating pressure) for 10 minutes.

9.1.2.4 Site tests

Site tests were performed including withstand voltage and partial discharge. Tests were performed on one phase at a time. The voltage was applied in levels up to 230 kV for 10 minutes. Partial discharge activity was monitored for at frequencies lower than 100 MHz using metallic foil electrode sensors and between 40 and 100 MHz using external antennas.

A load current test was performed in which a current of about 5100 A was applied in three cycles of 8 hours on and 16 hours off. The surface temperature of the enclosure was monitored using an optic fibre sensor with a resolution of $1^{O}C$, to detect possible temperature rise due to defective contact at the conductor joints. Expansion and contraction of the bellows was measured to confirm smooth movement.

9.1.3 PP9

In a project at the PP9 Power Plant in Saudi Arabia, 420 kV GIL is used for connections between transformers and a GIS substation [48]. The connections consist of eight three-phase circuits, totalling 17 km of single phase circuit. The project was completed in four stages, and was commissioned from May 1997 to March 2000

GIL was chosen as the only viable technical solution due to restrictions imposed by the route and the very corrosive environment (due to plant emissions and sand storms). In addition the GIL solution allows highly reliable transport of high powers with low losses.

The GIL was installed above ground at heights between 7 and 9 metres, to allow passage for transformer transportation. The ambient temperature varies between $-6^{O}C$ and $+55^{O}C$. The GIL is subject to winds of 120 km per hour with strong gusts of up to 150 km per hour.

Figure 15: Views of the 420 kV PP9 GIL: erection and layout.

9.1.3.1 Ratings

The GIL ratings are summarised in Table 6.

Table 6:
Ratings for PP9 GIL

Rated voltage	420 kV
Lightning Impulse Withstand Voltage	1425 kV
Switching Impulse Withstand Voltage	1050 kV
AC Withstand Voltage	630 kV
Frequency	60 Hz
Rated current	1200 A at +55°C
Short time withstand current	50 kA for 1 second

9.1.3.2 Design

Standard 420 kV GIS busbars, contacts, support insulators and adjustment and expansion bellows were used. The enclosures were of standard dimensions, but formed by extrusion as imposed by the specification. Pre-machined flanges were welded to the enclosures to allow bolted assembly at site. Unit lengths of enclosures were equipped to form shipping units. Shipping units were transported to site in 12.2 m containers.

The GIL design is summarised in Table 7.

Table 7:
Design of PP9 GIL

Outside diameter of enclosure	464 mm
Connection Method of enclosure	Bolted flanges
Total circuit length	5.6 km
Transport length	10.9 m
Insulating gas	SF_6
Gas Pressure at 20°C	6.5 bar abs

9.1.3.3 Installation

A clean workshop was created at site to prepare shipping units before assembly. In addition, a small shelter was used to provide a dust free zone in which to remove end covers and join shipping units to form a sub-assembly at ground level. A similar shelter was used when joining the sub-assembly to the previous GIL section in final position. The GIL was installed in supports with rollers to allow free expansion due to temperature. Bellows were used to absorb the expansion and positioning deviations.

9.1.3.4 Site tests

The GIL was energised using a conventional series resonant test set. The test was performed at 50 Hz, allowing lengths of more than 300 m to be tested at a time. The voltage was applied in levels up to 504 kV for 1 minute.

9.1.4 PALEXPO

A tunnel-installed GIL with two circuit lengths of 0.4 km has been installed in Geneva, where Energie Ouest Suisse has replaced a section of double circuit 245 kV overhead line to allow extension of the Palexpo exhibition centre. GIL was chosen since it offered similar operational characteristics to the overhead line and also due to the negligible electromagnetic field at ground level.

Installation began in September 2000. The GIL was assembled on site from 14 m transport lengths. The sections were welded at a foot of a shaft at one end of the tunnel in a temporarily installed assembly tent. From there the GIL was subsequently pulled into the tunnel. The elastic bending of the GIL allowed the curves of the tunnel to be followed without using elbow elements. Commissioning of the GIL took place in January 2001, followed by operational use early in 2001.

Figure 16: View of the 245 kV PALEXPO GIL.

9.1.4.1 Ratings

The GIL ratings are summarised in Table 8.

Table 8:
Ratings for PALEXPO GIL

Rated voltage	230 kV
Lightning Impulse Withstand Voltage	1050 kV
Switching Impulse Withstand Voltage	850 kV
AC Withstand Voltage	460 kV
Frequency	50 Hz
Rated current	2000 A
Short time withstand current	50 kA 3 s

9.1.4.2 Design

The GIL design is summarised in Table 9.

Table 9:
Design of PALEXPO GIL

Outside diameter of enclosure	512 mm
Connection Method of enclosure	Welded
Total circuit length	430 m x 2
Transport length	14 m
Insulating gas	20% SF_6 / 80% N_2
Gas Pressure at 20°C	7.0 bar abs

9.1.5 SAI NOI (Thailand)

From May to November 2001 a GIL for 550 kV, 4000 A rated current was installed near Bangkok, Thailand. It is part of the extension of an existing substation. During the installation, the existing substation remained in service. The GIL connects several bays of a GIS substation extension to outdoor busbars and overhead lines. GIL was chosen because of the high rating requirements and the lack of space within the substation. The total circuit length is approximately 1.2 km. The GIL was built of sections of up to 18 m length. Assembly was performed in a temporary tent on site.

Figure 17: View of the SAI NOI 550 kV GIL.

9.1.5.1 Ratings

The GIL ratings are summarised in Table 10.

Table 10:
Ratings of SAI NOI GIL

Rated voltage	550 kV
Lightning impulse Withstand Voltage	1550 kV
Switching Impulse Withstand Voltage	1175 kV
AC Withstand Voltage	740 kV
Frequency	50 Hz
Rated current	4000 A
Short time withstand current	63 kA 1 s

9.1.5.2 Design

The GIL design is summarised in Table 11.

Table 11:
Design of SAI NOI GIL

Outside diameter of enclosure	517 mm
Connection Method of enclosure	Welded
Total circuit length	1.2 km
Transport length	18 m
Insulating gas	60% SF_6 / 40% N_2
Gas Pressure at 20°C	7.0 bar abs

9.1.6 Hams Hall

A contract has been awarded by National Grid for 545 metres of GIL in the UK at Hams Hall substation in the Midlands. The GIL connects a conventional 400 kV substation to an overhead line. The configuration of the substation is such that access is very difficult due to other incoming lines and cables. The GIL of fully welded construction will be installed on supports above ground within the substation boundary. Outside the substation the GIL will be installed in separate trenches. Expansion of the GIL is accommodated by articulated bellows units which are situated at the mid-point. The GIL uses a gas mixture of 10% SF_6 and 90% N_2 as the insulating medium. Planned completion of installation is Summer 2003.

9.1.6.1 Ratings

The GIL ratings are summarised in Table 12.

Table 12:
Ratings of Hams Hall

Rated voltage	420 kV
Lightning impulse withstand voltage	1425 kV
AC withstand voltage	630 kV
Frequency	50 Hz
Switching impulse	1050 kV
Rated current	4000 A
Short time withstand current	63 kA for 1 second

9.1.6.2 Design of Hams Hall GIL

The GIL design is summarised in Table 13.

Table 13:
Design of Hams Hall

Outside diameter of enclosure	520 mm
Connection method of enclosure	Welded
Total circuit length	545 m
Transport length	11.5 m
Insulating gas	SF_6/N_2
Gas pressure at 20^{o}C	10.3 bar abs

9.2 Full-size Trials

9.2.1 420 kV GIL tests in Germany

At the IPH test laboratory in Berlin, tests have been performed on GIL designs for tunnel-installation and direct burial in co-operation with Bewag and other leading German utilities. The GIL uses an insulating gas mixture of 80% N_2 and 20% SF_6. Tests were performed to establish the reliability of all components, prove the on-site installation methods and provide experience. In the course of the tests, it was required to simulate the electrical and mechanical stresses that would occur over a 50 year life.

Short circuit withstand tests up to 63 kA, 3 s were performed on GIL prototypes containing all essential components. Internal arcing tests with 50 kA and 63 kA were performed on typical GIL arrangements.

9.2.1.1 Ratings

The GIL ratings are summarised in Table 14:

Table 14:
Ratings of 420 kV GIL tested in Germany

Rated voltage	420 kV
Lightning Impulse Withstand Voltage	1300 kV tunnel 1425 kV buried
Switching Impulse Withstand Voltage	1050 kV
AC Withstand Voltage	630 kV 1 min
Frequency	50 Hz
Rated current	3200 A tunnel 4000 A buried
Short time withstand current	63 kA for 3 second

The design for 420 kV GIL for tunnel is summarized in Table 15.

Table 15:
Design of 420 kV GIL for tunnel

Outside diameter of enclosure	520 mm
Connection Method of enclosure	Welded
Total circuit length	70 m
Transport length	11 m
Insulating gas	20% SF_6 / 80% N_2
Gas Pressure at 20°C	7.0 bar abs

The design for directly buried 420 kV GIL is summarized in Table 16.

Table 16:
Design for directly buried 420 kV GIL

Outside diameter of enclosure	600 mm
Connection Method of enclosure	Welded
Total circuit length	100 m
Transport length	14 m
Insulating gas	20% SF_6 / 80% N_2
Gas Pressure at 20°C	7.0 bar abs

9.2.1.2 Long term test on tunnel-installed GIL

Long term testing was performed in 1998 on a 70 m length including all major components of a typical GIL, which was installed in a section of tunnel of 3 m diameter. The GIL was assembled from 11 m long sections joined using a computer controlled, fully automated welding procedure. The test required the on-site welding method, the repair method, compensation of thermal expansion and UHF partial discharge monitoring to be demonstrated.

The test conditions are summarised in Table 17.

Table 17:
Test conditions for tunnel-installed GIL

Commissioning	AC withstand test, 1 min with PD monitoring	630 kV
	Lightning impulse test	1300 kV
	Switching impulse test	1050 kV
Load cycles	7 hours heating	3200 A
	5 hours cooling	480 kV cooling period only
Test duration		2500 hours
Intermediate tests every 480 h	Switching impulse test	1050 kV

All tests were successful.

9.2.1.3 Long term test on directly buried GIL

Long term testing was performed in 1999 on a 100 m length of directly buried GIL including a curved section, with the minimum permissible bending radius for the enclosures of 400 m, and an angle module. Realistic laying procedures were used and a repair under real conditions was required to be demonstrated. Conductor and enclosure temperatures and movement due to thermal expansion were recorded throughout the test.

The test conditions are summarised in Table 18.

Table 18:
Test conditions for directly buried GIL

Commissioning	AC withstand test, 10 s	550 kV
	AC withstand test, 1 min with PD monitoring	504 kV
	Lightning impulse test	1140 kV
Load cycles	8 hours heating	4000 A
	4/16 hours cooling (time parameters change every 480 h)	480 kV cooling period only
Test duration		2880 hours
Intermediate tests every 480 h	Lightning impulse test	1140 kV

All tests were successful.

9.2.2 EDF research programme

In 1993, EDF launched a comprehensive research programme with manufacturers to establish the feasibility of underground power transmission at 420 kV by GIL [54]. The programme addresses directly buried GIL with nitrogen based insulation. The aim is to have proven industrial technology available for use on the EDF system. The programme comprised two stages: a feasibility study and a long term test on a 300 m long directly buried GIL prototype.

9.2.2.1 Feasibility study and 420 kV GIL ratings

The feasibility study began in 1994 and was completed in 1997. Studies have been performed on dimensioning for insulation, thermal behaviour, mechanical constraints and corrosion protection. Laboratory tests have been performed on dielectric performance, short circuit performance, reliability studies, monitoring and fault location systems. All tests were successful. It was concluded that the required GIL technologies were accessible medium term.

The GIL ratings are summarised in Table 19.

Table 19:
Ratings of EDF GIL

Rated voltage	420 kV
Lightning impulse Withstand Voltage	1425 kV
Switching Impulse Withstand Voltage	1050 kV
AC Withstand Voltage	620 kV
Frequency	50 Hz
Rated current	3000 A
Short time withstand current	63 kA

9.2.2.2 Design

The GIL design is summarised in Table 20.

Table 20:
Design of EDF GIL

Outside diameter of enclosure	515 mm
Connection Method of enclosure	Welding
Total circuit length	300 m single phase
Transport length	15 m
Insulating gas	10% SF_6 / 90% N_2
Gas Pressure at 20°C	8.0 bars abs

9.2.2.3 Long term test on directly buried GIL

The second stage of the programme began in 1998. A 300 m long prototype of a 2000 MVA GIL was installed at Les Renardières for long duration testing [57]. The installation includes all components of a buried GIL. The test lasted for one year, simulating stresses equivalent to 50 years in service and including a simulated repair.

For this purpose, the prototype was subjected to heating cycles with simultaneously 420 kV phase to ground voltage application during 6000 hours. The objectives of the test were:

- Validation of procedures for laying and repairing underground GILs;
- Demonstration of the good long-term performance of the technology when stressed simultaneously by both the thermal and voltage stresses;
- First approach to the use of this type of link.

Table 21:
Test conditions for EDF directly buried 420 kV GIL

Commissioning	AC withstand test, 1 min with PD monitoring	570 kV
Load cycles	1/ for 22 hr/day over a period of 3 to 4 weeks, to raise the mean sheath temperature by at least 30 K	4000 A
	2/ for 10 to 15 days to bring the sheath temperature back to the level of the ambient temperature	0
	3/ resume of the cycle at step 1	
AC Voltage	Permanently applied	420 kV phase to ground
Test duration		6000 hours
Dielectric test after validation of procedures for repairing underground GILs	AC withstand test, 1 min with PD monitoring	570 kV

All the tests performed during the long term test were successful; but for economical reasons, the use of GIL's is not planned for the moment.

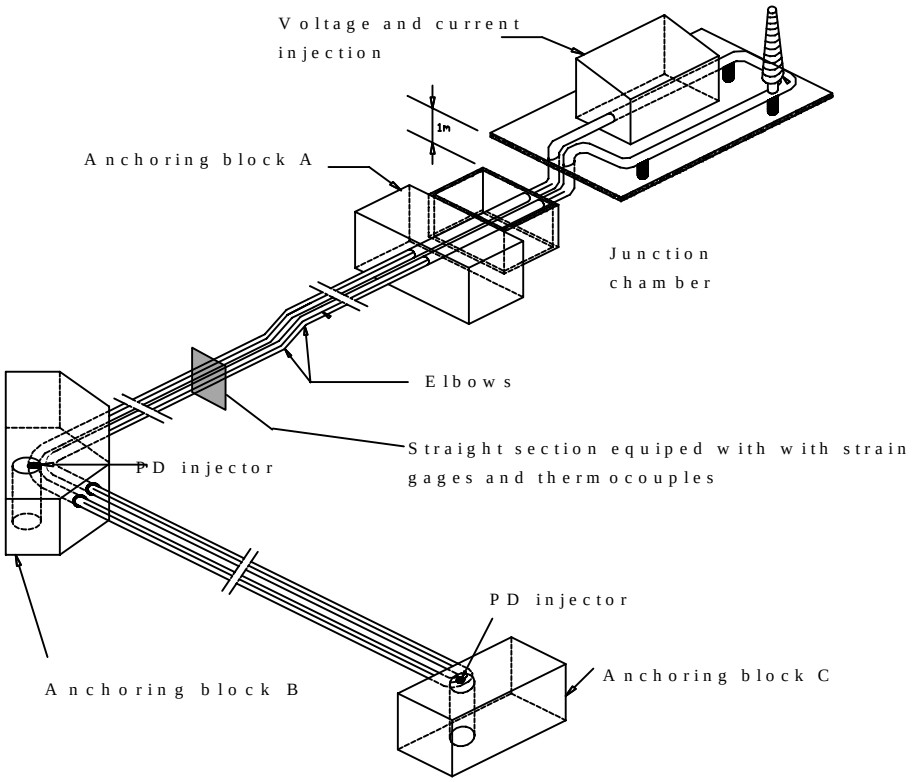

Figure 18: 300 m GIL prototype, 2000 MVA, constructed for the long duration tests. the concrete anchoring blocks were designed to remain immobile during the test in order to maximize the mechanical stresses in the enclosure elbows that concentrates the normal compression stresses of the enclosure. For a real GIL link, these anchorings are only used at the end of a link.

Figure 19: View of the elbows of the 300m GIL prototype and the thermally resistive backfill placed close to the GIL prototype before to bury it for the long term test.

10 Annex: GIL electrical parameters

For single phase type GIL with the enclosures solidly bonded at both ends, each phase has series inductance and shunt capacitance to earth. Coupling between phases is negligible.

The inductance *L* per unit length is:

$$L = \frac{\mu_0}{2\pi} \ln \frac{b}{a}$$

and the capacitance *C* per unit length is:

$$C = \frac{2\pi \varepsilon_0}{\ln \frac{b}{a}}$$

where *a* is the outer diameter of the conductor and *b* is the inner diameter of the enclosure.

Note that where special bonding is used, as is frequently the case for conventional cables, the inductance between phases will need to be considered as is also the case for overhead lines.

The resistance *R* per unit length depends not only on the conductor and enclosure dimensions and electrical resistivities, but also on the skin and proximity effects and the conductor and enclosure temperatures. A method for calculating the resistance is given in [13].

The shunt conductance *G* per unit length is not significant.

Assuming that *R* is less than the reactance of *L*, the surge impedance of the GIL is

$$Z_0 = \frac{1}{2\pi} \ln \frac{b}{a} \sqrt{\frac{\mu_0}{\varepsilon_0}}$$

11 References

[1] IEC 61640: 1998, Rigid high-voltage gas-insulated transmission lines for rated voltage of 72.5 kV and above

[2] IEC 60517: 1990, Gas-insulated metal-enclosed switchgear for rated voltages of 72.5 kV and above

[3] Nobuo, Amdo, Katsuya and Hayashida, 'New techniques for reduction of transmission loss in power cable', Hitchi Review Vol. 30, No 3, 1981

[4] Mukaiyama, Y, Ohshima, H, et al, 'Application of corrugated stainless steel sheath to high voltage XLPE cable', Fujikura Technical Review, 1994

[5] CIGRE Joint Working Group 21/22.01, technical brochure no 110, "Comparison of high voltage overhead lines and underground cables – report and guidelines", December 1996.

[6] R. Arrighi : "Operating characteristics of long links of AC high voltage of insulated cables" CIGRE session 1986, paper 21-13

[7] CIGRE Report - Calculation of the continuous rating of single core, rigid type, compressed gas insulated cables in still air with no solar radiation - Calcul de la capacité de transport en régime permanent des câbles unipolaires à isolant gaseux comprimé de type rigide posés en air calme et hors du rayonnement solaire, Electra No. 100, May 1985, pp 65 - 75.

[8] J. Jouaire: "Impacts techniques, environmentaux et économiques des technologies nouvelles", Réseaux électriques et environnement, Palais des Congrès, Versailles, 15 - 16 October 1996.

[9] ISO Standard 14040 'Environmental management – life cycle assessment – principles and framework', 1st edition 1997.

[10] CIGRE WG 23.02, Task Force 01, "Guide for SF6 gas mixtures (application and handling in electrical power equipment)", Cigre brochure 163, 2000.

[11] P. O'Connell and all (CIGRE WG23.02), "SF6 in the Electric Industry, Status 2000", Electra n°200, February 2002, pp16-25.

[12] CIGRE technical brochure 104 "Magnetic field in HV cable systems 1: Systems without ferromagnetic components".

[13] CIGRE Report – "Calculation of the continuous rating of single core, rigid type, compressed gas insulated cables in still air with no solar radiation - *Calcul de la capacité de transport en régime permanent des câbles unipolaires à isolant gaseux comprimé de type rigide posés en air calme et hors du rayonnement solaire"*, Electra No. 100, May 1985, pp 65 - 75.

[14] L.G. Christophorou and R.J. Van Brunt, "SF_6-N_2 mixtures Basic and HV insulation properties", IEEE Transactions on Dielectrics and Electrical Insulation, Vol. 2 No. 5, October 1995.

[15] L.G. Christophorou, Electron-molecule interactions and their applications, Volume 2, Academic Press inc., Orlando, 1984, ISBN 0-12-174402-7.

[16] A. Sabot, X. Waymel, D. Santos, D. Feldmann, Y. Maugain "Insulation co-ordination of 420 kV Gas Insulated Lines (GIL)" CIGRE General Session August 1998, paper 21/23/33-02

[17] A.R. Hileman, R.W. Flugum; T.F. Garrity: "Lightning insulation Coordination for a 600 kV DC Gas insulated cable", IEEE Transactions on Power Apparatus and Systems, Vol. PAS-101, No 11 November 1982

[18] A. Sabot: "Insulation co-ordination of Gas Insulated Lines (GIL) ",ISH 99, London 23-27August 1999, Invited lecture

[19] O. Völcker; H. Koch: "Insulation Co-ordination for Gas-Insulated Transmission Lines (GIL)" IEEE Transactions on power delivery, Vol. 16, No. 1, January 2001

[20] A. Schnettler, G Balzer; M. Hudasch M, B Johnnerfelt: "Protection of high voltage equipment by polymer housed surge arresters", CIGRE-Session 1998, paper 33-302

[21] B. Assmann : "Technische Mechanik", Band 2, Festigkeitslehre mit 97 Beispielen, 4 Auflage, R.Oldenbourg Verlag.

[22] ATV-A127, Richtlinie für die statische Berechnung von Abwasserkanälen undLeitungen, 3.Auflage 1997.

[23] G. Berger : Festigkeitslehre im Maschinenbau, Vogel Verlag.

[24] C. Peterson : "Grundlagen der Berechnung und baulichen Ausbildung von Stahlbauten", überarbeitete und erweiterte Auflage 1990

[25] R, Wendehorst : "Bautechnische Zahlentafeln", 1996 27 neub. Auflage.

[26] Chakir A., Koch H., zur FE-Berechnung der mechanischwen Beanspruchungen von erdverlegten, gasisolierten Übertragungsleitungen(GIL),17.CADFEM, internationale FEM technologietage , 6-8.Okt.1999

[27] DIN 18196 : "Erdbau; Bodenklassifikation für bautechnische Zwecke und Methoden zum Erkennen von Bodengruppen (06.70)"

[28] R. Nowack and H. Schneider : "Statische Berechnung von erdverlegten Entwässerungskanalen und –leitungen aus PVC-U (PVC hart), PE-HD(HDPE) und UP-GF (GFK)"

[29] DIN 1072, Straßen und Wegbrücken; Lastannahmen (11.67,E08,83)

[30] DIN 1072 Beiblatt ,, Straßen- und Wegbrücken; Lastannahme, Eräuterungen (11.67,E08.83)

[31] G. Connelly and G. Gaillard: « Three layer polyolefin pipe coatings»

[32] In : proceeding of the 7th International Conference on the Internal and External Protection of Pipes, paper C2 pp 41 to 46 – Sept. 21-23, 1987 – Cranfield UK, BHRA,. The Fluid Engineering Centre.

[33] G. Connelly, G. Gaillard, Y. Provou, G. Cavailie, C. Lamaire and R. Locatelli: « Three layer epoxy-polypropylene pipe coatings for use at elevated service temperatures »

[34] In : proceeding of the 8th International Conference on the Internal and External Protection of Pipes, pp 179 to 188 – 1990 – Cranfield UK, BHRA. The Fluid Engineering Centre.

[35] A.M. Schwab, M. Lambert and J. Voegel : "Corrosion protection of aluminium alloy sheaths of compressed gas-insulated cables" in E.D.F. Bulletin de la Direction des Etudes et Recherches, Série B, Réseaux électriques, Matériels électriques, n°3, 1980, pp 5 to 28.

[36] Cigre Working Group 21.12: "Compressed gas cables in use interntionally", Electra n°94, pp55, 1984.

[37] A. Cookson: "Gas-Insulated cables", IEEE Trans. on Electrical Insulation, Vol EI-20, n°5, October 1985, pp859-890.

[38] H. W. Graybill, J. A. Williams : "Underground power transmission with isolated-phase gas-insulated conductors", IEEE Transactions on Power Apparatus and Systems, Volume PAS-89, No 1, January 1970, pp 17-23

[39] G. W. Supplee, R. J. Kyle, R. V. Snow, P. C. Bolin : "Installation of a 230 kV compressed gas insulated bus", IEEE PES Summer Meeting, Vancouver, B.C., Canada, July 1973

[40] B. O. Pedersen, H. C. Doepken, P. C. Bolin : "Development of a compressed-gas-insulated transmission line", IEEE Winter Power Meeting, New York, N.Y., January 1971

[41] S. DeMaris : "500 kV CGI system is installed in the Cascades", Transmission and Distribution, April 1975, pp 50-54

[42] D. Feldmann, Y Maugain, M. Bourdet, M. Hopkins, P.M Lanquetin: "Development of a directly buried 400 kV Gas Insulated Line technology", CIGRE Session 2000, Report 21/23/33-02

[43] John Lewis WG 23.10 " Earthing of GIS – an application guide" , Electra N°151, pp 31 –51

[44] I. Murusawa, M. Ichihara, T. Kawai, A. Miyazaki, N. Takinami : "Development of long-distance 275 kV gas insulated transmission line (GIL)", The Eleventh International Conference on Gas Discharges and their Applications, Tokyo, 11 - 15 September, 1995.

[45] T. Nojima, M. Shimizu, A. Miyazaki, T. Araki, H. Nishima, H. Hata, H. Yamaguchi, T.Yamauchi, and M. Miyashita, :"Study on an after laying test for a long distance GIL", IEEE Transactions on Power Delivery, vol. 13, n°3, pp818-827 July 1998.

[46] T. Nojima, M. Shimizu, T. Araki, H. Hata, T. Yamauchi :"Installation of 275 kV - 3.3 km gas-isulated transmission line for underground large capacity transmission in Japan", CIGRE 1998 paper 21/23/33-01.

[47] A. Miyazaki, H. Hama, H. Nishima : "275 kV Shinmeika - Tokai GIL for long distance bulk-power transmission in a tunnel" IEEE PES Summer Meeting Panel Session on GIL, Berlin, 20-24 July 1997."

[48] J.M. Delcoustal: "A large GIL project: PP9", IEEE PES Summer Meeting Panel session on GIL, Berlin, 20 - 24 July 1997.

[49] Jess, H: IEEE PES Summer Meeting, Berlin, 20 - 24 July 1997.

[50] A. Schuette, H Koch : "Gas-insulated transmission lines (GIL). Type tests and prequalification", Jicable '99, pp 74-79

[51] C. G. Henningsen, G. Kaul, H. Koch, A. Schuette, R. Plath : "Electrical and mechanical long-time behaviour of gas-insulated lines", Paper 21/23/33-03, CIGRE Session 2000

[52] "Outline description of the gas-insulated line (GIL) application at the Palexpo Exhibition Centre, Geneva, Switzerland", Siemens press release, November 2000.

[53] J. Alter, M. Ammann, W. Boeck, W. Degen, A. Diessner, H. Koch, F. Renaud, S. Poehler: "N_2/SF_6 Gas-insulated Line of a new GIL generation in service", CIGRE session 2002, Report 21-204

[54] C. Aucourt, C. Boisseau, D. Feldmann : "Gas insulated cables: from the state of the art to feasibility for 400 kV transmission lines", Jicable 95, pp 133 - 138 (1995)

[55] C. Aucourt, C. Boisseau, D. Feldmann : “Les câbles à isolation gazeuse”, Epure, (France), October 1995, pp 13 - 24

[56] C. Menard : “Des pipelines électriques pour transporter la très haute tension”, L’Usine Nouvelle, October 1997, p 48.

[57] M. Bourdet, M. Hopkins, D. Feldmann, Y. Maugain, Y, “Long duration test of a directly buried GIL prototype”, Jicable ‘99, pp 86 - 91.

ANNEX A:

GIL Current Rating

Task Force 1 represented the following countries:

Abdellah Chakir,	Germany
Paul F Coventry,	UK,
Fabrizio Donazzi,	Italy
Dominique Feldmann,	France
Brian Gregory,	UK,*
Marcel Guillen,	France
Mel Hopkins,	USA +
T Okubo,	Japan
A Schuette,	Germany +
Markus Vestner,	Switzerland
Hiroaki Yamaguchi,	Japan

(+Corresponding)
(*Co-ordinator)

Table of Contents

1. Introduction

The objectives of the Task Force (TF) were to study and recommend methods for the calculation of the continuous and short time current ratings of gas insulated transmission line (GIL). The type of GIL installation differs from that previously studied in published CIGRE work in that the GIL is laid direct in the ground and employs a mixture of insulating gas. Much published work exists for a) SF_6 gas insulated busbar for in-air applications above ground and b) flexible cables for laid direct applications. However, the laid-direct application of GIL differs in the following respects:

- the GIL conductor is of larger diameter and is of annular geometry
- heat transfer through the primary insulation is by convection and radiation
- the insulation may comprise a mixture of gasses, such as N_2 and SF_6
- the gas is contained within a metallic enclosure of large diameter and low electrical resistance
- the high electrical conductivity of the metallic enclosure permits it to be earthed at its ends by the method of solid bonding and, although the circulating currents are of almost the same magnitude as those in the primary conductors, the heat generation is small.
- the diameter of the metallic enclosure and the horizontal spacing between the adjacent phases is large compared to the depth of burial, thereby influencing the calculation of heat dissipation through the surrounding ground.
- the conductor and metallic enclosure have larger cross sectional areas and higher thermal capacities, which are of benefit to short time overload ratings.

To determine the scope of work, the TF studied a) published rating methods for GIL and b) data on the experimental thermal performance of GIL. Sensitivity studies were then performed to identify those parameters having the greatest effect on continuous and short time ratings.

Annex A gives the recommended analytical formulae for continuous and short time rating followed by a brief guide to numerical modelling.

The results of the sensitivity studies on continuous and short time ratings are summarised. Annex A refers to the Appendices which give the source material for this work.

Recommendations for further work are given in Chapter 8.

2. Thermal Models for Continuous Rating

2.1 Description of GIL and trench layout

The GIL designs in this report are the single phase type in which the conductor is held concentric within a metallic, non-ferrous enclosure. The conductor is a solid cylindrical tube. The metallic enclosures are covered with a corrosion resistant polymeric oversheath. The enclosures are solidly bonded together and earthed at appropriate distances along the route. The advantages of solid bonding are a) that the induced voltages in the enclosures are limited to low values thus reducing the risk of corrosion and b) it is unnecessary to transpose either the metallic enclosures or the conductors. The disadvantage of solid bonding is that large circulating currents occur. This report includes calculations of the heating effects of circulating currents.

A typical trench cross section through a laid direct GIL circuit is shown in Figure 1. The depth of burial “L” depends upon the regulations in each particular country for the particular location in the route. For example, in farming land the depth has to be sufficient to avoid damage from agricultural ploughs. The centre line spacing “S” is determined by the clearances necessary to assemble each section of GIL in situ. Typical dimensions and material properties for the buried GIL are given in Appendix 1 and later in chapters 6 & 7 of this report. The values used in calculations were selected by averaging the dimensions and parameters employed by the TF members.

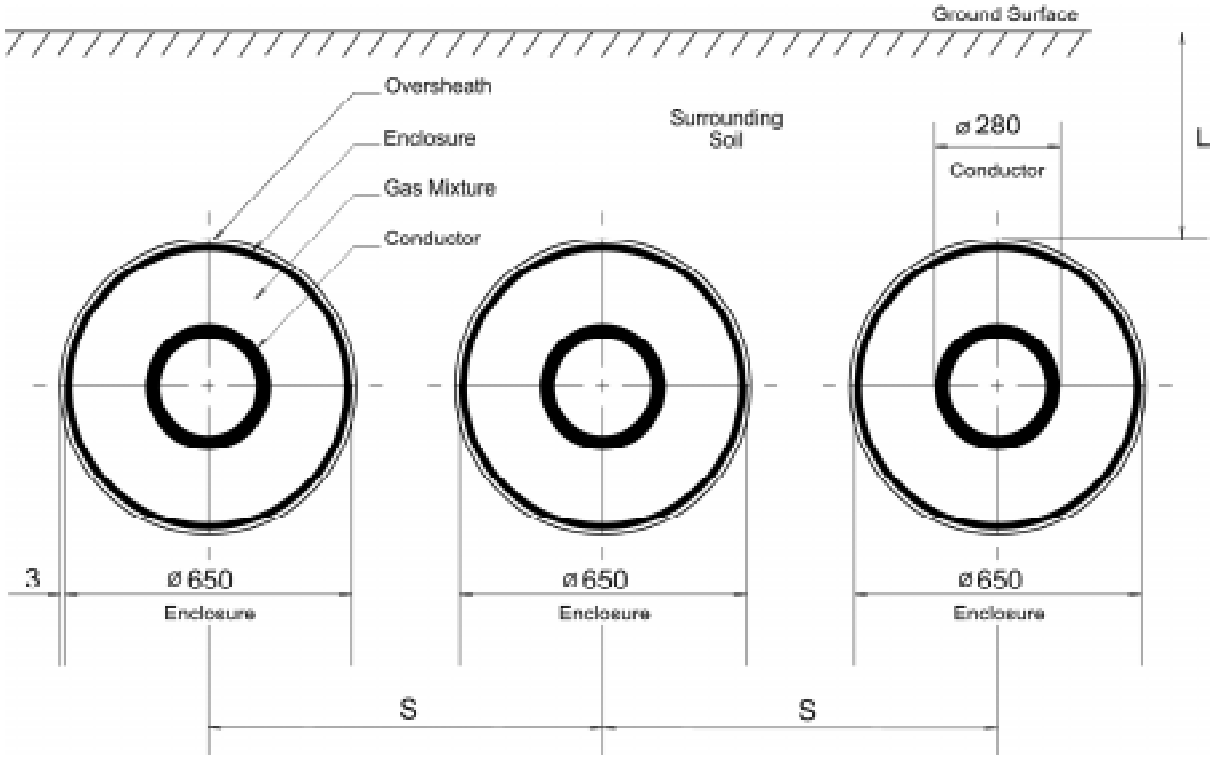

Figure 1 Cross Section of GIL Laid Direct in the Ground

2.2 Thermal circuit

The thermal circuit for one phase of a laid direct GIL is shown in (Figure 2). Heat is generated in the conductor by conduction losses. The heat is transferred from the conductor to the enclosure by radiation and convection through the insulating gas mixture. Heat is generated in the enclosure by circulating current conduction losses. The combined heat generation in the conductor and enclosure is transferred to the surroundings by conduction through the oversheath and soil and by convection in air at the ground surface. The soil is also heated by the two parallel GIL phases. Each phase has the same thermal circuit thus, as the thermal losses in each GIL are of similar magnitude, Figure 1-2 can be taken to represent all three phases. A mathematical adjustment of the components representing heat flow through the soil and to the surface air allows for the mutual heating from the parallel phases.

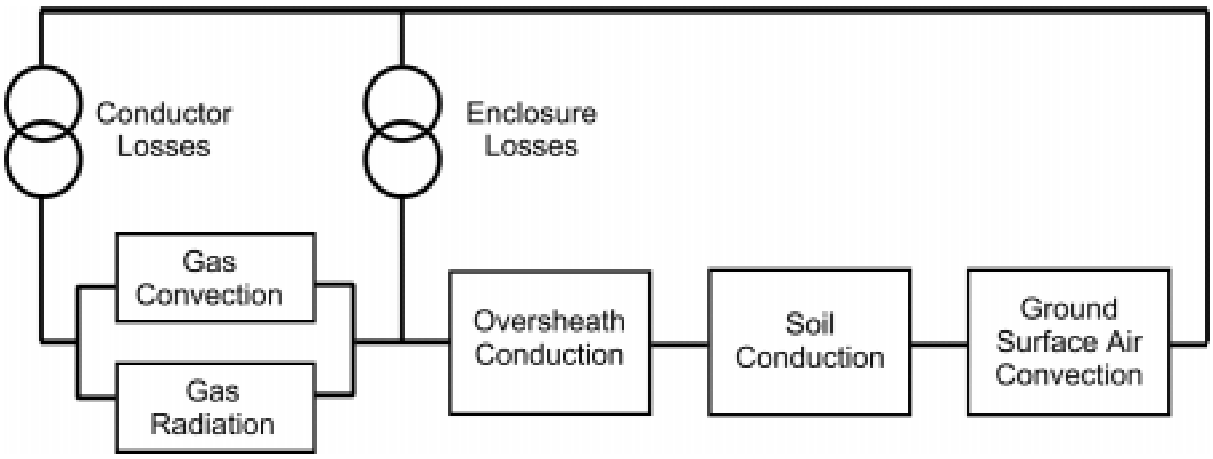

Figure 2 Thermal Circuit for One Phase of a Laid Direct GIL Circuit

The temperature rise of each component is determined by the heat flow through the network of thermal resistance and capacitance (short time rating only). The heat generated in the conductor and enclosure is temperature dependent. The thermal resistances associated with radiation and convection are highly temperature dependent. Thermal calculations are therefore normally performed in an iterative manner.

Rating calculations may be performed to determine either the magnitude of the current that can be sustained without exceeding the temperature limits of either the conductor or the soil adjacent to the oversheath. Alternatively the temperature of the conductor and soil can be calculated when the conductor carries a specified current.

The GIL cross section and thermal diagrams represent only part of a GIL installation. The GIL is assembled in comparatively short sections, at the ends of which sliding connectors are employed to join the conductors together. The conductor is supported on insulators at regular intervals and the enclosures may be divided into gas sections by barrier insulators. At some positions along the route, flanged connectors may be used to join enclosures together. At other positions the GIL may divert from the horizontal to inclined and vertical orientations. Concrete anchor blocks and foundations may be employed at selected positions along the route for thermo-mechanical and buoyancy reasons. At the ends of the route the GIL will normally be terminated into GIS switchgear or transformers. Each of the former items represent thermal discontinuities which may result in a locally higher or lower operating temperature. The thermal model taken in this study represents the majority of the route, i.e. the cross section containing the conductor and enclosure only, in which heat will only flow radially. This may be sufficient to determine the general rating of the circuit. At points of discontinuity the temperature is liable to differ and in consequence longitudinal heat flow in the conductor and enclosure will occur. At such positions it is advisable for the rating to be studied in greater detail and where necessary verified by experimental measurement.

Specifications for the continuous and short time maximum operating temperatures for GIL do not exists, although IEC 694 does give a maximum temperature for connectors in GIS. In selecting operating temperatures for buried GIL caution should be exercised as the depth of burial, spacing and soil thermal resistivity is likely to vary along the route. It is therefore prudent to include a factor of safety when selecting the maximum operating temperature.

A number of methods of calculating heat generation and thermal resistances applicable to GIL have been published. These are summarised below and compared in Appendix 2:

- Itaka et al[1] studied heat transfer characteristics using scale model GILs. Formulae were given for the heat transfer between conductor and enclosure by radiation, based on the Stefan-Boltzmann Law, and convection, based on the work of McAdams[2].
- Minaguchi et al[3] studied heat transfer characteristics in full sized GILs. The Stefan-Boltzmann formula for heat transfer by radiation was retained, but a new formula was proposed for the heat transfer by convection between conductor and enclosure. Measured and calculated values of temperature gave good agreement.
- A method for calculating the continuous rating of GIL in air was reported by CIGRE Working Group 21.12 in Electra 100[4]. Formulae were given for conductor and enclosure losses, taking into account skin and proximity effects, based on the work of Arnold[5]. A formula is given for heat transfer between conductor and enclosure by radiation, based on that given by Itaka[1]. A formula is given for heat transfer between conductor and enclosure by convection, based on the work of Vermeer[6]. A formula is given for the thermal resistance of the corrosion resistant over-sheath. The effects of solar radiation on GIL current ratings were reported by working group 21.12 in Electra 106[7].

- A report by Working Group 21.12 published in Electra 125[8] provides a method of calculating the continuous current ratings of three phase enclosed GIL, installed horizontally, both in still ambient air and laid direct. In the report, a formula is given for the thermal resistance of the surrounding soil. Since the diameter of the GIL is significant compared with the distance to the surface of the soil, the surface of the soil cannot be considered as an isothermal plane. The formula therefore includes a term to take into account the equivalent resistivity of the soil surface.
- Published information on field trials was given in the work of Minaguchi[3]. The members of the TF provided unpublished experimental results.
- IEC published a technical report IEC 61640[9] on the requirements for GIL in different applications, including an example of the method for the calculation of the current rating. This study supersedes giving the method of calculation in greater detail and provides recommendations for both continuous and short time current ratings.
- International Standard IEC 287-1-1[10] makes recommendations for calculation of the current rating of electric cables. Formulae are given for calculation of losses, taking into account skin and proximity effects based on the work of Arnold [5]. IEC 287-2-1[11] gives a formula for the thermal resistance of the corrosion resistant over-sheath which is the same as that given in Electra 100[4]. A formula is given which represents the external thermal resistance, i.e. the thermal resistance associated with conduction through the surrounding soil. This formula takes into consideration the mutual heating effect of adjacent phases and is given as an equivalent thermal resistance. The formula is given for the equivalent thermal resistance of the surrounding soil, based on the work of Kennelly [12].
- The Japanese Cable Makers' Association Standard 168-E makes recommendations for calculation of the current rating of electric cables. Formulae are given for calculation of losses, taking into account skin and proximity effects. A formula is given for the thermal resistance of the corrosion resistant over-sheath, which is essentially the same as that given in Electra 100[4] and IEC 287-2-1[11]. A formula is given for the equivalent thermal resistance of the surrounding soil, based on the work of Kennelly[12].

2.2.1 Review of Past Work

The review of past work identified that methodology needed to be developed for the following:

- The convective heat transfer through the gas mixture of SF_6 and N_2
- The use of finite element analysis and computational fluid dynamics software programs
- Conductors of large diameter (160mm or larger)
- Heat dissipation through the external thermal resistance taking into account the effect of heat transfer at the soil surface. This is needed as a result of the large diameter of the GIL when compared to the depth of burial.
- Heat transfer from large diameter GIL having a low heat flux, as affected by moisture migration and soil drying out.
- The short time rating of buried GIL.
- Operating temperature limits for the constituent materials of a GIL
- The rating of GIL inclined at an angle to the horizontal

2.2.2 Scope Selected for TF Work

The following key subjects were selected for study within the allocated time scale of the TF:

- Laid direct, horizontal single-phase GIL
- Comparison of methods for calculating ratings under continuous current loading;
  - Recommended formulae for rating calculations
  - Example calculation
  - Sensitivity study to assess the effect of parameters on the continuous rating
- Comparison of methods for calculating ratings under short time current loading;
  - Recommended formulae for rating calculations
  - Example calculation
  - Sensitivity study to assess the effect of parameters on the short time rating
- Recommended future work
- Bibliography

Insufficient published experimental information existed to justify the publication of new current rating formulae a) for heat dissipation from large conductors and b) for the phenomenon of soil drying out adjacent to large diameter enclosures.

After detailed study, the TF selected the use of a) proven and safe formulae for heat dissipation from smaller diameter bus bars published in Electra and b) the maximum permissible soil temperatures for smaller diameter flexible cables given in IEC 287.

2.3 References

[1] Itaka, K. Tomoo, A. Takushi, (Sept/Oct 1978) 'Heat transfer characteristics of gas spacer cables'. *IEEE Transactions on Power Apparatus and Systems*, Vol PAS-97, No. 5.

[2] McAdams, W H (1954), 'Heat transmission', *McGraw-Hill*, Chapter 7

[3] Minaguchi, D. Ginno, M. Itaka, K. Furukawa, H. Ninomiya, K. Hiyashi, T. (July 1985) 'Heat transfer characteristics of gas-insulated transmission lines' *IEEE/PES Summer Meeting, Vancouver, B.C., Canada,.*

[4] (May 1985) 'Calculation of the Continuous Rating of Single Core, Rigid type, Compressed Gas Insulated Cables in Still Air With No Solar Radiation.' *Electra No. 100* pp 65-75.

[5] Arnold, A. H. M. (1936) 'The alternating-current resistance of tubular conductors', *Jl. IEE*, vol 78, pp 580-593.

[6] Vermeer (March 1983) 'A simple formula for the Calculation of the Convective Heat Transfer between Conductor and Sheath in Compressed Gas Insulated Cables' *Electra No. 87* pp107-113.

[7] (May 1986) "Calculation of the continuous rating of single core, rigid type, compressed gas insulated cables in still air with solar radiation". *Electra No. 106* pp 23-31

[8](1989) 'Calculation of the continuous rating of three-core, rigid type, compressed gas insulated cables in still air and buried.' *Electra No 125* pp 104-111

[9]IEC 61640: 1998, 'Rigid high-voltage, gas-insulated transmission lines for rated voltage of 72,5 kV and above. *Lignes de transport rigides haute tension a isolation gaseuse de tension assignee egale ou superieure a 72,5 kV'*

[10] International Standard IEC 287-1-1 (1994) 'Electric cables – Calculation of the current rating – Part 1: Current rating equations and calculation of losses' First Edition.

[11] International Standard IEC 287-2-1 (1994) 'Electric cables – Calculation of the current rating – Part 2: Thermal resistance'.

[12] Kennelly, A. E. (1893) 'On the carrying capacity of electric cables submerged, buried or suspended in air' Minutes of IX annual meeting of the Association of Edison Illuminating Companies, p 79.

3. Recommended Formulae for Continuous Current Rating

The following formulae are recommended for the calculation of the continuous current rating of laid direct horizontal GIL.

An example calculation using the recommended formulae is given in Appendix 5.

The formulae have been selected from previous Electra[1] and IEC[2] publications and by documents. The formulae were utilised for the calculations carried out in the sensitivity study.

3.1 Permissible Current Rating

The permissible current rating is calculated from the equation [1,2,3]:

Eq. 1 $$I = \sqrt{\frac{\Delta\vartheta}{R_c \cdot \left[T_1 + (1+\lambda_1)\cdot(T_3 + T_4)\right]}}$$

Eq. 2 $$I = \sqrt{\frac{\Delta\vartheta}{R_c \cdot \left[T_1 + (1+\lambda_1)\cdot(T_3 + T_4)\right]}}$$

where:

- I : [A] rms current in one conductor
- R_c : [Ω/m] conductor ac resistance at maximum operating temperature
- T_1 : [K.m/W] effective thermal resistance of the insulating gas
- T_3 : [K.m/W] thermal resistance of the oversheath
- T_4 : [K.m/W] thermal resistance of the surrounding soil, allowing for mutual heating and heat transfer at the soil surface
- $\Delta\vartheta$: [K] permissible temperature rise of the conductor above ambient
- λ_1 : loss factor due to the enclosure conduction losses.

3.2 Calculation of Losses

The ac resistance per unit length of the conductor and of the enclosure are given by:

Eq. 3 Conductor : $R_c = R'_{oc} \cdot (1 + y_c)$ with $R'_{oc} = R_{oc} \cdot \left[1 + \alpha_c \cdot (\vartheta_c - 20)\right]$

Eq. 4 Enclosure : $R_e = R'_{oe} \cdot (1 + y_e)$ with $R'_{oe} = R_{oe} \cdot \left[1 + \alpha_e \cdot (\vartheta_e - 20)\right]$

where:

R_c : [Ω/m] conductor a.c. resistance at maximum operating temperature
R_{oc} : [Ω/m] conductor d.c. resistance at 20°C temperature
R'_{oc} : [Ω/m] conductor d.c. resistance at maximum operating temperature
α_c : [K^{-1}] temperature coefficient of conductor electrical resistivity at 20°C.
ϑ_c : [°C] conductor maximum operating temperature
y_c : conductor skin and proximity effect coefficient.
R_e : [Ω/m] enclosure a.c. resistance at its maximum operating temperature
R_{oe} : [Ω/m] enclosure d.c. resistance at 20°C temperature
R'_{oe} : [Ω/m] enclosure d.c. resistance at operating temperature
α_e : [K^{-1}] temperature coefficient of enclosure electrical resistivity at 20°C.
ϑ_e : [°C] enclosure maximum operating temperature
y_e : enclosure skin and proximity effect coefficient.

3.2.1 Calculation of the skin and proximity effect for conductor and enclosure

The skin and proximity effect for the conductor and enclosure can be calculated with the same expressions by changing the index j to j=c for the conductor and j=e for the enclosure, given by:

Eq. 5 $$\beta_j = \frac{2 \cdot t_j}{d_j} \qquad j = c, e$$

Eq. 6 $$z_j = \frac{\mu_o \omega}{2\pi} \cdot \frac{\beta_j}{\left(1 - \frac{\beta_j}{2}\right)} \cdot \frac{1}{R'_{oj}} = \frac{4\pi \cdot f \cdot \beta_j}{\left(1 - \frac{\beta_j}{2}\right) \cdot R'_{oj}} \cdot 10^{-7} \qquad j = c, e$$

where the symbols represent:

t_c, t_e :[m] the conductor and enclosure radial wall thickness,

d_c, d_e :[m] the conductor and enclosure external diameters

f :[Hz] frequency of mains supply

$\mu_0 = 4\pi.10^{-7}$: [H/m] magnetic permeability of free space

$\omega = 2\pi.f$: [s^{-1}] angular frequency of mains supply

for:

Eq. 7 $$z_j < 5 \qquad a(z_j) = \frac{7 \cdot z_j^2}{315 + 3 \cdot z_j^2} \qquad b(z_j) = \frac{56}{211 + z_j^2} \qquad j = c, e$$

Eq. 8 $$z_j > 30 \qquad a(z_j) = \sqrt{\frac{z_j}{2}} - 1 \qquad b(z_j) = \frac{2}{4\sqrt{z_j} - 5} \qquad j = c, e$$

Eq. 9 $$5 \le z_j \le 30 \qquad a(z_j) = \sum_{i=0}^{8} a_i \cdot z_j^i \qquad b(z_j) = \sum_{i=0}^{8} b_i \cdot z_j^i \qquad j = c, e$$

where the coefficients of the polynomial interpolation for Eq. 9 are shown in Table 1

Table 1 Coefficients of the polynomial interpolation

a_i coefficients	**b_i coefficients**
$a_0 = 1.97010\ 10^{-1}$	$b_0 = 2.53560\ 10^{-1}$
$a_1 = -1.56295\ 10^{-1}$	$b_1 = -2.1030734\ 10^{-1}$
$a_2 = 7.37960\ 10^{-2}$	$b_2 = 6.4955630\ 10^{-2}$
$a_3 = -9.02854\ 10^{-3}$	$b_3 = -1.0893730\ 10^{-2}$
$a_4 = 6.27032\ 10^{-4}$	$b_4 = 1.0372874\ 10^{-3}$
$a_5 = -2.69028\ 10^{-5}$	$b_5 = -5.8238557\ 10^{-5}$
$a_6 = 7.06740\ 10^{-7}$	$b_6 = 1.9109965\ 10^{-6}$
$a_7 = -1.04301\ 10^{-8}$	$b_7 = -3.3893677\ 10^{-8}$
$a_8 = 6.62315\ 10^{-11}$	$b_8 = 2.5096220\ 10^{-10}$

Finally the skin and proximity effect for the conductor and enclosure are:

Eq. 10
$$y_c = a(z_c) \cdot \left[1 - \frac{\beta_c}{2} - \beta_c^2 \cdot b(z_c)\right]$$
$$y_e = b(z_e) \cdot \left[1 + \frac{\beta_e}{2}\right]$$

3.2.2 Calculation of the loss factor λ due to induced currents circulating in the enclosure

Heat is generated in the enclosure by circulating currents and by eddy currents. The enclosures are electrically bonded together at discrete lengths along the route this permits current to circulate between the parallel enclosures. The heat generation due to localised eddy currents in the wall of the enclosure can be disregarded because of the low electrical resistance of the aluminium alloy enclosure. The circulating current losses are given as a fraction of the conductor losses. The fraction coefficient is named the loss factor λ.

The calculation of λ first needs the calculation of the reactance X of the enclosure and also the mutual reactance X_m between the enclosure of an external GIL in the flat formation and the conductors of the other two:

Eq. 11 $$X = \omega \cdot \mu_o \cdot \ln\left(\frac{2 \cdot s}{d_e - t_e}\right) = 4 \cdot \pi \cdot f \cdot 10^{-7} \cdot \ln\left(\frac{2 \cdot s}{d_e - t_e}\right)$$

Eq. 12 $$X_m = \omega \cdot \mu_o \cdot \ln(2) = 4 \cdot \pi \cdot f \cdot 10^{-7} \cdot \ln(2)$$

Eq. 13 $$P = X + X_m$$
$$Q = X - \frac{X_m}{3}$$

where s : [m] is the centre line distance between two adjacent GILs.

Eq. 14 $$\xi_1 = \frac{\frac{3}{4}P^2}{R_e^2 + P^2}$$
$$\xi_2 = \frac{\frac{1}{4}Q^2}{R_e^2 + Q^2}$$
$$\xi_3 = \frac{2 \cdot R_e \cdot P \cdot Q \cdot X_m}{\sqrt{3} \cdot \left(R_e^2 + P^2\right)\left(R_e^2 + Q^2\right)}$$

The circulating currents in the three enclosures are of different values, these are given by the following loss factors:

λ_{11} Lagging phase GIL:

Eq. 15 $$\lambda_{11} = \frac{R_e}{R_c} \cdot \left(\xi_1 + \xi_2 + \xi_3\right)$$

λ_{1m} Middle GIL:

Eq. 16 $$\lambda_{1m} = \frac{R_e}{R_c} \cdot \frac{4}{3}\xi_1$$

λ_{12} Leading phase GIL:

Eq. 17 $$\lambda_{12} = \frac{R_e}{R_c} \cdot \left(\xi_1 + \xi_2 - \xi_3\right)$$

3.3 Thermal Resistance Calculations

The formulae for the thermal resistances refer to a) the gas insulation within the GIL between the conductor and the enclosure, b) the GIL oversheath and c) the surrounding soil and surface air.

3.3.1 Thermal resistance between conductor and enclosure

This is the equivalent thermal resistance representing heat transfer due to convection and radiation.

The thermal resistance depends on both the conductor and the enclosure temperatures, which are not known before the calculation. A tentative value of the enclosure temperature must be assumed and an iterative calculation undertaken to achieve the convergence of the gas thermal resistance and of the enclosure temperature.

The thermal resistance of the gas insulation is the resultant of the equivalent convection resistance and the equivalent radiation resistance connected in parallel:

Radiation heat transfer:

Eq. 18 $$W_r = 5.69\pi d_c \left[\left(\frac{\vartheta_c + 273}{100}\right)^4 - \left(\frac{\vartheta_e + 273}{100}\right)^4\right] \frac{1}{\varepsilon_c + \frac{d_c}{d_w}\left(\frac{1}{\varepsilon_e} - 1\right)}$$

Convection heat transfer formula recommended by the task force is published in Electra 100[1] based on the work of Vermeer[2]:

Eq. 19 $$W_c = K_0 \left[p \cdot \Delta\vartheta^2\right]^{\frac{2}{3}} \cdot \frac{d_c \cdot \left[1 - \frac{d_c}{d_w}\right]^{2.167}}{\ln\left(\frac{d_w}{d_c}\right)}$$

where the symbols represent:

W_r, W_c : [W/m] heat transfer by radiation and convection

ϑ_c, ϑ_e : [°C] the conductor and enclosure temperatures

ε_c, ε_e : the conductor and enclosure surface emissivities

$\Delta\vartheta$: [K] temperature rise of the conductor above that of the enclosure

p : [bar] gas absolute pressure

K_0 : convection coefficient

d_w : [m] inner diameter of the enclosure

d_c : [m] outer diameter of the conductor

The convection coefficients are taken as follows:

SF_6 gas K_0=11.3

N_2 gas K_0= 5.83

For a mixture of SF_6 and N_2 gas with different volume percentages (Appendix 4):

Eq. 20 $$K_0 = (V_{SF_6})^{0.75} \cdot K_{0(SF_6)} + (1 - V_{SF_6})^{0.75} \cdot K_{0(N_2)}$$

where:

V_{SF_6} : is the per unit volume of SF_6 gas

$V_{N_2} = (1 - V_{SF_6})$: is the per unit volume N_2

$K_{0(SF_6)}, K_{0(N_2)}$: the convection coefficients for SF_6 and N_2.

The equivalent thermal resistances for radiation R_r and convection R_c, are calculated from Eq. 18and Eq. 19, as follows:

Eq. 21 $$R_r = \frac{\vartheta_c - \vartheta_e}{W_r}$$

$$R_c = \frac{\vartheta_c - \vartheta_e}{W_c}$$

and the resultant equivalent resistance T_1, from their parallel configuration, is:

Eq. 22 $$T_1 = \frac{1}{\frac{1}{R_r} + \frac{1}{R_c}} = \frac{\vartheta_c - \vartheta_e}{W_r + W_c}$$

3.3.2 Thermal resistance T_3 of the anti-corrosion oversheath

Eq. 23 $$T_3 = \frac{\rho_3}{2\pi} . \ln(1 - \beta_3)^{-1}$$

where:

T_3 : [K.m/W].thermal resistance of the oversheath

ρ_3 : [K.m/W] represents the thermal resistivity of the oversheath material,

$\beta_3 = \frac{2t_3}{d_3}$, Being t_3 and d_3 the thickness and the outer diameter of the oversheath [m].

3.3.3 Thermal resistance T_4 of the surrounding soil

The following calculations of T_4 are based on a uniform soil thermal resistivity. It is known that the phenomenon of moisture migration and soil drying will significantly increase the thermal resistivity of the adjacent soil. For conventional cables IEC286 records temperature limits for the soil at the interface with the oversheath to prevent soil drying-out. In the absence of information for the larger diameter GIL enclosures, it is recommended that these IEC 287 temperature limits be adopted.

The calculation of T_4 uses the full Kenelly formula which makes allowance for the ground surface above the GIL circuit being a non-isothermal plane (Appendix 3). This is necessary because the ratio of the depth of burial to the diameter of the GIL oversheath is significantly less than 10:1, thus the mathematical simplification of T_4 for smaller diameter conventional cables is not applicable to GIL.

Kenelly allows for the ground surface being non-isothermal by equating surface convection to a fictitious soil over-thickness δ[m] as given by:

Eq. 24 $$\delta = \frac{\beta_T}{\rho_T}$$

where:

$\beta_T = 0.20$ [Km^2/W]is the equivalent thermal resistivity of the soil per unit surface, representing convection[2].

ρ_T [Km/W] is the soil thermal resistivity.

The equivalent thermal resistance T_4 of the hottest of the three cables in flat formation, is given by:

Eq. 25 $$T_4 = \frac{\rho_T}{2\pi} \cdot \left[\ln\left(u + \sqrt{u^2 - 1}\right) + \frac{1 + 0.5 \cdot (\lambda_{11} + \lambda_{12})}{1 + \lambda_{1m}} \cdot \ln\left(1 + v^2\right) \right]$$

A typical configuration of the buried GIL is shown in Figure 1.

where:

Eq. 26 $$u = \frac{2(L + \delta)}{d_s}$$

$$v = \frac{2(L + \delta)}{s}$$

L = depth of burial

d_s = diameter over the oversheath

s = spacing between GIL

Eq. 25 for T_4 takes into account that since the three single core GIL cables are laid in flat formation with the sheaths bonded together this affects the equivalent thermal resistance of the hottest cable[3].

The formula is based on the centre cable being the hottest one, so that the value of loss factor to be used in Eq. 2 is that of the centre cable, that is:

Eq. 27 $$\lambda_1 = \lambda_{1m}$$

Where λ_{1m} is given in Eq. 16.

3.4 References

[1] (May 1995) 'Calculation of the continuous rating of single core, rigid type, compressed gas insulated cables in still air with no solar radiation' *Electra N°100*.

[2] (1989) 'Calculation of the continuous rating of three core, rigid type, compressed gas insulated cables in still air and buried' *Electra N°125*.

[3] IEC 287 (1994) 'Calculation of the continuous rating of cables (100% load factor)' First Edition.

4. Recommended Formulae For Short Time Current Rating

The calculation method takes into account the dependence of the gas thermal resistance on the conductor and enclosure temperatures and employs a finite difference method based on that given in Electra 87[1]. The dependence of the thermal resistance of the gas mixture on the conductor and enclosure temperatures has also been introduced. The thermal circuit for the short time rating is shown in Figure 3.

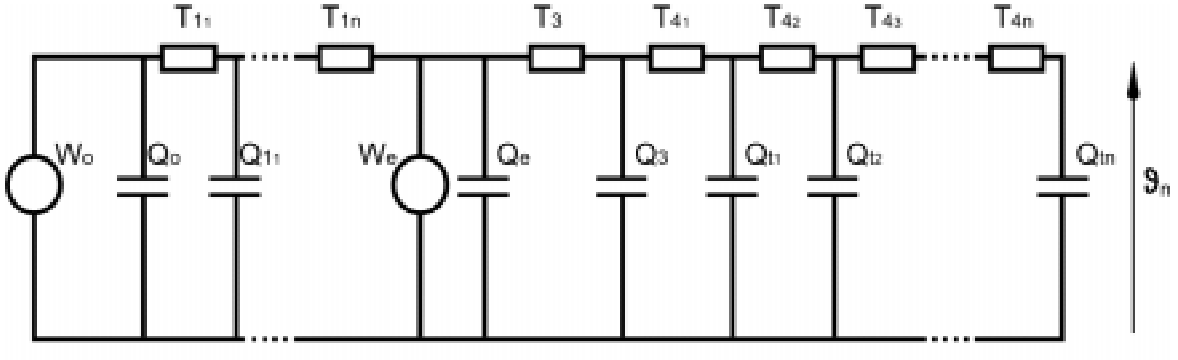

Figure 3: Thermal Circuit for Short Time Rating

4.1 Symbols

$A_{j,i}$ coefficient used in Chapter 4.3.5
Bj,i coefficient used in Chapter 4.3.5
D_0 [m] conductor inner diameter
D_c [m] conductor outer diameter
D_g [m] enclosure inner diameter
D_e [m] outer diameter of enclosure
D_s [m] outer diameter of the oversheath
D_t [m] boundary diameter in the soil at which a minimal temperature rise is set.
E_i exponential integral function
Q_j [J/K.m] thermal capacitance of an elementary layer between (j-1)'and j'.
Q_0 [J/K.m] thermal capacitance of the conductor
Q_{1j} [J/K.m] thermal capacitance of the j elementary layer of the gas insulation
Q_e [J/K.m] thermal capacitance of the enclosure
Q_s [J/K.m] thermal capacitance of the anticorrosion sheath
Q_{4j} [J/K.m] thermal capacitance of the j elementary layer of the soil
T_1 (ϑ_g) [K.m/W] thermal resistance of the gas insulation, as a function of the temperature rise of the gas
T_j [K.m/W] thermal resistance of an elementary layer between (j-1) and j.
W_i [W/m] step change of total heat dissipation per unit length of GIL at max operating temperature
W_o [W/m] heat generated by the conductor losses
W_e [W/m] heat generated by enclosure losses
i suffix of time,
j suffix of space,
n number of elementary layers in the gas insulation,
n_s number of elementary layers in the soil,
p [bar] absolute gas pressure
r [m] radius from GIL axis
r_j [m] external radius of an elementary layer
r_{j-1} [m] internal radius of an elementary layer
r_c [m] conductor outer radius
r_e [m] outer radius of GIL enclosure
r_g .[m] radius over the gas insulation – inner radius of the GIL enclosure
r_0 [m] inner radius of conductor

r_s [m] outer radius of the GIL oversheath

δ [m^2/s] soil thermal diffusivity

ρ_0 [Km/W] thermal resistivity of the conductor material

ρ_e [Km/W] thermal resistivity of the enclosure material

ρ_3 [Km/W] thermal resistivity of the oversheath material

ρ_t [Km/W] thermal resistivity of the soil

σ_0 [J/K.m^3] volumetric specific heat of the conductor material

σ_e [J/K.m^3] volumetric specific heat of the enclosure material

σ_s [J/K.m^3] volumetric specific heat of the oversheath material

σ_{SF6} [J/K.m^3] volumetric specific heat of SF_6

σ_{N2} [J/K.m^3] volumetric specific heat of N_2

ϑ_m [°C] average temperature of the gas layer j

ϑ_j [°C] temperature of the elementary layer j

ϑ_r [K] limit temperature rise at maximum soil radius

$\Delta\vartheta_{j,i}$ [K] temperature rise of node j at elapsed time i

t [s] time elapsed from beginning of transient

$\Delta\tau$ [s] time step duration

$\Delta\tau_i$ [s] time step duration at time i

4.2 General

Methods for calculating the transient temperature response of a GIL have not previously been published by CIGRE.

The application of the IEC 853-2[2] method for the calculation of GIL transient response is not appropriate for several reasons, a) the gas thermal resistance is temperature dependent b) the large diameter of the GIL has a negative influence on the precision of the soil thermal transient resistance calculation and c) the method is not appropriate for the calculation of the enclosure temperature.

A new method of calculation has been developed, taking into account the dependence of the gas thermal resistance on the conductor and enclosure temperatures and calculating more correctly the soil transient thermal resistance. The method is based on an adaptation of that given in Electra 87[1].

As in the Electra 87 method, the basic partial differential equations for transient heat transmission through the GIL and the soil are solved by finite difference methods for both the time and space domains. In terms of lumped constants this method describes the GIL and its surroundings by a network of thermal resistances in series and capacitances in parallel (Figure 3).

Heat flow is assumed to be radial both inside and outside the GIL so that it is possible to divide both the GIL and the soil into a number of concentric layers corresponding to lumped thermal elements within the network.

The radius of the soil into which heat disperses will increase with time. For practical purposes it is sufficient to consider only that particular radius within which a sensibly small temperature rise occurs. Beyond this radius there is no significant heat diffusion and the boundary of the cylinder formed by the radius can be considered to be at constant temperature. A method is given for determining the radius of the boundary cylinder as a function of transient duration and heat loss.

Unlike the Electra 87 method, the thermal properties of the gas insulation are temperature dependent and thus vary with time. Formulae for the radial thermal resistances of the metallic conductor and enclosure are given, but can be disregarded as being small.

4.3 Description of Method

4.3.1 Amount of soil to be considered for buried GIL

The soil thermal resistance in the transient calculation is taken to be a cylindrical layer, subdivided in a certain number of lumped thermal resistances in such a way that the temperature increase at the external surface of the cylindrical layer reaches a small preset value at the end of the duration. The temperature increase is taken at 0.1°C. This particular cylinder then becomes the boundary layer for the termination of that part of the calculation. This radius can be estimated from the exponential integral formula, which takes the GIL as a line source of heat.

Eq. 28 $$\Delta\vartheta_{r,\tau} = \frac{W_l}{4\pi}\rho_t \cdot \left[E_i\left(\frac{-r^2}{4\delta\tau}\right)\right]$$

4.3.2 Selection of the number of divisions within the insulation and soil

The thermal resistance of the conductor T_0 and the enclosure T_1 can each be represented in a single subdivision.

The gas insulation should be divided into at least two elementary layers.

The GIL oversheath is represented by one elementary layer.

The number, n_s of elementary layers in the soil should fulfill the following condition

$$\frac{D_t - D_s}{2 \cdot n_s D_s} < 0.16$$

where:

D_t =2r is the diameter of the soil within which the temperature rise at the end of the transient is approximately 0.1K. See the exponential integral formula Eq. 28.

D_s diameter of the oversheath.

4.3.3 Division of the GIL and soil into elements and allocation of losses

The thermal resistances of the conductor T_0 and enclosure T_1, if not disregarded as small, are given by:

Eq. 29 $$T_0 = \frac{\rho_0}{2\pi}\ln\left(\frac{r_c}{r_0}\right)$$

Eq. 30 $$T_e = \frac{\rho_3}{2\pi}\ln\left(\frac{r_e}{r_g}\right)$$

The equivalent thermal resistance of the gas is discussed in Appendix 4. Each elementary layer has a thermal resistance of the form:

Eq. 31 $$T_{1j} = \frac{\rho_g}{2\pi}\ln\left(\frac{r_j}{r_{j-1}}\right)$$

where:

Eq. 32 $$\rho_g = \frac{2 \cdot \pi \cdot T_g\left(\Delta\vartheta_g\right)}{\ln\left(\frac{r_e}{r_c}\right)}$$

is the thermal resistivity representation of heat transfer. The thermal resistance of the gas layer, $T_g\left(\Delta\vartheta_g\right)$ [Km/W] depends on the temperature difference of the gas layer and must be calculated by recursion at each step of the transient time.

The thermal resistance of the elementary layer of soil is given by:

Eq. 33 $$T_j = \frac{\rho_t}{2\pi}\ln\left(\frac{r_j}{r_{j-1}}\right)$$

The thermal capacitance of each layer is divided at the mid-layer radius and allocated to the nodes at the inner and outer radii of the layer to give a π network for the equivalent circuit of each layer.

The thermal capacitance of the elementary gas layer is given by:

Eq. 34 $$Q_{1j} = \pi \cdot \sigma_g \cdot \left[\left(\frac{r_j + r_{j+1}}{2}\right)^2 - \left(\frac{r_{j-1} + r_j}{2}\right)^2\right] \quad j = 1,\ldots n$$

Where [3]

Eq. 35 $$\sigma_g = \left[\frac{337.4}{273+\vartheta_m} V_{N_2} \cdot \frac{1037+0.101\cdot\vartheta_m}{1.4} + \frac{1666}{230+\vartheta_m} V_{SF_6} \cdot \frac{630+1.87\vartheta_m - 4.33\cdot 10^{-3}\cdot\vartheta_m^2}{1.33} \right] \cdot p$$

Where V_{N_2} and V_{SF_6} are the per unit fractions of nitrogen and SF_6 in the gas mixture.

Since the volumetric specific heat depends on the temperature of the gas layer it must be calculated by recursion at each step of the transient time.

4.3.4 The thermal capacitances of the conductor and enclosure are represented by:

Eq. 36 $$Q_c = \pi \cdot \sigma_0 \cdot \left[r_c^2 - r_0^{\,2} \right] + \pi \cdot \sigma_g \cdot \left[\left(\frac{r_c + r_1}{2} \right)^2 - r_c^2 \right]$$

Eq. 37 $$Q_e = \pi \cdot \sigma_e \cdot \left[r_e^2 - r_g^2 \right] + \pi \cdot \sigma_g \cdot \left[r_n^2 - \left(\frac{r_e + r_{n-1}}{2} \right)^2 \right] + \pi \cdot \sigma_s \cdot \left[\left(\frac{r_s + r_e}{2} \right)^2 - r_e^2 \right]$$

while the thermal capacitance of the anticorrosion oversheath is:

Eq. 38 $$Q_3 = \pi \cdot \sigma_s \cdot \left[r_s^2 - \left(\frac{r_s + r_e}{2} \right)^2 \right] + Q_{41}$$

where Q_{41} is the thermal capacitance of the first half layer of soil.

The thermal capacitance of the elementary soil layer is given by:

Eq. 39 $$Q_{4j} = \pi \cdot \sigma_t \cdot \left[\left(\frac{r_j + r_{j+1}}{2} \right)^2 - \left(\frac{r_{j-1} + r_j}{2} \right)^2 \right] \quad j = n+1, \ldots n_s$$

The gas insulation has zero dielectric losses.

4.3.5 Computation of temperature transient for a single GIL

The transient temperature rise of a single GIL can be computed from the system of equations corresponding to its equivalent thermal network as described in Figure 3.

This thermal network corresponds to the case of a GIL where the duration of the transient is sufficiently short that no adjacent GILs or heat transfer to the ground surface is involved. For transients of longer duration reference should be made to Chapter 5.

The steps required to compute the transient from the thermal network are as follows:

1) Compute for each node

$$A_{j,i} = \left[\left(1 - A_{j-1,i}\right) \left(\frac{T_{j+1}}{T_j} \right) + \left(\frac{Q_j T_{j+1}}{\Delta\tau_i} \right) \right]^{-1}$$

beginning at j=0 and going to j= n - 1, with

$$A_{-1,i} = 1$$

where

j = suffix representing the node j, see Figure 3

i = the suffix denoting a value at elapsed time t.

2) Compute initial values for each node of

$$B_{j,i} = A_{j,i} T_{j+1} \left[W_{j,i} + \Delta\vartheta_{j,i-1} \left(\frac{Q_j}{\Delta\tau_i} \right) + \frac{B_{j-1,i}}{T_j} \right]$$

beginning at j=0 and going to j=n-1, with

$$B_{-1} = 0$$

and $W_{j,i}$ is zero, at all nodes except at the node j=0, where W represents the conductor electric loss at time i and at the node corresponding to the enclosure, where W represents the enclosure electric loss at time i.

3) Compute values of temperature rise

$$\vartheta_{j,i} = \left(A_{j,i} + \Delta\vartheta_{j+1,i}\right) + B_{j,i}$$

starting at j= n - 1 and going to j = 0

where

$\Delta\vartheta_{j,i}$ = temperature rise at node j and time i

$\Delta\vartheta_{n,i}$ is always zero.

Repeat all the steps for as many times as is necessary to complete the transient

$$\Delta\tau_i = (\tau_i - \tau_{i-1})$$

At each time step, recalculate the thermal resistance and capacitance of the gas.

4.4 Mutual Heating Between the Parallel Phases

4.4.1 General principles

Each phase of the GIL circuit will have its own equivalent thermal network for which the transient temperature rise, caused by its own losses, is calculated. If the duration of the transient is sufficiently long for mutual heating from other GILs, or heat transfer to the ground surface to be significant, then this must be taken into account when calculating the true temperatures used to update GIL losses at each time step. Heat transfer to the ground surface is taken into account by locating the reflected images of the heat sources on the opposite side of the ground plane.

The true temperatures for each GIL are obtained at each time step by adding to its own temperature the temperature rise at the location of that GIL in the thermal field of each other GIL and of each image source. These thermal fields are computed from the equations corresponding to the equivalent networks being centred on each GIL or image source. In each of these networks there are nodes corresponding to the axial centre of other GILs and to the image sources. This process is carried out for all GILs and image sources in the group. Note that the thermal network of an image source is identical to that of its corresponding GIL except for the negative sign of its heat flux and temperature rise; separate networks for image sources are not therefore needed.

The total transient temperature rise of a GIL at any time is the sum of the temperature rise due to its own losses, given by its own network, and the temperature rise due to mutual heating given by the networks of other GILs and image sources.

4.4.2 Simplification for the case of three GILs in flat formation spaced from each other

A convenient simplification of the above treatment which adapts well to GIL, is the case of a circuit of three GILs in flat formation, spaced apart from each other, and for which it is assumed that the losses are equal.

The equivalent networks of all three GILs are identical and only the mutual heating between the middle and each outside GIL needs to be included. Thus it is only necessary to construct a network for the centre GIL.

The temperature rise in the centre GIL due to mutual heating from each outside GIL is given by the rise calculated at the node which corresponds to the centres of the outside GILs. This rise is arithmetically added at each time step to the temperature of the centre and outside GILs. This gives the true temperature of the centre GIL for the purpose of correcting GIL losses.

This simplification errs on the safe side.

An example calculation using the above method is given is given in Appendix 6

4.5 References

[1] Electra 87 ‘Computer Method For The Calculation Of The Response Of Single Core GILs To A Step Function Thermal Transient’

[2] IEC 853-2 (1989) ‘Cyclic Rating of Cables Greater Than 18/30 (36) kV And Emergency Ratings For Cables of All Voltages’ First Edition

[3] JWG 21/23/33-15 Document N°12 JWG 23/21/33 Volumetric specific heat. (Private Communication)

5. Guide To Numerical Modelling

Two types of software code were studied. Finite element analysis (FEA) divides the geometry into a number of discrete elements. Computations calculate heat transfer by thermal conduction. The advantage of FEA is that it can solve heat flow in complex asymmetrical and three dimensional geometries and can represent material properties that are temperature dependent. FEA can also be used to model current distribution in the conductor and enclosure and hence calculate the conduction losses. However, FEA cannot directly model gas flow and convective heat transfer through the gas insulation. Some FEA programs include a user sub-routine that calculates convective heat transfer through the insulating gas and at the ground surface. However these calculations are based on mathematical simplifications and do not truly model convective flow.

The second type of software, Computational Fluid Dynamics (CFD) directly models the convective movement and heat flow in a gas. It provides a completely different approach to the more traditional algorithms developed by Hitaka, Minaguchi and Vermeer. The success of the calculation is very dependent on the selection of the fluid properties and the type of fluid flow in the model, (i.e. turbulent or laminar flow conditions). Verification of the solution is required by practical measurement, or by comparison with traditional algorithms and simple annular geometry. Further CFD advantages are that complex asymmetrical and three dimensional geometries can be modelled with boundaries that are non-isothermal. For example modelling is possible of inclined GIL, the proximity of the ground surface and the presence of other GIL phases.

Important considerations when constructing the model are that boundary conditions should be sufficiently remote such that small variations in the boundary position do not effect the solution. This was achieved in the case of the buried GIL and cables studied in this work by placing the isothermal boundaries at a distance of 25m.

It is important that the GIL structure and the surrounding soil is modelled with sufficiently small elements of suitable geometry to make the calculations accurately represent heat flow. Having selected the geometry and set the initial boundary conditions of temperature and heat generation the computation is allowed to proceed until the required convergence is achieved.

Whichever software is used it is essential that the method be validated against calculations obtained by published formulae and experimental measurement.

5.1 The Application of FEA to Buried GIL

The FEA mesh accurately models both the distributed thermal resistances and the thermal capacitances of the solid materials both within the GIL and the surrounding soil.

FEA has been applied to both continuous and short time ratings with a good level of agreement with analytical methods. This would be expected as the same formulae were used to represent convection across the insulating gas mixture in both the FEA and the analytical models. (Appendix 6).

5.2 Application of CFD to Buried GIL

The solution of heat flow from buried GIL is an unusual application for CFD as there is a large volume of solid surrounding the gas filled enclosure. During the study it was necessary to adapt the CFD software to model both gas convection and to include conduction through the solid materials.

Satisfactory solutions were obtained using the properties of pure N_2 and the selection of a laminar flow convective model. The use of SF_6 properties and the selection of a turbulent gas model was unsuccessful as convergence of the solution could not be achieved. The physical properties of the SF_6-N_2 gas mixture had not been published and so convection in the gas mixture could not be studied.

The CFD method has much promise for GIL modelling and warrants further work in particular to its application to inclined and vertical GIL installations.

6. Sensitivity Study On Rating Parameters For Continuous Current Rating

The detailed sensitivity study is given in Appendix 7.

This study applies the recommended formulae given in chapter 3 to an example GIL application and assesses in detail the sensitivity of varying each of the key parameters by ±50%. The example application is for single phase GIL in flat formation under continuous loading. The purpose of this study is to rank the parameters in the order of the largest to the smallest effect on the magnitude of the rating, with the objectives of identifying:

1) The most important rating parameters when designing GIL for future applications.
2) The effect that inaccuracy in each design, installation or calculation parameter could have on the final rating.

6.1 Parameters

The parameters employed in the sensitivity study were derived from the dimensions of one particular hypothetical design of 400kV GIL. The list of parameters can be found in Appendix 7. The nominal target current rating chosen was 3000 Amps continuous. The UK summer ambient rating temperature of 15^{o}C, with a soil thermal resistivity of 1.2Km/W was taken. The individual parameters were calculated by taking the average values from those submitted by the Members of the Task Force, as used in their own Organisations or Countries. The example GIL was insulated with a gas mixture of 90% N_2 and 10% SF_6 at an absolute pressure of 6.7 bar. A design stress of 2kV/mm was taken at the outer surface of the conductor, which permitted a conductor diameter of 280mm to be selected in combination with an enclosure inner diameter of 630mm, these being close to the 'e' ratio, thereby giving a near optimum minimum enclosure diameter. The tubular aluminium conductor of 280mm external diameter had a wall thickness of 16mm giving a cross sectional area of 13270mm^2. The cylindrical aluminium alloy enclosure of 630mm internal diameter had a wall thickness of 10mm. An anticorrosion polyethylene oversheath of 3mm radial thickness was provided. The three single phase GIL enclosures were solidly bonded to each other and to earth at each end of the circuit to provide continuity for short circuit current. Thus circulating currents would flow in the enclosures under normal operation.

The example GIL circuit was laid at the same minimum depth as conventional flexible cable crossing farmland in the UK, i.e. 1050mm to the top of the anticorrosion oversheath. A nominal axial spacing of one diameter, 1312mm, was selected both to give adequate room within the trench to lay the GIL in flat formation and to connect longitudinal sections of GIL together.

The rating calculations were applied to yield the following results:

1) The resulting current ratings for either a range of selected maximum conductor operating temperatures or maximum soil temperature limits (i.e. the soil adjacent to the oversheath).
2) The resulting maximum operating temperatures of the conductor or soil for a rating of 3000 Amps.

It should be noted that recommended operating temperatures for GIL do not exist for buried applications. Recommended temperature limits exist for metalclad busbar installed in air with conductor connectors in SF_6, or a mixture of SF_6 [IEC694 Table 3][1]. The maximum continuous operating temperatures for connectors are given as 90^{o}C for tinned coated contacts, 105^{o}C for bare copper contacts and 105^{o}C for silver coated contacts. For the standard GIL dimensions studied, an arbitrary 71^{o}C conductor temperature resulted in a current rating of 3000 Amps.

Recommended limits exist for the maximum soil temperatures for conventional flexible cables to prevent thermal instability by the progressive increase of soil thermal resistivity as a result of moisture migration. The practices in each Country are listed in IEC287[2]. For example the maximum permissible soil temperature in the UK is taken as 50^{o}C and the maximum temperature in France as 60^{o}C. For the standard GIL dimensions studied a 60^{o}C soil emperature resulted in a current rating of 2886A. .

6.2 Conclusions on Continuous Rating Sensitivity Study

- The parameters that have the largest effect on the current rating are firstly the soil thermal resistivity and secondly the diameter of the enclosure.
- The parameter that has the largest effect on the operating temperature of the conductor is firstly the diameter of the enclosure and secondly the diameter of the conductor.
- The parameter that has the largest effect on the operating temperature of the enclosure is firstly the diameter of the enclosure and secondly the soil thermal resistivity.
- Increasing the conductor cross sectional area by reducing the inner diameter has only a small effect on the current rating and on reducing the operating temperatures, due to the adverse consequences

of skin effect to the ac resistance. In contrast, increasing the conductor cross sectional area by increasing the conductor diameter has a more significant benefit.

- As a first approximation the change in current rating is proportional to the square root of the change in the particular parameter. Thus the effect of the change on current rating is reduced.
- Variations of ±50% in the parameters involved with heat transfer within the gas have a minimal effect. Thus, although the Electra 100 formulae[3] for convection and radiation within the gas were chosen, the choice of alternative formulae will have a minimal effect on GIL ratings in buried applications. This is not so for in-air tunnel applications, where the external thermal resistance is small in comparison to the GIL internal resistance..
- At a constant current rating the effect of increasing the parameters on the operating temperature is significantly greater. To a first approximation the rise in temperature is directly proportional to the change in the parameter. In particular it is shown that a 50% increase in the soil thermal resistivity increases the rise in conductor operating temperature by 52.7% and the rise of the maximum soil temperature by 59.4%. Wide variations in the soil thermal resistivity can be experienced along the length of a GIL circuit due to changes in soil type, compaction and moisture content. This emphasises the importance of both accurate rating calculations and installation geometry, if overheating of the GIL and thermal instability are to be avoided.
- At the target current rating of 3000 Amps the conductor temperature is calculated to be 71^{o}C and the soil temperature adjacent to the enclosure is calculated to be 65^{o}C. Taking the recommended maximum figures to prevent soil drying out of 50^{o}C in the UK and 60^{o}C in France would limit the current rating to 2590 Amps and 2890 Amps respectively.

6.3 References

[1] IEC 694 (1996) 'Common Specifications for High Voltage Switchgear and Control Gear Standards' Table 3

[2] IEC 287 (1994) 'Electric Cables. Calculation of Current Rating. Part 1. Current Rating Equations (100% load factor) and Calculation of Losses.'

[3] Electra 100 (May 1985) 'Calculation of the Continuous Rating of Single Core, Rigid Type, Compressed Gas Insulated Cables in Still Air with No Solar Radiation'

7. Sensitivity Study On Rating Parameters For Short Time Current Rating

The detailed sensitivity study is given in Appendix 8.

7.1 Introduction

The sensitivity study on the short time rating of GIL is given in Appendix 7. The objectives of the study are to identify:

1) The most important rating parameters for prospective future GIL applications.
2) The effect that inaccuracy in each design, installation or calculation parameter could have on the short time rating.

The parameters employed in the sensitivity study were those of the 400kV GIL used for the continuous rating study, given in Appendix 6. The values of thermal heat capacities are recorded in Appendix 7.

A continuous 100% full load current rating of 3000 Amps was selected. The starting conditions for the short term rating were a) no previous current loading (0% preload) and b) 85% of full load current. A short term maximum operating temperature of 95°C was selected for the conductor. The UK summer ambient rating temperature of 15^{o}C, with a soil thermal resistivity of 1.2Km/W were taken. The rating conditions are summarised in Table 2.

Table 2 Sensitivity Study Conditions

Conductor short time temperature limit	95 °C
Pre-load starting current	0% and 85%
Duration of short time load	20 min and 12 h

7.2 Conclusions on Short Term Rating Sensitivity Study

- The GIL reference design was shown to have high short time ratings. In particular for the 12 hour period, the GIL was able to carry over twice the continuous load of 3000A starting from a 85% preload condition.

Table 3

Time	[Sort time rating / Continuous rating]	
	85% preload current	0% preload current
20 mins	6.39	9.06
12 hours	2.43	3.28

- The parameter that has the largest effect on the 20 minute short time rating is the volumetric specific heat of the conductor. An increase of 50% in the volumetric specific heat increased the short time rating by 19%, whereas a decrease, reduced the short time rating by 23%. These high ratings show the importance of performing current loading tests to verify the short time ratings, especially for the connectors, which may have a different thermal capacity and electrical resistance to the conductor.
- The other five parameters each had a small effect on the 20 minute short time rating indicating that the temperature rise of the conductor was almost adiabatic. The next most significant parameter was the convective parameter producing a current rating variation of less than 2%.
- The parameter that had the largest effect for the 12 hour period was K_0, the convection parameter for the gas mixture. A 50% increase in K_0 increased the short time rating by 6%. A 50% decrease, reduced it by 10~11%. This shows the importance of experimental verification of the short time rating as the properties of the mixture and the transient behaviour of the changing convection patterns are likely to have a significant effect.
- The parameter that had the second most significant effect on the 12 hour period was the soil thermal resistivity. An increase of 50% decreased the rating by 4~5% and a 50% decrease, increased the rating by 8~9%. This indicates that the thermal capacitances of the conductor and enclosure had become saturated within 12 hours.
- The study showed the sensitivity of the current rating to the thermal capacity of the conductor for the 20 minute rating and to the convection parameter K_0 for the 12 hour rating. If it is intended to employ these large short time ratings in a GIL application, it is recommended that:
    - A factor of safety is included to reduce the risk of overheating the conductor and connectors.

- The temperature is verified by experimental measurement. A factor of safety could be built into the selection of the maximum permissible conductor temperature. For this study an arbitrary value of 95°C was chosen.

8. Recommendations for Future Work

- The rating of GIL inclined at an angle to the horizontal.

  The majority of GIL circuits of long route length will include substantial lengths of GIL that are not horizontal. The work of Minaguchi et al[1] gives experimental results for GIL containing SF_6 gas installed in air. This shows that angles up to 15 degrees to the horizontal have little effect. Thus the effect of greater angles needs to be studied for laid direct applications. Three dimensional CFD methods can be applied to calculate the current rating, subject to the comments below:

- The use of CFD software programs

  Further work is required to provide input data and to validate the simulation of convection in SF_6 and N_2 gas mixtures.

- Convection from conductors of large diameter (160mm or larger)

  The work of Minaguchi[] in comparison to the work of Vermeer[] selected in this report, gives a slightly improved heat transfer in pure SF_6. The results of full size experiments on laid direct GIL containing SF_6 and N_2 mixtures have yet to be published, when these become available the convection formulae can be reviewed. However the sensitivity study has shown that the formulae will have little effect for buried GIL.

- Maximum operating temperatures

  Maximum operating temperatures for flexible cables are given in IEC 287, based on the safe working temperature of different types of insulation and conductor connections under continuous loading and short circuit conditions. It is recommended that similar values be studied for GIL.

- Soil drying out.

  The 60^{o}C maximum soil temperature employed in this report, to prevent moisture migration, was taken from IEC 287 as being the practice in France for laid direct cable installations. When experimental results are published for laid direct GIL, it is suggested that the applicability of the IEC 287 approach be reviewed.

8.1 References

[1] Minaguchi, D. Ginno, M. Itaka, K. Furukawa, H. Ninomiya, K. Hayashi, T. (1985) “Heat Transfer Characteristics of Gas-Insulated Transmission Lines” IEEE 85 SM 301-7

9. Bibliography

The bibliography in the Appendix 9 will be of use to those who wish to study the subject further.

Annex A: current rating / Appendixes

Table of Contents

1 Appendix 1: Reference Parameters

The GIL geometry shown in this report is given in Figure 1-1

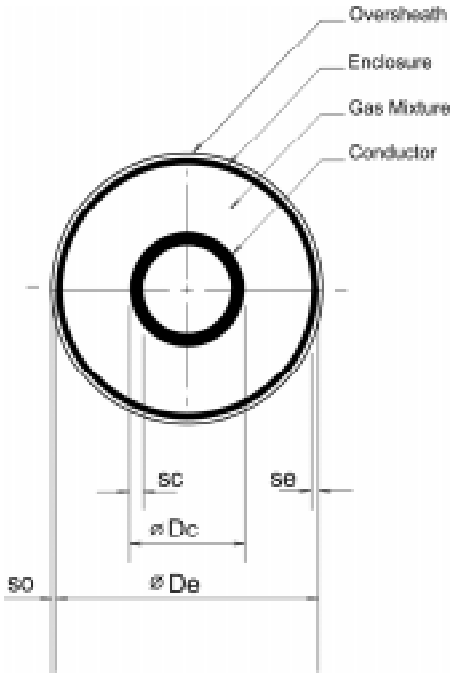

Figure 1-1: GIL Cross Section

The parameters employed in the sensitivity study were derived from the dimensions of one particular hypothetical design of 400kV GIL. The nominal target current rating chosen was 3000 Amps continuous. The UK summer ambient rating temperature of 15^{o}C with a soil thermal resistivity of 1.2Km/W was taken. The individual parameters were calculated by taking the average values from those submitted by the Members of the Task Force, as used in their own Organisations or Countries. The example GIL was insulated with a gas mixture of 90% N_2 and 10% SF_6 at an absolute pressure of 6.7 bar. A design stress of 2kV/mm was taken at the outer surface of the conductor, which permitted a conductor diameter of 280mm to be selected in combination with an enclosure inner diameter of 630mm, these being close to the 'e' ratio, thereby giving a near optimum minimum enclosure diameter. The tubular aluminium conductor of 280mm external diameter had a wall thickness of 16mm. The cylindrical aluminium alloy enclosure of 630mm internal diameter had a wall thickness of 10mm. An anticorrosion polyethylene sheath of 3mm radial thickness was provided. The three single phase GIL enclosures were solidly bonded to each other and to earth at each end of the circuit to provide continuity for short circuit current, thereby permitting circulating currents to flow under normal operation.

The example GIL circuit was laid at the same minimum depth as conventional flexible cable crossing farmland in the UK, i.e. 1050mm to the top of the anticorrosion sheath. A nominal axial spacing of two diameters, 1312mm, was selected both to give adequate room within the trench to lay the GIL in flat formation and to connect longitudinal sections of GIL together.

Table 1-1 GIL Parameters

Parameter	Symbol	Standard value	Unit
Axial Spacing	S	1312	mm
Burial depth (top of the anticorrosion sheath)	L	1050	mm
Conductor diameter	Dc	280	mm
Conductor thickness	sc	16	mm
Enclosure diameter	De	650	mm
Enclosure thickness	se	10	mm

Soil surface thermal resistivity	beta	0.2	$K.m^2/W$
Soil thermal resistivity	Rs	1.2	K.m/W
Conductor and enclosure thermal emissivity	sigma	0.2	
Gas mixture pressure	p	6.7	Bar abs.
SF_6 thermal convection constant	K1	11.3	
N_2 thermal convection constant	K2	5.83	
SF_6 Volume content	Vc	10	%
Conductor electric resistivity	Cr	$3.45.10^{-8}$	Ωm
Enclosure electric resistivity	Er	$5.9.10^{-8}$	Ωm

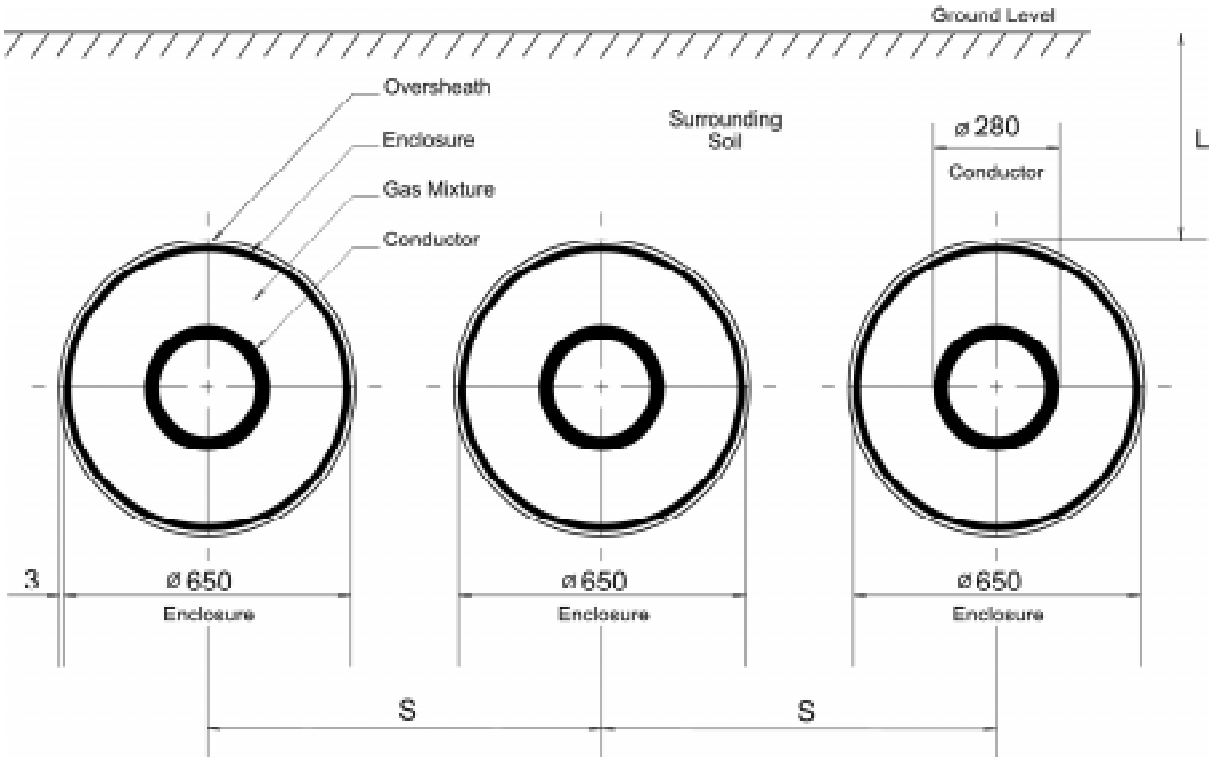

Figure 1-2: GIL Installation Arrangement

2 Appendix 2: Comparison of Methods and Measurements

A comparison was performed of methods for calculating ratings for laid direct, horizontal single phase GIL under continuous loading. The following methods of calculation were used:

2.1 Analytical methods:

2.1.1 IEC 287[1]

The formula given for the thermal resistance of the surrounding soil was used. The formula assumes that the soil surface is an isothermal plane, which is valid provided the GIL enclosure diameter is small compared with the distance to the surface (i.e. at least ten times less).

2.1.2 Japanese Cable Makers' Association Standard 168-E 1995 [2]

The formulae given for conductor and enclosure losses and the formula given for the thermal resistance of the surrounding soil were used. As above, the formula for thermal resistance of the surrounding soil assumes that the soil surface is an isothermal plane.

2.1.3 Itaka et al[3]

The formula given for convective heat transfer between conductor and enclosure was used.

2.1.4 Minaguchi et al[4]

The formula given for convective heat transfer between conductor and enclosure was used.

2.1.5 Electra 100[5]

The formulae given for conductor and enclosure losses and the formula given for convective heat transfer between conductor and enclosure were used.

2.1.6 Electra 125[6]

The correction applied to the formula for thermal resistance of the surrounding soil to take into account heat transfer at the soil surface was used. The formula therefore remains valid where the GIL diameter is not small compared with the distance to the surface.

2.1.7 Heat transfer at the soil surface as represented by an effective thermal resistivity

The formula proposed in the present document for heat transfer at the soil surface as represented by an effective thermal layer was used. The formula remains valid where the GIL diameter is not small compared with the distance to the surface.

The formula for radiative heat transfer between conductor and enclosure given by Itaka, Minaguchi and Electra 100 was used. The formula was the same in each case where a formula was given.

The formula for the thermal resistance of the corrosion resistant over-sheath given by IEC 287, The Japanese Cable Makers' Association Standard 168-E and Electra 100 was used. The formula was the same in each case where a formula was given.

2.2 Numerical Methods

2.2.1 Computational Fluid Dynamics (CFD)

A computational fluid dynamics model was used to model fluid flow and heat transfer. The model simulated heat transfer between conductor and enclosure by radiation and turbulent convection and heat transfer through the oversheath and soil by conduction.

2.2.2 Finite Element Method (FEM)

A finite element model was used to simulate the heat transfer through the oversheath and soil by conduction and the heat transfer by convection at the soil surface.

Calculations were performed for a GIL with the geometry, material properties and laying conditions specified in Appendix 1. Two depths of laying were considered; 1050 mm and 1350 mm from the surface of the soil to the top of the corrosion resistant oversheath. The 1050 mm depth is specified in the UK for urban installation of cable. The 1350 mm depth is specified in the UK for rural installation through ploughed farmland. Calculations were performed both with the soil surface assumed to be an isothermal plane and with a correction applied to take into account the heat transfer at the soil surface.

Initially, calculations were performed with a continuous current of 3000 A, this being a typical Summer continuous rating for overhead line circuits. Calculations were then performed to determine the continuous currents giving rise to a maximum soil temperature of 60^{O}C, this being the maximum temperature permitted in France to avoid drying out of the soil.

The formulae for heat transfer by convection between conductor and enclosure all include a constant that is dependent on gas properties. The formula of Itaka et al[3] includes a constant K_0, the value of which was determined by experiment. The value is given as 24.4 for SF_6 and 14.9 for N_2. The formula of Minaguchi et al[4] includes a constant K_1, the value of which was given as 4.40 for SF_6. The formula of Electra 100 includes a constant K_0, the value of which was derived from the physical properties of the gases by Vermeer[7] and is given as 11.3 for SF_6 and 5.83 for N_2. In the calculations, a value was taken to represent a nitrogen based gas mixture. The values given for N_2 and SF_6 were weighted in the ratio 19:1 and averaged.

2.3 Calculation Methods

Calculations were performed using the combinations of methods shown in Table 2-1

Table 2-1 Calculation methods

Calculation	Conductor and enclosure losses	Thermal resistances		
		Conductor to enclosure	Surrounding soil	Surface of soil
A	Electra 100	Electra 100	IEC 287	Electra 125
B	Electra 100	Itaka et al	IEC 287	Electra 125
C		Minaguchi et al	Japanese Cable Makers' Association	-
D	Electra 100	Electra 100	IEC 287	-
E	Electra 100	Electra 100	IEC 287	Equivalent layer
F		CFD	CFD	
G	IEC 287	Electra 87	FEM	FEM

2.4 Comparison of results

The results of calculations for the GIL with continuous current of 3000 A are shown in Table 2-2 and Table 2-3 for calculations where the soil surface was taken as an isothermal plane and in Table 2-4 and Table 2-5 for calculations where the heat transfer at the soil surface was taken into account.

Where the soil surface was taken as an isothermal plane, the mean values of conductor temperature were 64.0^{O}C for a depth of 1050 mm and 71.5^{O}C for a depth of 1350 mm. There was a significant difference of 10% between the maximum and minimum calculated temperature rise. The Computational Fluid Dynamics model gave a lower result for conductor temperature rise than the Finite Element Method and the analytical methods. The conductor temperature rises calculated by the analytical methods were in agreement to within 4%.

For all methods of calculation, the temperature difference between conductor and enclosure was small (of the order of 5^{O}C) compared with the temperature difference through the soil. However, the variation in temperature difference was large (of the order of +/- 16%) between the different methods.

The losses for the centre phase GIL were in agreement to +1%/-2%.

Where the heat transfer at the soil surface was taken into account, the results showed generally similar trends. The conductor and enclosure temperatures were significantly higher (of the order of 5^{O}C) compared with the results for the isothermal soil surface. The calculated values of soil thermal resistance were correspondingly higher.

Results showing the continuous current for a maximum soil temperature of 60^{O}C are shown in Table 2-5 and Table 2-6 for calculations where the soil surface was taken as isothermal and in Table 2-7 and Table 2-8 for calculations where the heat transfer at the soil surface was taken into account.

Where the soil surface was taken as an isothermal plane, the mean value of the continuous current for a 60^{O}C maximum soil temperature was 3042 A for a depth of 1050 mm and 2851 A for a depth of 1350 mm. At each depth of laying, the current values agreed to within 2.3%.

Where the heat transfer at the soil surface was taken into account, the continuous current was reduced by about 3% compared with the results for the isothermal soil surface. The mean value of continuous current was 2925 A for a depth of 1050 mm and 2765 A for a depth of 1350 mm. At each depth of laying, the current values agreed to within 5%.

Table 2-2: Temperature calculation for 1050 mm depth with ground surface isothermal 15^{O}C

	A	B	C	D	E	F	G	Mean value
Current	3000	3000	3000	3000	3000	3000	3000	3000
depth of laying (mm)	1050	1050	1050	1050	1050	1050	1050	1050
conductor temperature	65.1	63.6	64.6	65.0	65.2	60.3	64.1	64.0
enclosure temperature	59.4	59.0	59.5	59.0	59.2	56.0	58.2	58.6
maximum soil temperature	59.1	58.7	59.1	58.7	58.9	54.5	57.9	58.1
conductor losses (Wm^{-1})	29.6	29.1	29.9	29.2	29.2	28.3	30.7	29.4
enclosure losses (Wm^{-1})	30.9	30.8	30.6	30.7	31.3	30.3	29.2	30.5
total losses	60.5	59.9	60.5	59.9	60.6	58.6	59.8	60.0
gas thermal resistance	0.192	0.158	0.171	0.204	0.204	0.152	0.191	0.182
external thermal resistance	0.730	0.730	0.729	0.729	0.725	0.674	0.717	0.719

Table 2-3: Temperature calculation for 1350 mm depth with ground surface isothermal 15^{O}C

	A	B	C	D	E	F	G	Mean Value
Current	3000	3000	3000	3000	3000	3000	3000	3000
depth of laying (mm)	1350	1350	1350	1350	1350	1350	1350	1350
conductor temperature	72.4	70.9	70.5	72.2	72.4	68.5	73.4	71.5
enclosure temperature	66.7	66.2	66.2	66.2	66.4	63.0	67.6	66.0
Maximum soil temperature	66.4	65.9	65.9	65.9	66.1	61.4	67.3	65.6
conductor losses (Wm^{-1})	30.2	29.7	30.3	29.8	29.8	29.1	31.3	30.0
Enclosure losses (Wm^{-1})	31.6	31.6	31.3	31.5	32.1	31.0	29.6	31.2
total losses	61.8	61.2	61.6	61.3	61.9	60.1	60.9	61.3
gas thermal resistance	0.189	0.158	0.139	0.201	0.201	0.189	0.186	0.18
External thermal resistance	0.832	0.830	0.826	0.831	0.825	0.772	0.859	0.825

Table 2-4: Temperature calculation for 1050 mm depth with ground surface heat transfer coefficient

	A	B	E	F	G	Mean value
Current	3000	3000	3000	3000	3000	3000
depth of laying (mm)	1050	1050	1050	1050	1050	1050
Conductor temperature	70.5	65.4	69.3	65.3	69.6	68.0
Enclosure temperature	64.8	60.7	63.3	60.6	63.8	62.6
Maximum soil temperature	64.4	60.4	63.0	59.0	63.5	62.1
conductor losses (Wm^{-1})	30.0	29.2	29.6	28.8	30.8	29.7
Enclosure losses (Wm^{-1})	31.4	31.0	31.8	30.8	28.7	30.7
total losses	61.4	60.2	61.4	59.6	58.8	60.3
gas thermal resistance	0.191	0.159	0.202	0.163	0.195	0.182
External thermal resistance	0.805	0.755	0.782	0.738	0.825	0.781

Table 2-5: Temperature calculation for 1350 mm depth with ground surface heat transfer coefficient

	A	B	E	F	G	Mean Value
Current	3000	3000	3000	3000	3000	3000
depth of laying (mm)	1350	1350	1350	1350	1350	1350
Conductor temperature	76.9	72.3	78.1	71.2	76.3	75.0
enclosure temperature	71.2	67.7	72.1	66.8	70.5	69.7
Maximum soil temperature	70.9	67.3	71.8	61.4	70.2	68.3
conductor losses (Wm^{-1})	30.5	29.8	30.2	29.4	30.5	30.1
enclosure losses (Wm^{-1})	32.1	31.7	32.7	31.4	29.1	31.4
total losses	62.6	61.5	62.9	60.8	59.5	61.5
gas thermal resistance	0.186	0.156	0.199	0.150	0.192	0.177
external thermal resistance	0.892	0.851	0.903	0.763	0.928	0.867

Table 2-6: Current rating calculation for 1050 mm depth, soil max 60^{O}C, ground surface isothermal 15^{O}C

	A	B	C	D	E	G	Mean value
Current	3025.0	3039.7	3028.0	3037.7	3028.7	3092.0	3041.9
depth of laying (mm)	1050	1050	1050	1050	1050	1050.0	1050
Conductor temperature	65.7	65.1	65.2	66.3	66.4	66.3	65.8
enclosure temperature	60.3	60.3	60.4	60.4	60.3	60.3	60.3

maximum soil temperature	60.0	60.0	60.0	60.0	60.0	60.0	60.0
conductor losses (Wm^{-1})	30.2	30.0	30.5	30.1	29.9	31.8	30.4
enclosure losses (Wm^{-1})	31.5	31.7	31.3	31.6	32.1	30.2	31.4
total losses	61.7	61.7	61.8	61.7	61.9	62.0	61.8
gas thermal resistance	0.179	0.160	0.159	0.202	0.202	0.194	0.183
external thermal resistance	0.730	0.729	0.728	0.729	0.727	0.730	0.729

Table 2-7 Current rating calculation for 1350 mm depth, soil max 60^{O}C, ground surface isothermal

	A	B	C	D	E	G	Mean Value
Current	2835.0	2847.0	2841.0	2846.0	2838.1	2897.6	2850.8
depth of laying (mm)	1350	1350	1350	1350	1350	1350	1350
conductor temperature	65.5	64.5	64.7	65.7	65.7	65.7	65.3
enclosure temperature	60.3	60.3	60.3	60.3	60.3	60.3	60.3
maximum soil temperature	60.0	60.0	60.0	60.0	60.0	60.0	60
conductor losses (Wm^{-1})	26.5	26.3	26.8	26.3	26.2	27.8	26.7
enclosure losses (Wm^{-1})	27.7	27.9	27.5	27.8	28.1	26.5	27.6
total losses	54.1	54.2	54.3	54.1	54.3	54.4	54.2
gas thermal resistance	0.197	0.160	0.162	0.208	0.208	0.200	0.189
external thermal resistance	0.832	0.830	0.829	0.831	0.828	0.832	0.830

Table 2-8 Current rating calculation for 1050 mm depth, soil max 60^{O}C, ground surface heat transfer coefficient

	A	B	E	G	Mean value
Current	2882.0	2988.4	2918.4	2911.0	2924.9
depth of laying (mm)	1050	1050	1050	1050	1050
conductor temperature	65.6	64.9	66.0	65.1	65.1
enclosure temperature	60.3	60.3	60.3	60.3	60.3
maximum soil temperature	60.0	60.0	60.0	60.0	60.0
conductor losses (Wm^{-1})	27.4	29.0	27.7	28.0	28.0
enclosure losses (Wm^{-1})	28.6	30.7	29.8	26.6	28.9
total losses	55.9	59.7	57.5	54.6	56.9
gas thermal resistance	0.194	0.159	0.206	0.171	0.183
external thermal resistance	0.804	0.754	0.783	0.824	0.791

Table 2-9 Current rating calculation for 1350 mm depth, soil max 60^{O}C, ground surface heat transfer coefficient

	A	B	E	G	Mean Value
Current	2739.0	2813.6	2760.5	2745.5	2764.5
depth of laying (mm)	1350	1350	1350	1350	1350
conductor temperature	65.1	64.4	65.5	64.7	64.9
enclosure temperature	60.3	60.3	60.3	60.3	60.3
maximum soil temperature	60.0	60.0	60.0	60.0	60.0
conductor losses (Wm^{-1})	24.7	25.7	24.8	24.9	25.0
enclosure losses (Wm^{-1})	25.8	27.2	26.6	23.7	25.8
total losses	50.5	52.9	51.4	48.6	50.9
gas thermal resistance	0.194	0.161	0.211	0.176	0.186
external thermal resistance	0.891	0.851	0.875	0.926	0.886

2.5 Comments

Although there was general agreement in the values of conductor temperature at 3000 A and in the values of current for a maximum soil temperature of 60^{O}C, there were significant variations. There are a number of areas where errors may be incurred.

2.5.1 Analytical methods

The analytical methods may be subject to errors resulting from assumptions made in derivation of the formulae used.

The formula used in IEC 287 for the thermal resistance of the soil is valid where the enclosure diameter is at least 10 times less than the depth of laying. This condition is not met in either of the two installation geometries considered, and some error in the calculated values of temperature is to be expected.

The method of Electra 100 allows losses in each of the three phases to be calculated, taking into account the skin and proximity effects. However, the method does not take into account the lower temperatures of the outer phases compared with the centre phase. Hence, the calculated losses for the outer phases are likely to be greater than the actual losses.

The formulae used for convective heat transfer between conductor and enclosure are empirical in nature and their use may entail some error in the value of thermal resistance for the gas. The variation in results obtained using the different formulae merits investigating by comparison with experimental results.

2.5.2 Numerical methods

Where numerical methods are used, the distance to the boundary of the model and the boundary condition imposed may have a significant effect on the results obtained.

Calculations were performed using a finite element method where the limit of the area modelled was varied and three different boundary conditions were imposed. The boundary conditions were (i) a constant temperature of 15^{O}C, (ii) a zero temperature gradient and (iii) a simulated condition for a boundary at infinity. The geometry modelled was as defined in Appendix 1, with a depth of laying of 1050 mm and a continuous current of 3000 A.

Results of calculated temperature of the GIL external surface as the limit of the area modelled was varied are shown in for each of the boundary conditions.

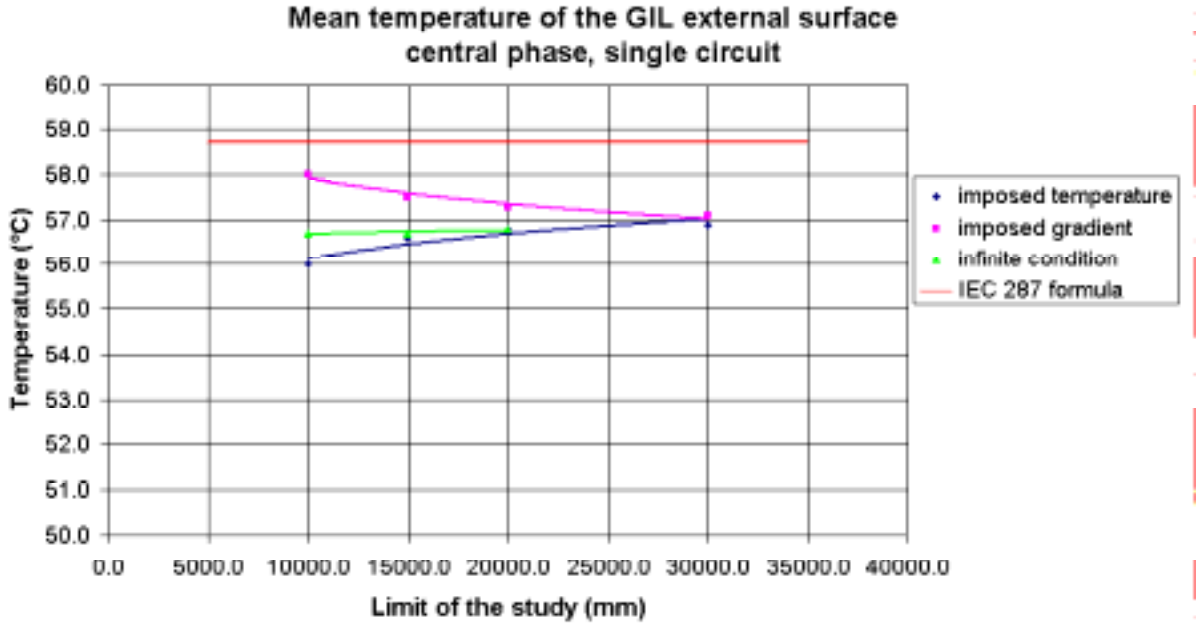

Figure 2-1: Temperature of the GIL external surface as the limit of the area modelled

The temperature calculated using the formula of IEC 287 is shown for comparison. In general, the finite element method gave a lower temperature than that of the IEC 287 formula. This may be due to limitations in the range of applicability of the formula, as discussed above. Of the finite element calculations, the imposed temperature boundary condition gave the lowest calculated temperatures. The imposed gradient boundary condition gave the highest temperatures. Results calculated for all three boundary conditions tended to converge as the limit of the area modelled was increased to about 30 m, approximately an order of magnitude greater than the GIL depth and spacing.

2.5.3 Heat transfer by convection at soil surface

Taking into account the heat transfer by convection at the soil surface had a significant effect on the calculated values of conductor temperature at 3000 A and values of current for a maximum soil temperature of 60^{O}C. Current ratings for horizontal, laid direct gas-insulated transmission lines under continuous loading: Calculation of thermal resistance.

2.6 Comparison of formulae for thermal resistance

The published methods for calculating the thermal resistances are compared

2.6.1 Thermal resistance between conductor and enclosure

Heat is transferred between conductor and enclosure of the GIL by radiation and convection.

2.6.2 Heat transfer by radiation

Formulae for the heat transfer by radiation are given by Itaka *et al*[3] and Minaguchi *et al*[4] and Electra 100. There is general agreement that the heat transfer by radiation is described by the Stefan-Boltzmann Law and may be expressed as follows:

$$W_r = \sigma\left(\theta_i^4 - \theta_o^4\right)\pi\, D_{ti} \frac{1}{\frac{1}{\varepsilon_{ti}} + \frac{D_{ti}}{D'_{to}}\left(\frac{1}{\varepsilon_{to}} - 1\right)}$$

where

D_{ti} = outer diameter of conductor

D'_{to} = inner diameter of enclosure

θ_i = temperature of conductor [K]

θ_o = temperature of enclosure [K]

σ = Stefan-Boltzmann constant = 5.67 x 10^{-8} [W/(m^2K^4)]

ε_{ti} = emissivity coefficient of conductor

ε_{to} = emissivity coefficient of enclosure

2.6.3 Heat transfer by convection

A number of formulae have been published for the heat transfer by convection.

2.6.3.1 Method of Itaka *et al*[3]

$$W_c = \frac{K_0 P^{0.6} D_{ti}^{0.75} (\theta_i - \theta_o)^{1.25}}{\left[\ln\left(\frac{D'_{to}}{D_{ti}}\right) + a\right]\left[1 + \left(\frac{D_{ti}}{D'_{to}}\right)^{0.6}\right]^{1.25}}$$

where

a = a constant determined experimentally

K_0 = a constant depending on the physical properties of the gas

P = absolute gas pressure (in kg/cm^2)

2.6.3.2 Method of Minaguchi *et al*[4]

According to Minaguchi *et al*[4], the heat transfer by convection is described by the following relationship:

$$W_c = K_1 P^{0.65} D_{ti}^{0.75} (\theta_i - \theta_o)^{1.25}$$

where

K_1 = convection constant between conductor and enclosure

P = absolute gas pressure (in kg/cm^2)

2.6.3.3 Method of Electra 100[5]

$$W_c = \frac{K_0 \left[D_{ti}\left(1 - \frac{D_{ti}}{D_{to}}\right)^{2.167}\right] P^{0.67} (\theta_i - \theta_o)^{1.33}}{\ln\left(\frac{D'_{to}}{D_{ti}}\right)}$$

where

K_0 = constant depending on the gas

P = absolute gas pressure (in bar)

2.7 Comparison of methods for calculation of thermal resistances of the gas

In all three methods, the convective heat transfer is expressed as the product of four terms: A constant *K*, which is dependent on gas properties, a term which is dependent on the conductor and enclosure dimensions ('form factor'), pressure to the power *n* and temperature difference to the power *m*.

The value of K_0 in the formula of Itaka *et al* was determined by experiment. The value is given as 24.4 for SF_6 and 14.9 for N_2. In the formula of Minaguchi *et al*, the value of K_1 is given as 4.40 for SF_6 and 2.69 for N_2. The value of K_0 in the formula of Electra 100 is given as 11.3 for SF_6 and 5.83 for N_2. The values are derived from the physical properties of the gases by Vermeer[7].

The formulae of Itaka *et al*, Minaguchi *et al* and Electra 100 differ in the way that the form factors are expressed. However, the conductor and enclosure diameters encountered in practice will fall within a limited range. In Figure 2-2, the form factors of the three formulae are shown for a geometry where the inner diameter of the enclosure is constant at 630 mm and the outer diameter of the conductor is varied across the range 150 – 300 mm. The form factors have been normalised with respect to their values for a conductor diameter of 280 mm. For all three formulae, the form factors show similar variation across the range of conductor diameters of interest. It would appear that, effectively, the three form factors vary only by a scale factor.

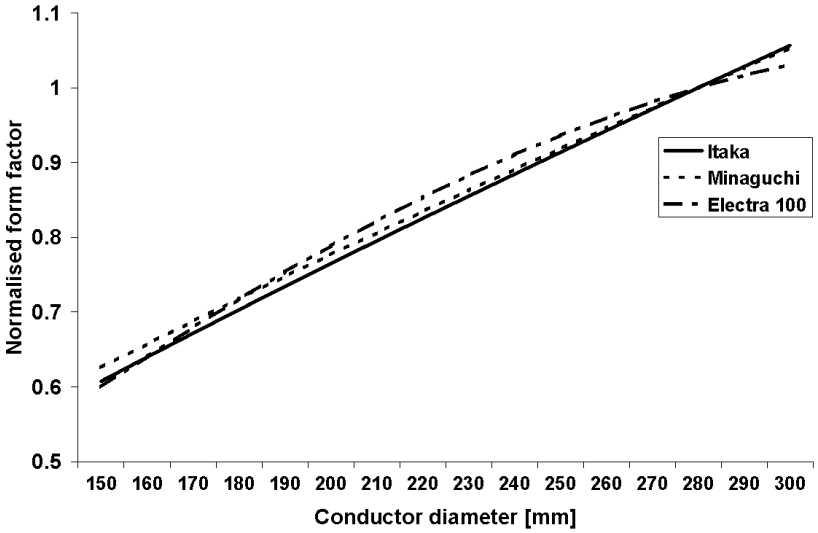

Figure 2-2: Normalised Form Factor Variation with Conductor Diameter

In all three formulae, convective heat transfer varies with pressure to the power *n*, where *n* varies from 0.6 in the formula of Itaka *et al* to 0.67 in the formula of Electra 100. In practice, the pressures used are likely to fall within a limited range and the value of *n* is unlikely to be significant.

In the formulae of Itaka *et al* and Minaguchi *et al*, the convective heat transfer varies with temperature difference to the power 1.25, while in the formula of Electra 100, it varies with temperature difference to the power 1.33. A discrepancy between the formulae of a few percent is to be expected across the temperature range of interest.

The convective heat transfer as a function of temperature difference between conductor and enclosure as calculated using each of the three methods is shown in Figure 2-3 for a GIL the geometry of which is given below:

Conductor outer diameter	280 mm
Enclosure inner diameter	630 mm
Gas pressure	670 kPa
Gas composition	95% N_2 , 5% SF_6

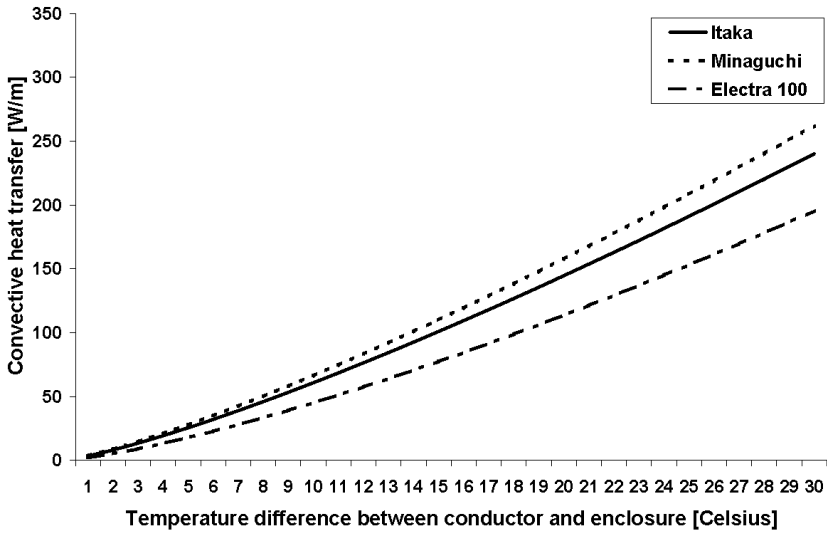

Figure 2-3: Convective Heat Transfer between Conductor and Enclosure

The corresponding thermal resistances between conductor and enclosure due to convective heat transfer are shown in Figure 2-4. The convective heat transfer calculated by the three methods showed significant differences. The method of Electra 100 gave a convective heat transfer that was below the average for the three methods by 16 – 32% across the temperature range, while the method of Minaguchi *et al* gave a value that was higher than the average by 13 – 21%. The method of Itaka *et al* gave a value that was higher than the average by 3 – 11%. The percentage differences between the three methods were greatest at lower temperatures.

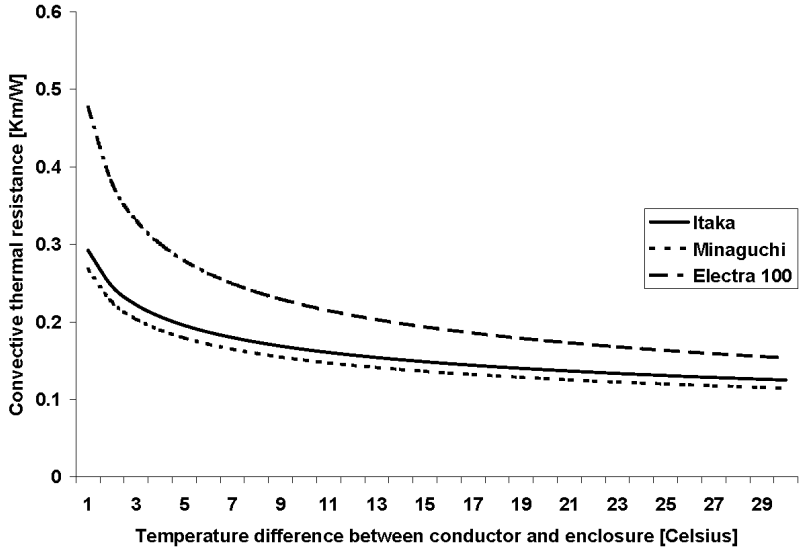

Figure 2-4: Convective heat transfer thermal resistance variation with temperature difference

The total heat transfer between conductor and enclosure was calculated by adding the radiated component, where an emissivity constant for the conductor and enclosure surfaces of 0.2 and an enclosure temperature of 60^{O}C were assumed. The results are shown in Figure 2-5. The corresponding thermal resistances between conductor and enclosure are shown in Figure 2-6. The methods used to calculate the convective component of heat transfer account for significant differences in the total heat transfer.

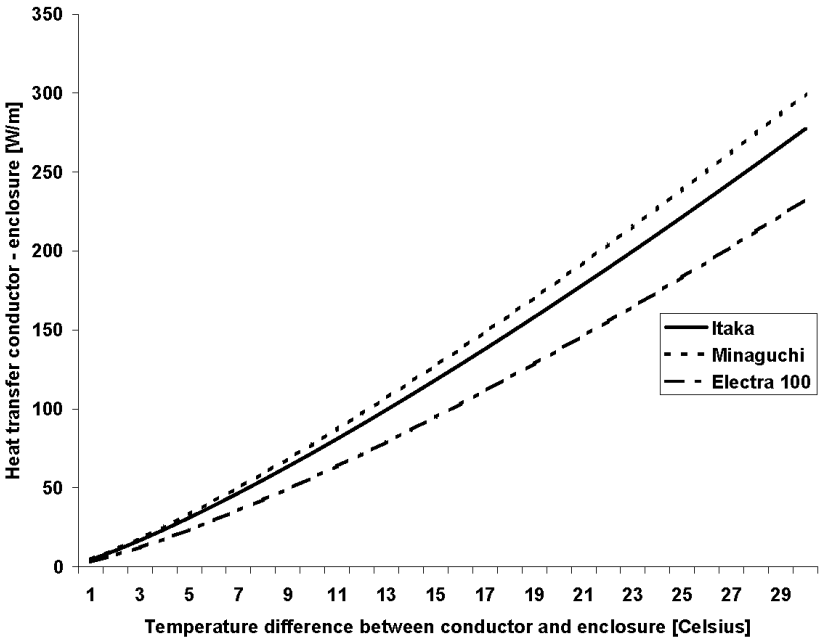

Figure 2-5: Combined Radiative and Convective Heat Transfer between Conductor and Enclosure as a Function of Temperature Difference

The lack of agreement between the methods used to calculate the heat transfer by convection merits further investigation by comparison with experimental results. It is, however, unlikely to have a significant influence on the ratings of directly buried GIL: In practice, the temperature difference, under continuous loading, between the conductor and enclosure is likely to be small compared with the temperature difference through the surrounding soil. Moreover, ratings are most likely to be limited by the enclosure temperature.

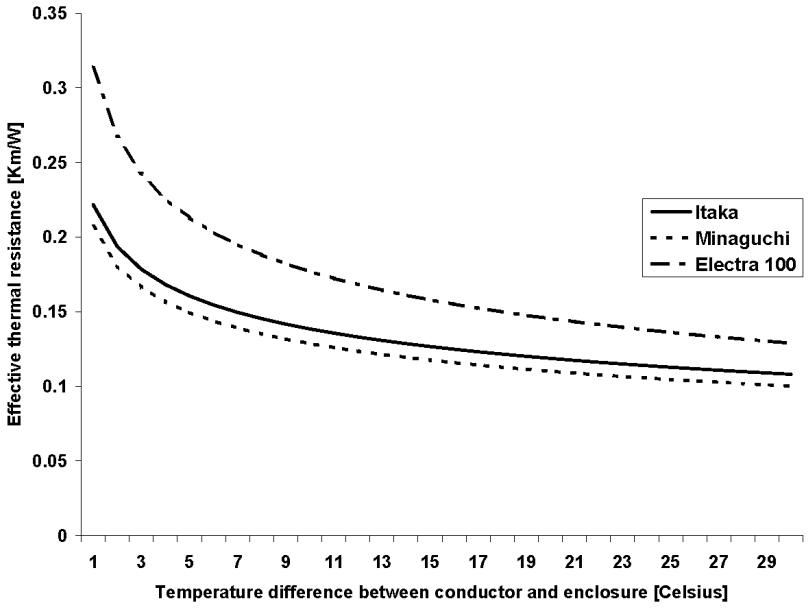

Figure 2-6: Effective Thermal Resistance Between Conductor and Enclosure as a Function of Temperature Difference

2.8 Thermal resistance of corrosion protective oversheath

Formulae for the thermal resistance of the corrosion protective oversheath are given in Electra 100[5], the Japanese Cable Makers Association Standard 168-E 1995[2] and IEC 287-2-1: 1994[1]. There is general agreement that the thermal resistance is given by:

$$T_3 = \frac{\rho_t}{2\pi} \ln \frac{D_e}{D_{to}}$$

where:

D_e = Outer diameter of corrosion protective oversheath

D_{to} = Outer diameter of enclosure

Δ_t = thermal resistivity of the oversheath material

2.9 Thermal resistance of surrounding soil

Formulae for the thermal resistance of the surrounding soil are given in the Japanese Cable Makers Association Standard 168-E 1995 and IEC 287.

2.10 Method of Japanese Cable Makers Association Standard JCS 168-E 1995

The thermal resistance of the surrounding soil, for the central cable, is given as:

$$T_4 = \frac{\rho_T}{2\pi}\left[\ln\left(\frac{4L}{D_e}\right) + \ln\left(\frac{4L^2}{s_1^2}+1\right)\right]$$

where

L = axial depth of laying

s_1 = axial separation between phases

Δ_T = thermal resistivity of surrounding soil

2.11 Method of IEC 287

Two formulae are given for the thermal resistivity of the surrounding soil, for the central cable. Where the losses in each phase are approximately equal, the thermal resistance is given as:

$$T_4 = \frac{\rho_T}{2\pi}\left[\ln\left(\frac{2L}{D_e} + \sqrt{\frac{4L^2}{D_e^2}-1}\right) + \ln\left(\frac{4L^2}{s_1^2}+1\right)\right]$$

Where the losses are unequal, the thermal resistance is given as:

$$T_4 = \frac{\rho_T}{2\pi}\left[\ln\left(\frac{2L}{D_e} + \sqrt{\frac{4L^2}{D_e^2}-1}\right) + \left[\frac{1+0.5(\lambda'_{11}+\lambda'_{12})}{1+\lambda'_{1m}}\right]\ln\left(\frac{4L^2}{s_1^2}+1\right)\right]$$

where

λ'_{11} = loss factor for outer phase, lagging phase angle

λ'_{1m} = loss factor for centre phase

λ'_{12} = loss factor for outer phase, leading phase angle

It may be seen that where the loss factors are equal, the two formulae become the same.

2.12 Comparison of methods

Assuming the loss factors are approximately equal, it may be seen that the formulae of the Japanese Cable Makers Association and IEC 287 are equivalent when $4L^2/D_e^2 >> 1$. For a geometry where the outer diameter of the GIL is 0.656 m, the axial separation between phases is 1.3 m and the axial depth of laying is 1.38 m (1.05 m to the top of the corrosion protective oversheath), the values of thermal resistance calculated using the two methods differ by 0.38%. When the axial depth of laying is increased to 1.68 m (1.35 m to the top of the corrosion protective oversheath), the difference reduces to 0.22%. The effect on the calculated rating of such a difference will be insignificant.

In the derivation of the above formulae, the soil surface is assumed to be isothermal. In practice, the assumption is not true and the actual value of the thermal resistance of the surrounding soil will be higher.

2.13 Conclusions

Published methods for calculating the thermal resistances of components applicable to directly buried GIL have been compared.

There is agreement that the heat transfer by radiation from conductor to enclosure is described by the Stefan-Boltzmann Law.

Three methods for calculating the heat transfer by convection from conductor to enclosure have been compared for a typical GIL geometry over a range of temperatures. The differences between the results obtained using the three methods were significant. However, for directly buried GIL, the convective heat transfer between conductor and enclosure is unlikely to have a critical influence on ratings.

There is agreement regarding the formula for conduction through the corrosion protective oversheath.

Two methods for calculating conduction through the surrounding soil were compared. The difference between the results obtained using the two methods was not significant.

2.14 References

[1] International Standard IEC 287-1-1 (1994 First Edition) 'Electric cables - Calculation of the current rating - Part 1: Current rating equations (100% load factor) and calculation of losses - Section 1: General'

International Standard IEC 287-2-1 (1994 First Edition) 'Electric cables - Calculation of the current rating - Part 2: Thermal resistance - Section 1: Calculation of thermal resistance'

[2] Japanese Cable Makers' Association Standard 168 - E 1995.

[3] Itaka, K. Araki, T. and Hara, T. 'Heat transfer characteristics of gas spacer cables, IEEE Transactions on Power Apparatus and Systems', Vol. PAS-97, No. 5, Sept/Oct 1978, pp 1579-1585

[4] Minaguchi, D. Ginno, M. Itaka, K. Furukawa, H. Ninomiya, K. and Hayashi, T. 'Heat Transfer Characterstics of Gas-Insulated Transmission Lines', IEEE 85 SM 301-7.

[5] Cigré Report 'Calculation of the continuous rating of single core, rigid type, compressed gas insulated cables in still air with no solar radiation - *Calcul de la capacité de transport en régime permanent des câbles unipolaires à isolant gazeux comprimé de type rigide posés en air calme et hors du rayonnement solaire*.' *Electra No. 100* (May 1985) pp 65-75

[6] Electra No. 125 'Calculation of the Continuous Rating of Three Core, Rigid Type, Compressed Gas Insulated Cables in Still Air and Buried." (1989) pp 104-111

[7] Vermeer, J. 'A Simple Formula For The Calculation Of The Convective Heat Transfer Between Conductor And Sheath In Compressed Gas Insulated Cables – *Une Formule Simple Pour Le Calcul De La Transmission De Chaleur Par Convection Entre Le Conducteur Et La Gaine Dans Les Câbles À Isolation Gazeuse*.' *Electra No. 87*, (March 1983), pp107-113

3 Appendix 3: Heat Transfer from the Ground Surface to Air - Method Employing an Equivalent Soil Layer

3.1 Introduction

The determination of the soil thermal resistivity for a group of equally load cables is a complex problem that has been worked out in the known terms by considering some simplifying mathematical hypotheses. The two most important are:

- the surfaces of the cables are isothermal
- the cables are buried at a suitable depth, quantified by recommending that $\frac{2 \cdot L}{D} \geq 10$

where:

- L is the burial depth
- D is the external cable diameter

When the cables are not buried deeply, that is $\frac{2 \cdot L}{D} < 10$, the hypothesis of isothermicity of the soil surface can produce a sensible error in the soil thermal resistance evaluation, since the thermal resistance of the soil must take into account also the heat transfer from the soil surface to the surrounding air. GILs suffer from the effect of this additional thermal term, due to their large external diameter that reduces the ratio 2L/D, (generally the burial depth does not exceed the value of 1.5m).

In the past, for a three-core GIL[1], it has been worked out a formula for the evaluation of the thermal resistance additional term to take into account said heat transfer.

In the present document said formula is extended to a three single core cables in flat formation.

3.2 Method using the superimposition of the effects

In Neher [2] the problem to determine the thermal resistance of the soil for a single cable close to the surface (2L/D<10) has been analytically resolved for a single core cable, and an additional term to the classic Kennelly formula, has been carried out.

By using the symbols of Figure 3-1 the thermal resistance of the soil is summarised by the sum of the:

Kennelly term:

Eq. 3-1 $$T_4 = \frac{\rho}{2\pi} \cdot \ln\left(\frac{2 \cdot L + \sqrt{4 \cdot L^2 - D^2}}{D}\right)$$

Additional term, to take into account of the soil surface heat transfer:

Eq. 3-2 $$T_4' = \frac{\rho}{2\pi} \cdot \left(1.9 \cdot \frac{\beta \cdot \cos\vartheta}{\rho \cdot d'}\right)$$

where:

β is the soil surface thermal resistivity expressed in K.m^2/W,

ρ is the soil thermal resistivity expressed in K.m/W,

ϑ is the angular position of the isotherm of the reference cable,

and the other terms have the meaning shown in Figure 3-1.

In Eq. 3-2, looking to Figure 3-1, d' is the distance between the two thermal charges which are not in the cable centres, due to the thermal proximity effect. In a first approximation, by disregarding the terms of inferior order, it is possible to write:

$$d' = 2 \cdot (L - \varepsilon_1)$$

where :

$$\varepsilon_1 = \frac{D^2}{8L}$$

is the displacement of the thermal charge from the cable geometric centre Figure 3-1

Inserting d' in Eq. 3-2, taking the point P as reference, and hence $\vartheta = 0$, the additional thermal resistance results:

Eq. 3-3 $$T_4' = \frac{1}{2\pi} \cdot \left(1.9 \cdot \frac{\beta}{\left(2L - \frac{D^2}{4L} \right)} \right)$$

When three single core cables in flat formation are considered, the thermal resistance of the hottest cable, that is the central one, is carried out with superimposition principle, which states that the thermal resistance is the sum of the Kennelly term referred to the central cable, plus two terms of mutual heating each with the following expression:

Eq. 3-4 $$T_4' = \frac{\rho}{2\pi} \ln \left(\frac{\sqrt{4L^2 + s^2}}{s} \right)$$

and three terms of soil surface resistance with formal expressions like those of Electra 125[2] and King *et al*[3] that is:

Eq. 3-5 $$T_{4a}' = \frac{\rho}{2\pi} \cdot \left(1.9 \cdot \frac{\beta \cdot \cos\vartheta}{\rho \cdot d'} \right)$$

where, for each of the other two cables, d' can be approximated with a good precision by Figure 3-2:

Eq. 3-6 $$d' \cong \sqrt{4 \cdot L^2 + s^2}$$

Moreover taking into account that with a good approximation

Eq. 3-7 $$\cos(\vartheta) = \frac{2L}{\sqrt{4 \cdot L^2 + s^2}}$$

the sum of the additional terms of mutual heating, by inserting in Eq. 3-5 the Eq. 3-6 and Eq. 3-7, and doubling, is:

Eq. 3-8 $$T_{4a}' = \frac{1}{\pi} \cdot \left(1.9 \cdot \frac{\beta \cdot 2L}{\left(4 \cdot L^2 + s^2 \right)} \right)$$

In conclusion the additional term due to the soil surface thermal resistance is expressed by the sum of Eq. 3-3 and Eq. 3-8.

3.3 Method using an Equivalent Layer

In order to verify the additional thermal term previously defined, a method using an equivalent layer is adopted[3]. Using this method, the heat transfer q at the soil surface is assumed as:

Eq. 3-9 $$q = \frac{(\vartheta_s - \vartheta_a)}{\beta}$$

where ϑ_s and ϑ_a the soil and air temperatures respectively, while the others terms have known meaning. This term takes into account the convection and the radiation heath transfer.

The main assumptions in the approach are:

1) there is on the soil surface a very thin layer over which the temperature is isothermal,

2) the thickness of this layer is evaluated in such a way that its equivalent thermal resistivity is equal to that of the soil

3) the thickness - δ - of the layer is such that $\delta << L$, so that it is possible to assume a temperature linear variation in it.

Due to this last assumption it is possible to write along the normal to the surface of the soil:

Eq. 3-10 $$q = \frac{1}{\rho}\frac{\partial \vartheta}{\partial n} = \frac{\left(\vartheta_s - \vartheta_a\right)}{\delta}$$

where the symbols have the known meaning.

Equating Eq. 3-9 and Eq. 3-10:

Eq. 3-11 $$\delta = \frac{\beta}{\rho}$$

The thermal resistance of the soil can be written, by using the symbols of Figure 3-3, as follows:

Eq. 3-12 $$T_4 = \frac{\rho}{2\pi}\cdot\left[\ln\left(\frac{2\cdot h_1 + \sqrt{4\cdot h_1^2 - D^2}}{D}\right) + 2\cdot\ln\left(\frac{\sqrt{h_1^2 + s^2}}{s}\right)\right]$$

The aim of this document is to show that this approach gives the same results of that considered in the previous paragraph.

By inserting in Eq. 3-12 the expression of h_1 (see Figure 3-3), it is possible to write:

Eq. 3-13 $$T_4 = \frac{\rho}{2\pi}\cdot\left[\ln\left(\frac{2\cdot(L+\delta) + \sqrt{4\cdot(L+\delta)^2 - D^2}}{D}\right) + 2\cdot\ln\left(\frac{\sqrt{4\cdot(L+\delta)^2 + s^2}}{s}\right)\right]$$

The first term of the T_4 can be rewritten after some algebraic passages and developments in series (see paragraph 3.5), as follows:

Eq. 3-14 $$T_4 = \frac{\rho}{2\pi}\cdot\left[\ln\left(\frac{2\cdot L + \sqrt{4\cdot L^2 - D^2}}{D}\right) + \frac{2\delta}{\sqrt{4\cdot L^2 - D^2}}\right]$$

Inserting the expression of δ from Eq. 3-11 the additional term which accounts for the soil surface thermal resistance (second term in square bracket) is written as:

$$T_{4a} = \frac{1}{2\pi}\cdot\frac{2\cdot\beta}{\sqrt{4\cdot L^2 - D^2}}$$

which, by the development in series of $\sqrt{4\cdot L^2 - D^2} = 2L - \frac{D^2}{4L}$, gives the same term (Eq. 3-3), apart from the value 2 in place of the value 1.9:

Eq. 3-15 $$T_4' = \frac{1}{2\pi}\cdot\left(2\cdot\frac{\beta}{\left(2L - \frac{D^2}{4L}\right)}\right)$$

The second term in T_4 of Eq. 3-13 is the mutual thermal resistance due to the two adjacent cables and, after some algebraic passages and developments in series (see Appendix I), can be written as follows:

Eq. 3-16 $$T_{4a}' = \frac{\rho}{2\pi}\cdot\left[2\cdot\ln\left(\frac{\sqrt{4\cdot L^2 + s^2}}{s}\right) + 2\cdot\frac{2L\delta}{4\cdot L^2 + s^2}\right]$$

The second term in square bracket accounts for the additional soil surface thermal resistance due to the two adjacent cables. Inserting in it the Eq. 3-11 it can be written as:

Eq. 3-17 $$T'_{4a} = \frac{1}{2\pi} \cdot \frac{2 \cdot \beta \cdot L}{4 \cdot L^2 + s^2}$$

which is, apart from the value 2 in place of the value 1.9, the same as Eq. 3-8.

3.4 Conclusions

The thermal resistance of three single core cables buried in flat formation and equally loaded, has been written taking into account of the additional thermal resistance due to the heat exchange at the soil surface. This formula applies to cables not deeply buried, namely to GIL.

The development has been obtained starting from two different approach that, in any case, give the same practical results.

For calculation purposes the formula for the additional thermal resistance due to the soil surface thermal resistivity given in Electra 125[4], that is:

$$T'_4 = \frac{3.8 * \beta_t}{D_s \cdot \left(\frac{2 * L}{Ds} - 1 \right)} \cdot n_c$$

has been determined as a sum of three terms equal to that related to the central cable (Eq. 3-3).

Here a new formula here recommended for its simplicity since it takes into account the thermal resistance of the soil in its globality, is (Eq. 3-12) one, namely

$$T_4 = \frac{\rho}{2\pi} \cdot \left[\ln\left(\frac{2 \cdot h_1 + \sqrt{4 \cdot h_1^2 - D^2}}{D} \right) + 2 \cdot \ln\left(\frac{\sqrt{h_1^2 + s^2}}{s} \right) \right]$$

where:

$$h_1 = 2 \cdot \left(L + \frac{\beta}{\rho} \right)$$

L is the burial depth [m]

β is the soil surface thermal resistivity [m^2K/W]

ρ is the soil thermal resistivity [mK/W]

The formula has been verified by using a FEM method and its validity has been checked for a range of thickness δ of:

$$\delta \leq 0.5 \text{ m}$$

that, assuming a soil thermal resistivity of conduction of 1.2 mK/W gives:

$$\beta \leq 0.6 \ \frac{K \cdot m^2}{W}$$

3.5 Mathematical Developments

The first term in Eq. 3-13 is expressed in the argument:

$$2 \cdot (L + \delta) + \sqrt{4 \cdot (L + \delta)^2 - D^2} = 2 \cdot (L + \delta) + \sqrt{4L^2 + 8L\delta + 4\delta^2 - D^2}$$

where δ^2 can be disregarded being of second order. By following with the development it is:

$$2 \cdot (L + \delta) + \sqrt{4L^2 + 8L\delta - D^2} = 2 \cdot (L + \delta) + \sqrt{\left(4L^2 - D^2\right) \cdot \left(1 + \frac{8L\delta}{4L^2 - D^2}\right)} = 2 \cdot (L + \delta) + \sqrt{\left(4L^2 - D^2\right)} \cdot \sqrt{\left(1 + \frac{8L\delta}{4L^2 - D^2}\right)}$$

and by developing in series the last square row being $\frac{8L\delta}{4L^2 - D^2} << 1$ it is:

$$2\cdot(L+\delta)+\sqrt{\left(4L^2-D^2\right)}\cdot\sqrt{\left(1+\frac{8L\delta}{4L^2-D^2}\right)} = 2\cdot(L+\delta)+\sqrt{\left(4L^2-D^2\right)}\cdot\left(1+\frac{4L\delta}{4L^2-D^2}\right) = 2\cdot(L+\delta)+\sqrt{\left(4L^2-D^2\right)}+\frac{4L\delta}{\sqrt{\left(4L^2-D^2\right)}}$$

After some algebraic passage, this last is rewritten in:

$$\left(2\cdot L+\sqrt{\left(4L^2-D^2\right)}\right)\cdot\left[1+\frac{2\delta}{\sqrt{\left(4L^2-D^2\right)}}\right]$$

Inserting this expression in the logarithm of Eq. 3-13 it is, by applying the log rules:

$$T_4 = \frac{\rho}{2\pi}\cdot\left[\ln\left(\frac{2\cdot L+\sqrt{4\cdot L^2-D^2}}{D}\right)+\ln\left(1+\frac{2\delta}{\sqrt{4\cdot L^2-D^2}}\right)\right]$$

and by developing in series the last log, possible since $\frac{2\delta}{\sqrt{4\cdot L^2-D^2}} << 1$ the Eq. 3-14 is obtained.

The second term in Eq. 3-13 is expressed in the argument:

$$\sqrt{4\cdot(L+\delta)^2+s^2} = \sqrt{4L^2+8L\delta+\delta^2+s^2}$$

where δ^2 can be disregarded being of second order. By following with the development it is:

$$\sqrt{4L^2+8L\delta+s^2} = \sqrt{\left(4L^2+s^2\right)\cdot\left(1+\frac{8L\delta}{4L^2+s^2}\right)} = \sqrt{\left(4L^2+s^2\right)}\cdot\sqrt{\left(1+\frac{8L\delta}{4L^2+s^2}\right)}$$

By developing in series the last square row, possible, since $\frac{8L\delta}{4L^2+s^2} << 1$ it is:

$$\sqrt{\left(4L^2+s^2\right)}\cdot\left(1+\frac{4L\delta}{4L^2+s^2}\right)$$

Inserting this expression in the logarithm of Eq. 3-13 it is, by applying the log rules:

$$T_4 = \frac{\rho}{2\pi}\cdot\left[\ln\left(\frac{\sqrt{4\cdot L^2+s^2}}{s}\right)+\ln\left(1+\frac{4L\delta}{4\cdot L^2+s^2}\right)\right]$$

and by developing in series the last log, possible since $\frac{4L\delta}{4\cdot L^2+s^2} << 1$ the Eq. 3-16 is obtained.

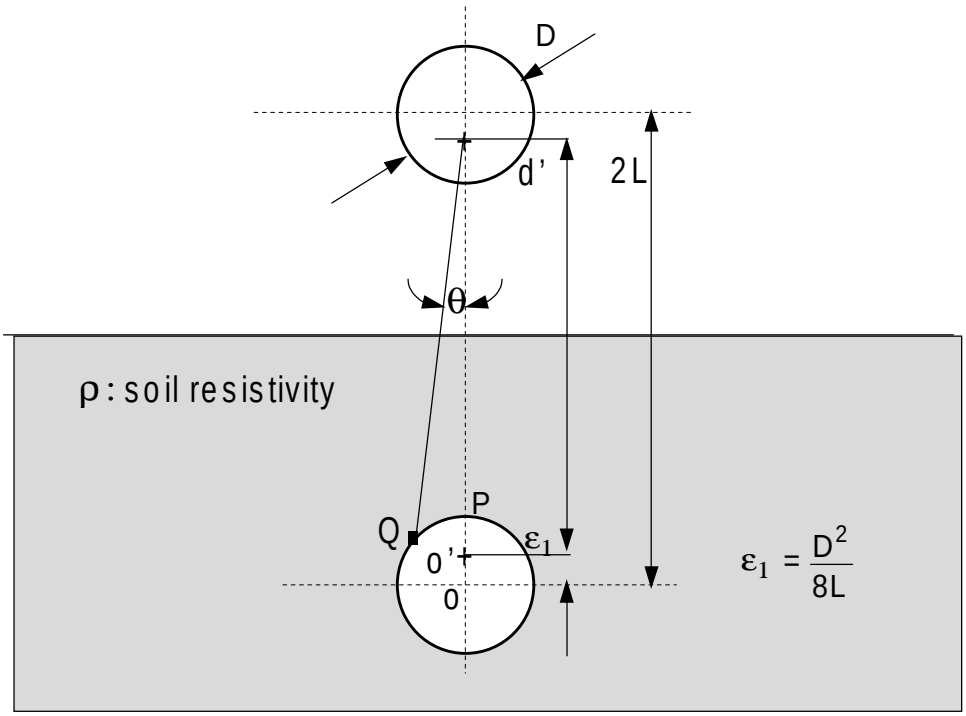

Figure 3-1: One cable and its image

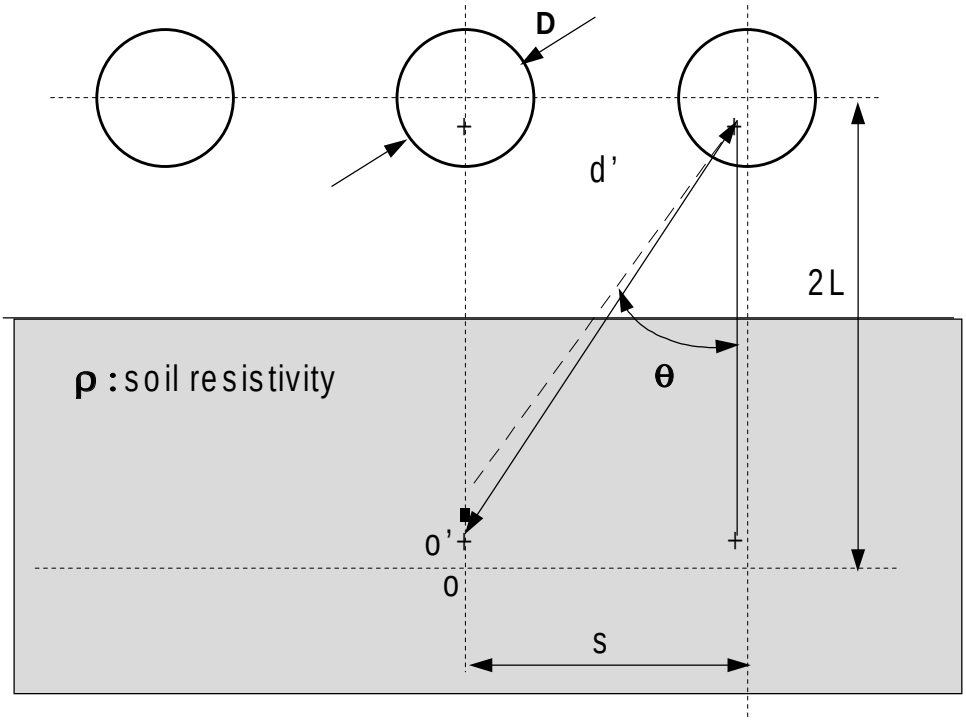

Figure 3-2: Three cables and their images

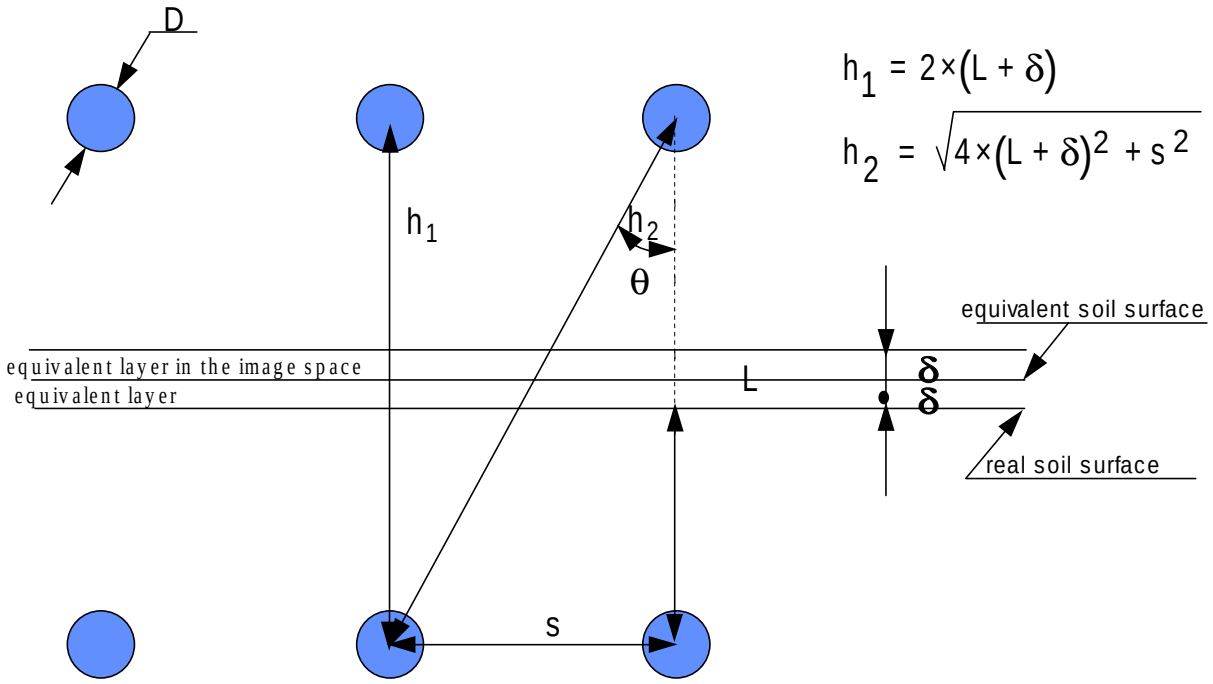

Figure 3-3: Method using an equivalent layer

3.6 References

[1] Electra N°125 (1989) 'Calculation of the continuous rating of three core, rigid type, compressed gas insulated cables in still air and buried'

[2] Neher, J.H. (1949) 'The Temperature Rise of Buried Cables and Pipes' AIEE Trans. Vol 68

[3] King, S.Y. Halfter, N.A. (1977) 'Underground Power Cables' Hong Kong University Press

[4] Electra N° 125, (1988) 'Calculation of the continuous rating of three-core, rigid type, compressed gas insulated cables in still air and buried' p.103,111

4 Appendix 4: Properties of the Gas Mixture

4.1 Free Convection Thermal Resistance of the Gas Mixture

Following the development carried out by Vermeer[1] a new formulation for the convective heat transfer between conductor and sheath in GIL has been reported in the present document.

The hypotheses for the new development, verified with extensive measurements by Lis *et al* [2] are:

The development of Vermeer[1], well represented by formula (10)[1], holds both for SF_6, N_2 and their mixtures.

In the range of temperature rise on the gas mixture prevailing for the GIL, the thermal resistivity of SF_6 and N_2 are very insensitive to the pressure and pressure variation[2].

The coefficient $C = c \cdot K$ (represented by the coefficient K0 in the previous CIGRÉ works[3], for example) is sensibly constant and fairly independent on the pressure and temperature rise of the gas mixture.

From equations (11), (14) and (18) of Vermeer[1] the expression of "C" :

$$C = 0.1638 \cdot F(p = 1, t)$$

and by equation (13)[1]:

Eq. 4-1
$$C = 0.1638 \cdot \left[\frac{\left(\rho \big|_{p=1} \right)^2 \cdot \lambda^2 \cdot c_p}{\eta} \right]^{\frac{1}{3}}$$

Since from the hypotheses 1, 2 and 3 the coefficient C in Eq. 4-1 is fairly independent on the partial pressures of the gas mixture, it is possible to draw out from Eq. 4-1 an equivalent expression by substituting its parameters by their sum, weighted in volume content.

Assuming a mixture of the two gases SF_6 and N_2, and indicating for simplicity $\bar{\rho} = \rho \big|_{p=1}$, the constant C_m, representing C for the gas mixture, is:

Eq. 4-2
$$C_m = 0.1638 \cdot \left[\frac{\left(\bar{\rho}_{SF6} \cdot V_{SF6} + \bar{\rho}_{N2} \cdot V_{N2} \right)^2 \cdot \left(\lambda_{SF5} \cdot V_{SF6} + \lambda_{N2} \cdot V_{N2} \right)^2 \cdot \left(c_{pSF6} \cdot V_{SF6} + c_{pN2} \cdot V_{N2} \right)}{\eta_{sf6} \cdot V_{SF6} + \eta_{N2} \cdot V_{N2}} \right]^{\frac{1}{3}}$$

where

V_{SF6} and V_{N2} indicate the percentage content in volume of the two gases

Taking into account that $V_{SF6} + V_{N2} = 1$, it is also:

Eq. 4-3
$$V_{N2} = 1 - V_{SF6}$$

Eq. 4-2 is a cumbersome expression, but a very good approximation is carried out by the following linear combination, that works for every volume content in the case of mixtures of gases SF_6 and N_2.

Eq. 4-4
$$C_m = 0.1638 \cdot \left\{ \left(V_{SF6} \right)^{0.75} \left[\frac{\bar{\rho}_{SF6}^{2} \cdot \lambda_{SF6}^{2} \cdot c_{pSF6}}{\eta_{SF6}} \right]^{\frac{1}{3}} + \left(V_{N2} \right)^{0.75} \left[\frac{\bar{\rho}_{N2}^{2} \cdot \lambda_{N2}^{2} \cdot c_{pN2}}{\eta_{N2}} \right]^{\frac{1}{3}} \right\}$$

On the basis of the development by Vermeer[1], since it is:

Eq. 4-5

$$\begin{cases} 0.1638 \cdot \left[\dfrac{\rho_{SF6}^{-2} \cdot \lambda_{SF6}^{\ 2} \cdot c_{pSF6}}{\eta_{SF6}} \right]^{\frac{1}{3}} = 11.3 \\ 0.1638 \cdot \left[\dfrac{\rho_{N2}^{-2} \cdot \lambda_{N2}^{2} \cdot c_{pN2}}{\eta_{N2}} \right]^{\frac{1}{3}} = 5.83 \end{cases}$$

the Eq. 4-4 can be rewritten by:

$$C_m = (V_{SF6})^{0.75} \cdot 11.3 + (V_{N2})^{0.75} \cdot 5.83$$

and introducing the Eq. 4-3

Eq. 4-6 $$C_m = (V_{SF6})^{0.75} \cdot 11.3 + (1 - V_{SF6})^{0.75} \cdot 5.83$$

Since, as already outlined the coefficient C is in different CIGRÉ papers indicated by the coefficient K_0 the Eq. 4-6 is rewritten by using this notation from now on.

Then it is:

Eq. 4-7 $$K_0 = (V_{SF6})^{0.75} \cdot 11.3 + (1 - V_{SF6})^{0.75} \cdot 5.83$$

The Figure 4-1 shows the behaviour of the Eq. 4-7, compared with the Eq. 4-2 and with a linear approximation represented by an equivalent expression given by a weighted average of the volume content of the two gases. This formula used in previous reports has the same structure of the of the Eq. 4-7, but the exponent of the percentage in volume is equal to 1 instead of 0.75, that is:

Eq. 4-8 $$K_0 = (V_{SF6}) \cdot 11.3 + (1 - V_{SF6}) \cdot 5.83$$

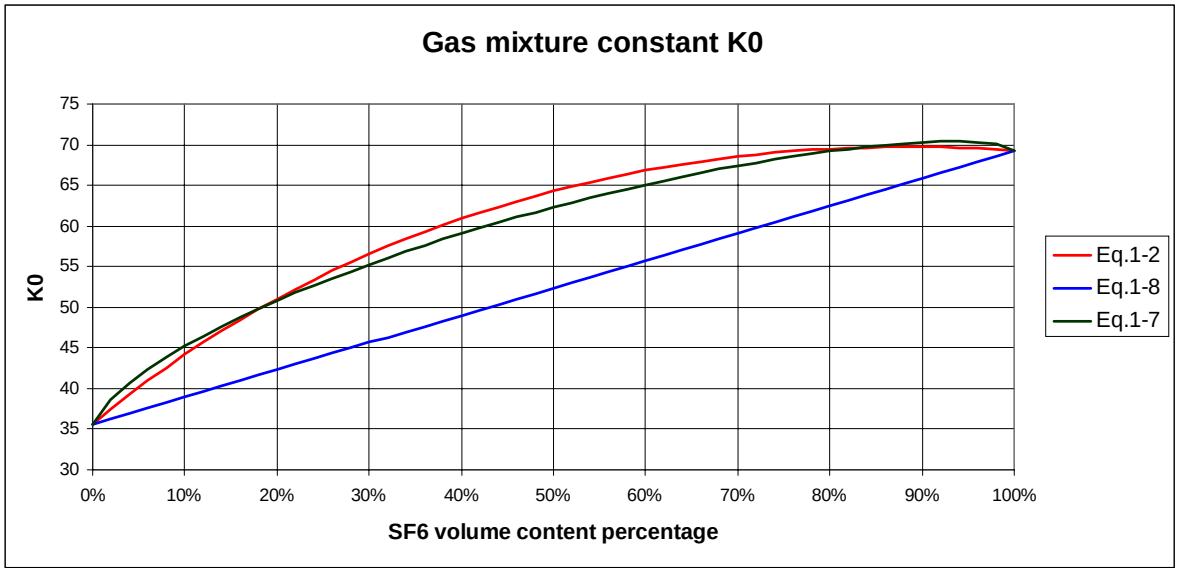

Figure 4-1: Method using an equivalent layer

As the Figure 4-1 shows the Eq. 4-7 fits the Eq. 4-8 with an error less than 3% everywhere, but with a better approximation in the interval of SF6 content up to 30% centred on the 20%.

In order to verify the formula Eq. 4-7, against the Eq. 4-8 chosen in previous documents, the same calculations reported in document[4] now followed.

Table 4-1 lists the data used in the calculations.

Table 4-1 Parameters, assumed in the calculations.

Quantity	Value	Unit
Conductor outside diameter	180.0	mm
Conductor thickness	11.0	mm
Conductor Electric Resistivity	$3.0\ 10^{-8}$	Ω.m
Conductor outer surface thermal emissivity	0.2	
Enclosure outside diameter	520.0	mm
Enclosure thickness	10	mm
Enclosure Electric Resistivity	3.510^{-8}	Ω.m
Enclosure inner surface thermal emissivity	0.2	
Anticorrosion external sheath thickness	0	mm
Gas mixture volume content	90% N_2 + 10% SF_6	
Absolute pressure of the gas mixture	9.0	bar
Ambient temperature	19.5	°C
Burial depth at the top of the anticorrosion sheath	1000	mm
Axial spacing	1120	mm

The GIL is in air, insulated with a layer of wool rock of 100 mm wound on the enclosure.

Since the enclosure temperature has been measured, in the calculations an equivalent external thermal resistivity suitable to find said enclosure temperature, is considered. Then, the enclosure temperature is assumed as reference value and the conductor temperature is calculated.

In calculations the following hypotheses have been applied:

The thermal resistance of the gas mixture insulation are carried out by using whether the Vermeer formula[1] or that of Itaka[5].

The convection coefficient K0 of the gas mixture is assumed as average, in volume content, of the coefficients of the two gases.

Table 4-2 shows the results obtained by using the old formula (Eq. 4-8), while Table 4-3 contains the results carried out with the new formula (Eq. 4-7).

Table 4-2 420 kV GIL.: Temperatures Measured and Calculated with the formula Eq. 4-8

	Measured	Calculated					
		Vermeer	**Itaka**	**Vermeer**	**Itaka**	**Vermeer**	**Itaka**
Equivalent Thermal resistivity		0.8	0.8	0.85	0.85	1	1
Current (A)	3000	3000	3000	3000	3000	3000	3000
Thermal resistivity eq.		0.8	0.8	0.85	0.85	1	1
Conductor losses (W/m)		56.8	56.5	57.3	56.9	58.7	58.3
Enclosure losses (W/m)		22.9	22.9	23.1	23.1	23.7	23.6
Total losses		79.7	79.4	80.4	80	81.4	81.9
Conductor temperature	67.3	**66.1**	**63.9**	**68.7**	**66.4**	**76.5**	**74.3**
Enclosure temperature	56.4	**54.6**	**54.4**	**57.1**	**56.8**	**64.8**	**64.6**
Temperature rise	10.9	11.5	9.5	11.6	9.6	11.7	9.7
Equivalent T4 (K.m/W)		0.44	0.44	0.467	0.467	0.55	0.55
T1 (W/m)		**0.203**	**0.169**	**0.202**	**0.168**	**0.200**	**0.166**

Table 4-3 420 kV GIL.: Temperatures Measured and Calculated with the formula Eq. 4-7

	Measured	Calculated					
		Vermeer	**Itaka**	**Vermeer**	**Itaka**	**Vermeer**	**Itaka**
Equivalent Thermal resistivity		0.8	0.8	0.85	0.85	1	1
Current (A)	3000	3000	3000	3000	3000	3000	3000
Thermal resistivity eq.		0.8	0.8	0.85	0.85	1	1
Conductor losses (W/m)		56.8	56.5	57.3	56.9	58.7	58.3
Enclosure losses (W/m)		22.9	22.9	23.1	23.1	23.7	23.6
Total losses		79.7	79.4	80.4	80	81.4	81.9
Conductor temperature	67.3	**66.3**	**64.0**	**68.8**	**66.6**	**76.7**	**74.4**
Enclosure temperature	56.4	**54.6**	**54.4**	**57.1**	**56.9**	**64.8**	**64.6**
Temperature rise	10.9	11.5	9.5	11.6	9.6	11.7	9.7
Equivalent T4 (K.m/W)		0.44	0.44	0.467	0.467	0.55	0.55
T1 (W/m)		**0.206**	**0.170**	**0.205**	**0.169**	**0.202**	**0.168**

Looking at the results, the new formula Eq. 4-7 shows:

- a maximum increase of the conductor temperatures in about $\frac{66.3-66.1}{66.1}=0.3\%$,
- the same enclosure temperature,
- a maximum increase of the gas mixture thermal resistance in about $\frac{0.205-0.202}{.202}=1.5\%$:

4.2 Conclusion

A method of calculating the convection coefficient for a mixture of gases has been developed. following the suggestions reported in Vermeer[1] and Lis et al[2].

The gas mixture convection coefficient, Ko, can be expressed by Eq. 4-7. This is consistent with the “similarity principle’ used to calculate heat transmission by convection.

4.3 Volumetric Specific Heat

Values of volumetric specific heats that may be useful in GIL overload calculations are given in Table 4-4, together with the thermal resistivity and electric resistivity at 20 °C.

Table 4-4 Thermal and electric parameters for overload calculations

Material	Thermal resistivity [K.m / W]	Volumetric specific heat [J / m^3.K]	Electric Resisistivity at 20 °C [Ω.m]
Copper	-	$3.45\ 10^6$	$1.7241\ 10^{-6}$
Aluminium	-	$2.5\ 10^6$	$2.8264\ 10^{-6}$
Lead or Lead alloy	-	$1.45\ 10^6$	$21.4\ 10^{-6}$
Steel	-	$3.8\ 10^6$	$13.8\ 10^{-6}$
Stainless Steel	-	$3.8\ 10^6$	$70\ 10^{-6}$
Bronze	-	$3.4\ 10^6$	$3.5\ 10^{-6}$
Paper oil filled	5.0	$2.0\ 10^6$	-

PE	3.5	$2.4\ 10^6$	-
XLPE	3.5	$2.4\ 10^6$	-
PVC	6.0	$1.7\ 10^6$	-
EPR	5.0	$2.0\ 10^6$	-
Rubber	5.0	$2.0\ 10^6$	-
Butyl Rubber	5.0	$2.0\ 10^6$	-
Concrete	1.0	$1.9\ 10^6$	-
Fibre for duct	4.8	$2.0\ 10^6$	-
Earthenware	1.2	$1.7\ 10^6$	-

Concerning to the insulating gas specific heat the following considerations apply:

from Vermeer[1] the nitrogen (N_2) physical characteristics, within the operating ranges:

$10 < p_{N2}$ (pressure) < 30 bar

30 °C < t (temperature) < 90°C

are:

Eq. 4-9 density $\rho = \frac{337.4}{273 + t} \cdot p_{N2}$ $\frac{kg}{m^3}$

Eq. 4-10 specific heat at constant pressure $c_p = 1037 + 0.101 \cdot t$ $\frac{J}{K\,kg}$

and for SF_6 gas, within the operating ranges:

$2 < p_{SF6}$ (pressure) < 6 bar

30 °C < t (temperature) < 90°C

Eq. 4-11 density $\rho = \frac{1666}{230 + t} \cdot p_{SF6}$ $\frac{kg}{m^3}$

Eq. 4-12 specific heat at constant pressure $c_p = 630 + 1.87 \cdot t - 4.33 \cdot 10^{-3} \cdot t^2$ $\frac{J}{K\,kg}$

In the thermal transient calculation the specific heat must be taken at constant volume, so that the following formulae applies for the two gases:

Eq. 4-13 $c_v = \frac{c_p \cdot \rho}{k}$ $\frac{J}{K\,m^3}$

Where ‘k’ is the ratio between the specific heats at constant pressure and constant volume.

The values of k are:

N_2 gas k = 1.4

SF_6 gas k = 1.33

In gas mixtures the volumetric specific heat is given by:

Eq. 4-14 $c_v = \sum_i p_i \cdot c_{vi}$

being

p_i the partial pressure of each gas

c_{vi} the volumetric specific heat of each gas

Indicating with V_i the volume ratio of the two gases, that is

V_{N2} = 95%

V_{SF6} = 5%

the partial pressures of each gas is given by

Eq. 4-15
$$p_{N2} = V_{N2} \cdot p$$
$$p_{SF6} = V_{SF6} \cdot p$$

being p the total pressure of the mixture.

Inserting the Eq. 4-15 in Eq. 4-9 and Eq. 4-11, and using the Eq. 4-13 together with Eq. 4-10 and Eq. 4-12 , the volumetric specific heat of the mixture is carried out with the Eq. 4-14:

Eq. 4-16
$$c_v = \left[\frac{337.4}{273+t} V_{N2} \cdot \frac{1037 + .101 \cdot t}{1.4} + \frac{1666}{230+t} V_{SF6} \cdot \frac{630 + .1.87t - 4.33 \cdot 10^{-3} \cdot t^2}{1.33} \right] \cdot p$$

Figure 4-2 shows the Eq. 4-16 evaluated for different mixture pressure and as a function of the temperature. The temperature range has been extrapolated up to 120 °C; the suitability of that extrapolation must be carefully discussed in the next meeting.

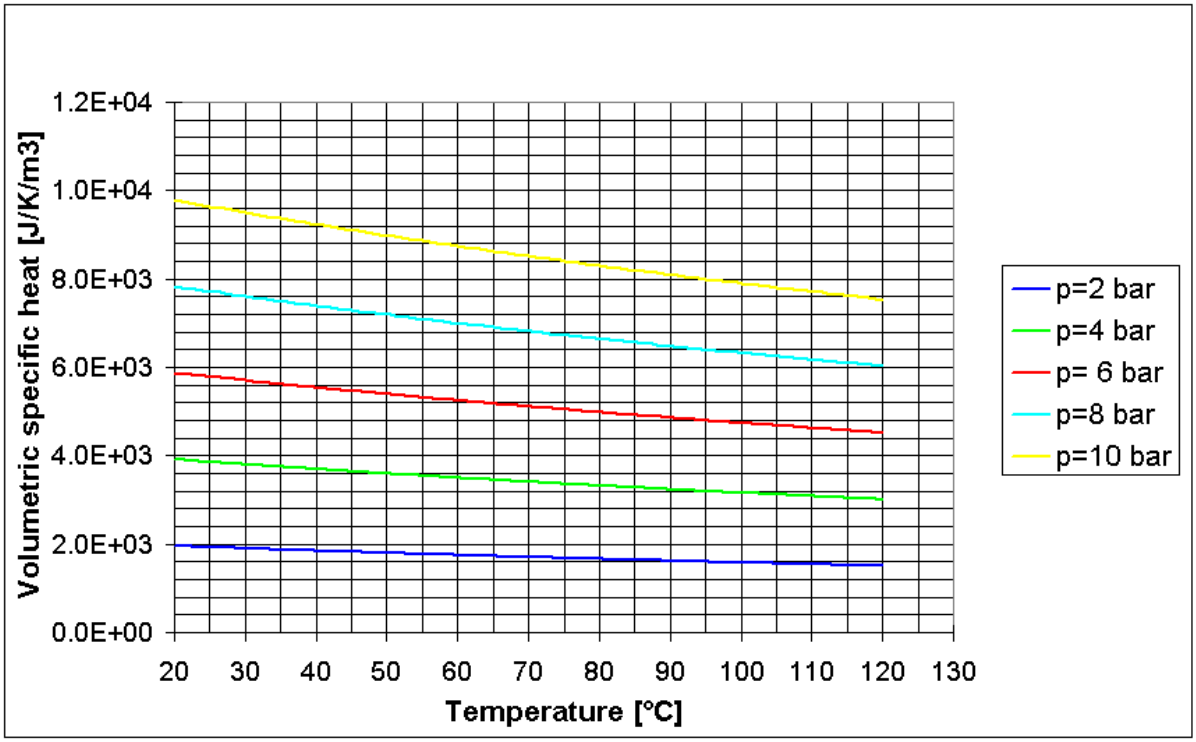

Figure 4-2: Example of volumetric specific heat Gas Mixture with volumetric ratio 95% N2 + 5% SF6

4.4 References

[1] Vermeer, J. 'A Simple Formula for the Calculation of the Convective Heat Transfer Between Conductor and Sheath in Compressed Gas Insulated Cables.' Electra No.87.

[2] Lis, J. and Kellard, P.O. (1965) 'Measurements of the thermal conductivity of sulphur hexafluoride and a 50% (volume) mixture of sulphur hexafluoride and nitrogen.' *BRIT. J. APLL. PHYS.* Vol. 16.

[3] Electra No. 100 (May 1985) 'Calculation of the Continuous Rating of Single Core, Rigid Type, Compressed Gas Insulated Cables in Still Air with No Solar Radiation' pp 65-75.

[4] Cigre JWG33 'Comparison between experimental results and calculation for 420 kV GIL'.

[5] Itaka, K. Araki, T. and Hara, T. (1978) 'Heat Transfer Characteristics of Gas Spacer Cables' *IEEE Transactions on Power Apparatus and Systems* Vol PAS – 97 No. 5 Sept/Oct 1978 pp 1579 -1585.

5 Appendix 5: Example of Continuous Rating Calculation

The results of continuous current ratings for a GIL having the dimensions given in Appendices 1 and 7 are shown below.

Table 5-1 shows the calculated maximum current rating to be 2886A where the maximum soil temperature is limited to 60°C.

Table 5-2 shows the calculated maximum soil temperature to be 64°C when the GIL is carrying 3000A.

Table 5-1 First calculation maximum soil temperature equal to 60°C

Current rating	2885.84	(A)
C.c Conductor resistance at the maximum temperature	3.08E-06	(Ω/m)
Conductor skin effect	1.21E-01	
C.a Conductor resistance at the maximum temperature	3.45E-06	(Ω/m)
C.c Enclosure resistance at the maximum temperature	3.41E-06	(Ω/m)
Enclosure skin effect	7.45E-03	
Loss factor due to current in the enclosure	9.93E-01	
C.a Enclosure resistance at the maximum temperature	3.44E-06	(Ω/m)
Convection heat losses between conductor and enclosure	2.24E+01	(W/m)
Radiation heat losses between conductor and enclosure	6.41E+00	(W/m)
Total power losses (conductor-enclosure)	2.88E+01	(W/m)
Thermal resistence between conductor and enclosure	1.99E-01	(K.m/W)
Thermal resistance of the surrounding soil	7.85E-01	(K.m/W)
Thermal resistance of outer serving	5.12E-03	(K.m/W)
Conductor losses	28.76	(W/m)
Enclosure losses	**28.56**	(W/m)
Current circulating in the eclosure	2882.75	(A)
Conductor temperature	66	(°C)
Enclosure temperature	60.29	(°C)
Maximum soil temperature (on outer serving)	60	(°C)

Table 5-2 Second calculation current rating equal to 3000A

Current rating	**3000.0**	(A)
C.c Conductor resistance at the maximum temperature	**3.13E-06**	(Ω/m)
Conductor skin effect	**1.17E-01**	
C.a Conductor resistance at the maximum temperature	**3.5E-06**	(Ω/m)
C.c Enclosure resistance at the maximum temperature	**3.46E-06**	(Ω/m)
Enclosure skin effect	**7.24E-03**	
Loss factor due to current in the enclosure	**9.95E-01**	
C.a Enclosure resistance at the maximum temperature	**3.49E-06**	(Ω/m)
Convection heat losses between conductor and enclosure	**2.44E+01**	(W/m)
Radiation heat losses between conductor and enclosure	**7.12E+00**	(W/m)

Total power losses (conductor-enclosure)	**31.48E+00**	(W/m)
Thermal resistance between conductor and enclosure	**1.94E-01**	(K.m/W)
Thermal resistance of the surrounding soil	**7.85E-01**	(K.m/W)
Thermal resistance of outer serving	**5.12E-03**	(K.m/W)
Conductor losses	**31.48**	(W/m)
Enclosure losses	**31.31**	(W/m)
Current circulating in the enclosure	**2996.69**	(A)
Conductor temperature	**70.71**	(°C)
Enclosure temperature	**64.62**	(°C)
Maximum soil temperature	**64.30**	(°C)

6 Appendix 6: Short Time Current Rating

The results of short time current ratings for a GIL having the dimensions given in Appendices 1 and 8 are given below using the method recommended in Section 3, which is based on Electra 87. The starting conditions for each of the following three cases is 100% full load (3000A) with a conductor temperature of 70.5°C and enclosure temperature of 65°C.

The data assumed for the calculations are the standard one and are reported in Table 6-1

Table 6-1 Parameters and values in GIL assumed as reference

Quantity	Value	Unit
Line Voltage	400	kV
Frequency	50	Hz
Current Rating 100% of the load factor	3000	A
Conductor outside diameter	280	Mm
Conductor thickness	16	Mm
Conductor Electric Resistivity	$3.45.10^{-8}$	Ω.m
Conductor outer surface emissivity	0.2	
Enclosure outside diameter	650	Mm
Enclosure thickness	10	Mm
Enclosure Electric Resistivity	$5.9.10^{-8}$	Ω.m
Enclosure inner surface emissivity	0.2	
Anticorrosion external sheath diameter	656	Mm
Anticorrosion external sheath thickness	3	Mm
Anticorrosion sheath thermal resistivity	3.5	K.m/W
Dielectric (Gas mixture)	90% N_2 + 10% SF_6	
Absolute pressure of the gas mixture	6.7	Bar
Soil and stabilised backfill thermal resistivity	1.2	K.m/W
Soil surface thermal resistivity	0.20	$K.m^2/W$
Soil ambient temperature	15	°C
Burial depth at the top of the anticorrosion sheath	1050	Mm
Conductor volumetric specific heat	$2.5\ 10^6$	$J/K/m^3$
Enclosure volumetric specific heat	$2.5\ 10^6$	$J/K/m^3$
Anticorrosion sheath volumetric specific heat	$2.4\ 10^6$	$J/K/m^3$
Soil thermal diffusivity	$0.4\ 10^{-6}$	m^2/s
Earthing	Enclosure solid bonded	
Axial spacing	1312	Mm

Figure 6-1 applies a 33% overload (4000A). The temperatures after 50hrs are 80.5°C on the conductor and 71°C on the enclosure.

Figure 6-2 applies a 166% overload (8000A). The temperatures after 8hrs are 115°C on the conductor and 87°C on the enclosure.

Figure 6-3 applies a 300% overload (12000A). The temperatures after 2.5hrs are 129°C on the conductor and 87°C on the enclosure.

The results are compared with calculations using the finite element method. The formulae par. 3.1 (Eq. 17, 18 & 19) were programmed, where necessary as user subroutines within the computational code, to represent the heat transfer by convection and radiation.

The Figure 6-1 to Figure 6-3 show the comparison between the two methods.

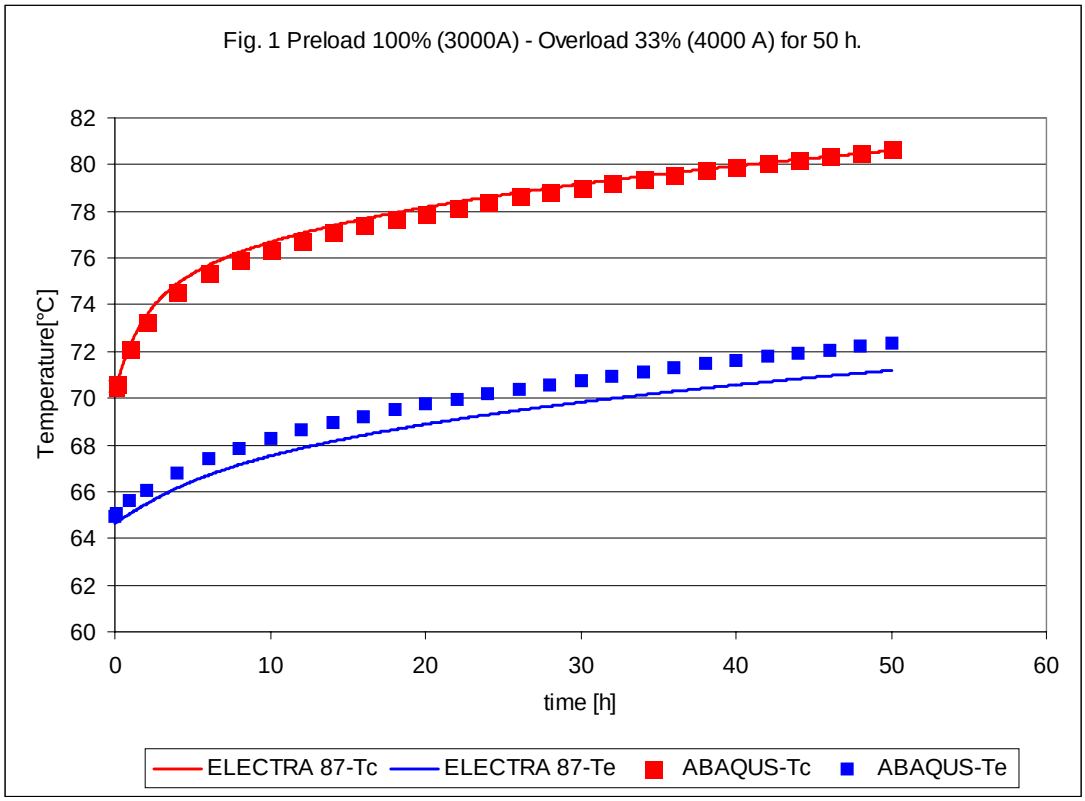

Figure 6-1: Preload 100% (3000A) – Overload 33% (4000A) for 50h

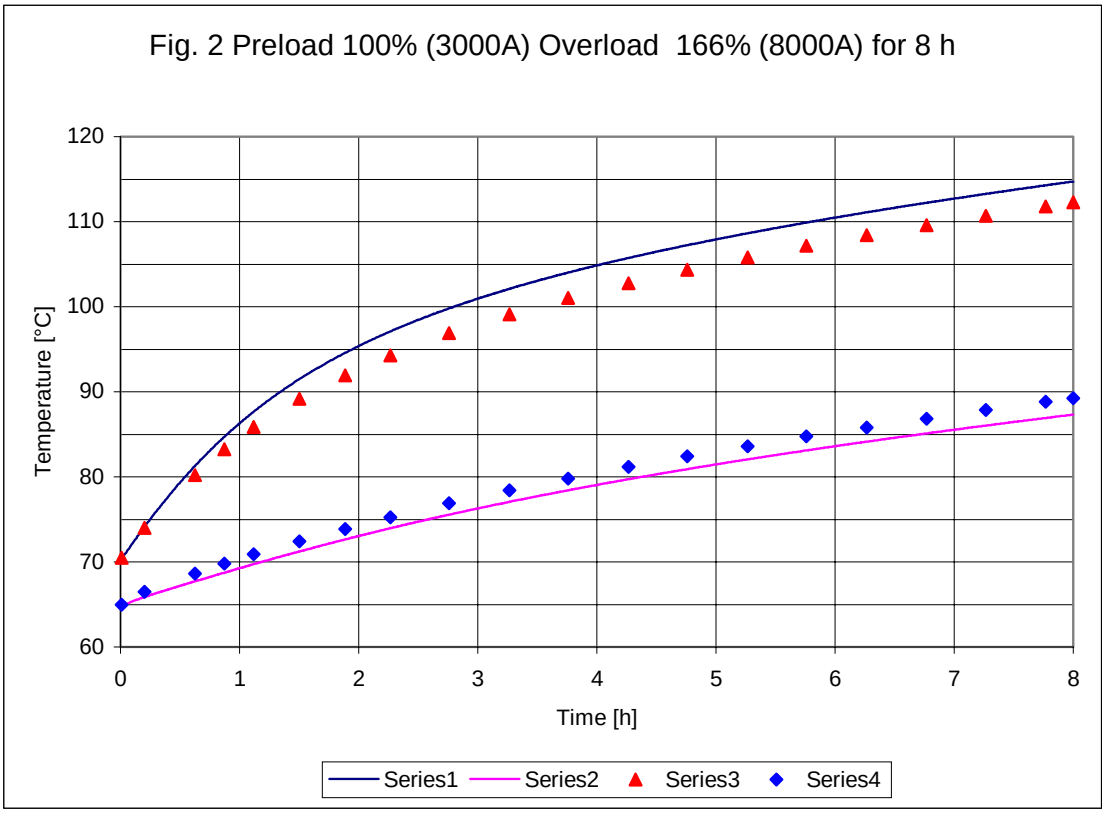

Figure 6-2: Preload 100% (3000A) – Overload 166% (8000A) for 8h

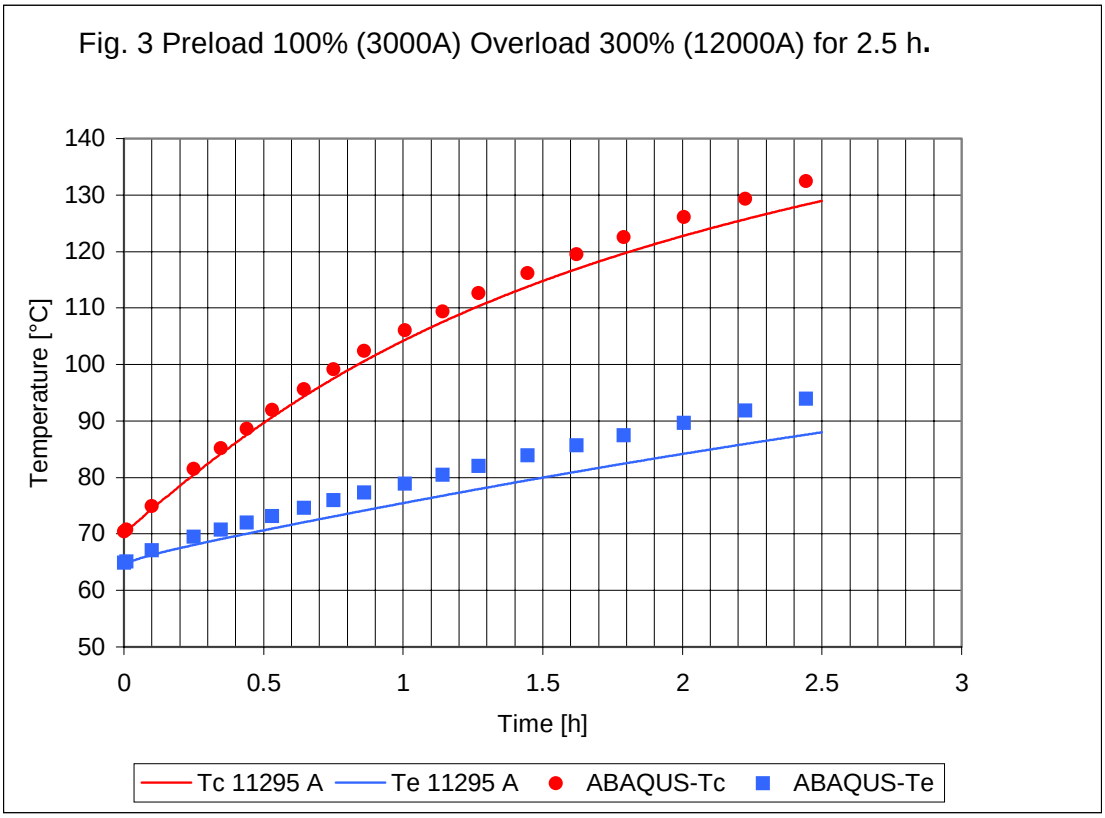

Figure 6-3: Preload 100% (3000A) – Overload 300% (12000A) for 2.5

7 Appendix 7: Continuous Rating Sensitivity Study

7.1 GIL Rating Parameter Sensitivity Study

This study applies the recommended formulae for continuous rating (given in Part A Section 2) to an example GIL application. The study assesses the sensitivity of the GIL current rating to variations in the value of each of its key parameters.

The example application is for single phase GIL in flat formation under continuous loading. The purpose of this study is to rank the parameters in the order of the largest to the smallest effect on the magnitude of the rating, with the objectives of identifying**:**

1) The most important rating parameters for prospective future GIL applications.

2) The effect that inaccuracy in each design, installation or calculation parameter could have on the final rating.

The rating calculations were applied to yield the following results:

1) The resulting current ratings for either a range of selected maximum conductor operating temperatures or maximum soil temperature limits (i.e. the soil adjacent to the sheath).

2) The resulting maximum operating temperature of the conductor or soil for a rating of 3000 Amps.

It should be noted that recommended operating temperatures for GIL do not exist for buried applications. Recommended temperature limits exist for the conductor connectors in SF_6, or a mixture of SF_6 [IEC694 Table 3][1]. The maximum continuous operating temperatures for connectors are given as 90^{o}C for tinned coated contacts, 105^{o}C for bare copper contacts and 105^{o}C for silver coated contacts. For the standard GIL dimensions studied, an arbitrary 75^{o}C conductor temperature resulted in a current rating of 3098 Amps.

Recommended limits exist for the maximum soil temperatures for conventional cables to prevent thermal instability by the progressive increase of soil thermal resistivity as a result of moisture migration. The practices in each Country are listed in IEC287 [2]. For example the maximum permissible soil temperature in the UK is taken as 50^{o}C and the maximum temperature in France as 60^{o}C. For the standard GIL dimensions studied a 60^{o}C soil temperature resulted in a current rating of 2886A.

Table 7-1: Reference parameters and values taken for the GIL sensitivity study

Quantity	Value	Unit
Conductor outside diameter	280	mm
Conductor thickness	16	mm
Conductor electric resistivity	$3.45\ 10^{-8}$	Ω.m
Conductor outer surface emissivity	0.2	
Enclosure outside diameter	650	mm
Enclosure thickness	10	mm
Enclosure electric resistivity	$5.9.10^{-8}$	Ω.m
Enclosure inner surface emissivity	0.2	
Anticorrosion external sheath diameter	656	mm
Anticorrosion external sheath thickness	3	mm
Anticorrosion sheath thermal resistivity	3.5	K.m/W
Dielectric (gas mixture)	90% N_2 + 10% SF_6	
Absolute pressure of the gas mixture	6.7	bar
Soil and stabilised backfill thermal resistivity	1.2	K.m/W
Soil surface thermal resistivity	0.20	$K.m^2/W$
Soil ambient temperature	15	°C
Burial depth to the top of the anticorrosion sheath	1050	mm

Earthing	Enclosure solid bonded	
Axial spacing	1312	mm

The individual parameters are listed in Table 7-1. In the sensitivity study, the magnitude of each parameter was changed by ±50%. The resulting effect on either current rating or operating temperature was then calculated as a percentage variation, with the convention: '+' increasing and '-' decreasing.

It should be noted that this sensitivity study is not meant to give either the optimum GIL dimensions, installation dimensions, operating temperatures or current ratings. These are best left to the designer for each particular application.

Table 7-2 shows the parameters taken into consideration in the sensitivity study with the main values and their identifying symbols. The central column of the table shows the standard value of each parameter. Note that the axial spacing of 656 mm corresponds to a 'just touching' cable situation. Also the ±25% variation of each parameter is considered in the calculations in order to check that the rate of change is the same as for ±50%.

Table 7-2: Interval of variation of the parameters in the sensitivity study

Parameter	Symbol	-50% of the standard value	Standard value	+50% of the standard value	Unit
Axial Spacing	AS	656	1312	1968	mm
Burial depth (top of the anticorrosion sheath)	L	525	1050	1575	mm
Conductor diameter	Dc	140	280	420	mm
Conductor thickness	sc	8	16	24	mm
Enclosure diameter	De	325	650	975	mm
Enclosure thickness	se	5	10	15	mm
Soil surface thermal resistivity	beta	0.1	0.2	0.3	$K.m^2/W$
Soil thermal resistivity	Rs	0.6	1.2	1.8	K.m/W
Conductor and enclosure thermal emissivity	sigma	0.1	0.2	0.3	
Gas mixture pressure	p	3.35	6.7	10.05	Bar abs.
SF_6 thermal convection constant	K1	5.65	11.3	16.95	
N_2 thermal convection constant	K2	2.915	5.83	8.745	
SF_6 Volume content	Vc	5	10	15	%
Conductor electric resistivity	Cr	$1.725.10^{-8}$	$3.45.10^{-8}$	$5.175.10^{-8}$	Ωm
Enclosure electric resistivity	Er	$2.95.10^{-8}$	$5.9.10^{-8}$	$8.85.10^{-8}$	Ωm

7.2 Sensitivity study on Current Rating for Selected Maximum Conductor or Soil Temperature Limits

The Tables and Figures from 1 to 30 show the current rating calculated at the parameter values of Table 7-2 and their intermediate values. The current rating calculations are referred to the maximum soil temperature (temperature at the anticorrosion sheath and soil interface) and to the conductor temperature respectively.

In the last two columns of each table the percentage variations of the current rating, for the assumed ±50% variation of the parameter, are shown, calculated as in the following expression:

$$Crpv(\pm 50\%) = \frac{I(\pm 50\%)}{I(std)} - 1$$

where:

Crpv(±50%) is the current rating percent variation for the ±50% parameter variation,

I(std) is the current rating calculated at the parameter standard value

I(±50%) is the current rating calculated at the parameter variations.

The average value of the current rating variations are assessed and shown in the last two cells of each table.

7.2.1 Parameterised quantity: spacing between adjacent enclosures

Starting from the conditions of Table 7-1the spacing between adjacent GIL enclosures has been assumed to vary, with different pitches, starting from the space between enclosures equal to a 'just touching' condition (-50%) GIL diameter, up to +50% on GIL diameter. The current ratings have been reported in Table 7-3, Table 7-4 and Figure 7-1 Figure 7-2.

Table 7-3: Current rating (A) as a function of the GIL axial spacing and of the maximum soil temperature

Max soil temperature (°C)	AS= 656 [mm]	AS= 984 [mm]	AS= 1312 [mm]	AS= 1640 [mm]	AS= 1968 [mm]	Crpv(-50%)	Crpv(+50%)
40	1948	2099	2223	2328	2417	-12.4%	8.7%
50	2267	2442	2587	2708	2812	-12.4%	8.7%
60	2530	2725	2886	3021	3137	-12.3%	8.7%
70	2753	2966	3141	3288	3413	-12.3%	8.7%
80	2949	3175	3362	3520	3654	-12.3%	8.7%
90	3121	3361	3559	3725	3867	-12.3%	8.7%
100	3276	3527	3734	3909	4057	-12.3%	8.6%
					Average =	-12.3%	8.7%

Table 7-4 Current rating (A) as a function of the GIL axial spacing and of the conductor temperature

Conductor temperature (°C)	AS= 656 [mm]	AS= 984 [mm]	AS= 1312 [mm]	AS= 1640 [mm]	AS= 1968 [mm]	Crpv(-50%)	Crpv(+50%)
45	2007	2149	2263	2359	2439	-11.3%	7.7%
55	2292	2455	2587	2697	2789	-11.4%	7.8%
65	2533	2714	2861	2983	3086	-11.5%	7.9%
75	2742	2938	3098	3231	3343	-11.5%	7.9%
85	2926	3136	3308	3451	3571	-11.5%	8.0%
95	3091	3314	3496	3647	3775	-11.6%	8.0%
105	3240	3474	3665	3825	3959	-11.6%	8.0%
					Average=	-11.5%	7.9%

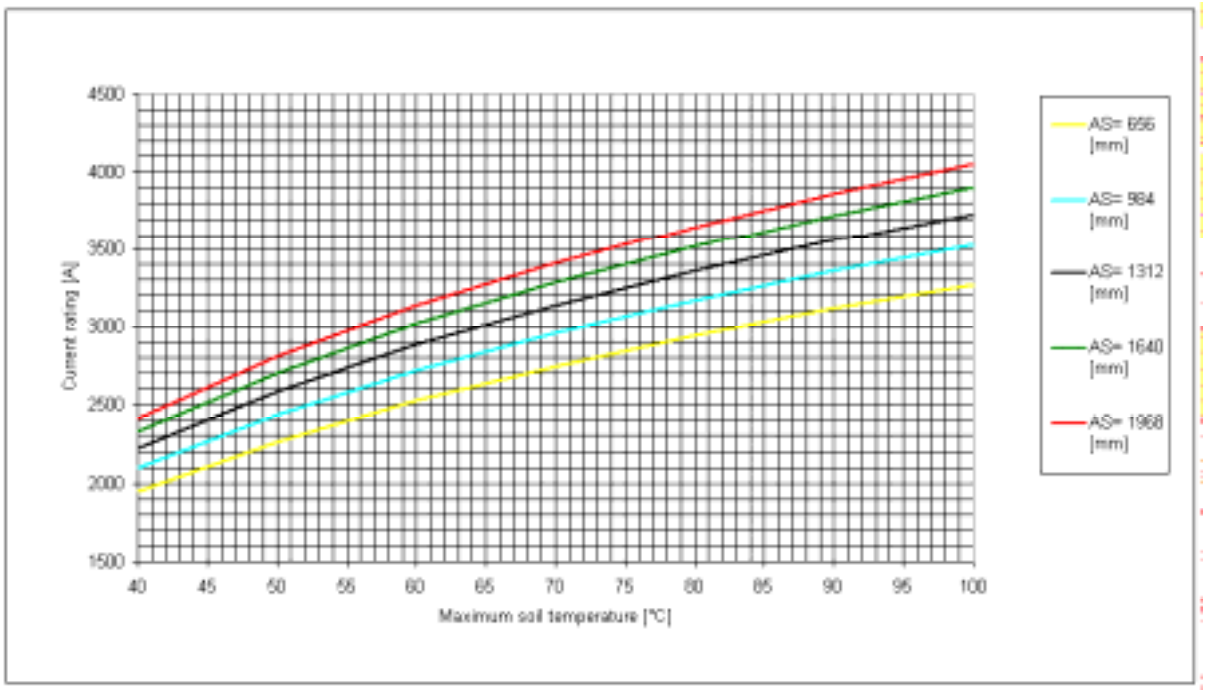

Figure 7-1: Current rating vs. Maximum soil temperature. Variable dimension: Axial Spacing (As) V=400 kV

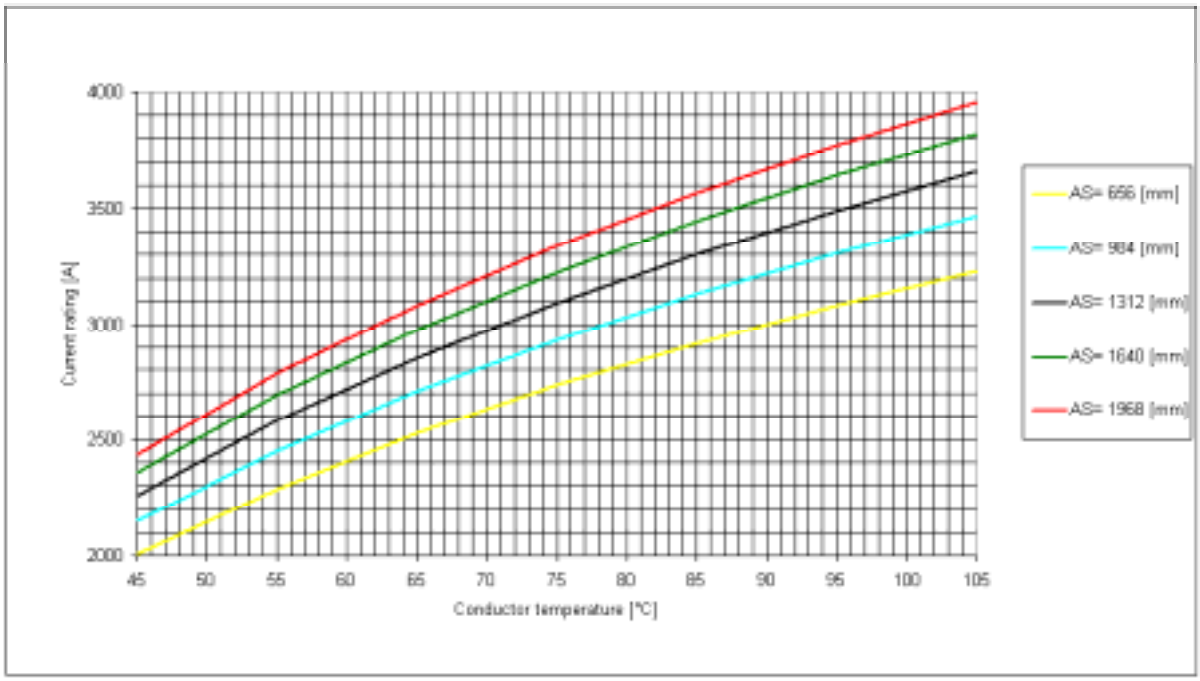

Figure 7-2: Current rating vs. Conductor temperature. Variable dimension: Axial Spacing. V=400 kV

From the Table 7-3 and Table 7-4 it is possible to see that the current rating variation at a given maximum soil temperature is of the order 15% for a variation in axial spacing of ±50%.

7.2.2 Parameterised Quantity: Burial Depth

Starting from the value of 1050 mm, measured at the top of the anticorrosion sheath, the burial depth increases with suitable pitches from 525mm to 1575mm.

The current ratings have been reported in Table 7-5 Table 7-6 and Figure 7-3 Figure 7-4. The last column shows the current rating variation for a variation burial depth of between ±50%.

Table 7-5: Current rating (A) as a function of the burial depth and of the maximum soil temperature

Max soil temperature (°C)	L = 525 [mm]	L =787.5 [mm]	L=1050 [mm]	L=1312.5 [mm]	L =1575 [mm]	Crpv(-50%)	Crpv(+50%)
40	2588	2371	2223	2115	2032	16.4%	-8.6%
50	3010	2758	2587	2461	2365	16.4%	-8.6%
60	3358	3077	2886	2746	2638	16.3%	-8.6%
70	3653	3348	3141	2989	2872	16.3%	-8.6%
80	3911	3584	3362	3200	3075	16.3%	-8.6%
90	4139	3793	3559	3387	3254	16.3%	-8.6%
100	4342	3980	3734	3554	3415	16.3%	-8.5%
					Average=	16.3%	-8.6%

Table 7-6 Current rating (A) as a function of the burial depth and of the conductor temperature

Conductor temperature (°C)	L = 525 [mm]	L =787.5 [mm]	L =1050 [mm]	L =1312.5 [mm]	L =1575 [mm]	Crpv(-50%)	Crpv(+50%)
45	2589	2397	2263	2164	2087	14.4%	-7.8%
55	2963	2741	2587	2472	2383	14.6%	-7.9%
65	3280	3032	2861	2733	2634	14.7%	-7.9%
75	3556	3285	3098	2959	2851	14.8%	-8.0%
85	3799	3509	3308	3159	3043	14.9%	-8.0%
95	4017	3709	3496	3338	3215	14.9%	-8.0%
105	4215	3890	3665	3499	3370	15.0%	-8.1%
					Average=	14.7%	-7.9%

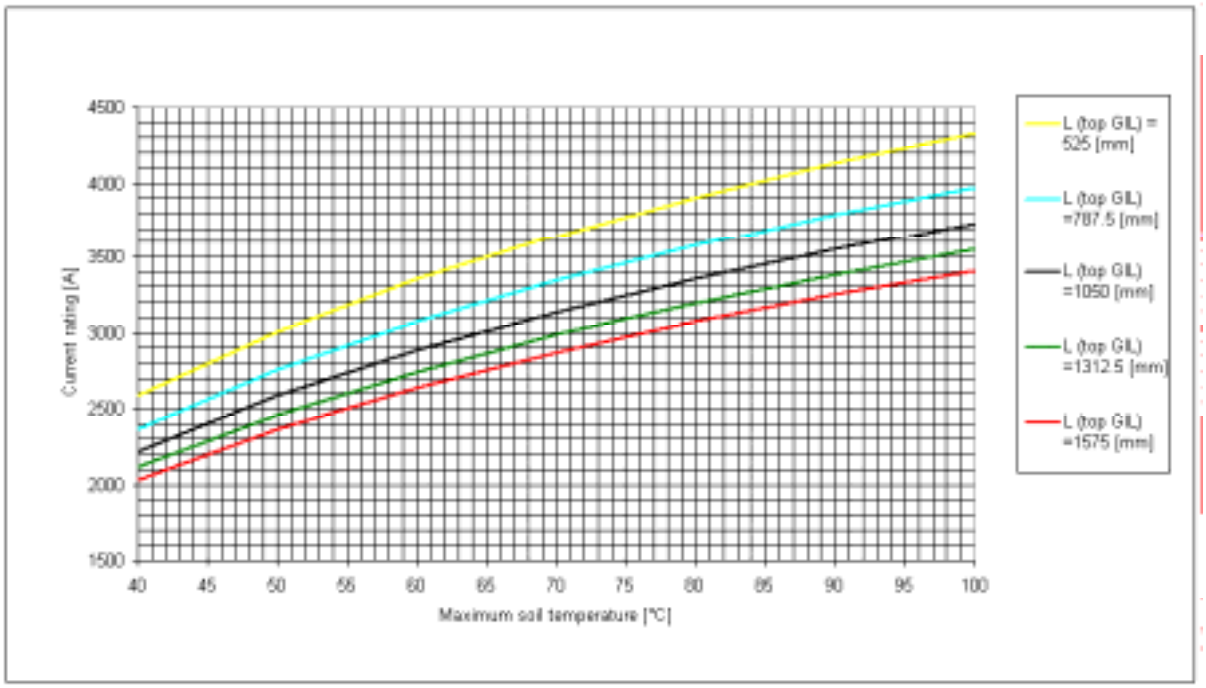

Figure 7-3: Current rating vs. Conductor temperature. Variable dimension: Axial Spacing. V=400 kV

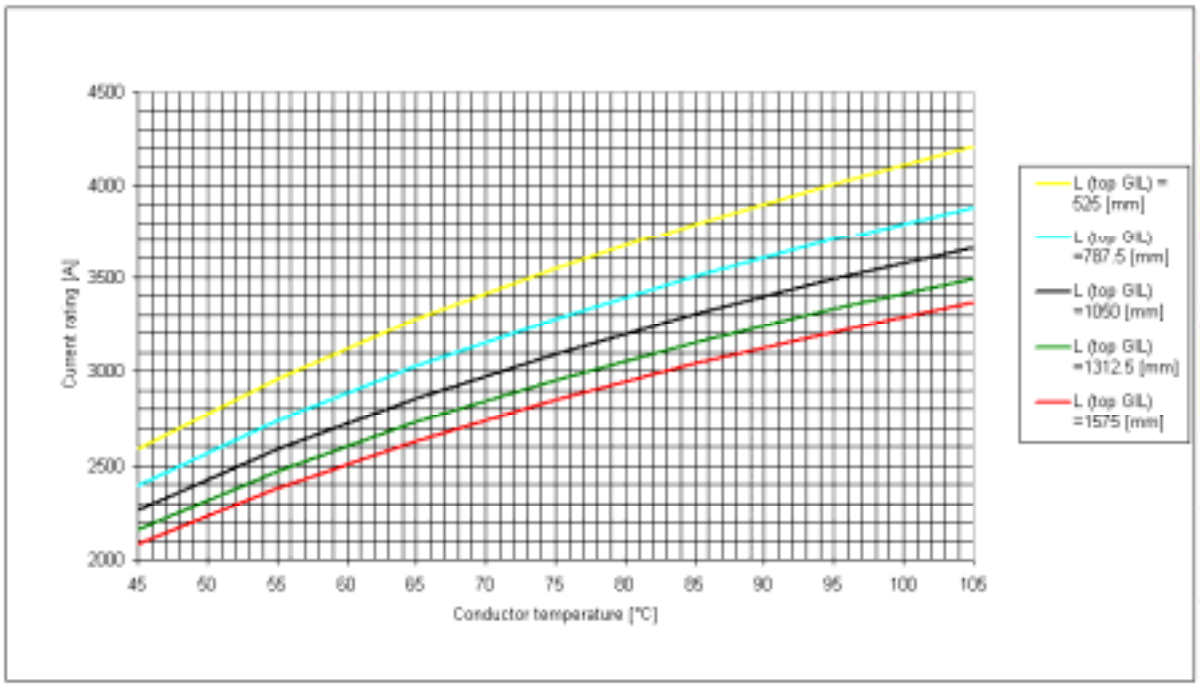

Figure 7-4 Current rating vs. Conductor temperature. Variable dimension: Burial depth. V=400 kV

7.2.3 Parameterised Quantity: Conductor Diameter

The conductor thickness was kept constant at 16 mm.

Table 7-7: Current rating (A) as a function of the conductor diameter and of the maximum soil temperature

Max soil temperature (°C)	Dc=140 [mm]	Dc=210 [mm]	Dc=280 [mm]	Dc=350 [mm]	Dc=420 [mm]	Crpv(-50%)	Crpv(+50%)
40	1774	2045	2223	2351	2447	-20.2%	10.1%
50	2062	2379	2587	2735	2847	-20.3%	10.1%
60	2300	2654	2886	3051	3176	-20.3%	10.0%
70	2501	2888	3141	3320	3455	-20.4%	10.0%
80	2677	3092	3362	3555	3699	-20.4%	10.0%
90	2833	3272	3559	3762	3915	-20.4%	10.0%
100	2972	3434	3734	3948	4108	-20.4%	10.0%
					Average=	-20.3%	10.0%

Table 7-8: Current rating (A) as a function of the conductor diameter and of the conductor temperature

Conductor temperature (°C)	Dc=140 [mm]	Dc=210 [mm]	Dc=280 [mm]	Dc=350 [mm]	Dc=420 [mm]	Crpv(-50%)	Crpv(+50%)
45	1704	2044	2263	2415	2523	-24.7%	11.5%
55	1956	2340	2587	2758	2880	-24.4%	11.3%
65	2171	2590	2861	3048	3182	-24.1%	11.2%
75	2358	2808	3098	3299	3443	-23.9%	11.1%
85	2524	3001	3308	3521	3674	-23.7%	11.1%

95	2673	3174	3496	3719	3880	-23.5%	11.0%
105	2809	3330	3665	3898	4066	-23.4%	10.9%
					Average=	-24.0%	11.2%

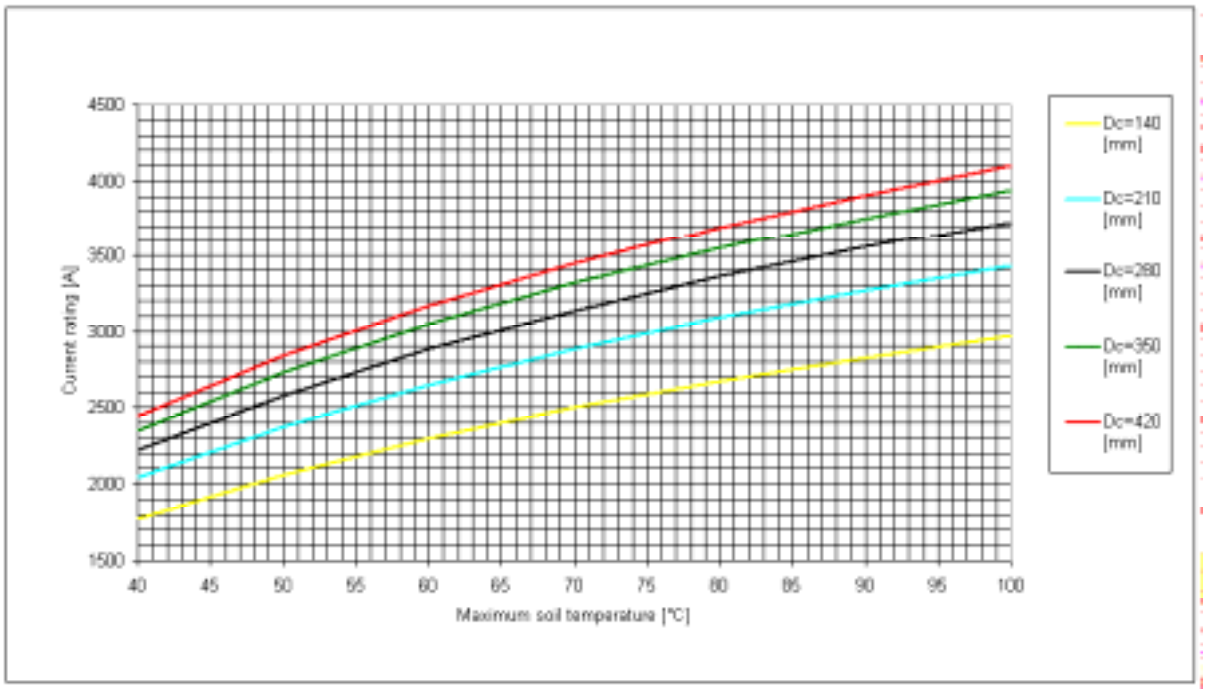

Figure 7-5 Current rating vs. Maximum soil temperature. Variable dimension: Conductor diameter. V=400 kV

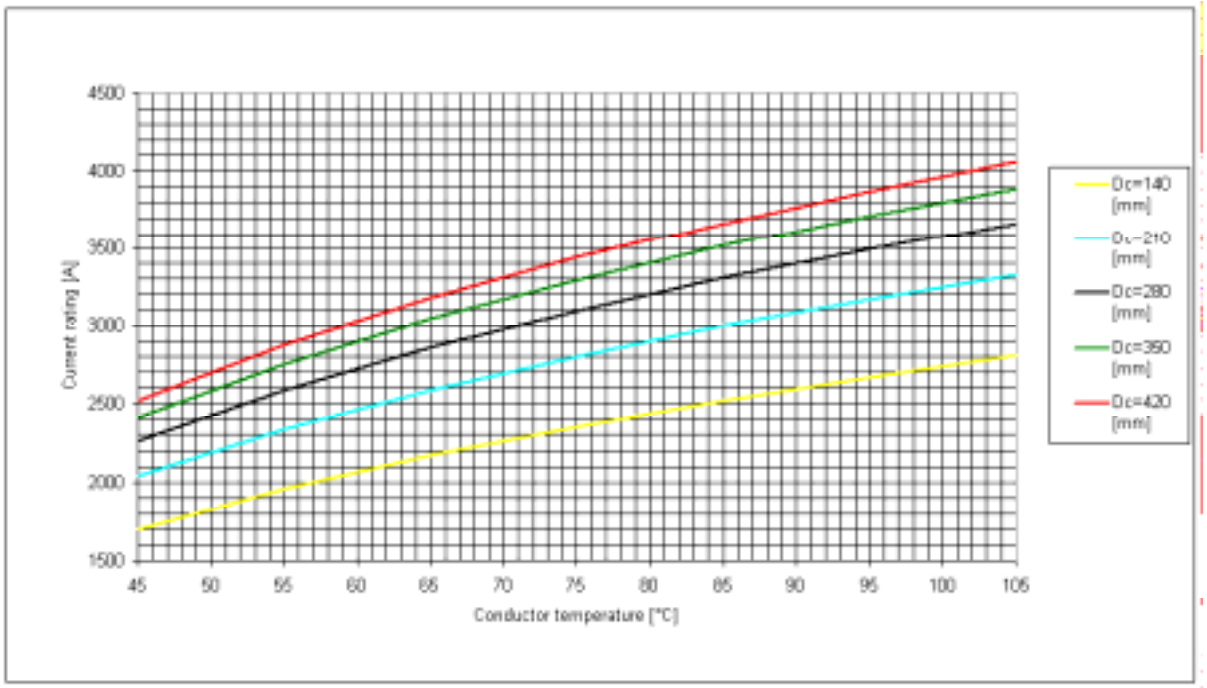

Figure 7-6: Current rating vs. Conductor temperature. Variable dimension: Conductor diameter. V=400 kV

7.2.4 Parameterised Quantity: Conductor Thickness

The conductor outer diameter was kept constant at 280 mm.

Table 7-9: Current rating (A) as a function of the conductor thickness and of the maximum soil temperature

Max soil temperature (°C)	sc=8 [mm]	sc=12 [mm]	sc=16 [mm]	sc=20 [mm]	sc=24 [mm]	Crpv(-50%)	Crpv(+50%)
40	1903	2115	2223	2263	2262	-14.4%	1.8%
50	2208	2458	2587	2637	2640	-14.6%	2.1%
60	2458	2738	2886	2946	2953	-14.8%	2.3%
70	2670	2976	3141	3211	3222	-15.0%	2.6%
80	2854	3183	3362	3442	3459	-15.1%	2.9%
90	3015	3365	3559	3648	3669	-15.3%	3.1%
100	3160	3528	3734	3832	3859	-15.4%	3.3%
					Average =	-14.9%	2.6%

Table 7-10: Current rating (A) as a function of the conductor thickness and of the conductor temperature

Conductor temperature (°C)	sc=8 [mm]	sc=12 [mm]	sc=16 [mm]	sc=20 [mm]	sc=24 [mm]	Crpv(-50%)	Crpv(+50%)
45	1914	2144	2263	2308	2308	-15.4%	2.0%
55	2185	2448	2587	2642	2645	-15.6%	2.2%
65	2413	2704	2861	2925	2932	-15.7%	2.5%
75	2610	2926	3098	3172	3184	-15.8%	2.8%
85	2783	3121	3308	3391	3407	-15.9%	3.0%
95	2938	3296	3496	3588	3609	-15.9%	3.2%
105	3078	3454	3665	3766	3793	-16.0%	3.5%
					Average=	-15.7%	2.7%

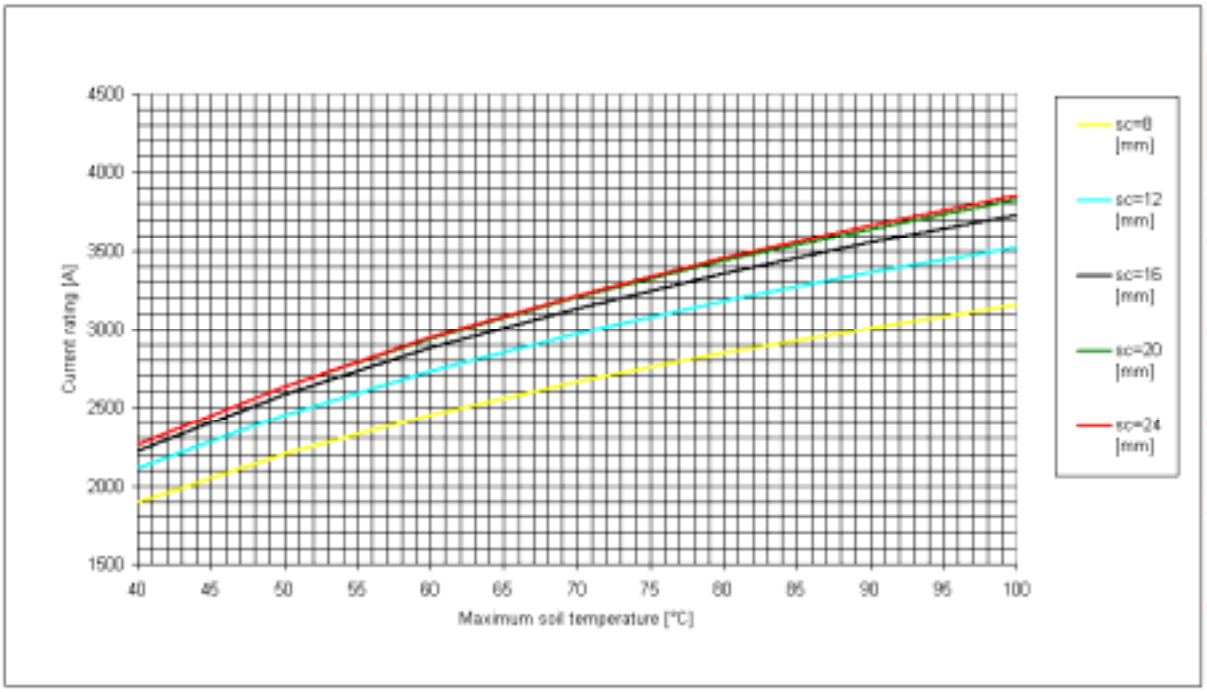

Figure 7-7: Current rating vs. Maximum soil temperatureVariable dimension: Conductor thickness. V=400 kV

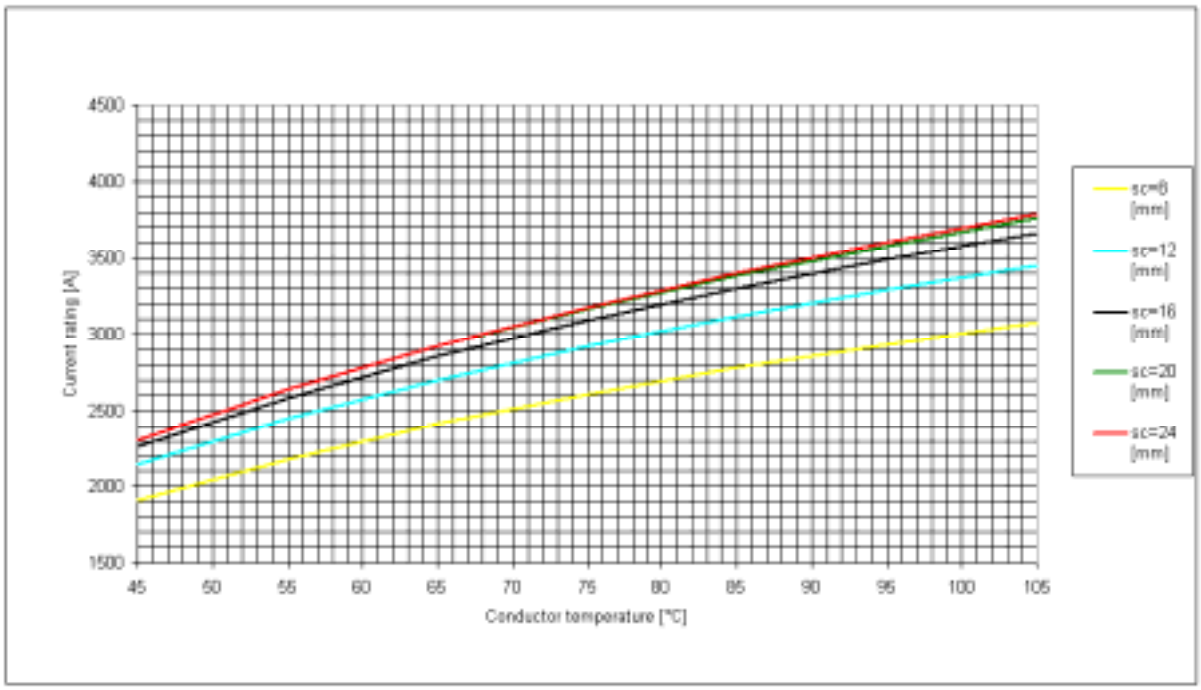

Figure 7-8: Current rating vs. Conductor temperature. Variable dimension: Conductor thickness. V=400 kV

7.2.5 Parameterised Quantity: Enclosure Diameter.

The enclosure thickness was kept constant at 10 mm.

Table 7-11: Current rating (A) as a function of the enclosure diameter and of the maximum soil temperature

Max soil temperature (°C)	De=325 [mm]	De=487.5 [mm]	De=650 [mm]	De=812.5 [mm]	De=975 [mm]	Crpv(-50%)	Crpv(+50%)
40	1671	1988	2223	2411	2569	-24.9%	15.5%
50	1942	2312	2587	2806	2989	-24.9%	15.6%
60	2165	2579	2886	3131	3335	-25.0%	15.6%
70	2355	2806	3141	3407	3630	-25.0%	15.6%
80	2520	3004	3362	3648	3887	-25.0%	15.6%
90	2666	3179	3559	3862	4115	-25.1%	15.6%
100	2797	3336	3734	4053	4318	-25.1%	15.6%
					Average=	-25.0%	15.6%

Table 7-12: Current rating (A) as a function of the enclosure diameter and of the conductor temperature

Conductor temperature (°C)	De=325 [mm]	De=487.5 [mm]	De=650 [mm]	De=812.5 [mm]	De=975 [mm]	Crpv(-50%)	Crpv(+50%)
45	1619	2024	2263	2445	2592	-28.5%	14.5%
55	1857	2312	2587	2796	2966	-28.2%	14.6%
65	2061	2557	2861	3093	3282	-27.9%	14.7%
75	2239	2768	3098	3351	3557	-27.7%	14.8%

85	2398	2956	3308	3579	3800	-27.5%	14.9%
95	2541	3123	3496	3783	4018	-27.3%	14.9%
105	2671	3274	3665	3968	4215	-27.1%	15.0%
					Average=	-27.8%	14.8%

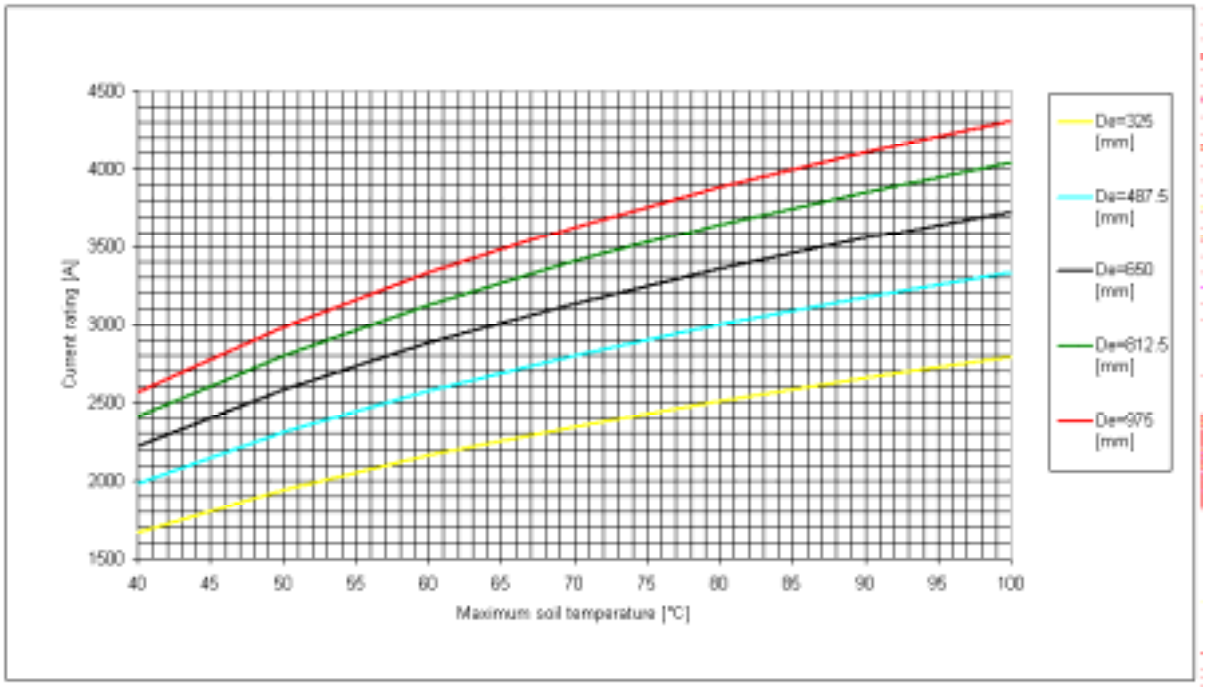

Figure 7-9: Current rating vs. Maximum soil temperature, Variable dimension: Enclosure diameter. V=400 kV

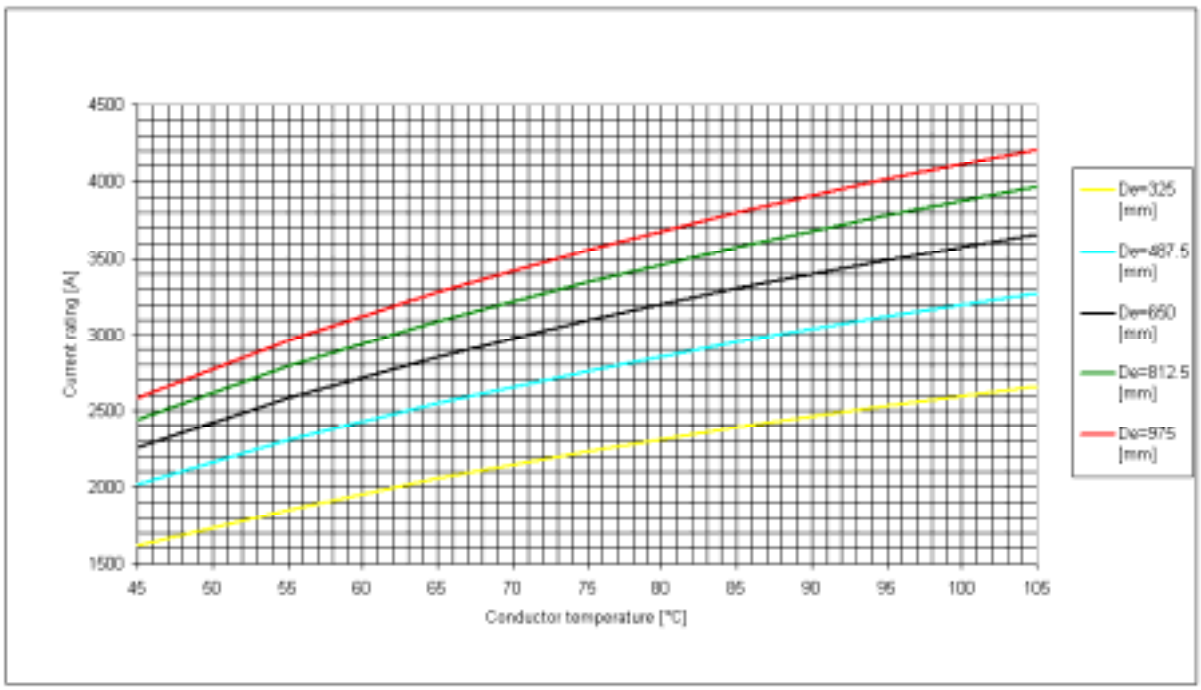

Figure 7-10: Current rating vs. Conductor temperature. Variable dimension: Enclosure diameter. V=400 kV

7.2.6 Parameterised Quantity: Enclosure Thickness

The enclosure outer diameter was kept constant at 650mm.

Table 7-13: Current rating (A) as a function of the enclosure thickness and of the maximum soil temperature.

Max soil temperature (°C)	se=5 [mm]	se=7.5 [mm]	se=10 [mm]	Se=12.5 [mm]	se=15 [mm]	Crpv(-50%)	Crpv(+50%)
40	1830.71	2066.39	2223.24	2333.33	2411.8	-17.7%	8.5%
50	2129.22	2403.76	2586.79	2715.49	2807.71	-17.7%	8.5%
60	2374.59	2681.2	2885.86	3030.14	3133.95	-17.7%	8.6%
70	2583.41	2917.38	3140.61	3298.32	3412.23	-17.7%	8.6%
80	2765.15	3122.97	3362.47	3532.01	3654.9	-17.8%	8.7%
90	2925.82	3304.77	3558.74	3738.85	3869.83	-17.8%	8.7%
100	3069.55	3467.43	3734.4	3924.06	4062.39	-17.8%	8.8%
					Average=	-17.7%	8.6%

Table 7-14: Current rating (A) as a function of the enclosure diameter and of the conductor temperature.

Conductor temperature (°C)	se=5 [mm]	se=7.5 [mm]	se=10 [mm]	Se=12.5 [mm]	se=15 [mm]	Crpv(-50%)	Crpv(+50%)
45	1894.47	2118.05	2263.47	2363.72	2434.21	-16.3%	7.5%
55	2161.2	2418.82	2586.97	2703.33	2785.6	-16.5%	7.7%
65	2386.14	2672.85	2860.55	2990.88	3083.46	-16.6%	7.8%
75	2580.92	2893.12	3098.05	3240.77	3342.58	-16.7%	7.9%
85	2752.65	3087.53	3307.87	3461.74	3571.95	-16.8%	8.0%
95	2906.03	3261.33	3495.62	3659.65	3777.56	-16.9%	8.1%
105	3044.39	3418.24	3665.27	3838.62	3963.64	-16.9%	8.1%
					Average=	-16.7%	7.9%

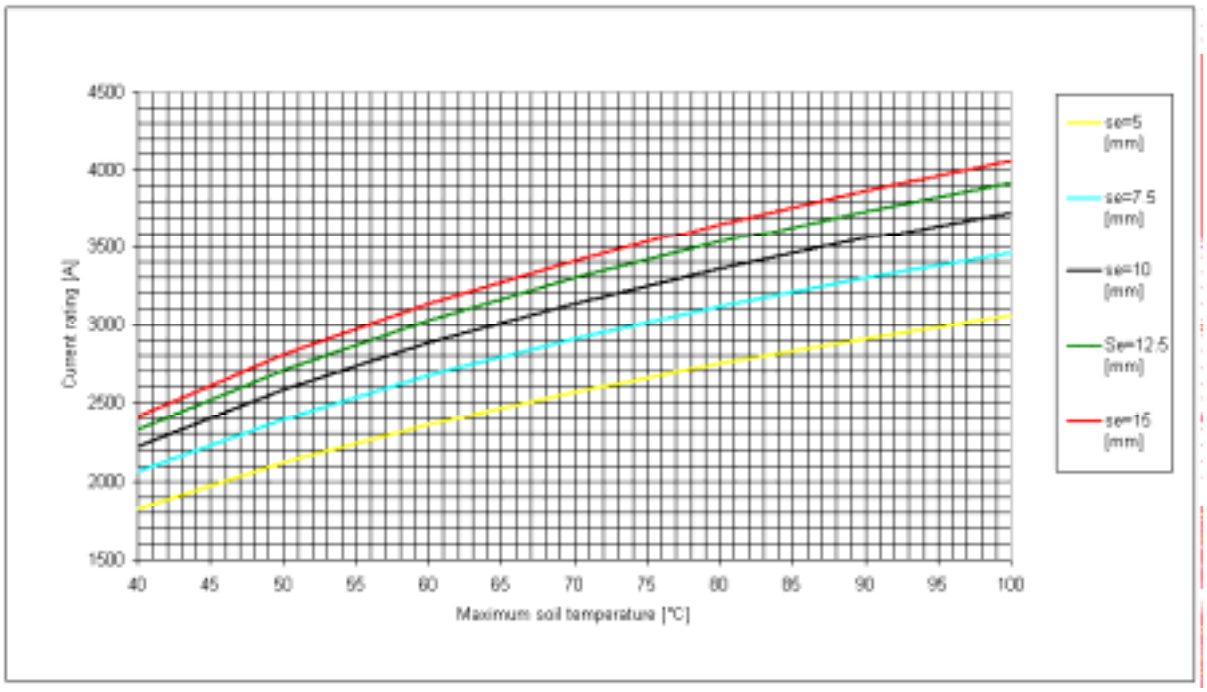

Figure 7-11: Current rating vs. Maximum soil temperature. Variable dimension: Enclosure thickness. V=400 kV

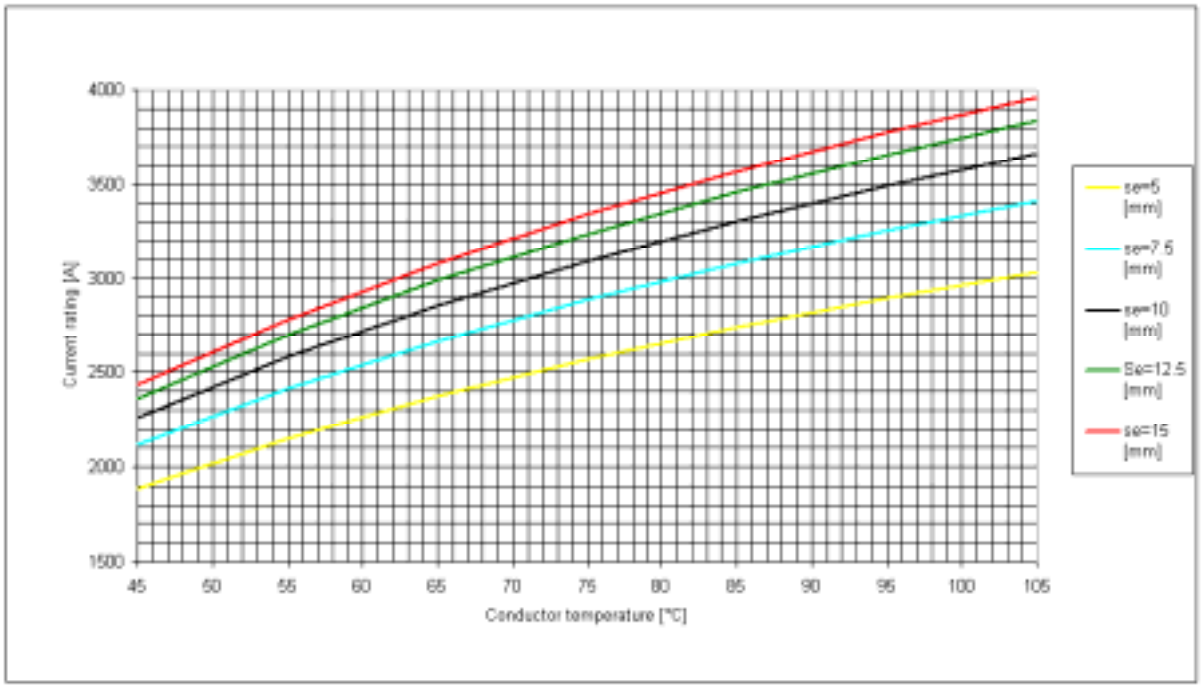

Figure 7-12: Current rating vs. Conductor temperature.Variable dimension: Enclosure thickness .V=400 kV

7.2.7 Parameterised Quantity: Heat Transfer At The Soil Surface, As Represented By An Effective Thermal Resistivity

The soil surface thermal resistivity varies from 0.1 to 0.3 $\frac{K \cdot m^2}{W}$, with a pitch of 0.05 $\frac{K \cdot m^2}{W}$. The current ratings have been reported in Table 7-15 Table 7-16 and Figure 7-13 Figure 7-14

Table 7-15: Current rating (A) as a function of soil surface thermal resistivity and of the maximum soil temperature

Max soil temperature (°C)	beta=0.1 [K.m²/W]	beta=0.15 [K.m²/W]	beta=0.2 [K.m²/W]	beta=0.25 [K.m²/W]	beta=0.3 [K.m²/W]	Crpv(-50%)	Crpv(+50%)
40	2264.79	2243.51	2223.24	2203.98	2185.61	1.9%	-1.7%
50	2635.03	2610.3	2586.79	2564.4	2543.05	1.9%	-1.7%
60	2939.62	2912.06	2885.86	2860.91	2837.12	1.9%	-1.7%
70	3199.05	3169.09	3140.61	3113.48	3087.61	1.9%	-1.7%
80	3424.99	3392.94	3362.47	3333.45	3305.78	1.9%	-1.7%
90	3624.85	3590.96	3558.74	3528.05	3498.78	1.9%	-1.7%
100	3803.74	3768.19	3734.4	3702.21	3671.52	1.9%	-1.7%
					Average =	1.9%	-1.7%

Table 7-16: Current rating (A) as a function of soil surface thermal resistivity and of the conductor temperature

Conductor temperature (°C)	beta=0.1 [K.m²/W]	beta=0.15 [K.m²/W]	beta=0.2 [K.m²/W]	beta=0.25 [K.m²/W]	beta=0.3 [K.m²/W]	Crpv(-50%)	Crpv(+50%)
45	2301.35	2281.95	2263.47	2245.82	2228.95	1.7%	-1.5%
55	2630.66	2608.29	2586.97	2566.62	2547.18	1.7%	-1.5%
65	2909.2	2884.29	2860.55	2837.9	2816.26	1.7%	-1.5%
75	3151.04	3123.9	3098.05	3073.38	3049.81	1.7%	-1.6%
85	3364.73	3335.61	3307.87	3281.41	3256.13	1.7%	-1.6%
95	3555.96	3525.05	3495.62	3467.54	3440.73	1.7%	-1.6%
105	3728.77	3696.25	3665.27	3635.72	3607.51	1.7%	-1.6%
					Average=	1.7%	-1.6%

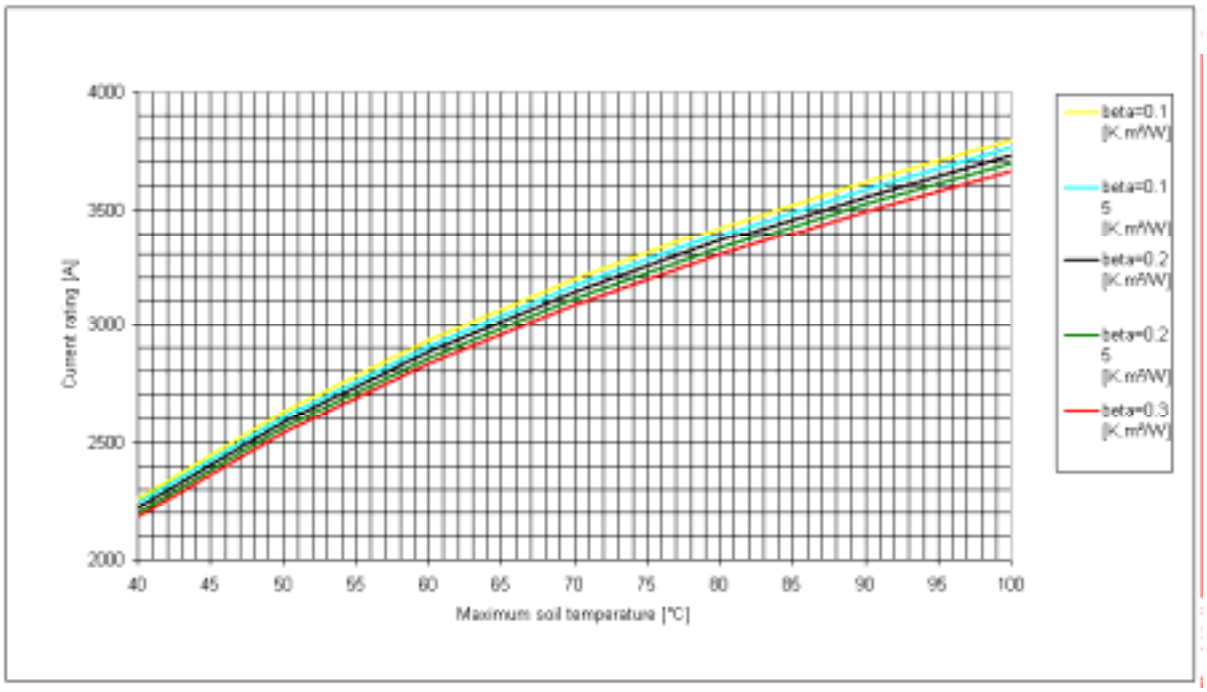

Figure 7-13: Current rating vs. Maximum soil temperature. Variable dimension: Soil surface thermal resistivity (beta).V=400 kV

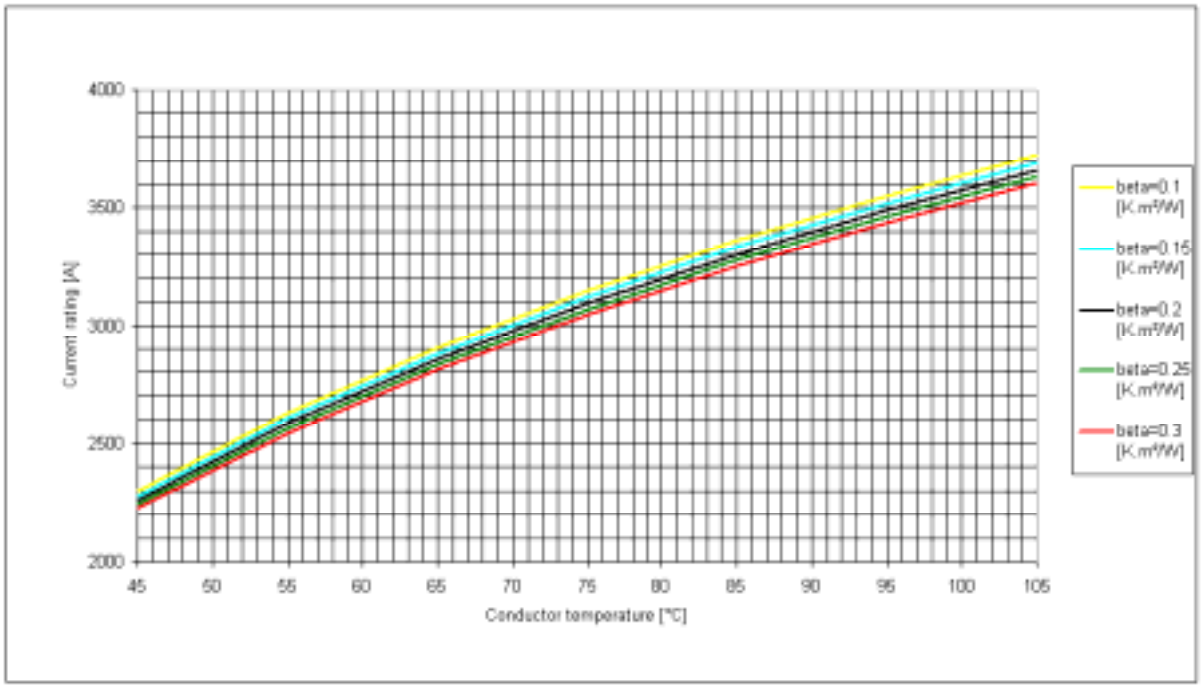

Figure 7-14: Current rating vs. Conductor temperature. Variable dimension: Soil surface thermal resistivity (beta). V=400 kV

7.2.8 Parameterised Quantity: Soil Thermal Resistivity

The soil resistivity has been assumed varying from 0.6 to 1.8 $\frac{K \cdot m}{W}$ with different pitches, in order to consider characteristic values. The current ratings have been reported in Table 7-17, Table 7-18, Figure 7-15 and Figure 7-16.

Table 7-17: Current rating (A) as a function of the soil thermal resistivity and of the maximum soil temperature

Max soil temperature (°C)	rs =0.6 [K.m/W]	rs=0.9 [K.m/W]	rs=1.2 [K.m/W]	rs=1.5 [K.m/W]	rs=1.8 [K.m/W]	Crpv(-50%)	Crpv(+50%)
40	3036.08	2535.87	2223.24	2003.94	1839.08	36.6%	-17.3%
50	3530.69	2949.94	2586.79	2331.86	2140.17	36.5%	-17.3%
60	3937.16	3290.48	2885.86	2601.73	2388.03	36.4%	-17.3%
70	4283.05	3580.45	3140.61	2831.65	2599.23	36.4%	-17.2%
80	4584.04	3832.92	3362.47	3031.93	2783.23	36.3%	-17.2%
90	4850.13	4056.2	3558.74	3209.14	2946.04	36.3%	-17.2%
100	5088.16	4256	3734.4	3367.76	3091.8	36.3%	-17.2%
					Average=	36.4%	-17.2%

Table 7-18: Current rating (A) as a function of the soil thermal resistivity and of the conductor temperature

Conductor temperature (°C)	rs =0.6 [K.m/W]	rs=0.9 [K.m/W]	rs=1.2 [K.m/W]	rs=1.5 [K.m/W]	rs=1.8 [K.m/W]	Crpv(-50%)	Crpv(+50%)
45	2969.7	2544	2263.47	2060.16	1903.89	31.2%	-15.9%
55	3404.45	2910.92	2586.97	2352.77	2173.08	31.6%	-16.0%
65	3773.39	3221.63	2860.55	2600.02	2400.38	31.9%	-16.1%
75	4094.61	3491.66	3098.05	2814.49	2597.45	32.2%	-16.2%
85	4379.15	3730.45	3307.87	3003.84	2771.35	32.4%	-16.2%
95	4634.37	3944.32	3495.62	3173.18	2926.8	32.6%	-16.3%
105	4865.49	4137.73	3665.27	3326.1	3067.12	32.7%	-16.3%
					Average=	32.1%	-16.1%

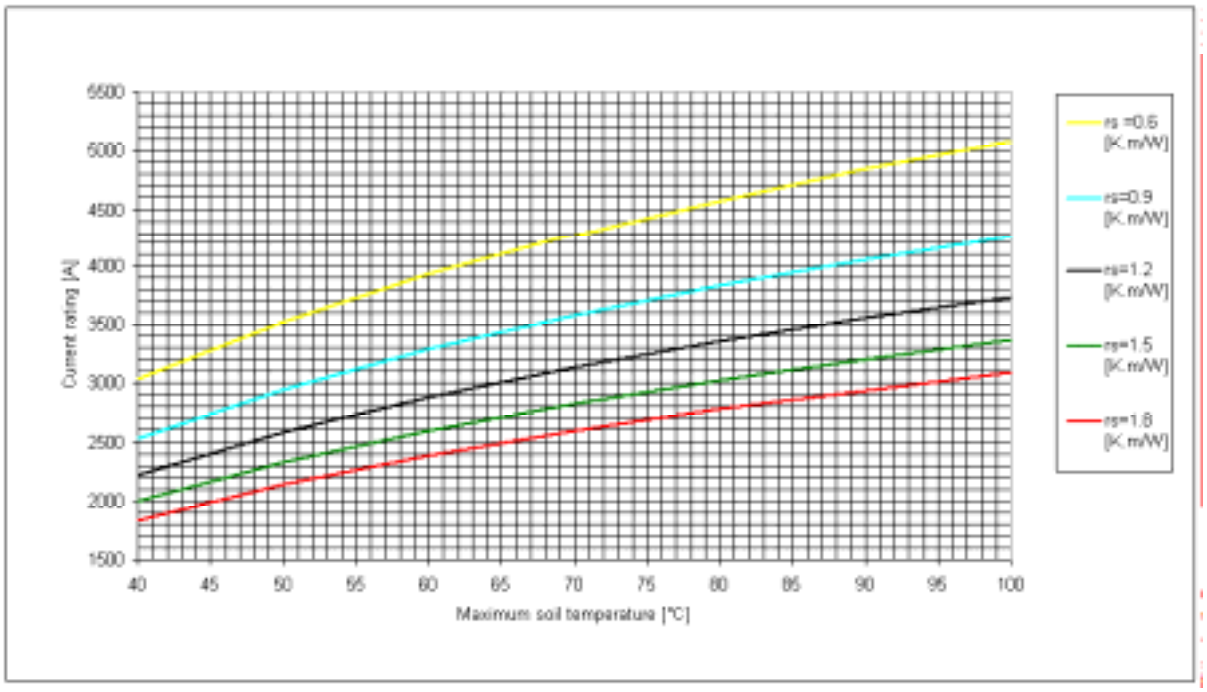

Figure 7-15: Current rating vs. Maximum soil temperature. Variable dimension: Soil thermal resistivity (rs).V=400kV.

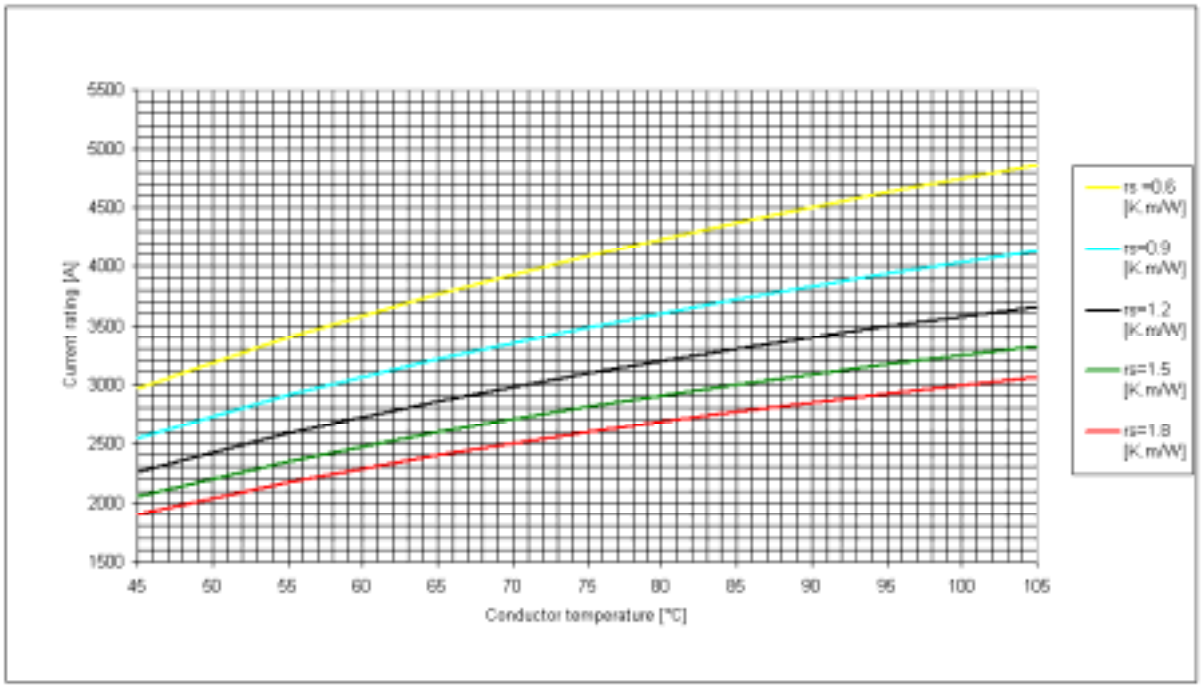

Figure 7-16 Current rating vs. Conductor temperature.Variable dimension: Soil thermal resistivity (rs).V=400 kV

7.2.9 Parameterised Quantity: Thermal Emissivity Of The Conductor And Enclosure Surfaces

The conductor outer surface thermal emissivity has been assumed equal to that of the enclosure inner surface. Their values vary between 0.1 to 0.3

The current ratings calculated as a function of said emissivity are shown in Table 7-19, Table 7-20, Figure 7-17 and Figure 7-18.

Table 7-19: Current rating (A) as a function of the conductor and enclosure surfaces emissivity and of the maximum soil temperature

Max soil temperature (°C)	sigma= 0.1	sigma= 0.15	sigma= 0.2	sigma= 0.25	sigma= 0.3	Crpv(-50%)	Crpv(+50%)
40	2222.71	2223	2223.24	2223.51	2223.77	-0.02%	0.02%
50	2585.96	2586.38	2586.79	2587.17	2587.51	-0.03%	0.03%
60	2884.74	2885.31	2885.86	2886.38	2886.87	-0.04%	0.03%
70	3139.19	3139.92	3140.61	3141.26	3141.88	-0.05%	0.04%
80	3360.73	3361.62	3362.47	3363.27	3364.02	-0.05%	0.05%
90	3556.66	3557.73	3558.74	3559.68	3560.57	-0.06%	0.05%
100	3731.97	3733.22	3734.4	3735.5	3736.52	-0.07%	0.06%
					Average=	-0.05%	0.04%

Table 7-20: **Current rating (A) as a function of the conductor and enclosure surfaces emissivity and of the conductor temperature**

Conductor temperature (°C)	sigma= 0.1	sigma= 0.15	sigma= 0.2	sigma= 0.25	sigma= 0.3	Crpv(-50%)	Crpv(+50%)
45	2250.05	2256.9	2263.47	2269.77	2275.83	-0.6%	0.5%
55	2572.67	2579.97	2586.97	2593.68	2600.11	-0.6%	0.5%
65	2845.41	2853.15	2860.55	2867.63	2874.41	-0.5%	0.5%
75	3082.09	3090.26	3098.05	3105.48	3112.57	-0.5%	0.5%
85	3291.12	3299.7	3307.87	3315.63	3323.01	-0.5%	0.5%
95	3478.09	3487.09	3495.62	3503.7	3511.36	-0.5%	0.5%
105	3646.98	3656.39	3665.27	3673.65	3681.57	-0.5%	0.4%
Average=						-0.5%	0.5%

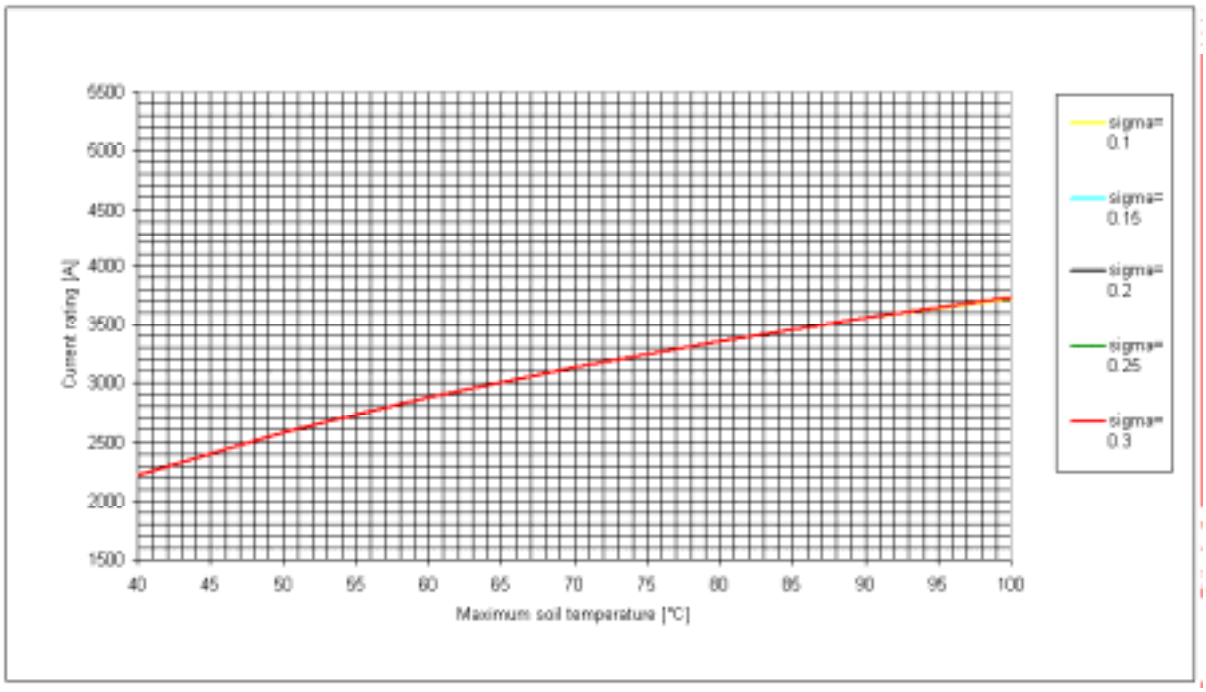

Figure 7-17: Current rating vs. Maximum soil temperature. Variable dimension: Emissivity of conductor and enclosure surfaces (sigma). V=400 kV

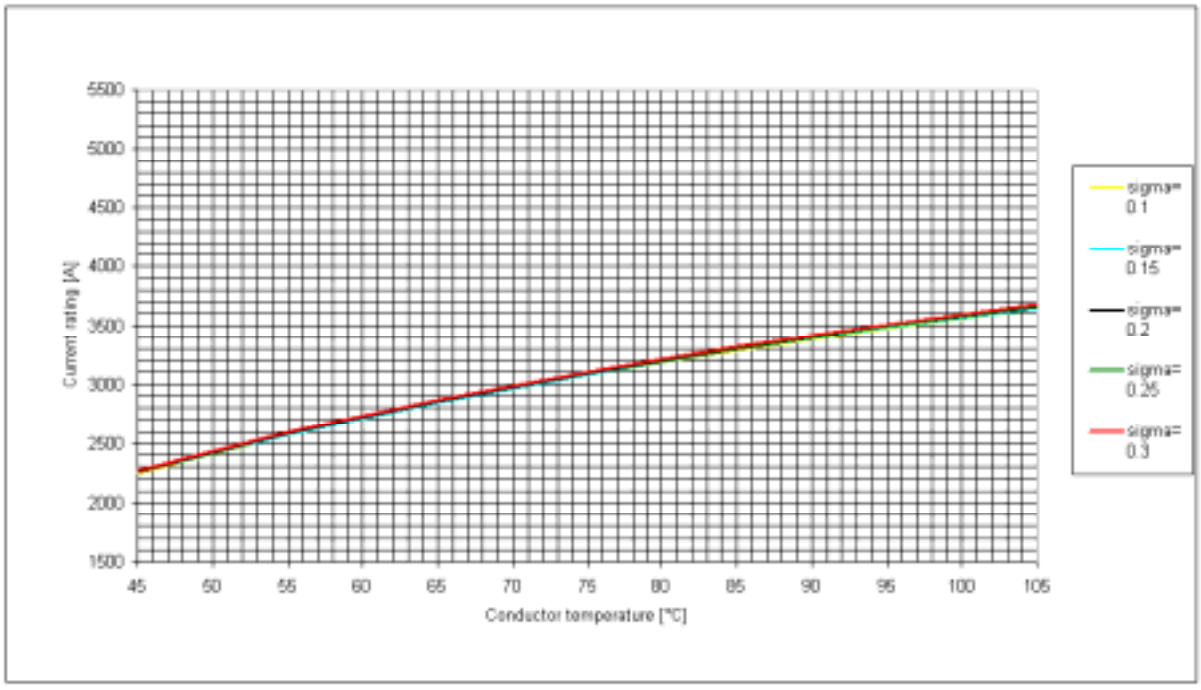

Figure 7-18: Current rating vs. Conductor temperature. Variable dimension: Emissivity of conductor and enclosure surfaces (sigma).V=400

7.2.10 Parameterised Quantity: Gas Mixture Pressure

The absolute pressure of gas mixture has been assumed between 3.35 to 10.05 bar.

The current ratings calculated as a function of the gas pressure are shown in Table 7-21, Table 7-22, Figure 7-19, Figure 7-20.

Table 7-21: Current rating (A) as a function of the gas pressure and of the maximum soil temperature

Max soil temperature (°C)	p= 3.35 [bar abs]	p= 5.03 [bar abs]	p= 6.7 [bar abs]	p= 8.38 [bar abs]	p= 10.05 [bar abs]	Crpv(-50%)	Crpv(+50%)
40	2221.37	2222.54	2223.24	2223.79	2224.2	-0.08%	0.04%
50	2584.03	2585.71	2586.79	2587.53	2588.12	-0.11%	0.05%
60	2882.3	2884.47	2885.86	2886.86	2887.59	-0.12%	0.06%
70	3136.31	3138.93	3140.61	3141.82	3142.74	-0.14%	0.07%
80	3357.51	3360.53	3362.47	3363.88	3364.95	-0.15%	0.07%
90	3553.17	3556.55	3558.74	3560.32	3561.53	-0.16%	0.08%
100	3728.31	3732	3734.4	3736.14	3737.48	-0.16%	0.08%
					Average=	-0.13%	0.07%

Table 7-22 Current rating (A) as a function of the gas mixture pressure and of the conductor temperature.

Conductor temperature (°C)	p= 3.35 [bar abs]	p= 5.03 [bar abs]	p= 6.7 [bar abs]	p= 8.38 [bar abs]	p= 10.05 [bar abs]	Crpv(-50%)	Crpv(+50%)
45	2218.73	2245.85	2263.47	2276.3	2286.12	-2.0%	1.0%
55	2540.01	2568.5	2586.97	2600.4	2610.68	-1.8%	0.9%
65	2812.46	2841.64	2860.55	2874.3	2884.81	-1.7%	0.8%
75	3049.54	3078.97	3098.05	3111.92	3122.53	-1.6%	0.8%
85	3259.45	3288.81	3307.87	3321.74	3332.35	-1.5%	0.7%
95	3447.65	3476.73	3495.62	3509.39	3519.94	-1.4%	0.7%
105	3618.01	3646.63	3665.27	3678.87	3689.29	-1.3%	0.7%
					Average=	-1.6%	0.8%

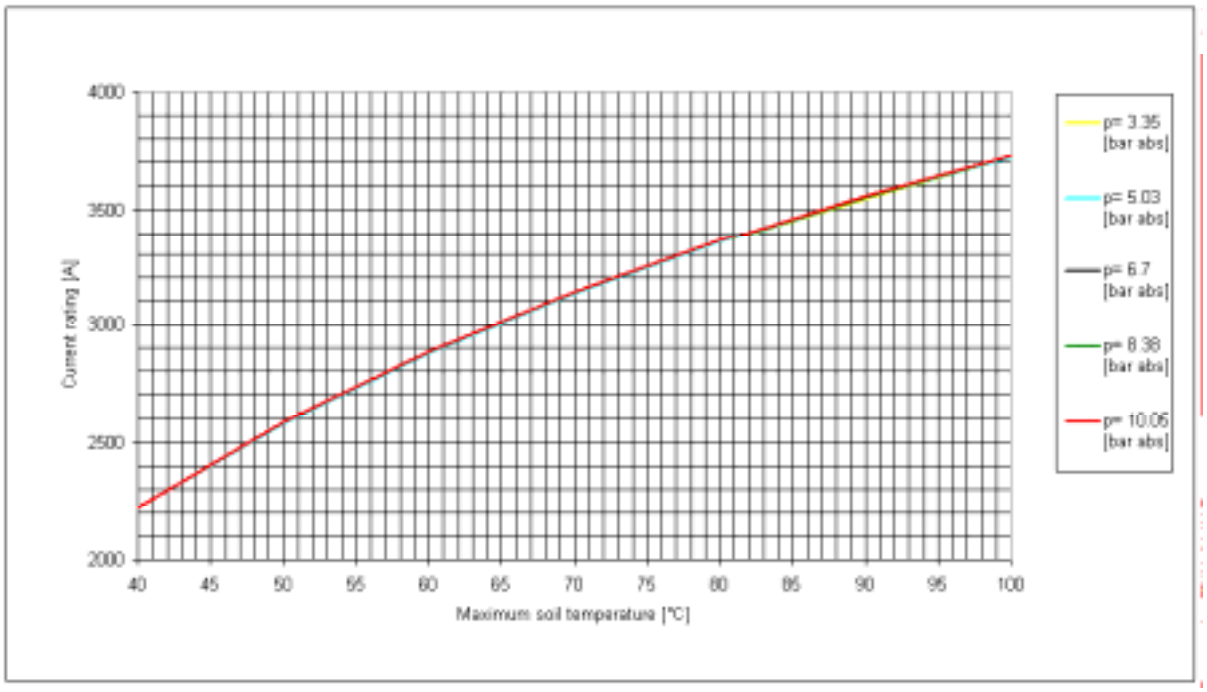

Figure 7-19 Current rating vs. Maximum soil temperature Variable dimension: Gas mixture absolute pressure (p). V=400 kV

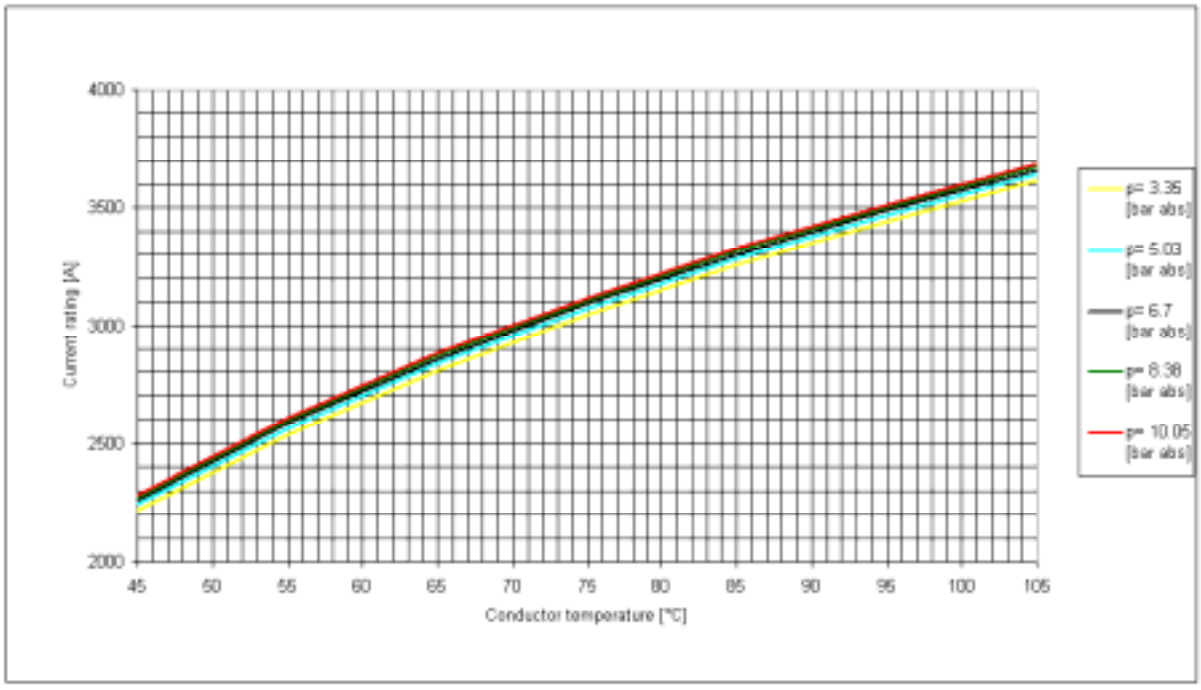

Figure 7-20 Current rating vs. Conductor temperature. Variable dimension:Gas mixture absolute pressure (p). V=400 kV

7.2.11 Parametrised Quantity: Thermal Convection Constant Of The SF_6

Table 7-23: Current rating (A) as a function of the SF_6 convection constant and of the maximum soil temperature.

Max soil temperature (°C)	K1=5.65	K1=8.48	K1=11.3	K1=14.13	K1=16.95	Crpv(-50%)	Crpv(+50%)
40	2222.93	2223.11	2223.24	2223.41	2223.56	-0.01%	0.01%
50	2586.28	2586.54	2586.79	2587.02	2587.23	-0.02%	0.02%
60	2885.2	2885.54	2885.86	2886.16	2886.44	-0.02%	0.02%
70	3139.81	3140.22	3140.61	3140.97	3141.31	-0.03%	0.02%
80	3361.55	3362.02	3362.47	3362.89	3363.28	-0.03%	0.02%
90	3557.7	3558.23	3558.74	3559.21	3559.65	-0.03%	0.03%
100	3733.26	3733.85	3734.4	3734.92	3735.41	-0.03%	0.03%
					Average =	-0.02%	0.02%

Table 7-24 Current rating (A) as a function of the SF6 convection constant and of the conductor temperature.

Conductor temperature (°C)	K1=5.65	K1=8.48	K1=11.3	K1=14.13	K1=16.95	Crpv(-50%)	Crpv(+50%)
45	2255.08	2259.41	2263.47	2267.29	2270.87	-0.4%	0.3%
55	2578.18	2582.72	2586.97	2590.97	2594.72	-0.3%	0.3%
65	2851.55	2856.21	2860.55	2864.64	2868.48	-0.3%	0.3%
75	3088.97	3093.66	3098.05	3102.18	3106.05	-0.3%	0.3%
85	3298.8	3303.49	3307.87	3312	3315.87	-0.3%	0.2%
95	3486.62	3491.27	3495.62	3499.72	3503.56	-0.3%	0.2%
105	3656.39	3660.98	3665.27	3669.31	3673.11	-0.2%	0.2%
					Average =	-0.3%	0.3%

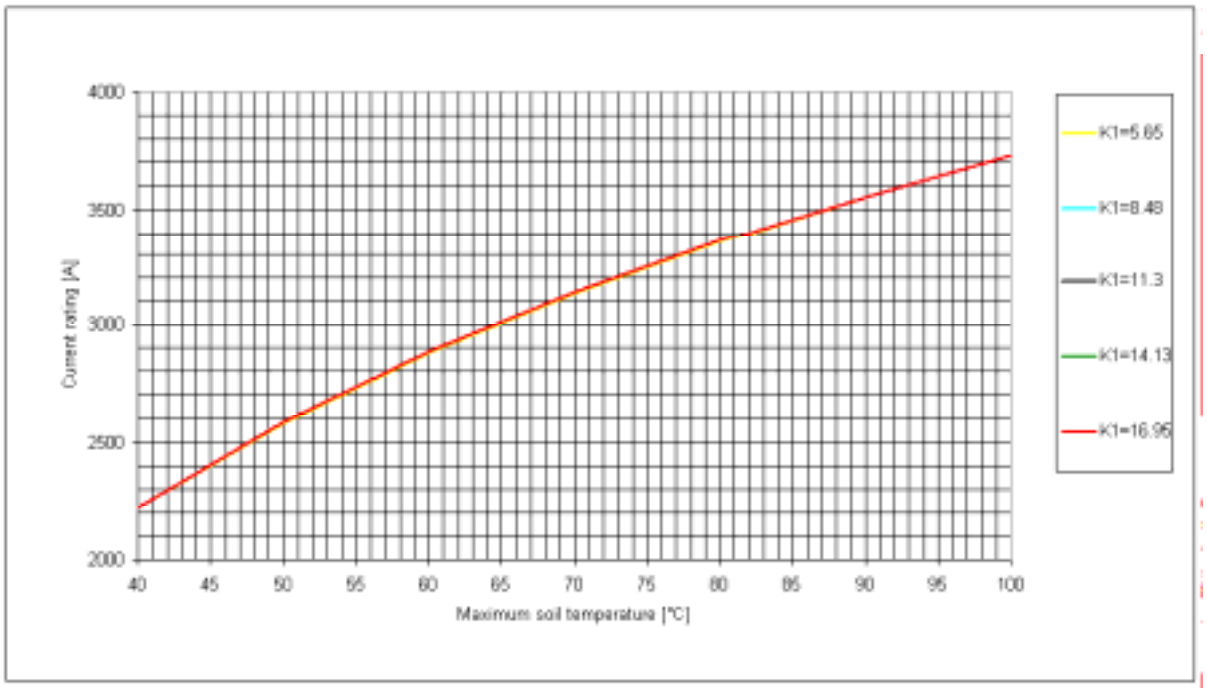

Figure 7-21 Current rating vs. Maximum soil temperature. Variable dimension: Thermal convection constant of the SF6 (K1). V=400 kV.

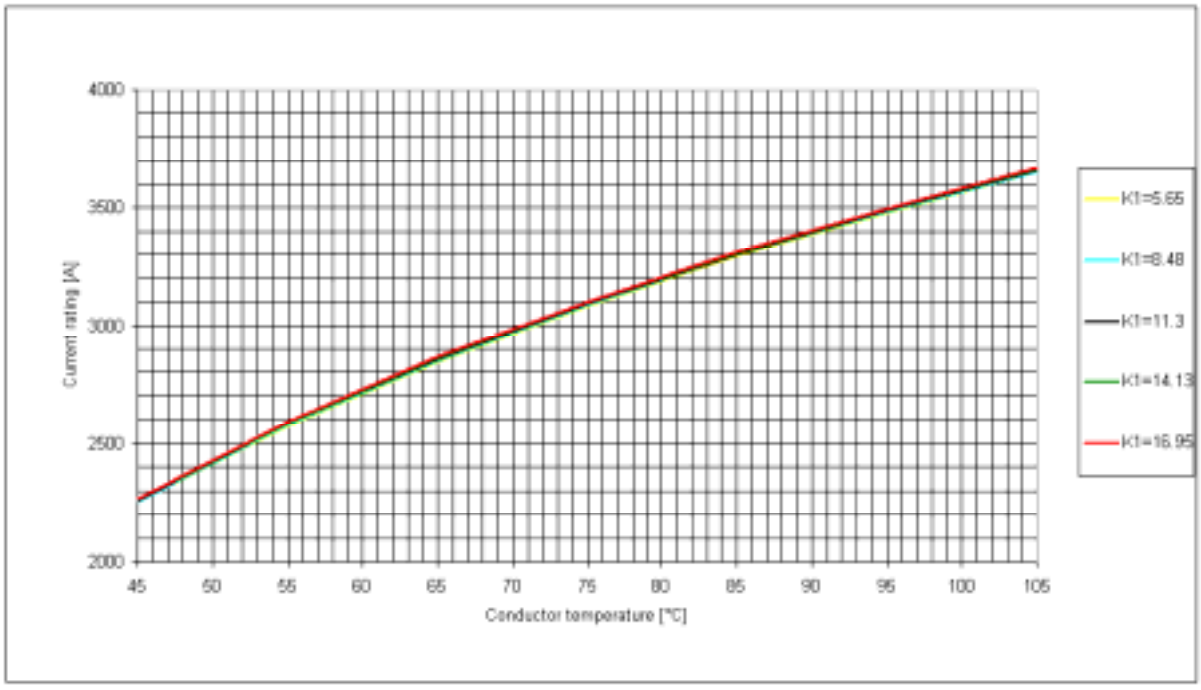

Figure 7-22 Current rating vs. Conductor temperature. Variable dimension: Thermal convection constant of the SF6 (K1). V=400 kV

7.2.12 Parameterised Quantity: Thermal Convection Constant Of The N_2

.

Table 7-25 Current rating (A) as a function of the N_2 convection constant and of the maximum soil temperature

Max soil temperature (°C)	K2=2.92	K2=4.37	K2=5.83	K2=7.29	K2=8.75	Crpv(-50%)	Crpv(+50%)
40	2221.06	2222.37	2223.24	2223.92	2224.44	-0.10%	0.05%
50	2583.59	2585.48	2586.79	2587.72	2588.47	-0.12%	0.06%
60	2881.73	2884.17	2885.86	2887.1	2888.04	-0.14%	0.07%
70	3135.63	3138.56	3140.61	3142.12	3143.26	-0.16%	0.08%
80	3356.72	3360.1	3362.47	3364.22	3365.56	-0.17%	0.09%
90	3552.3	3556.08	3558.74	3560.71	3562.23	-0.18%	0.10%
100	3727.36	3731.48	3734.4	3736.57	3738.25	-0.19%	0.10%
					Average =	-0.15%	0.08%

Table 7-26 Current rating (A) as a function of the N_2 convection constant and of the conductor temperature.

Conductor temperature (°C)	K2=2.92	K2=4.37	K2=5.83	K2=7.29	K2=8.75	Crpv(-50%)	Crpv(+50%)
45	2211.69	2242.04	2263.47	2279.45	2291.91	-2.3%	1.3%
55	2532.61	2564.5	2586.97	2603.7	2616.73	-2.1%	1.2%
65	2804.88	2837.55	2860.55	2877.68	2891.01	-1.9%	1.1%
75	3041.89	3074.84	3098.05	3115.33	3128.79	-1.8%	1.0%
85	3251.82	3284.69	3307.87	3325.15	3338.61	-1.7%	0.9%
95	3440.11	3472.64	3495.62	3512.78	3526.16	-1.6%	0.9%
105	3610.6	3642.61	3665.27	3682.22	3695.45	-1.5%	0.8%
					Average =	-1.85%	1.0%

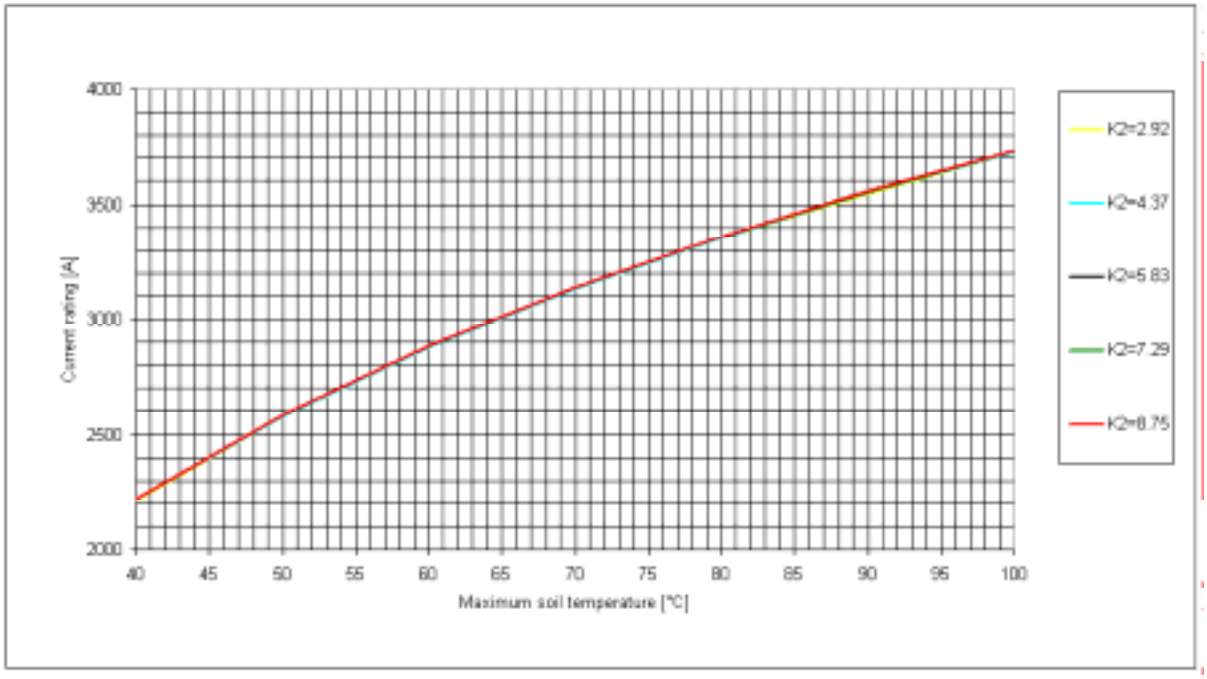

Figure 7-23 Current rating vs. Maximum soil temperature. Variable dimension: Thermal convection constant of the N2 (K2).V=400 kV.

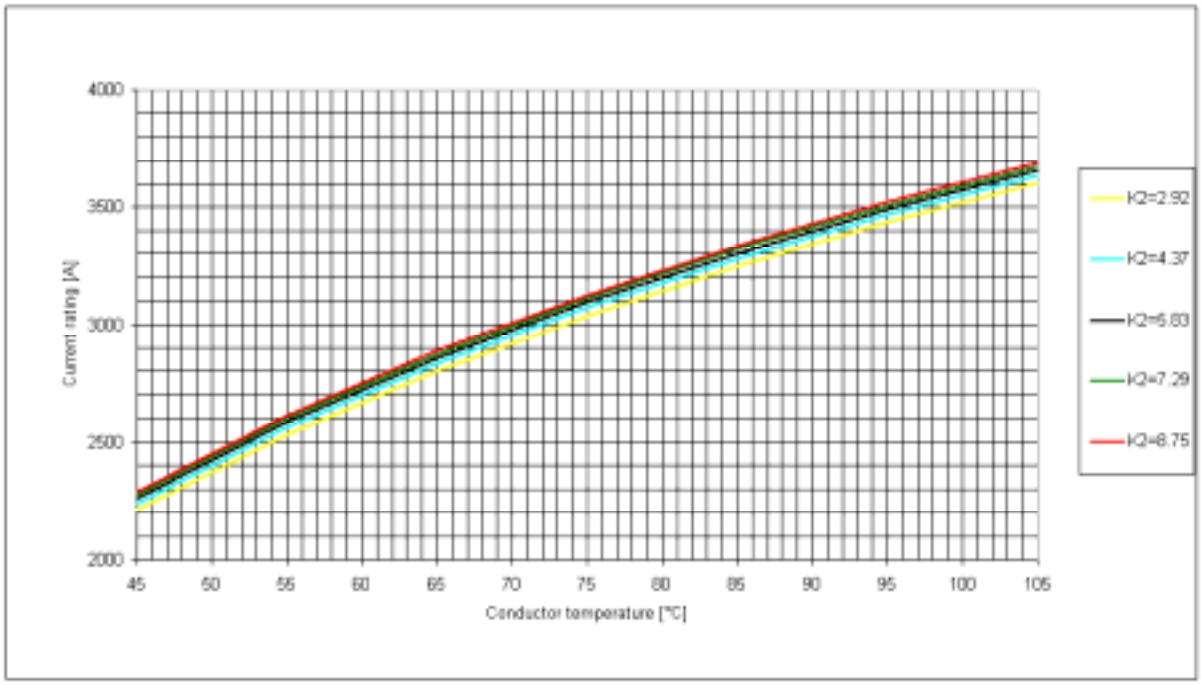

Figure 7-24 Current rating vs. Conductor temperature. Variable dimension: Thermal convection constant of the N_2 (K2). V=400 kV

7.2.13 Parameterised Quantity: Volumetric Percentage Of SF_6 In The Gas Mixture

Table 7-27 Current rating (A) as a function of the SF_6 volume content in gas mixture and of the maximum soil temperature.

Max soil temperature (°C)	Vc=5 [%]	Vc=7.5 [%]	Vc=10 [%]	Vc=12.5 [%]	Vc=15 [%]	Crpv(-50%)	Crpv(+50%)
40	2223.11	2223.2	2223.24	2223.32	2223.4	-0.01%	0.01%
50	2586.55	2586.67	2586.79	2586.9	2587.01	-0.01%	0.01%
60	2885.55	2885.71	2885.86	2886.01	2886.15	-0.01%	0.01%
70	3140.23	3140.42	3140.61	3140.78	3140.96	-0.01%	0.01%
80	3362.04	3362.26	3362.47	3362.68	3362.88	-0.01%	0.01%
90	3558.25	3558.5	3558.74	3558.97	3559.19	-0.01%	0.01%
100	3733.87	3734.14	3734.4	3734.65	3734.9	-0.01%	0.01%
					Average=	-0.01%	0.01%

Table 7-28 Current rating (A) as a function of the SF6 volume content in gas mixture and of the conductor temperature

Conductor temperature (°C)	Vc=5 [%]	Vc=7.5 [%]	Vc=10 [%]	Vc=12.5 [%]	Vc=15 [%]	Crpv(-50%)	Crpv(+50%)
45	2259.54	2261.53	2263.47	2265.34	2267.16	-0.2%	0.2%
55	2582.85	2584.94	2586.97	2588.93	2590.84	-0.2%	0.1%
65	2856.34	2858.48	2860.55	2862.56	2864.51	-0.1%	0.1%
75	3093.8	3095.95	3098.05	3100.07	3102.04	-0.1%	0.1%
85	3303.62	3305.78	3307.87	3309.9	3311.86	-0.1%	0.1%
95	3491.41	3493.55	3495.62	3497.63	3499.58	-0.1%	0.1%
105	3661.11	3663.22	3665.27	3667.25	3669.18	-0.1%	0.1%
					Average =	-0.1%	0.1%

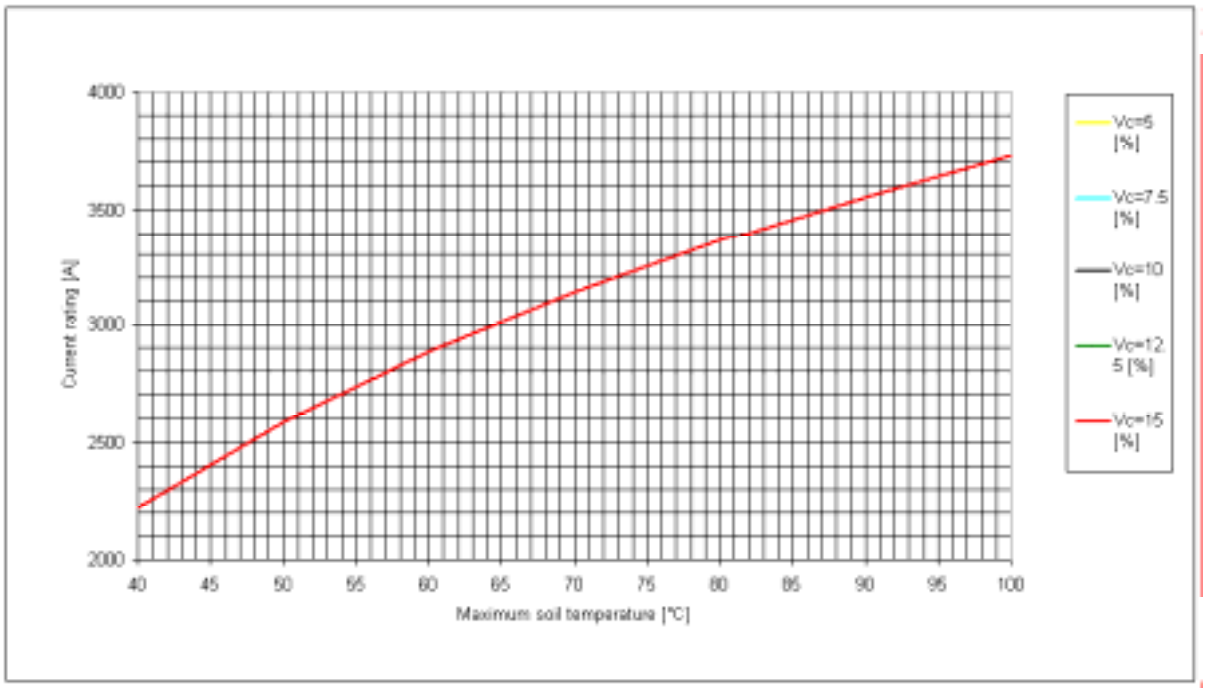

Figure 7-25 Current rating vs. Maximum soil temperature. Variable dimension: SF6 Volume content (Vc). V=400 kV.

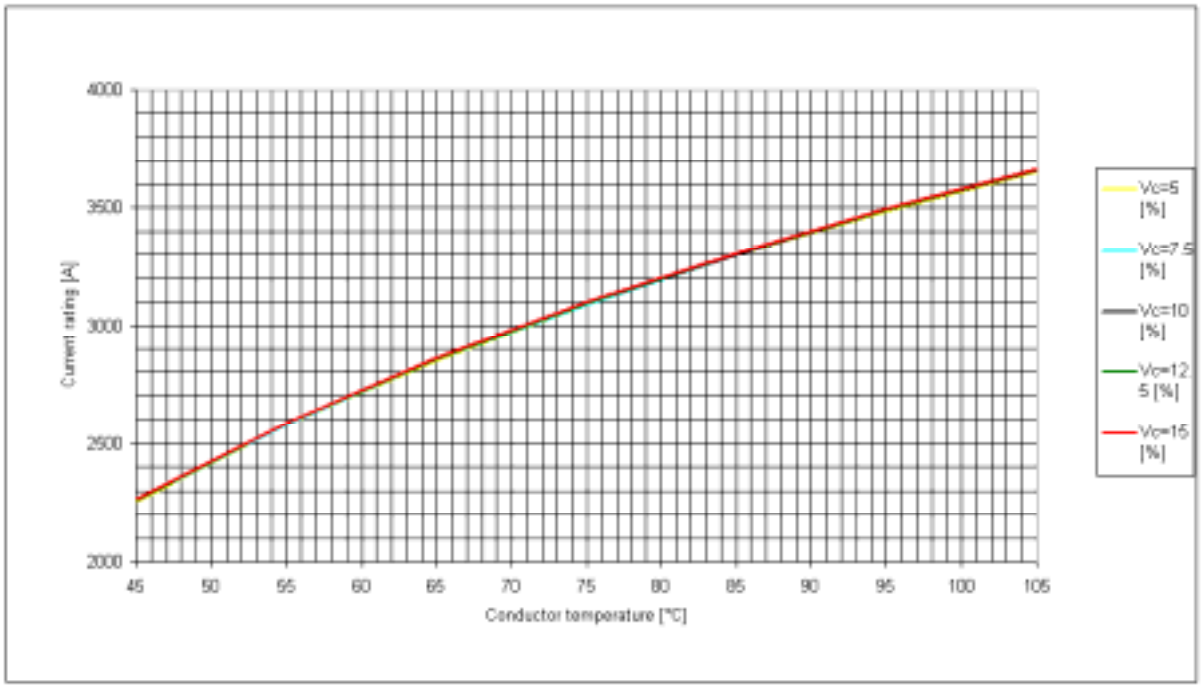

Figure 7-26 Current rating vs. Conductor temperature. Variable dimension: SF6 Volume content (Vc). V=400 kV

7.2.14 Parameterised Quantity: Conductor Electric Resistivity

Table 7-29 Current rating (A) as a function of the electric resistivity of the conductor and of the maximum soil temperature.

Max soil temperature (°C)	Cr= 1.73E-8 [Ωm]	Cr= 2.59E-8 [Ωm]	Cr= 3.45E-8 [Ωm]	Cr= 4.31E-8 [Ωm]	Cr= 5.18E-8 [Ωm]	Crpv(-50%)	Crpv(+50%)
40	2453.31	2335.64	2223.24	2120.22	2026.36	10.3%	-8.8%
50	2860.09	2720	2586.79	2465.19	2354.86	10.5%	-8.9%
60	3197.15	3037.04	2885.86	2748.52	2624.31	10.8%	-9.0%
70	3485.34	3307.67	3140.61	2989.49	2853.22	10.9%	-9.1%
80	3737.56	3543.84	3362.47	3199.08	3052.14	11.1%	-9.2%
90	3961.69	3753.13	3558.74	3384.26	3227.75	11.3%	-9.3%
100	4163.14	3940.75	3734.4	3549.84	3384.66	11.4%	-9.3%
					Average =	10.9%	-9.1%

Table 7-30 Current rating (A) as a function of the electric resistivity of the conductor and of the conductor temperature.

Conductor temperature (°C)	Cr= 1.73E-8 [Ωm]	Cr= 2.59E-8 [Ωm]	Cr= 3.45E-8 [Ωm]	Cr= 4.31E-8 [Ωm]	Cr= 5.18E-8 [Ωm]	Crpv(-50%)	Crpv(+50%)
45	2524.96	2389.93	2263.47	2149.4	2046.91	11.5%	-9.5%
55	2888.85	2732.74	2586.97	2455.92	2338.44	11.6%	-9.6%
65	3198.44	3023.18	2860.55	2714.84	2584.52	11.8%	-9.6%
75	3467.78	3275.71	3098.05	2939.39	2797.77	11.9%	-9.7%
85	3706.65	3499.15	3307.87	3137.58	2985.89	12.0%	-9.7%
95	3921.15	3699.36	3495.62	3314.79	3154.01	12.1%	-9.7%
105	4115.61	3880.47	3665.27	3474.81	3305.75	12.2%	-9.8%
					Average =	11.9%	-9.7%

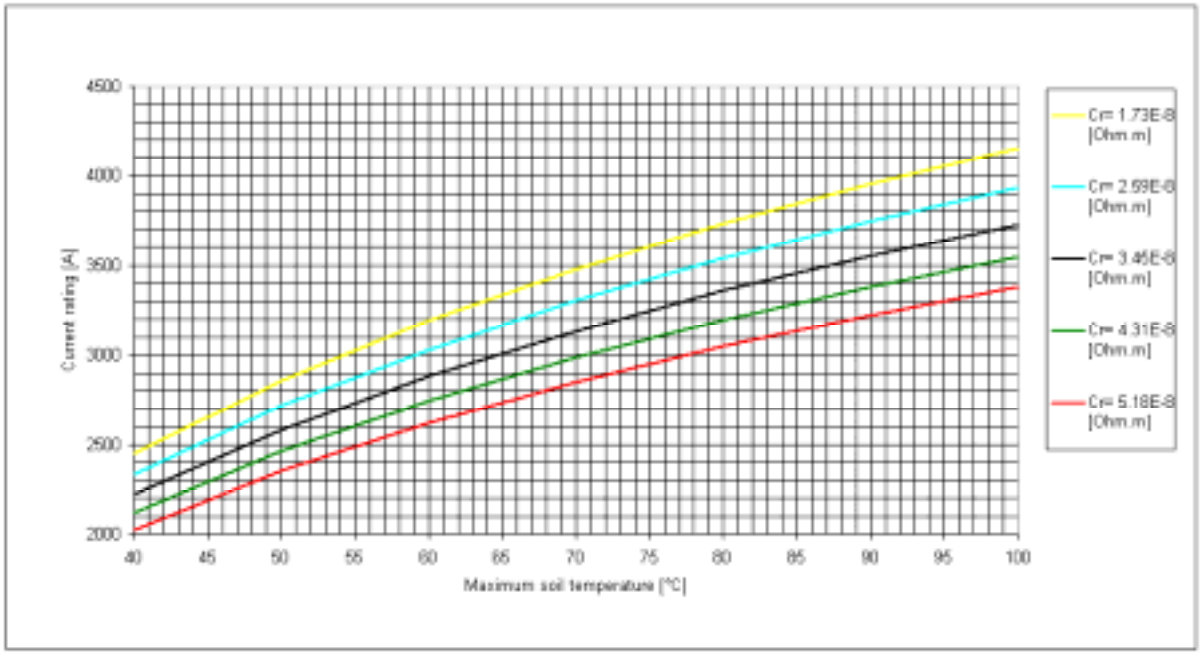

Figure 7-27 Current rating vs. Maximum soil temperature. Variable dimension: Conductor electric resistivity [Cr]. V=400 kV

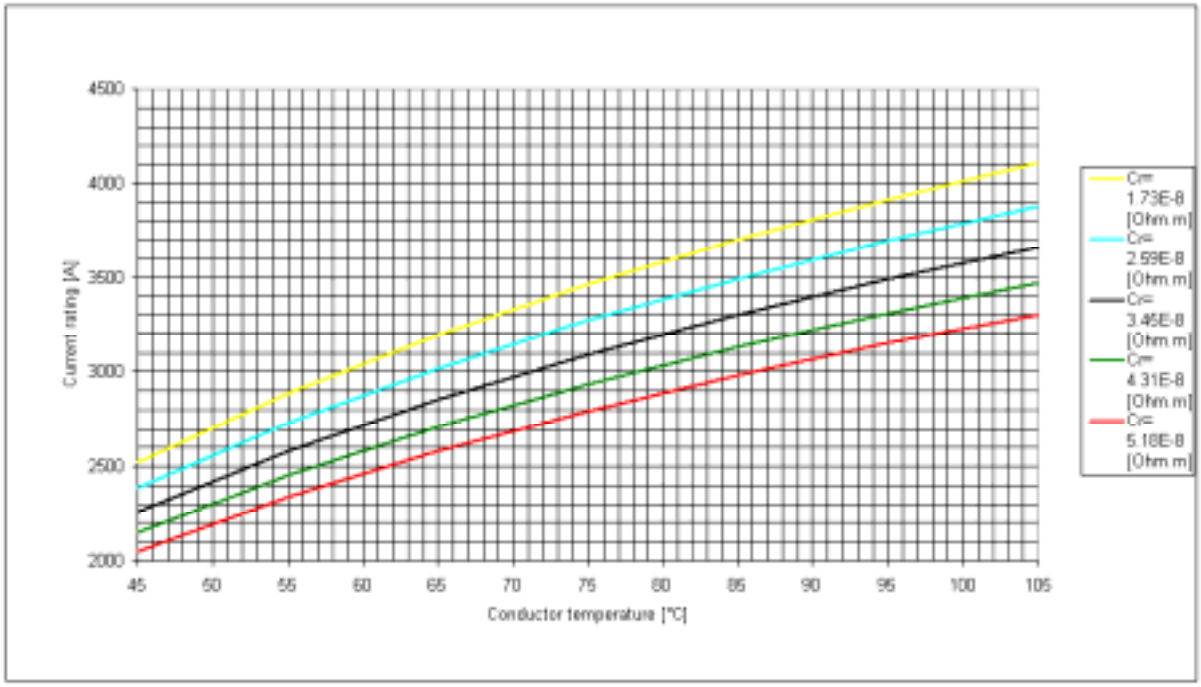

Figure 7-28 Current rating vs. Conductor temperature. Variable dimension: Conductor electric resistivity [Cr]. V=400 kV

7.2.15 Parameterised Quantity: Enclosure Electric Resistivity

Table 7-31: Current rating (A) as a function of the electric resistivity of the enclosure and of the maximum soil temperature.

Max soil temperature (°C)	Er= 2.95E-8 [Ω.m]	Er= 4.43E-8 [Ω.m]	Er= 5.9E-8 [Ω.m]	Er= 7.38E-8 [Ω.m]	Er= 8.85E-8 [Ω.m]	Crpv(-50%)	Crpv(+50%)
40	2550.51	2370.45	2223.24	2099.33	1994.7	14.7%	-10.3%
50	2968.86	2758.51	2586.79	2442.26	2320.31	14.8%	-10.3%
60	3313.55	3077.96	2885.86	2724.33	2588.04	14.8%	-10.3%
70	3607.53	3350.2	3140.61	2964.48	2815.96	14.9%	-10.3%
80	3863.87	3587.41	3362.47	3173.57	3014.36	14.9%	-10.4%
90	4090.88	3797.34	3558.74	3358.48	3189.79	15.0%	-10.4%
100	4294.28	3985.31	3734.4	3523.94	3346.75	15.0%	-10.4%
					Average =	14.9%	-10.3%

Table 7-32 Current rating (A) as a function of the electric resistivity of the enclosure and of the conductor temperature.

Conductor temperature (°C)	Er= 2.95E-8 [Ω.m]	Er= 4.43E-8 [Ω.m]	Er= 5.9E-8 [Ω.m]	Er= 7.38E-8 [Ω.m]	Er= 8.85E-8 [Ω.m]	Crpv(-50%)	Crpv(+50%)
45	2559.01	2397.82	2263.47	2148.56	2050.28	13.1%	-9.4%
55	2929.71	2742.55	2586.97	2454.16	2340.77	13.2%	-9.5%
65	3244.1	3034.43	2860.55	2712.37	2586.02	13.4%	-9.6%
75	3517.72	3288.09	3098.05	2936.33	2798.6	13.5%	-9.7%
85	3760.02	3512.41	3307.87	3134.05	2986.17	13.7%	-9.7%
95	3977.31	3713.32	3495.62	3310.85	3153.81	13.8%	-9.8%
105	4174.03	3895.01	3665.27	3470.51	3305.13	13.9%	-9.8%
					Average=	13.5%	-9.6%

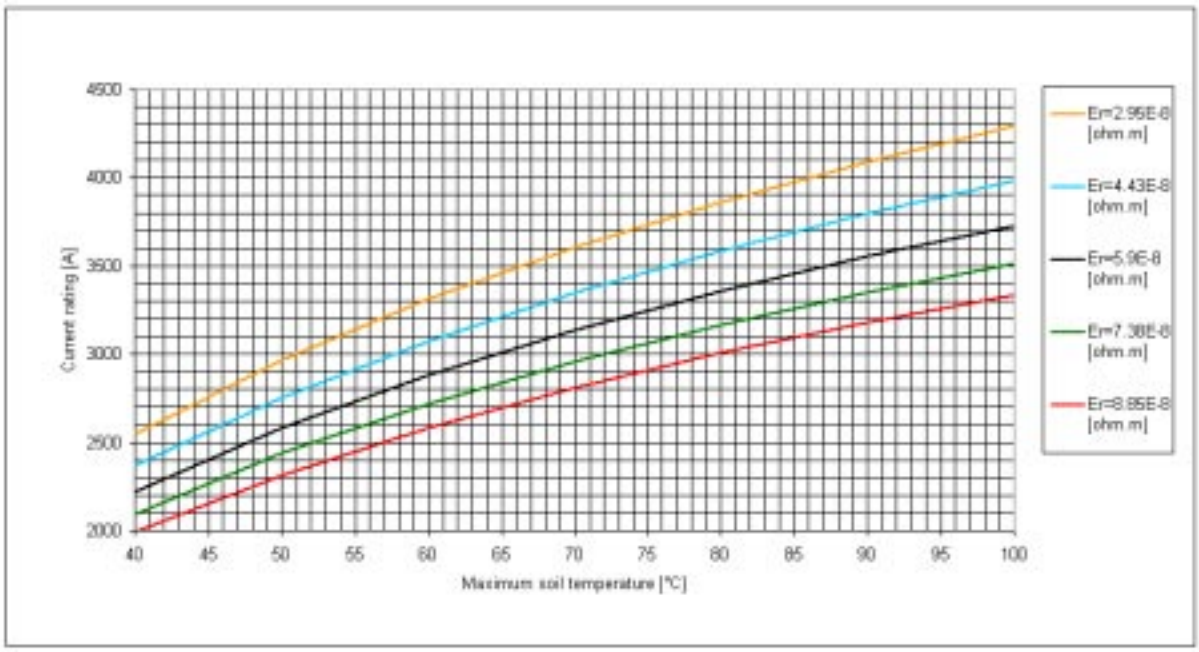

Figure 7-29 Current rating vs. Maximum soil temperature. Variable dimension: Enclosure electric resistivity [Er]. V=400 kV

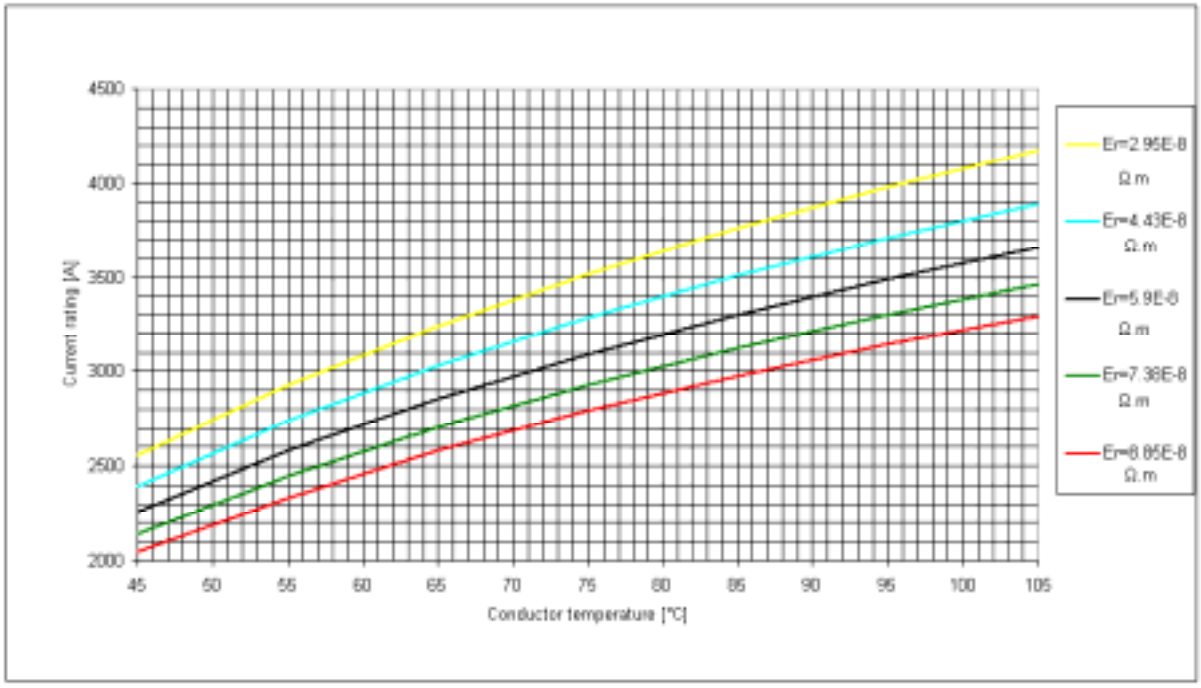

Figure 7-30 Current rating vs. Conductor temperature. Variable dimension: Enclosure electric resistivity [Er]. V=400 kV

7.2.16 Resultant Percentage Variations In Current Rating For A ±50% Change In Each Parameter

Table 7-33 Table 7-34 show the percentage variations of the current rating for the ±50% range of the numerical value of the reference parameters. The results of **Table 7-33** take as reference the maximum soil temperature, while **Table 7-34** takes as reference the conductor temperature.

Figure 7-31 and Figure 7-32 show the results in graphic form.

Table 7-33 **Current rating percentage variation for a ±50% of variation of the parameter values, related to the maximum soil temperature.**

Parameters	Parameter variation = -50%	Parameter variation = +50%	Total abs. values
Soil thermal resistivity	36.4%	-17.2%	53.6%
Enclosure diameter	-25.0%	15.6%	40.6%
Conductor diameter	-20.3%	10.0%	30.4%
Enclosure thickness	-17.7%	8.6%	26.4%
Enclosure electric resistivity	14.9%	-10.3%	25.2%
Burial depth	16.3%	-8.6%	24.9%
Axial Spacing	-12.3%	8.7%	21.0%
Conductor electric resistivity	10.9%	-9.1%	20.1%
Conductor thickness	-14.9%	2.6%	17.5%
Soil surface thermal resistivity	1.9%	-1.7%	3.5%
K2 Constant of N2 thermal convection	-0.15%	0.08%	0.23%
Gas mixture pressure	-0.13%	0.07%	0.20%
Conductor and enclosure thermal emissivity	-0.05%	0.04%	0.09%
K1 Constant SF6 thermal convection	-0.02%	0.02%	0.05%
SF6 Volume content	-0.01%	0.01%	0.02%

Table 7-34 Current rating percentage variation for a ±50% of variation of the parameter values, related to the conductor temperature

Parameters	Parameter variation = -50%	Parameter variation = +50%	Total abs. values
Soil thermal resistivity	32.1%	-16.1%	48.2%
Enclosure diameter	-27.8%	14.8%	42.6%
Conductor diameter	-24.0%	11.2%	35.1%
Enclosure thickness	-16.7%	7.9%	24.5%
Enclosure electric resistivity	13.5%	-9.6%	23.2%
Burial depth	14.7%	-7.9%	22.7%
Conductor electric resistivity	11.9%	-9.7%	21.6%
Axial Spacing	-11.5%	7.9%	19.4%
Conductor thickness	-15.7%	2.7%	18.5%
Soil surface thermal resistivity	1.7%	-1.6%	3.3%
K2 Constant of N2 thermal convection	-1.8%	1.0%	2.9%
Gas mixture pressure	-1.6%	0.8%	2.4%
Conductor and enclosure thermal emissivity	-0.5%	0.5%	1.0%
K1 Constant SF6 convection	-0.3%	0.3%	0.6%
SF6 Volume content	-0.1%	0.1%	0.3%

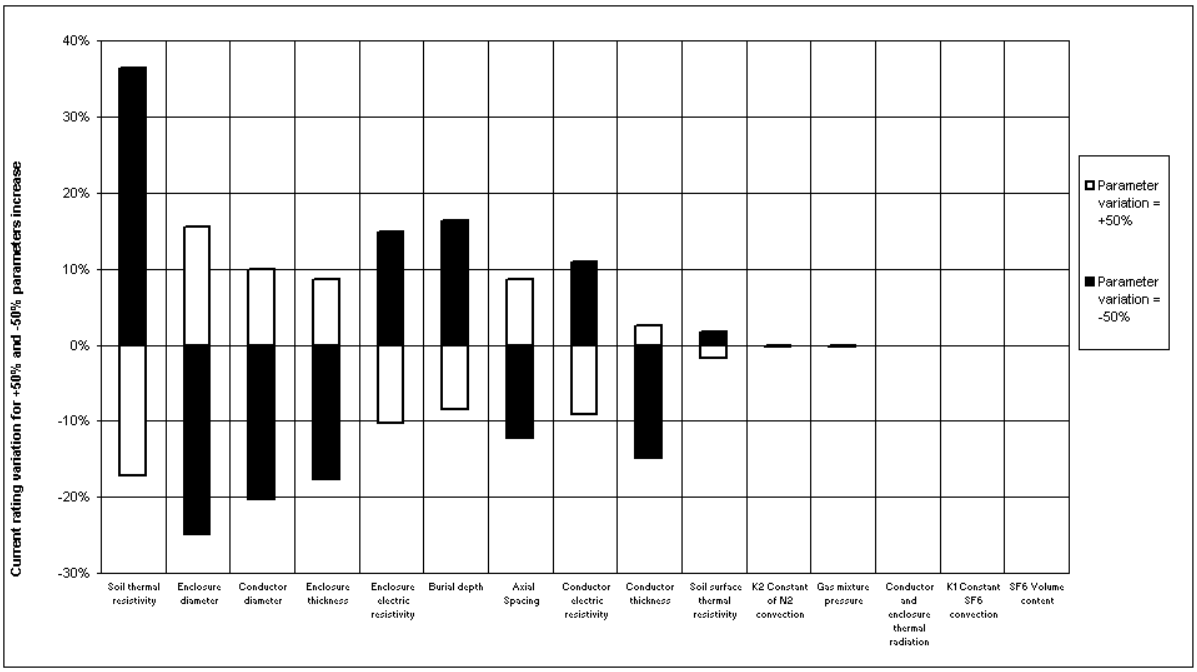

Figure 7-31 Current rating variation for -50% and +50% of the design parameters increase. Maximum soil temperature. V=400kV

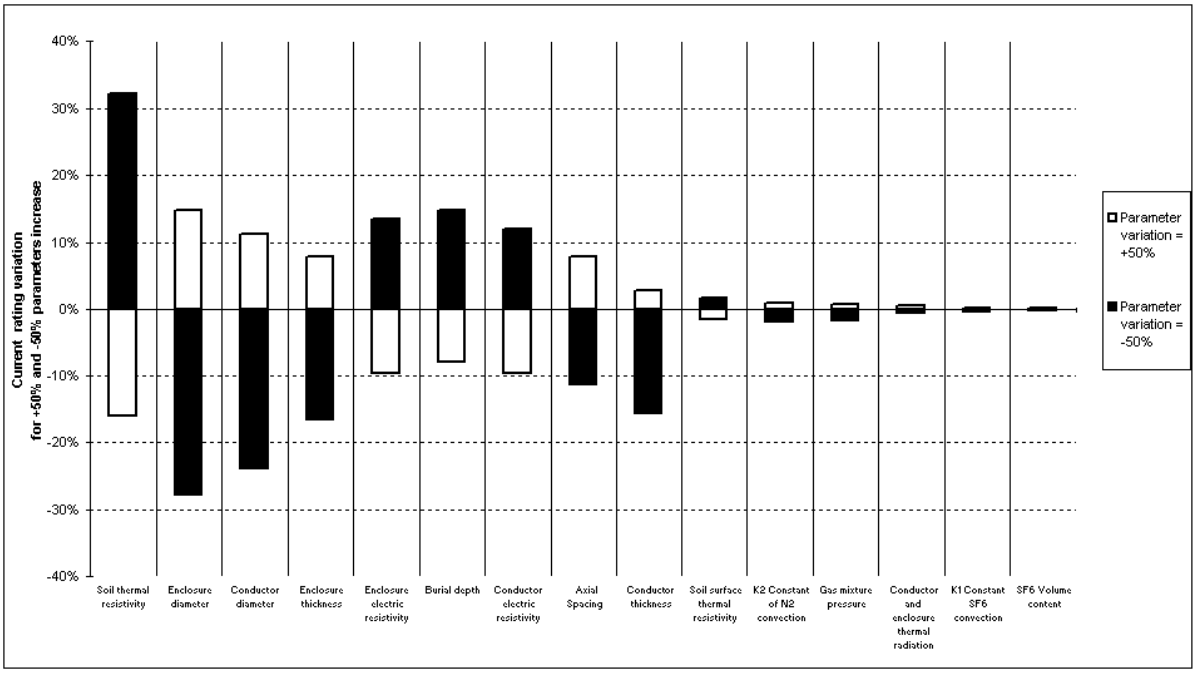

Figure 7-32 Current rating percentage variation for -50% and +50% of the design parameters increase. Conductor temperature. V=400kV

7.3 Sensitivity Study On Conductor And Maximum Soil Temperatures At Constant Current Rating

In the previous paragraph the sensitivity study has been carried out with the aim to analyse the effect of the different GIL design parameters on the current rating. In the present chapter the sensitivity study considers the effect of the different GIL design parameters on the conductor temperature and on the maximum soil temperature, at a constant current rating, equal to 3000A.

The tables and Figures from 33 to 47 show the maximum soil temperatures and the conductor temperatures calculated at the parameter values of Table 7-2 and their intermediate values. In the last two rows of each Table the percentage variations of the maximum soil and conductor temperatures respectively are shown, for the assumed ±50% variation of the parameter. They are calculated as in the following expression:

$$\mathrm{Tpv}(\pm 50\%) = \frac{\vartheta(\pm 50\%) - \vartheta_a}{\vartheta(\mathrm{std}) - \vartheta_a} - 1$$

where:

Tpv(±50%) is the temperature rise to the ambient temperature percentage variation for the ±50% parameter variation,

$\vartheta(\pm 50\%) - \vartheta_a$ is the temperature rise to the ambient temperature, calculated at the parameter variations

$\vartheta(\mathrm{std}) - \vartheta_a$ is the temperature rise to the ambient temperature, calculated at the standard value

7.3.1 Parameterised Quantity: Axial Spacing Between Adjacent Enclosures

Table 7-35 Maximum soil and conductor temperature as a function of the axial spacing at a current rating of 3000A

Axial Spacing (mm)	Conductor Temperature (°C)	Max.Soil Temperature (°C)
656	89.3	82.9
984	78.0	71.6
1312	70.7	64.3
1640	65.7	59.3
1968	62.0	55.6
Tpv(-50%) =	33.4%	37.6%
Tpv(+50% =	-15.7%	-17.7%

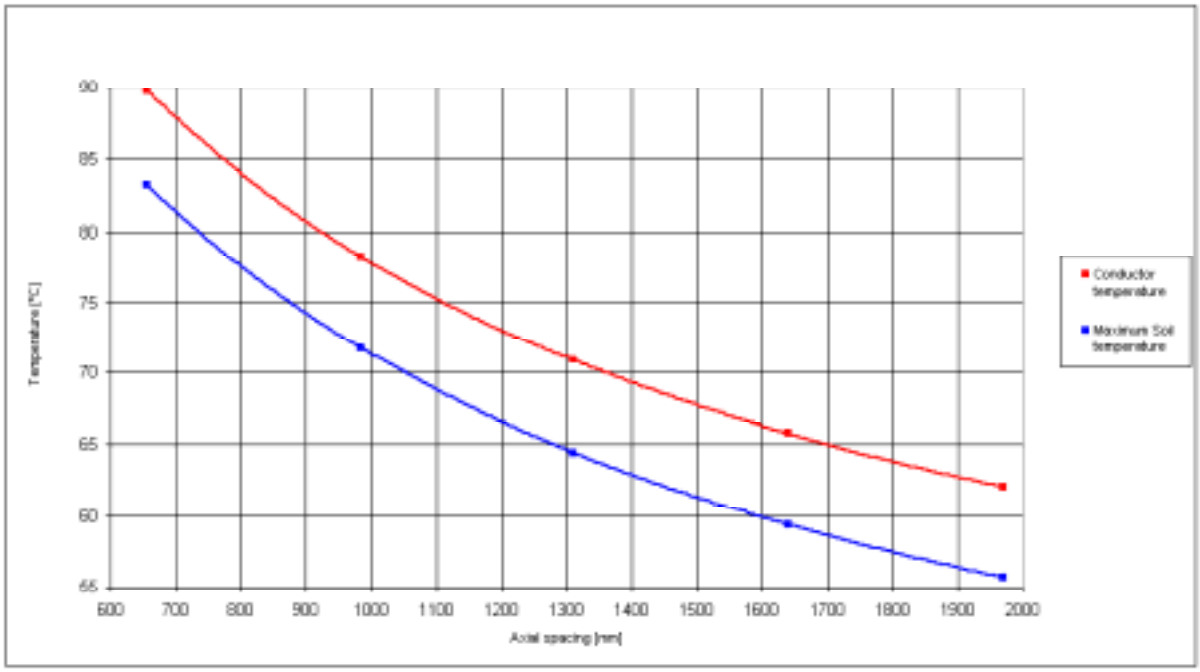

Figure 7-33 Conductor and maximum soil temperature vs. axial spacing. I=3000A,V=400kV

7.3.2 Parameterised Quantity: Depth Of Burial

Table 7-36 Maximum soil and conductor temperature as a function of the burial depth at a current rating of 3000A.

Burial depth (mm)	Conductor Temperature (°C)	Max.Soil Temperature (°C)
525.0	56.1	49.7
787.5	63.8	57.4
1050.0	70.7	64.3
1312.5	76.9	70.5
1575.0	82.6	76.2
Tpv(-50%) =	-26.3%	-29.5%
Tpv(+50% =	21.4%	24.1%

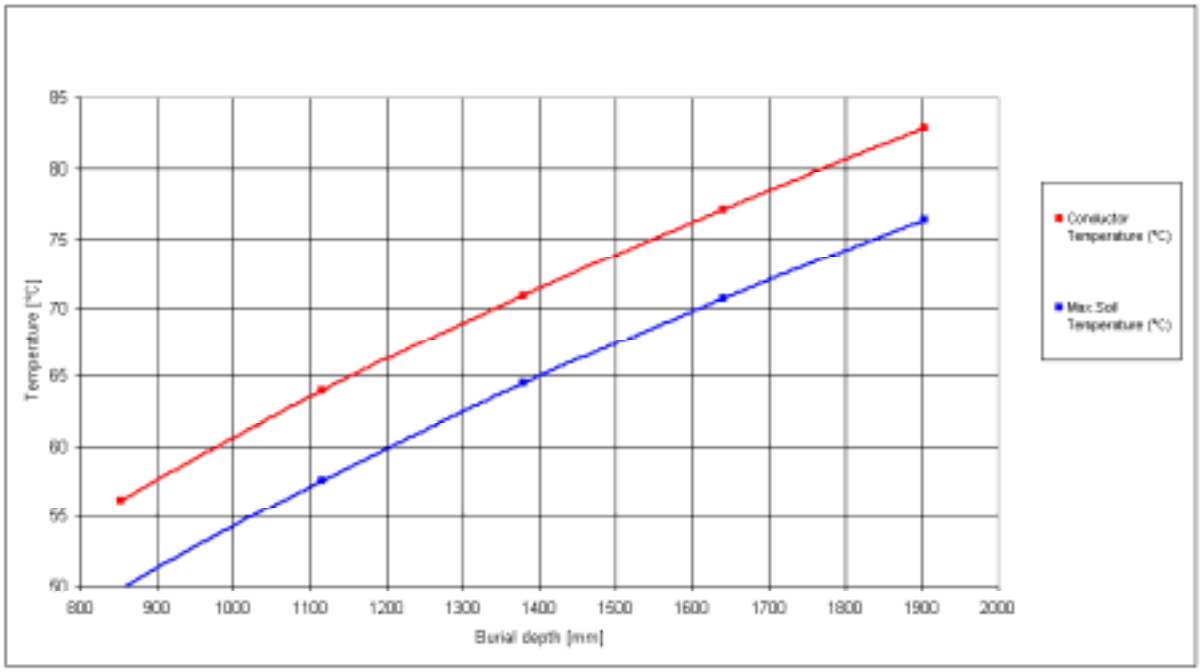

Figure 7-34 Conductor and Maximum soil temperature vs. Burial depth. I=3000A V=400kV

7.3.3 Parameterised quantity: Conductor diameter

Table 7-37 Maximum soil and conductor temperature as a function of the conductor diameter at a current rating of 3000A.

Conductor diameter (mm)	Conductor Temperature (°C)	Max.Soil Temperature (°C)
140	120.9	102.2
210	85.0	75.3
280	70.7	64.3
350	63.2	58.3
420	58.8	54.4
Tpv(-50%) =	90.0%	76.8%
Tpv(+50% =	-21.4%	-20.0%

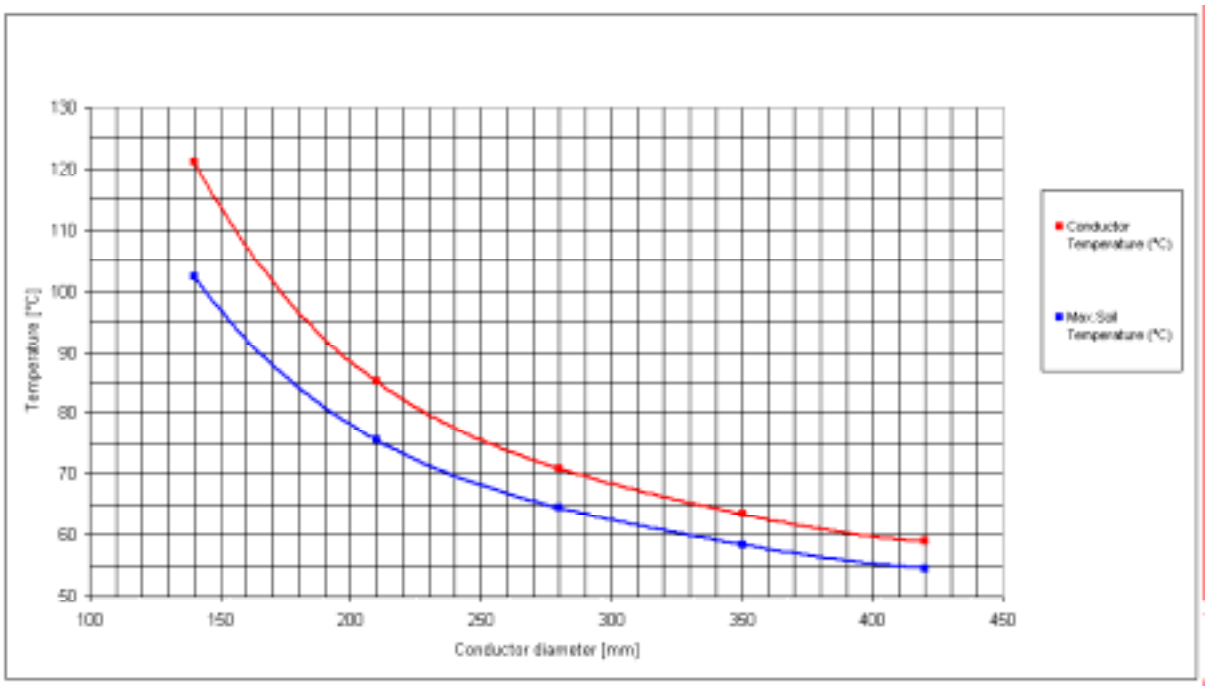

Figure 7-35 Conductor and Maximum soil temperature vs. Conductor diameter. I=3000A V=400kV

7.3.4 Parameterised Quantity: Conductor Radial Thickness

Table 7-38 Maximum soil and conductor temperature as a function of the conductor thickness at a current rating of 3000A.

Conductor thickness (mm)	Conductor Temperature (°C)	Max.Soil Temperature (°C)
8	99.3	89.0
12	78.7	71.1
16	70.7	64.3
20	67.9	61.9
24	67.6	61.6
Tpv(-50%) =	51.3%	50.1%
Tpv(+50% =	-5.6%	-5.4%

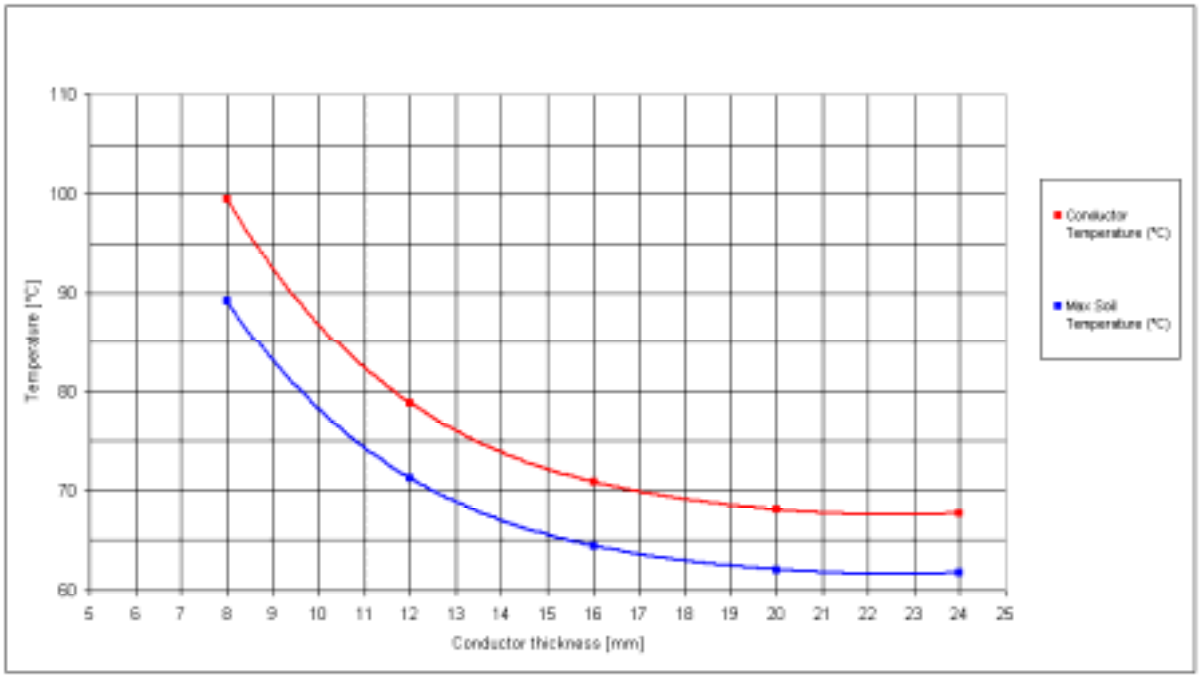

Figure 7-36 Conductor and Maximum soil temperature vs. Conductor thickness. I=3000A V=400kV

7.3.5 Parameterised Quantity: Enclosure Diameter

Table 7-39 **Maximum soil and conductor temperature as a function of the enclosure diameter at a current rating of 3000A.**

Enclosure diameter (mm)	Conductor Temperature (°C)	Max.Soil Temperature (°C)
325	135.1	117.9
487.5	87.6	79.8
650	70.7	64.3
812.5	61.7	55.8
975	56.0	50.3
Tpv(-50%) =	115.0%	109.0%
Tpv(+50% =	-26.4%	-28.4%

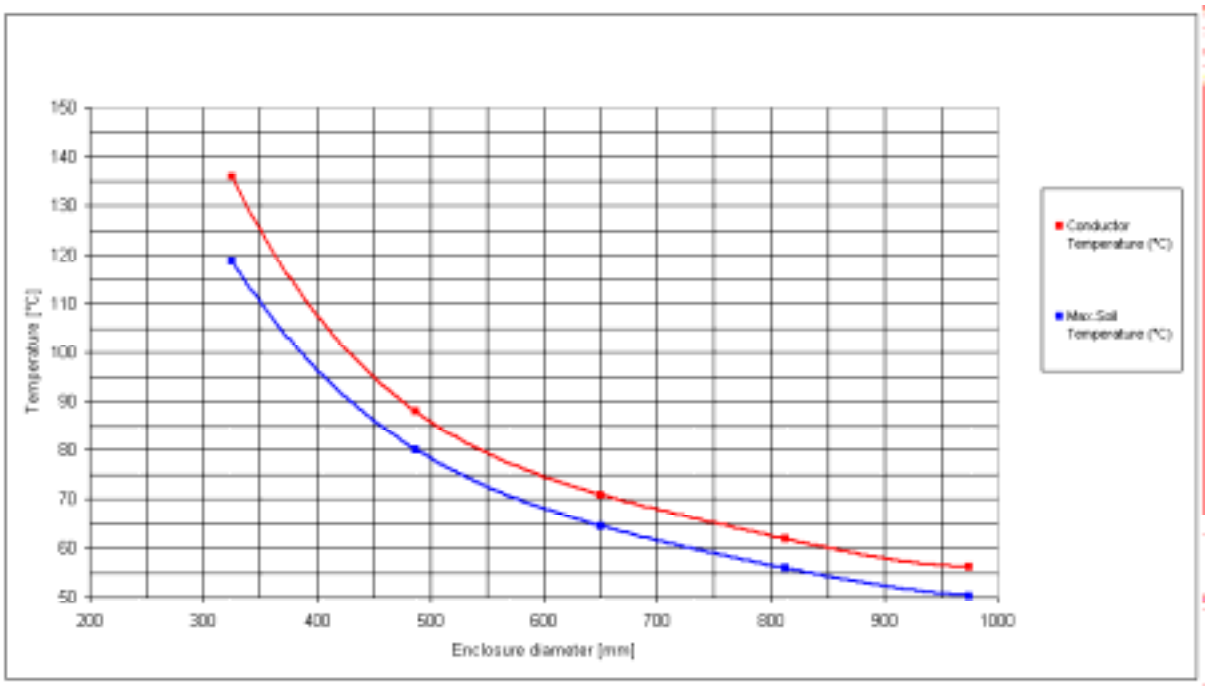

Figure 7-37 Conductor and Maximum soil temperature vs. Enclosure Diameter. I=3000A V=400kV

7.3.6 Parameterised Quantity: Enclosure Thickness

Table 7-40 Maximum soil and conductor temperature as a function of the enclosure thickness at a current rating of 3000A.

Enclosure thickness (mm)	Conductor Temperature (°C)	Max.Soil Temperature (°C)
5	101.7	95.0
7.5	80.4	73.9
10	70.7	64.3
12.5	65.3	59.0
15	62.1	55.7
Tpv(-50%) =	55.6%	62.3%
Tpv(+50% =	-15.6%	-17.5%

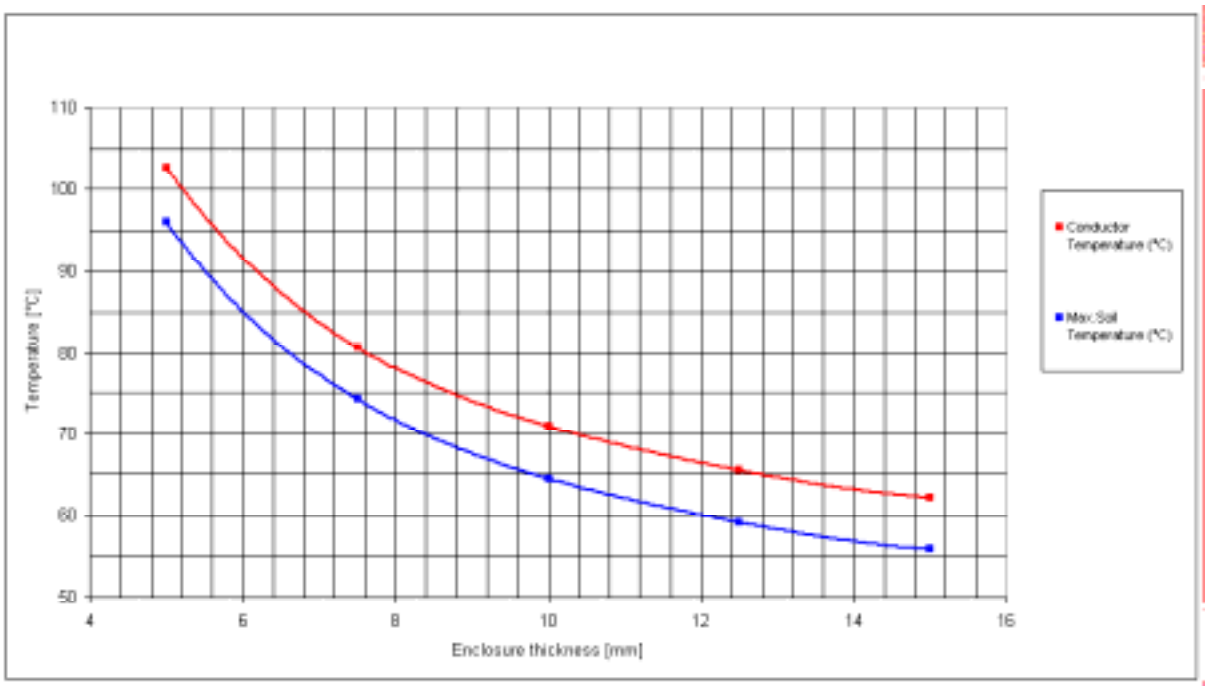

Figure 7-38 Conductor and Maximum soil temperature vs. Enclosure thickness. I=3000A V=400kV

7.3.7 Parameterised Quantity: Heat Transfer At The Soil Surface, As Represented By An Effective Thermal Resistivity

Table 7-41 Maximum soil and conductor temperature as a function of the soil surface thermal resistivity at a current rating of 3000A.

Soil surface thermal resistivity ($K.m^2/W$)	Conductor Temperature (°C)	Max.Soil Temperature (°C)
0.1	68.6	62.2
0.15	69.7	63.3
0.2	70.7	64.3
0.25	71.7	65.3
0.3	72.8	66.3
Tpv(-50%) =	-3.8%	-4.3%
Tpv(+50% =	3.7%	4.1%

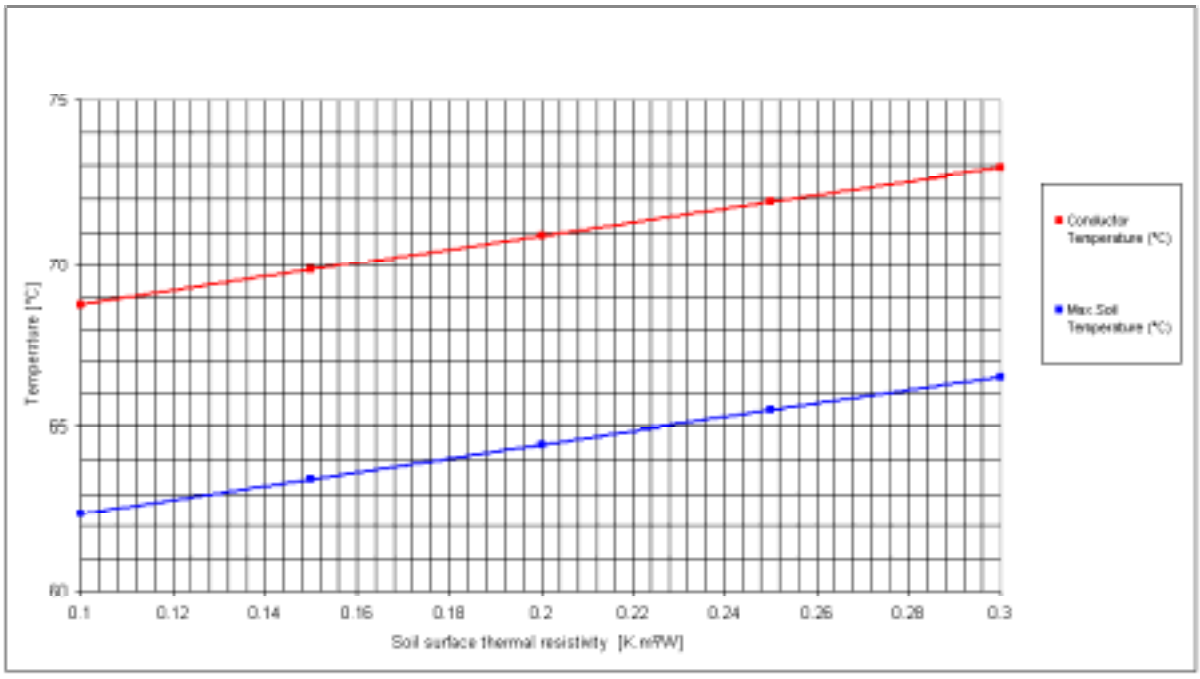

Figure 7-39 Conductor and Maximum soil temperature vs. Soil surface thermal resistivity (beta). I=3000A V=400kV

7.3.8 Parameterised Quantity: Soil Thermal Resistivity

Table 7-42 Maximum soil and conductor temperature as a function of the soil thermal resistivity at a current rating of 3000A.

Soil thermal resistivity (K.m/W)	Conductor Temperature (°C)	Max.Soil Temperature (°C)
0.6	45.6	39.4
0.9	57.7	51.4
1.2	70.7	64.3
1.5	84.8	78.3
1.8	100.1	93.6
Tpv(-50%) =	-45.0%	-50.6%
Tpv(+50% =	52.7%	59.4%

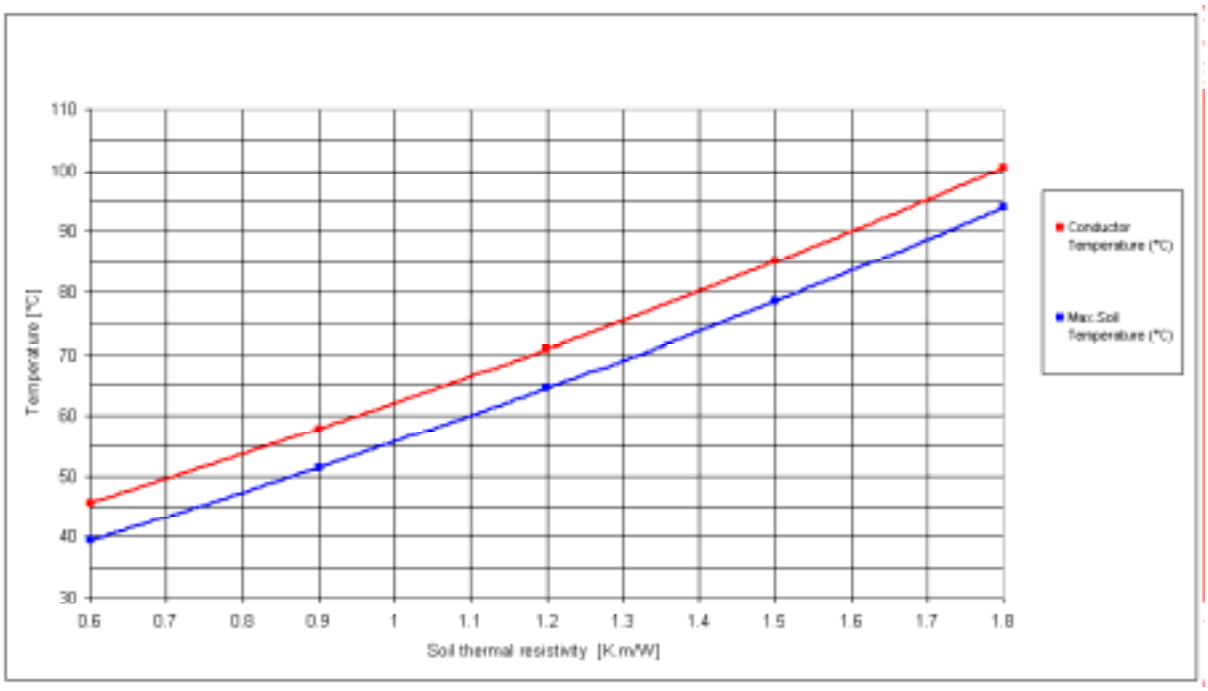

Figure 7-40 Conductor and Maximum soil temperature vs. Soil thermal resistivity. I=3000A V=400kV

7.3.9 Parameterised Quantity: Conductor And Enclosure Emissivity

Table 7-43 Maximum soil and conductor temperature as a function of the conductor and enclosure emissivity at a current rating of 3000A.

Emissivity of conductor and enclosure surfaces	Conductor Temperature (°C)	Max.Soil Temperature (°C)
0.1	71.4	64.4
0.15	71.0	64.3
0.2	70.7	64.3
0.25	70.4	64.3
0.3	70.1	64.3
Tpv(-50%) =	1.2%	0.1%
Tpv(+50% =	-1.1%	-0.1%

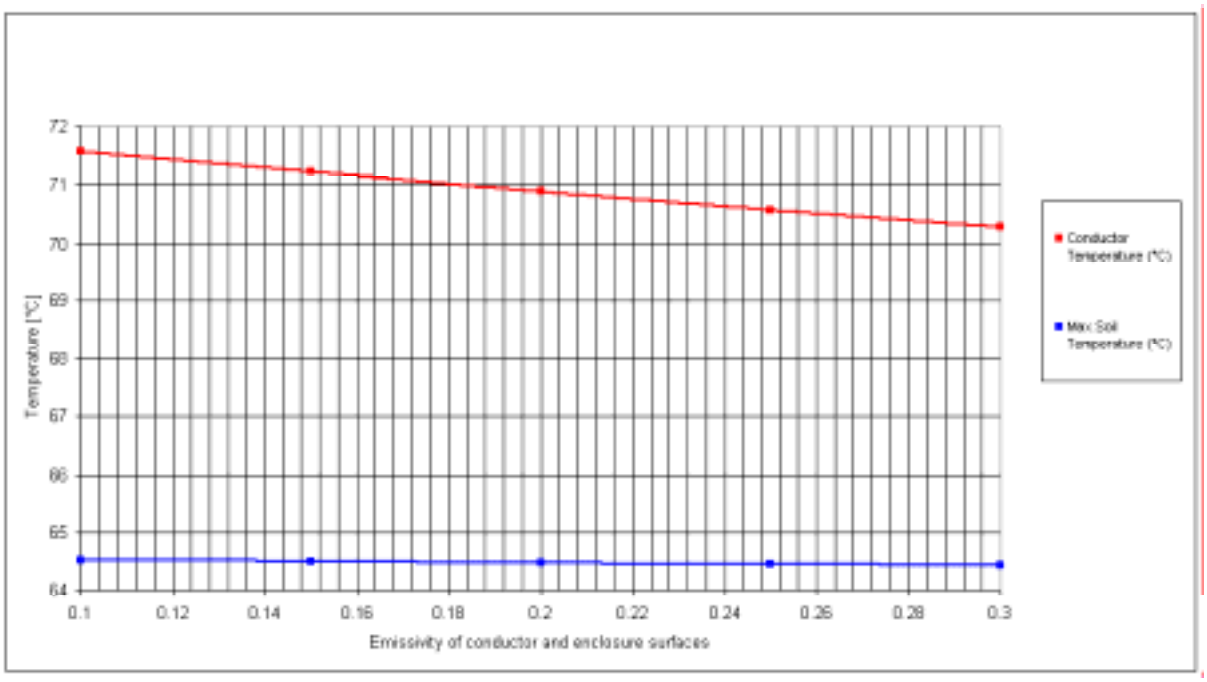

Figure 7-41 Conductor and Maximum soil temperature vs. Emissivity of conductor and enclosure surfaces. I=3000A V=400kV

7.3.10 Parameterised Quantity: Gas Mixture Pressure

Table 7-44 Maximum soil and conductor temperature as a function of the gas mixture pressure at a current rating of 3000A.

Gas mixture absolute pressure (bar abs.)	Conductor Temperature (°C)	Max.Soil Temperature (°C)
3.35	72.8	64.5
5.03	71.5	64.4
6.7	70.7	64.3
8.38	70.1	64.3
10.05	69.7	64.2
Tpv(-50%) =	3.8%	0.3%
Tpv(+50% =	-1.9%	-0.2%

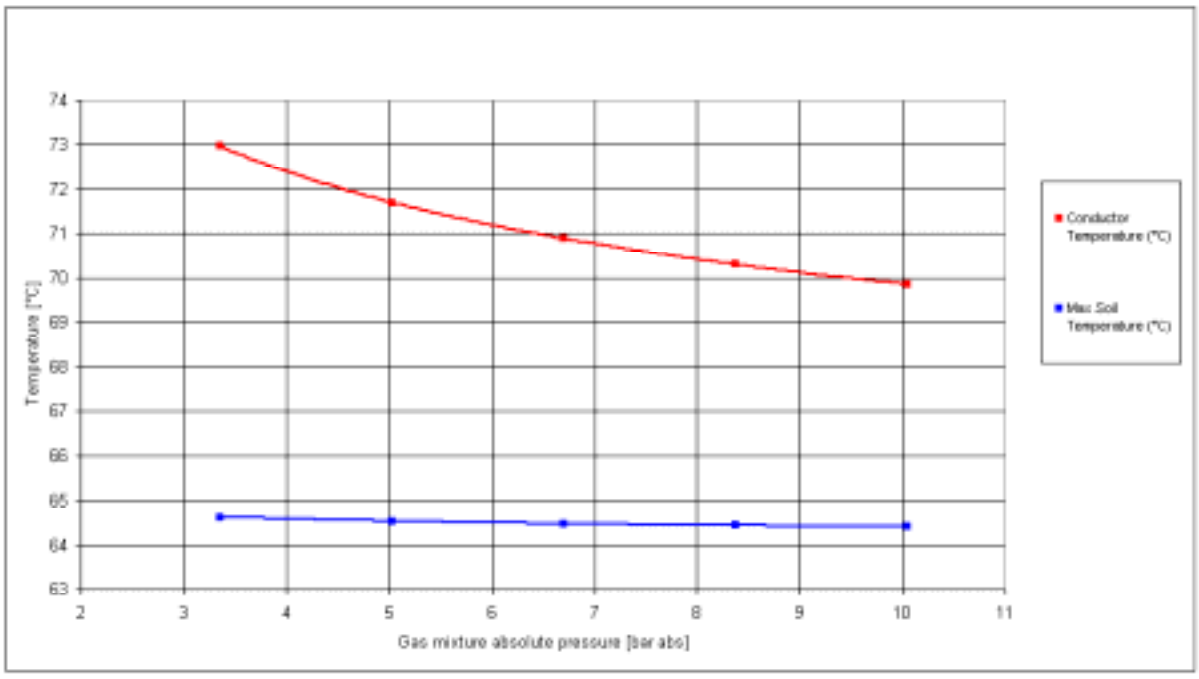

Figure 7-42 Conductor and Maximum soil temperature vs. Gas mixture absolute pressure. I=3000A V=400kV

7.3.11 Parameterised Quantity: Thermal Convection Constant Of The SF_6

Table 7-45 Maximum soil and conductor temperature as a function of the thermal convection constant of the SF_6 at a current rating of 3000A.

Thermal convection constant of the SF_6	Conductor Temperature (°C)	Max.Soil Temperature (°C)
5.65	71.1	64.3
8.48	70.9	64.3
11.3	70.7	64.3
14.13	70.5	64.3
16.95	70.4	64.3
Tpv(-50%) =	0.7%	0.06%
Tpv(+50% =	-0.6%	-0.05%

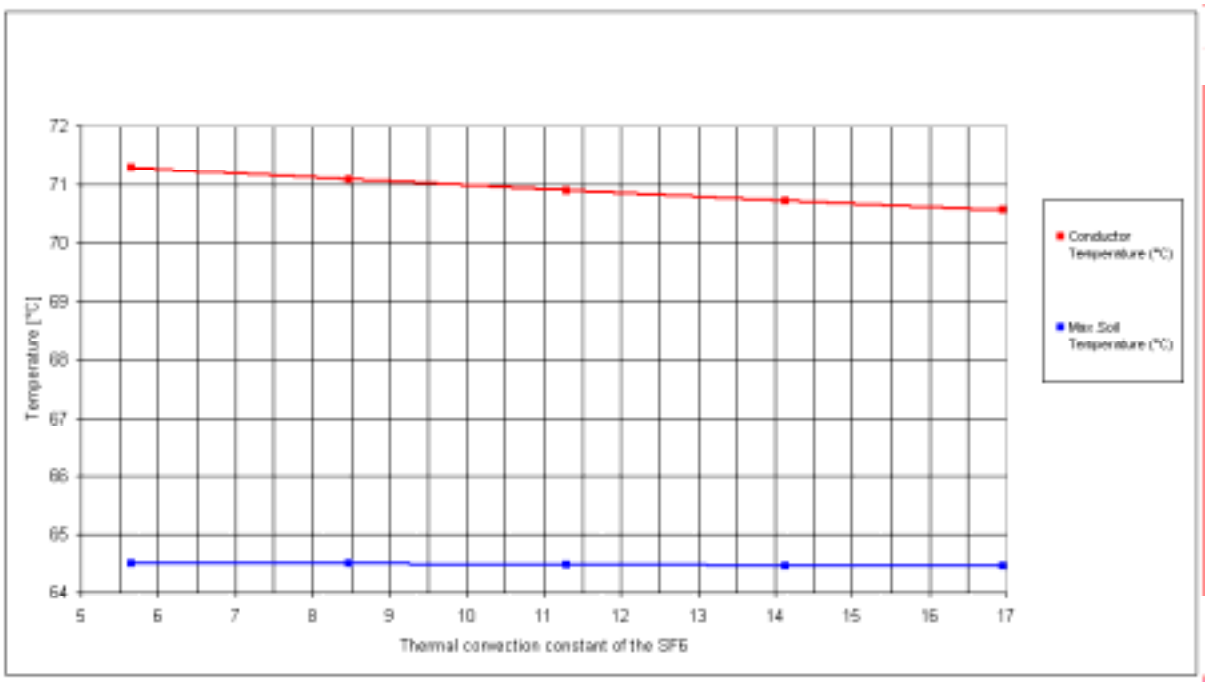

Figure 7-43 Conductor and Maximum soil temperature vs. Thermal convection constant of the SF6. I=3000A V=400kV

7.3.12 Parameterised Quantity: Thermal Convection Constant Of The N_2

Table 7-46 Maximum soil and conductor temperature as a function of the thermal convection constant of the N_2 at a current rating of 3000A.

Thermal convection constant of the N2	Conductor Temperature (°C)	Max.Soil Temperature (°C)
2.92	73.1	64.5
4.37	71.7	64.4
5.83	70.7	64.3
7.29	70.0	64.3
8.75	69.4	64.2
Tpv(-50%) =	4.4%	0.4%
Tpv(+50% =	-2.3%	-0.2%

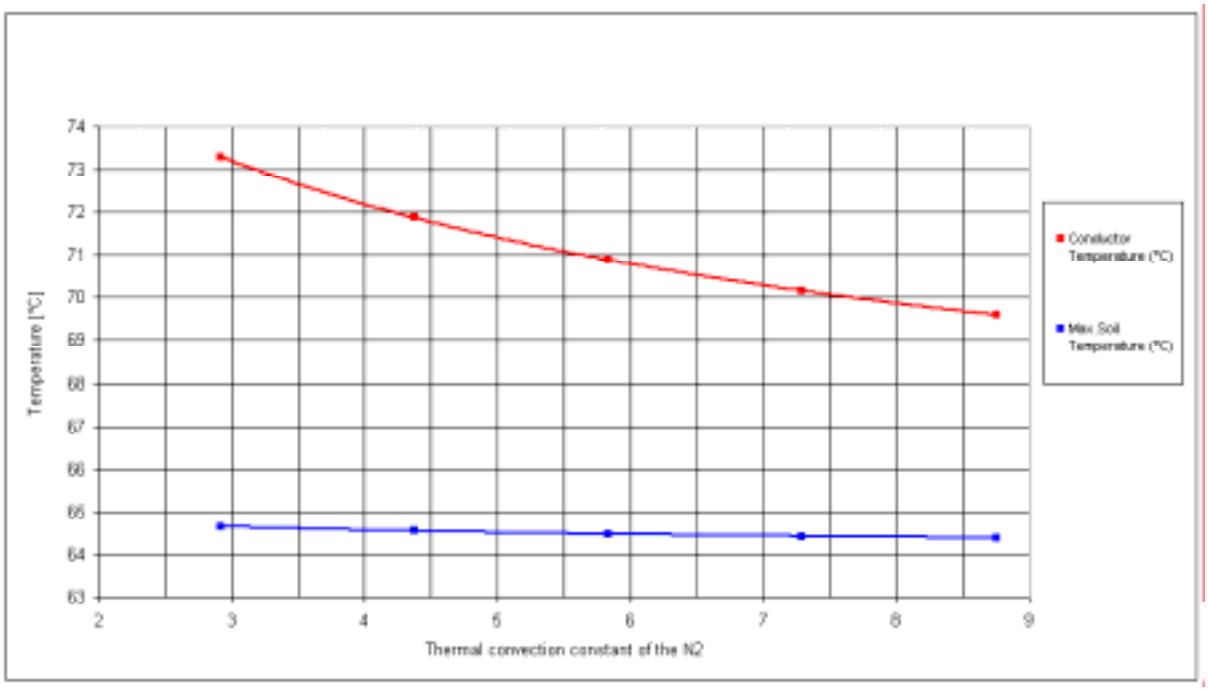

Figure 7-44 Conductor and Maximum soil temperature vs. Thermal convection constant of the N2. I=3000A V=400kV

7.3.13 Parameterised Quantity: SF_6 Percent Of Volume Content In Gas Mixture

Table 7-47 Maximum soil and conductor temperature as a function of the SF_6 percent of volume content in gas mixture at a current rating of 3000A.

SF6 Volume content (%)	Conductor Temperature (°C)	Max.Soil Temperature (°C)
5	70.9	64.3
7.5	70.8	64.3
10	70.7	64.3
12.5	70.6	64.3
15	70.5	64.3
perc(-50%) =	0.3%	0.03%
perc(+50% =	-0.3%	-0.02%

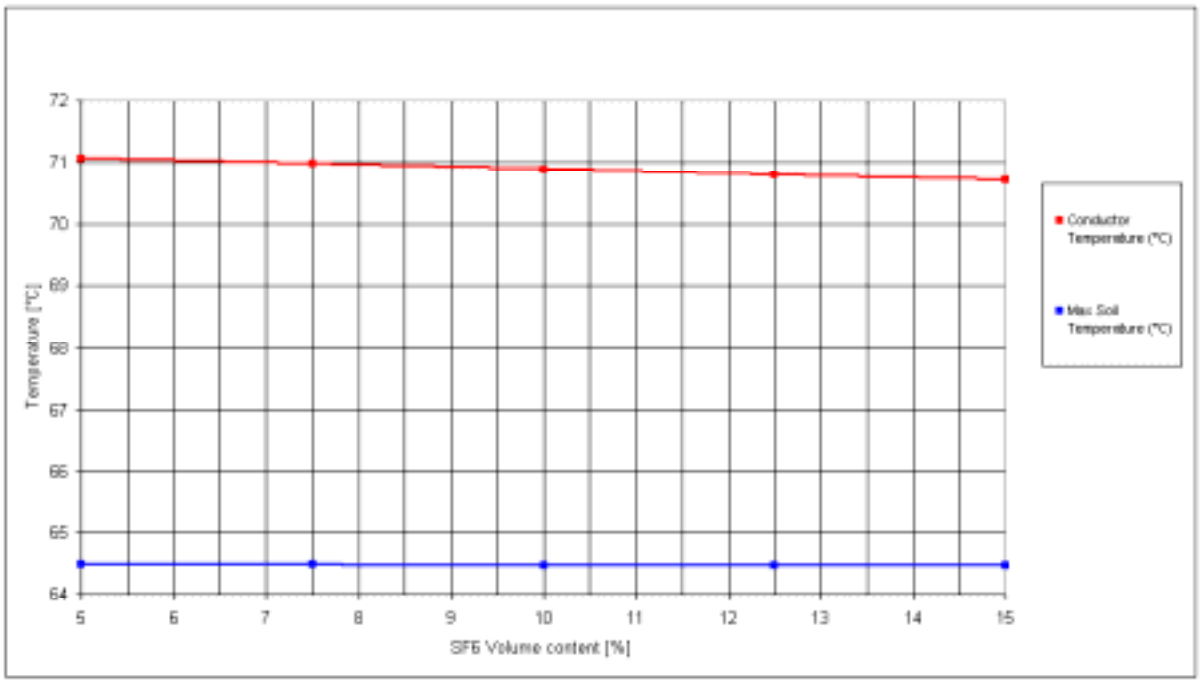

Figure 7-45 Conductor and Maximum soil temperature vs. SF6 Volume content. I=3000A V=400kV

7.3.14 Parameterised Quantity: Conductor Electric Resistivity

Table 7-48 Maximum soil and conductor temperature as a function of the conductor electric resistivity at a current rating of 3000A.

Conductor electric resistivity (Ω.m)	Conductor Temperature (°C)	Max.Soil Temperature (°C)
1.73E-08	58.4	54.0
2.59E-08	64.2	58.7
3.45E-08	70.7	64.3
4.31E-08	77.9	70.5
5.18E-08	85.8	77.3
Tpv(-50%) =	-22.1%	-21.0%
Tpv(+50% =	27.1%	26.3%

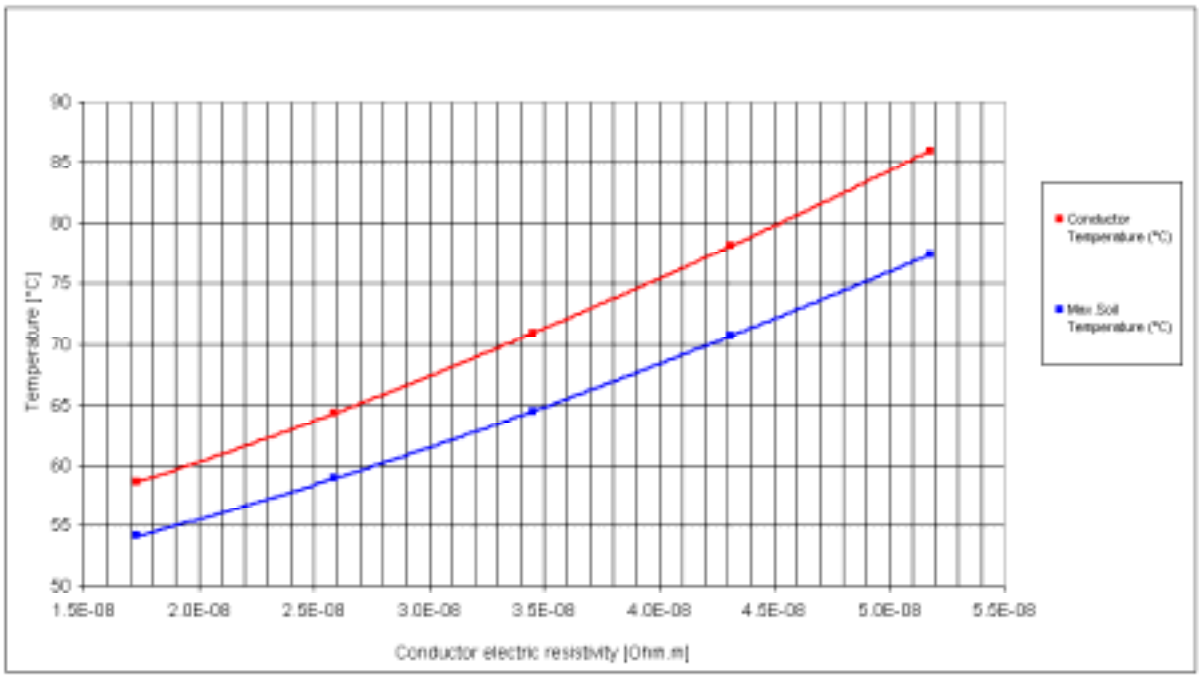

Figure 7-46 Conductor and Maximum soil temperature vs. Conductor electric resistivity. I=3000A V=400kV

7.3.15 Parameterised Quantity: Enclosure Electric Resistivity

Table 7-49 Maximum soil and conductor temperature as a function of the enclosure electric resistivity at a current rating of 3000A.

Enclosure electric resistivity (Ω.m)	Conductor Temperature (°C)	Max.Soil Temperature (°C)
2.95E-08	57.1	50.8
4.43E-08	63.7	57.4
5.90E-08	70.7	64.3
7.38E-08	78.1	71.6
8.85E-08	85.8	79.2
Tpv(-50%) =	-24.4%	-27.3%
Tpv(+50% =	27.1%	30.3%

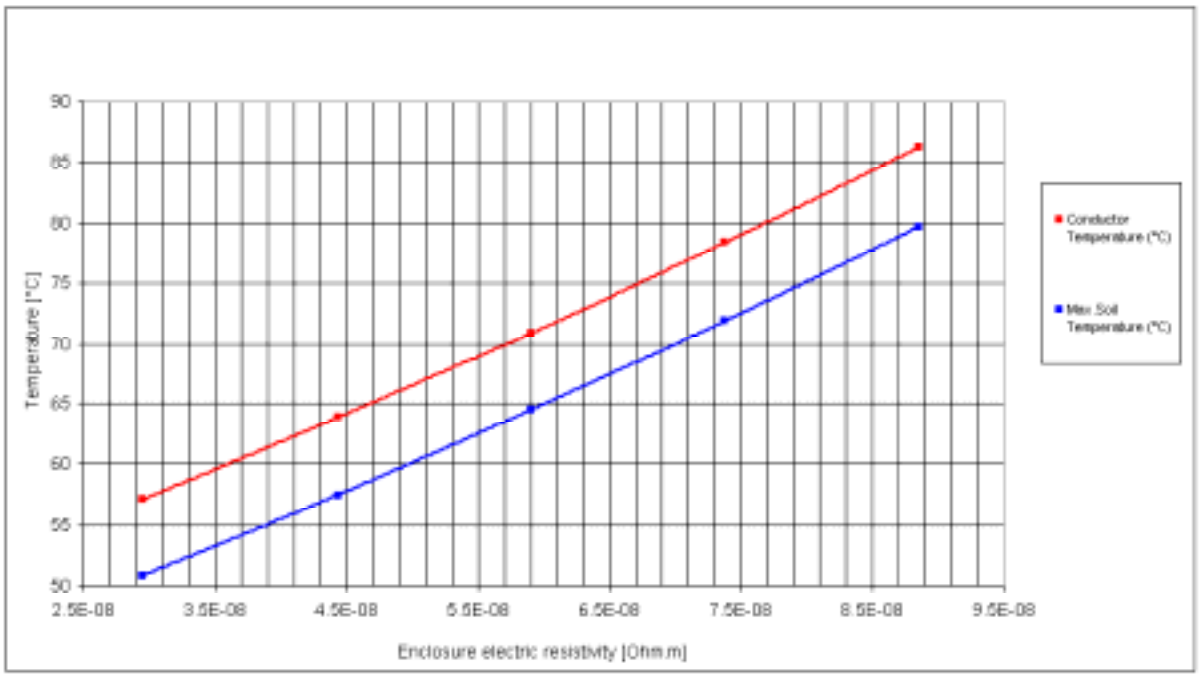

Figure 7-47 Conductor and Maximum soil temperature vs. Enclosure electric resistivity. I=3000A V=400kV

7.3.16 Resultant Percentage Variations In Operating Temperatures For A ±50% Change In Each Parameter

Table 7-50 and Table 7-51 show respectively the percentage variations of the maximum soil temperature and of the conductor temperature for the ±50% increase of the numerical value of the reference parameter. The change in parameter value was based upon the reference value i.e. the one used in the standard calculation, from which the current rating was calculated and the percentage variation evaluated. The percentages are referred to the conductor (or maximum soil temperature) rise to the ambient temperature. Figure 7-48 and Figure 7-49 show the results in graphic form.

The results show that the most important parameters in designing the GIL is the soil thermal resistivity and that means, from the physical point of view, that any mechanism that tends to alter the thermal resistivity, like drying out of the soil due to moisture migration promoted by the heat dissipated by the GIL, should be carefully considered. Moreover, from the numerical point of view, it also means that calculation of the soil thermal resistance should be rigorously undertaken.

Table 7-50 Maximum soil temperature percentage variation for a ±50% variation of the parameter values.

Parameters	Parameter variation = -50%	Parameter variation = +50%	Total abs. values
Enclosure diameter	109.0%	-28.4%	137.4%
Soil thermal resistivity	-50.6%	59.4%	110.0%
Conductor diameter	76.8%	-20.0%	96.8%
Enclosure thickness	62.3%	-17.5%	79.8%
Enclosure electric resistivity	-27.3%	30.3%	57.6%
Axial Spacing	37.6%	-17.7%	55.3%
Conductor thickness	50.1%	-5.4%	55.5%
Burial depth	-29.5%	24.1%	53.6%
Conductor electric resistivity	-21.0%	26.3%	47.3%
Soil surface thermal resistivity	-4.3%	4.1%	8.4%
K2 Constant of N2 convection	0.4%	-0.2%	0.5%

Gas mixture pressure	0.3%	-0.2%	0.46%
Conductor and enclosure thermal radiation	0.10%	-0.09%	0.19%
K1 Constant SF6 convection	0.06%	-0.05%	0.11%
SF6 Volume content	0.03%	-0.02%	0.05%

Table 7-51 Conductor temperature percentage variation for a ±50% variation of the parameter values.

Parameters	Parameter variation = -50%	Parameter variation = +50%	Total abs. values
Enclosure diameter	115.0%	-26.4%	141.4%
Conductor diameter	90.0%	-21.4%	111.4%
Soil thermal resistivity	-45.0%	52.7%	97.7%
Enclosure thickness	55.6%	-15.6%	71.2%
Conductor thickness	51.3%	-5.6%	56.9%
Enclosure electric resistivity	-24.4%	27.1%	51.5%
Axial Spacing	33.4%	-15.7%	49.1%
Conductor electric resistivity	-22.1%	27.1%	49.2%
Burial depth	-26.3%	21.4%	47.7%
Soil surface thermal resistivity	-3.8%	3.7%	7.5%
K2 Constant of N2 convection	4.4%	-2.3%	6.7%
Gas mixture pressure	3.8%	-1.9%	5.6%
Conductor and enclosure thermal radiation	1.2%	-1.1%	2.3%
K1 Constant SF6 convection	0.7%	-0.6%	1.3%
SF6 Volume content	0.3%	-0.3%	0.6%

7.3.17 Summary

- The percentage changes in current ratings at a constant conductor operating temperature and the equivalent changes at a constant maximum soil temperature are listed below in Table 7-52

Table 7-52

Parameters	+50%		-50%	
	Conductor	Soil max.	Conductor	Soil max.
Parameters which reduces the rating				
Soil thermal resistivity	-16.1%	-17.2%	32.1%	36.5%
Enclosure electric resistivity	-9.6%	-10.3%	13.5%	14.9%
Conductor electric resistivity	-9.7%	-9.1%	11.9%	10.9%
Burial depth	-7.9%	-8.6%	14.7%	16.3%
Soil surface thermal resistivity	-1.6%	-1.7%	1.7%	1.9%
Parameters which increase the rating				
Enclosure diameter	14.8%	15.6%	-27.8%	-25.0%
Conductor diameter	11.2%	10.0%	-24.0%	-20.3%

Enclosure thickness	7.9%	8.6%	-16.7%	-17.7%
Axial Spacing	7.9%	8.7%	-11.5%	-12.3%
Conductor thickness	2.7%	2.6%	-15.7%	14.9%
K2 constant of N_2 thermal convection	1.0%	0.08%	1.8%	-0.15%
Gas pressure	0.8%	0.07%	-1.6%	-0.13%
Soil surface convection thermal resistivity	0.5%	1.9%	-0.5%	-1.7%
Surfaces thermal emissivity	0.5%	0.04%	-0.5%	-0.05%
K1 constant of SF_6 thermal convection	0.3%	0.02%	-0.3%	-0.02%
SF6 volumetic content	0.1%	0.01%	-0.1%	-0.01%

The effect of ± 50% variation in each parameter are graphically shown in Figure 7-31 Figure 7-32 for conductor rating and Figure 7-48 and Figure 7-49 for operating temperatures.

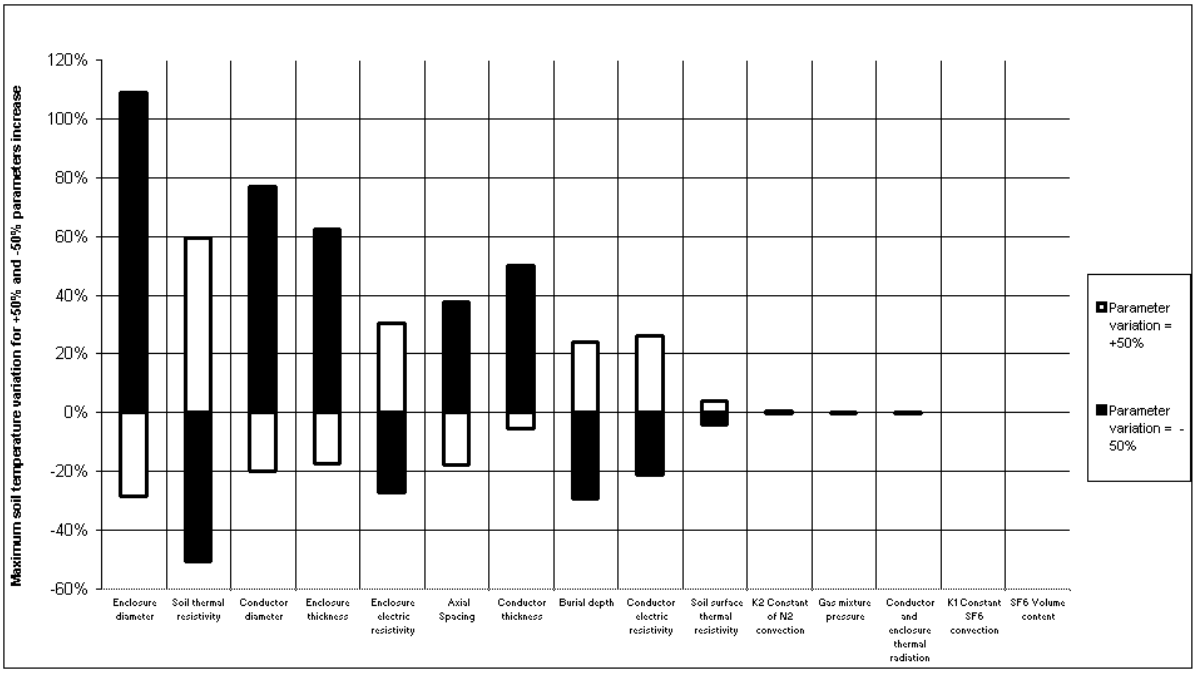

Figure 7-48 Maximum soil temperature variation for -50% and +50% of the design parameters increase. I= 3000 A. V=400kV

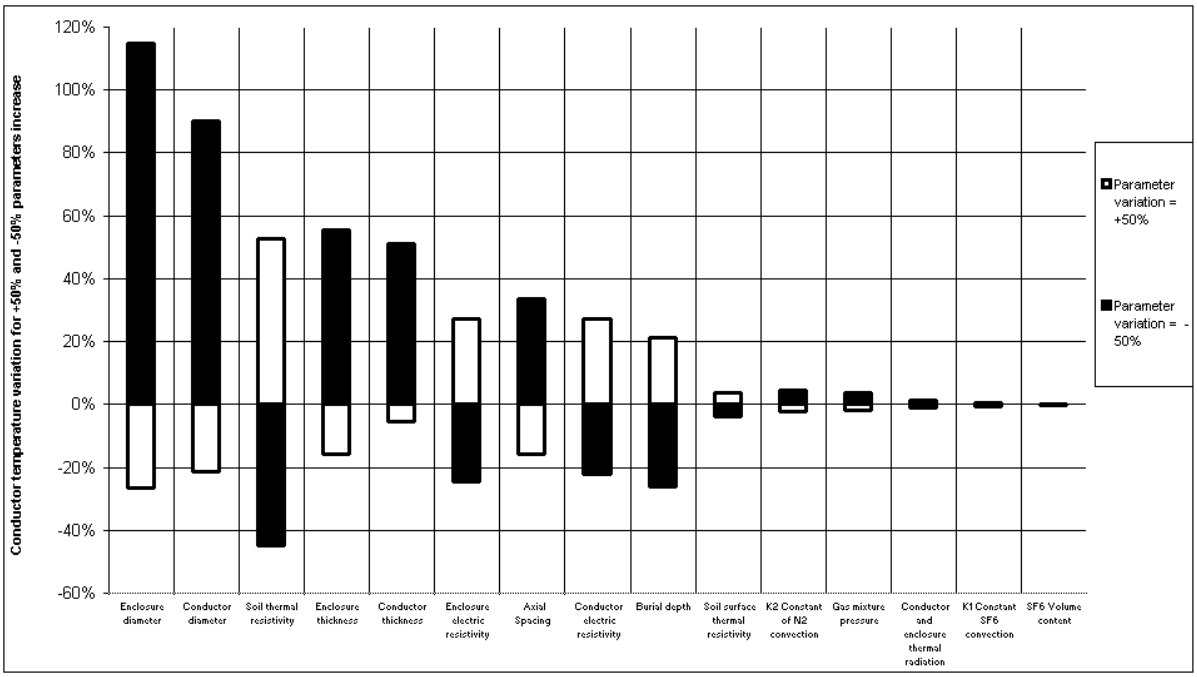

Figure 7-49 Conductor temperature variation for -50% and +50% of the design parameters increase. I= 3000 A.V=400kV

7.4 Conclusions

- The parameter that has the largest effect on the current rating is firstly the soil thermal resistivity and secondly the enclosure diameter.
- The parameter that has the largest effect on the operating temperature of the conductor is firstly the enclosure diameter and secondly the conductor diameter.
- The parameter that has the largest effect on the operating temperature of the enclosure is firstly the enclosure diameter and secondly the soil thermal resistivity.
- Increasing the conductor cross sectional area by increasing its thickness has a small effect on the current rating and on the operating temperatures due to the skin effect. In contrast, increasing the conductor cross sectional area by increasing the conductor diameter has a more significant effect.
- As a first approximation the change in current rating is proportional to the square root of the change in the particular parameter. Thus the effect of the change on current rating is reduced.
- Variations of ±50% in the parameters involved with heat transfer within the gas have a minimal effect. Thus, although the Electra 100 formula for convection and radiation within the gas was chosen, the choice of alternative formulae will have a minimal effect on GIL ratings in buried applications.
- At a constant current rating the effect of increasing the parameters on the operating temperature is significantly greater. To a first approximation the rise in temperature is directly proportional to the change in the parameter. In particular it is shown that 50% increase in the soil thermal resistivity increases the rise in conductor operating temperature by 52.7% and the rise of the maximum permissible soil temperature by 59.4%. Wide variations in the soil thermal resistivity can be experienced due to changes in soil type, compaction and moisture content and this emphasises the importance of accurate rating calculations and accurate installation geometry if overheating of the GIL and thermal instability are to be avoided.
- At the target current rating of 3000 Amps the conductor temperature is calculated to be 71^{o}C and the soil temperature adjacent to the enclosure is calculated to be 65^{o}C. Taking the recommended maximum figures to prevent soil drying out (50^{o}C in the UK and 60^{o}C in France), would reduce the current rating to 2590 Amps and 2890 Amps respectively.

7.5 References

[1] IEC 694 (Second Edition 1996) ‘Common Specifications for High Voltage Switchgear and Controlgear Standards.’

[2] IEC 287-1-1 (First Edition 1994) ‘Electric Cables – Calculation of the Current Rating – Part 1: Current Rating Equations (100% Load Factor) and Calculation of Losses – Section 1 : General’

8 Appendix 8: Sensitivity Study On Rating Parameters For Short Time Current Rating

8.1 Introduction

The sensitivity study on the overload of GIL has the purpose of ranking the parameters in the order of the largest to the smallest effect on the magnitude of the rating, with the objectives of identifying:

1) The most important rating parameters for prospective future GIL applications.

2) The effect that inaccuracy in each design, installation or calculation parameter could have on the final short terms rating.

The parameters employed in this sensitivity study were derived from the dimensions of the 400kV GIL used for the study of continuous rating given in Appendix 1. The nominal target current rating chosen was 3000 Amps continuous. The UK summer ambient rating temperature of 15^{o}C, with a soil thermal resistivity of 1.2Km/W was taken.

The rating calculations were applied with the conditions reported in the following Table 8-1:

Table 8-1 Sensitivity Study

Conductor temperature limit	95 °C
Pre-load current	0% and 85%
Overload duration	20 min and 12 h

to yield the following results

1) The resulting short term current for reference parameters as in Table 8-2 and for a suitable variation of the said parameters, as reported in Table 8-3.

Table 8-2 Reference parameters and values taken for the GIL short time rating sensitivity study.

Quantity	**Value**	**Unit**
Soil Thermal resistivity	1.2	K.m/W
Conductor Volumetric specific heat	2.5x10^6	J/K/m^3
Enclosure Volumetric specific heat	2.5x10^6	J/K/m^3
Gas Mixture volumetric specific heat	1010 (*)	J/K/m^3
Anticorrosion oversheath thermal resistivity	3.5	K.m/W
Anticorrosion oversheath volumetric specific heat	2.4 10^6	J/K/m^3
Convective parameter K0 for mixture	$K0_{SF6}$=11.3, $K0_{N2}$=5.83 (**)	

(*) Average value=90%*Cv_{N2}(average between 15-90°C)+10%*Cv_{SF6}(average between 15-90°C)

(**) being K0 = ($K0_{SF6}$ * (V_{SF6}%)^ 0.75 + $K0_{N2}$x(V_{N2}%) ^ 0.75)

The individual parameters are listed in Table 8-2. In the sensitivity study, the magnitude of each parameter was changed by ±50%. The resulting effect on either short current was then calculated as a percentage variation, with the convention: '+' representing increase and '-' a decrease.

Table 8-3 shows the parameters taken into consideration in the sensitivity study with the main values and their identifying symbols. The central column of the table shows the standard value of each parameter.

Table 8-3 Parameters selected in the short time rating sensitivity study

Parameter	Symbol	-50% of the standard value	Standard value	+50% of the standard value	Unit
Soil Thermal resistivity	Rs	0.6	1.2	1.8	K.m/W
Cond. Volumetric specific heat	Cvc	1.25 10^6	2.5 10^6	3.75 10^6	J/K/m^3

Encl. Volumetric specific heat	Cve	1.25 10^6	2.5 10^6	3.75 10^6	J/K/m^3
Mixture volumetric specific heat	Cvgas	505	1010 (*)	1515	J/K/m^3
Anticorrosion thermal resistivity	Rpe	1.75	3.5	5.25	K.m/W
Antic. Volumetric specific heat	Cvpe	1.2 10^6	2.4 10^6	3.6 10^6	J/K/m^3
Convective parameter K0 for mixture	K0	$K0_{SF6}$=5.65, $K0_{N2}$=2.915	$K0_{SF6}$=11.3, $K0_{N2}$=5.83	$K0_{SF6}$=16.95 $K0_{N2}$=8.745	

8.2 Sensitivity Study On Short Terms Rating. Time To Over-Temperature Equal To 20 min.

The Tables from Table 8-4 to Table 8-10 show the short term current rating variations calculated at the parameter values of Table 8-3. The current calculations are referred to the GIL conductor over-temperature of 95°C reached in 20 min. The starting pre-load current is either 0 A or 2550 A which is the 85% of the steady state condition, equal to 3000 A.

In the last two columns of each table the percentage variations of the current rating, for the assumed ±50% variation of the parameter, are shown, calculated as in the following expression:

$$Crpv(\pm 50\%) = \left(\frac{I(\pm 50\%) - 1}{I(std)}\right) x100\%$$

where:

Crpv(±50%) is the current rating percent variation for the ±50% parameter variation,

I(std) is the current rating calculated at the parameter standard value

I(±50%) is the current rating calculated at the parameter variations.

8.2.1 Parameterised quantity: soil thermal resistivity.

Table 8-4 Short terms Current rating (A) as a function of the soil thermal resistivity

Pre-load %	-50%	0	50%	-50% Variation %	+50% Variation %
0	27,252	27,190	27,153	0.2	-0.1
85	23,046	19,181	14,088	0.2	-0.1

Since the diffusivity of the soil has been taken constant and equal to the value suggested in IEC853-2[1] (0.4 x 10^{-6} m^2/s), assumption justified by the short time of the thermal transient, the results also apply to a ±50% soil volumetric specific heat variation at a constant thermal resistivity. Thus Table 8-4 also indicates the sensitivity of the current rating to the inverse related parameter i.e. the soil specific heat.

8.2.2 Parameterised quantity: conductor volumetric specific heat.

Table 8-5 Short terms Current rating (A) as a function of the Conductor volumetric specific heat

Pre-load %	-50%	0	50%	-50% Variation %	+50% Variation %
0	20,818	27,190	32,412	-23.4	19.2
85	14,691	19,181	22,848	-23.4	19.1

8.2.3 Parameterised quantity: enclosure volumetric specific heat.

Table 8-6 Short terms Current rating (A) as a function of the Enclosure volumetric specific heat

Pre-load %	-50%	0	50%	-50% Variation %	+50% Variation %
0	26,936	27,190	27,371	-0.9	0.7
85	19,023	19,181	19,287	-0.8	0.6

8.2.4 Parameterised quantity: mixture volumetric specific heat.

Table 8-7 Short terms Current rating (A) as a function of the Mixture volumetric specific heat

Pre-load %	-50%	0	50%	-50% Variation %	+50% Variation %
0	27,095	27,190	27,284	-0.3	0.3
85	19,117	19,181	19,245	-0.3	0.3

8.2.5 Parameterised quantity: anticorrosion layer thermal resistivity.

Table 8-8 Short terms Current rating (A) as a function of the Anticorrosion layer thermal resistivity.

Pre-load %	-50%	0	50%	-50% Variation %	+50% Variation %
0	27,282	27,190	27,119	0.3	-0.3
85	19,268	19,181	19,107	0.3	-0.2

8.2.6 Parameterised quantity: anticorrosion layer volumetric specific heat.

Table 8-9 Short terms Current rating (A) as a function of the Anticorrosion layer volumetric specific heat.

Pre-load %	-50%	0	50%	-50% Variation %	+50% Variation %
0	27,148	27,190	27,229	-0.2	0.1
85	19,154	19,181	19,206	-0.1	0.1

8.2.7 Parameterised quantity: convective parameter K0.

Table 8-10 Short terms Current rating (A) as a function of the Convective parameter K0

Pre-load %	-50%	0	50%	-50% Variation %	+50% Variation %
0	26,651	27,190	27,704	-2.0	1.9
85	18,298	19,181	19,737	-1.7	1.6

8.3 Sensitivity Study on Short Time Rating. Time To Over-Temperature Equal to 12 Hours.

The Tables from Table 8-11 to Table 8-17 show the short term current rating variations calculated at the parameter values of Table 8-3. The current calculations are referred to the GIL conductor over-temperature of 95°C reached in 12 hours. The starting pre-load is 0 A or 2550 A which is the 85% of the steady state condition, equal to 3000 A.

8.3.1 Parameterised quantity: soil thermal resistivity.

Table 8-11 Short terms Current rating (A) as a function of the Soil thermal resistivity

Pre-load %	-50%	0	50%	-50% Variation %	+50% Variation %
0	10,762	9,847	9,333	9.3	-5.2
85	9,356	7,278	5,321	7.6	-4.1

Since the diffusivity of the soil has been taken constant and equal to the value suggested in IEC853-2[2] (0.4×10^{-6} m^2/s), assumption justified by the short time of the thermal transient, the results also apply to a ±50% soil volumetric specific heat variation at a constant thermal resistivity. Thus Table 4-4 also indicates the sensitivity of the current rating to the inverse related parameter i.e. the soil specific heat.

8.3.2 Parameterised quantity: conductor volumetric specific heat.

Table 8-12 Short terms Current rating (A) as a function of the Conductor volumetric specific heat

Pre-load %	-50%	0	50%	-50% Variation %	+50% Variation %
0	9,670	9,847	10,039	-1.8	2.0
85	7,165	7,278	7,403	-1.6	1.7

8.3.3 Parameterised quantity: enclosure volumetric specific heat.

Table 8-13 Short terms Current rating (A) as a function of the Enclosure volumetric specific heat

Pre-load %	-50%	0	50%	-50% Variation %	+50% Variation %
0	9,739	9,847	9,953	-1.1	1.1
85	7,212	7,278	7,342	-0.9	0.9

8.3.4 Parameterised quantity: mixture volumetric specific heat.

Table 8-14 Short terms Current rating (A) as a function of the Mixture volumetric specific heat

Pre-load %	-50%	0	50%	-50% Variation %	+50% Variation %
0	9,841	9,847	9,853	-0.1	0.1
85	7,274	7,278	7,281	0.0	0.0

8.3.5 Parameterised quantity: anticorrosion layer thermal resistivity.

Table 8-15 Short terms Current rating (A) as a function of the Anticorrosion layer thermal resistivity.

Pre-load %	-50%	0	50%	-50% Variation %	+50% Variation %
0	9,951	9,847	9,747	1.1	-1.0
85	7,352	7,278	7,206	0.9	-0.8

8.3.6 Parameterised quantity: anticorrosion layer volumetric specific heat.

Table 8-16 Short terms Current rating (A) as a function of the Anticorrosion layer volumetric specific heat.

Pre-load %	-50%	0	50%	-50% Variation %	+50% Variation %
0	9,817	9,847	9,877	-0.3	0.3
85	7,259	7,278	7,296	-0.3	0.3

8.3.7 Parameterised quantity: convective parameter K0.

Table 8-17 Short terms Current rating (A) as a function of the Convective parameter K0

Pre-load %	-50%	0	50%	-50% Variation %	+50% Variation %
0	8723	9847	10430	-11.4	5.9
85	6379	7278	7764	-10.3	5.7

8.4 Conclusions

- The parameters that have the largest effect on the short term current rating are: the volumetric specific heat of the conductor, the convective parameter K0 for the insulation gas mixture and the thermal resistivity of the soil.
- The volumetric specific heat of the conductor has the largest effect in case of short time overloads like 20 min, as in the calculations. This effect is fairly independent of the pre-load value.
- The convective parameter K0 for the insulation gas mixture has the largest effect for medium time overloads, like 12 hours, as in the calculations. Such an effect is due to the fact that the temperature rise between the conductor and the enclosure remains high and this activate the increasing of the gas mixture thermal resistance.
- The thermal resistivity of the soil has the largest effect for high time overloads, greater than 12 hours. Such an effect is due to the fact that the thermal capacitance of the conductor (and in some extends of the enclosure) “saturates” and the heat begins to transit across the thermal resistances.

From Figure 8-1 to Figure 8-4 the effects of the parameters variations are represented arranged from the biggest to the lowest.

- The GIL reference design was shown to have high short time ratings. In particular for the 12 hour period, the GIL was able to carry over twice the continuous load of 3000A starting from an 85% preload condition.

Time	[Sort time rating / Continuous rating]	
	85% preload current	0% preload current
20 mins	6.39	9.06
12 hours	2.43	3.28

- The parameter that has by far the largest effect on the 20 minute duration short time rating is the volumetric specific heat of the conductor. An increase of 50% in the volumetric specific heat increased the short time rating by 19%, whereas a decrease, decreased the short time rating by 23%. This also shows the importance of performing current loading tests to verify short time ratings, especially for the conductor connectors, which are likely to have a different thermal capacity to the conductor.
- The other five parameters all had a small effect on the 20 minute short time rating with variations of less than 2% (convective parameter).
- The percentage sensitivity variations in current for the 12 hour period were significantly different from the 20 hour period.
- The parameter that had the largest effect for the 12 hour period was the convection parameter, K0 for the gas mixture. A 50% increase in the convective parameter increased the short time rating by 6% and a 50% decrease in K0, decreased it by 10~11%. This shows the importance of experimental verification of the short time rating, as the properties of the mixture and the transient behaviour of the changing convection patterns are likely to have a significant effect.
- The parameters that have the second most significant effect on the 12 hour period were the soil thermal resistivity and its inversely related parameter, the soil specific heat. An increase of 50% in the soil resistivity decreased the rating by 4~5% and a 50% decrease, increased the rating by 8~9%.
- The two most significant factors were shown to be the thermal capacity of the conductor for the 20 minutes rating and heat transfer coefficient through the gas for the12 hour rating. As a result of this sensitivity it is recommended that:
  - a factor of safety is included to reduce the risk of overheating of the conductor and connectors. The factor of safety could be built into the selection of the maximum permissible conductor temperature, for this study an arbitrary value of 95°C was chosen, which is less than the temperature limit for connectors given in IEC 60694 Table 3.
  - the temperature be verified by experimental measurement.

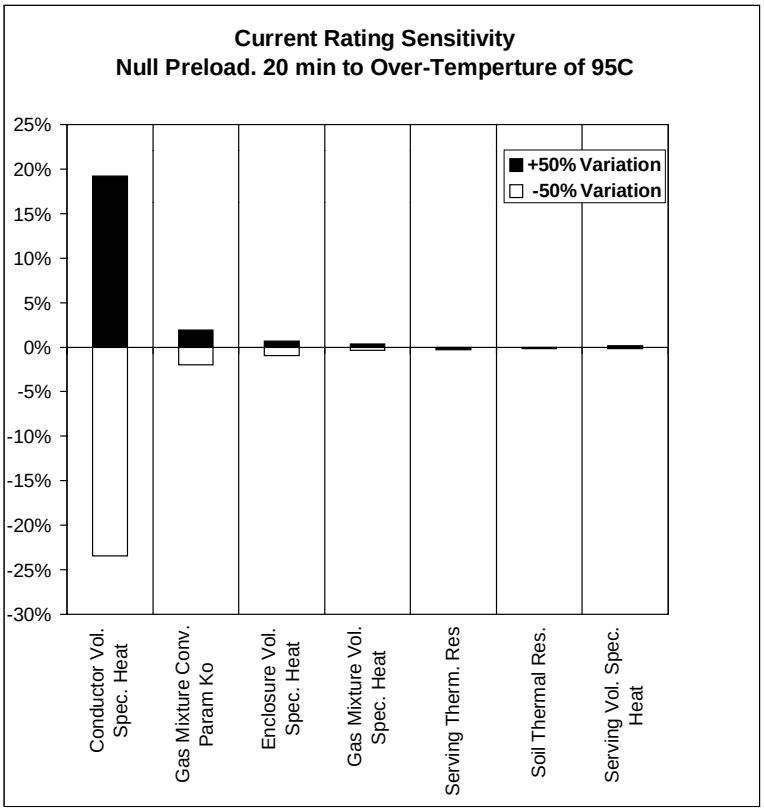

Figure 8-1

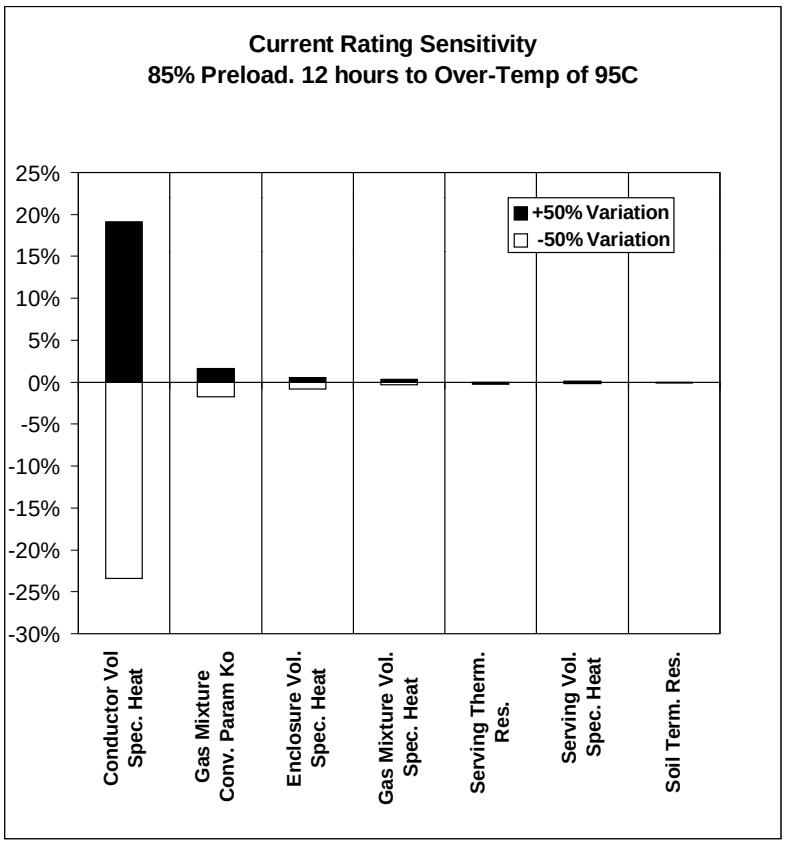

Figure 8-2

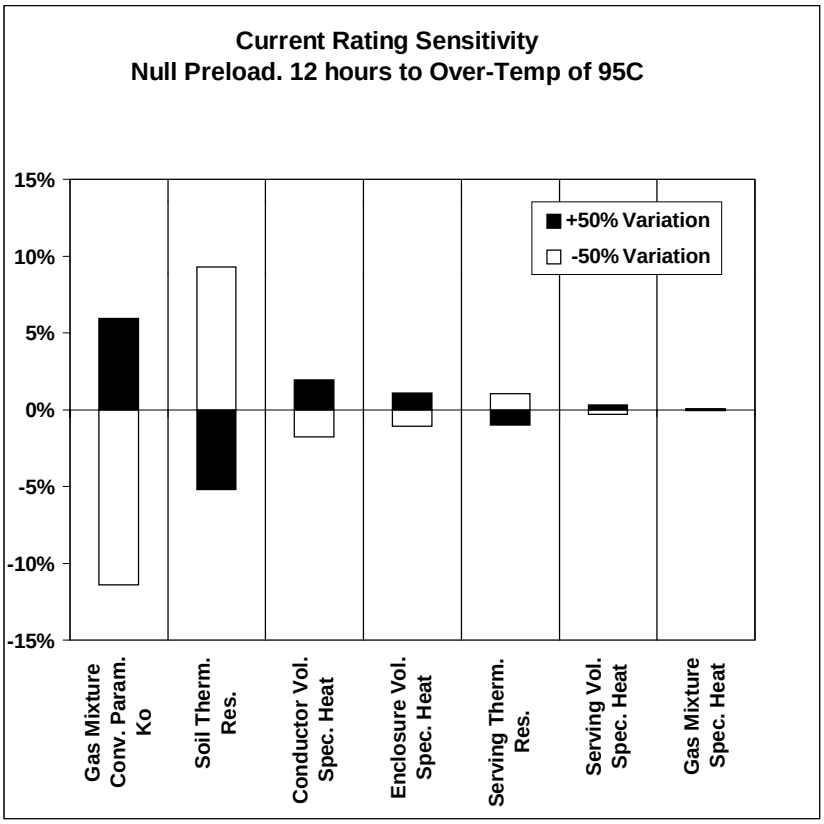

Figure 8-3

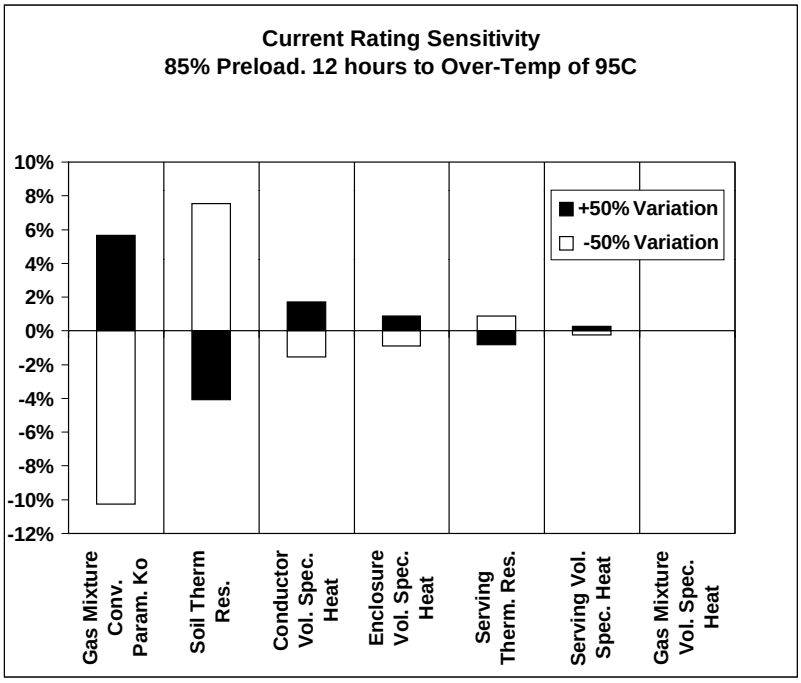

Figure 8-4

8.5 References

[1] IEC853-2 (First Edition 1989) 'Calculation of the Cyclic and Emergency Current Rating of Cables' Appendix D Table D1

[2] IEC60694 (Second Edition 1996) 'Common Specifications for High Voltage Switchgear and Control Gear Standards' Table 3.

9 Appendix 9: Bibliography

Vermeer, J. (March 1983) 'A simple formula for the calculation of the convective heat transfer between conductor and sheath in compressed gas insulated cables - *Une formule simple pour le calcul de la transmission de chaleur par convection entre le conducteur et la gaine dans les câbles à isolation gazeuse.'* Electra No 87 pp 107-113

Lis, J. (1966) 'Experimental investigation of natural convection heat transfer in simple and obstructed horizontal annuli' *International Heat Transfer Conference*, Chicago, pp 196-204

Cigré Report (May 1985) 'Calculation of the continuous rating of single core, rigid type, compressed gas insulated cables in still air with no solar radiation - *Calcul de la capacité de transport en régime permanent des câbles unipolaires à isolant gazeux comprimé de type rigide posés en air calme et hors du rayonnement solaire.'* Electra No. 100, pp 65-75

Cigré Report (1989) 'Calculation of the continuous rating of three-core, rigid type, compressed gas insulated cables in still air and buried.' Electra No 125, pp 104-111

Minaguchi, D. Ginno, M. Itaka, K. Furukawa, H. Ninomiya, K. and Hayashi, T. 'Heat transfer characterstics of gas-insulated transmission lines' IEEE 85 SM 301-7

Itaka, K. Araki T. and Hara T. (Sept/Oct 1978) 'Heat transfer characteristics of gas spacer cables' *IEEE Transactions on Power Apparatus and Systems* Vol. PAS-97 No. 5 pp 1579-1585

Lis J. and Kellard P. O. (1965) 'Measurements of the thermal conductivity of sulphur hexafluoride and a 50% (volume) mixture of sulphur hexafluoride and nitrogen' *Brit. J. Appl. Phys.*, Vol 16, pp 1099-1104

Cigré Report (1986) 'Calculation of the continuous rating of single core, rigid type, compressed gas insulated cables in still air with solar radiation - *Calcul de la capacité de transport en régime permanent des câbles unipolaires à isolant gazeux comprimé de type rigide, posés en air calme et exposés au rayonnement solaire.' Electra No. 106* pp 23-31.

Doepken H. C. (1970) 'Calculated heat transfer characteristics of air and SF_6' *IEEE Transactions on Power Apparatus and Systems* Vol PAS-89, No. 8 pp 1979-1985.

International Standard IEC 287-1-1 'Electric cables - Calculation of the current rating - Part 1: Current rating equations (100% load factor) and calculation of losses - Section 1: General'

International Standard IEC 287-2-1 'Electric cables - Calculation of the current rating - Part 2: Thermal resistance - Section 1: Calculation of thermal resistance'

IEC 61640 'HV gas-insulated transmission lines for rated voltages 72.5 kV and above'

Kennelly A. E. (1893) 'On the carrying capacity of electric cables submerged, buried or suspended in air' *Minutes of IX annual meeting of the Association of Edison Illuminating Companies* p 79.

Arnold A. H. M. (1936) 'The alternating-current resistance of tubular conductors' JI. IEE, vol 78 pp 580-593.

Japanese Cable Makers' Association Standard 168 - E 1995.

Cigré Report (October 1972) 'Current ratings of cables for cyclic and emergency loads - Part 1: Cyclic ratings (load factor less than 100%) and response to a step function - *capacités de transport des cables pour les régimes de charge cycliques et de secours d'urgence - Premiere partie: Capacités de transports cycliques (facteur de charge inférieur a 100%) et réponse a l'application d'un échelon.'* Electra No 24 pp 63 – 97

Norme Internationale International Standard CEI IEC 853 – 2 '*Calcul des capacités de transport des cables pour les régimes de charges cycliques et de surcharge de secours – Deuxieme partie: Régime cyclique pour des cables de tensions superiéures B 18/30 (36) kV et régimes de secours pour des cables de toutes tensions* – Calculation of the cyclic and emergency current rating of cables Part 2: Cyclic rating of cables greater than 18/30 (36) kV and emergency ratings for cables of all voltages'

ERA Report 90 – 0170 (November 1990) 'Calculation of the cyclic and emergency current ratings of cables for voltages greater than 19/33 kV'

Cigré report (January 1976) 'Capacités de transport des cables pour les régimes de charge cycliques et de secours d'urgence - Deuxieme partie: Régimes de secours et réponse de court durée a l'application d'un échelon unité (pour des durées inférieures a celles considérées dans la premiere partie et pouvant descendre jusqu'B dix minutes) - *Current ratings of cables fore cyclic and emergency loads – Part 2: Emergency ratings and short duration response to a step function (for time periods shorter than those applicable to Part 1 and down to 10 minutes).*' Electra No 44 pp 3 – 16

Cigré report - M*é*thode digitale de calcul de la r*é*ponse des cables unipolaires B l'application d'un *é*chelon thermique transitoire – *Computer method for the calculation of the response of single-core cables to a step function thermal transient'* Electra No 87, pp 41 – 63

ANNEX B:

GIL Insulation coordination, on site test, long duration test, monitoring and grounding

written by TF2 members:

A. Sabot France (Convenor),

A. Girodet France (formerly M. Guillen),

E. Kynast Germany,

S. Meijer Netherland,

A. Miyazaki Japan,

G. Rizzi Italy

Table of Contents

1. General Insulation Co-ordination Process

As given in IEC 60071-1 [1], figure 1 displays the Insulation Coordination flow chart in which there are four main steps:

- a first one to determine the insulation characteristic of the equipment: characterisctic of the insulating mediums involved in the insulation (volt-time V-t curves, electric aging V-n curves,....), self restoring, non self restoring, mix insulation but also the associated chosen test procedures for withstand type, routine and on site tests; indeed these test procedures charaterizes the discharge probability associated with the test voltage levels which are chosen.

- a second one to characterize the distribution of the overvoltage amplitude through a set of value called representative overvoltage U_{rp}. Depending on the Insulation Coordination approach (determinist or probabilistic) chosen for the class of stressing voltages and overvoltages, the U_{rp} characteristics can be just one amplitude in case of a determinist approach for a very short piece of equipment (i.e. circuit breaker, measuring transformer,....) or a Probability Density Function (PDF) of amplitudes. For long piece of equipment in case of a probabilistic approach the amplitudes PDF is needed in each point as for example for overhead lines or cables [2],[3] or long GIL [4], [5]. Of course a mixture of probabilistic and deterministic approach is always possible.

- a third one to adjust the insulation characteristic of the equipment with the stessing voltages and overvoltages for the chosen accepted risk of failure (derived from the accepted Insulation Major Failure Rate) thus giving the so called coordination withstand voltage U_{cw},

$$U_{cw} = K_c \times V_2 \quad (1)$$

  V_2 component of U_{rp} being the overvoltage amplitude having a 2% probability to be exceeded and K_c being the coordination factor.

- A fourth one intended to take into account the aging of the insulation and other random factors which affect the insulation characteristic of the equipment through the so called safety factor K_s. It should be emphasized that this Safety Factor must also cover to some extent all kinds of aging impacting the insulation and not only the electrical aging of the insulation. With this Safety Factor, the so called required withstand voltages U_{rw} are derived (2); depending on them, the so called withstand voltages U_w of the equipment are then selected in IEC standards of the equipment according to:

$$U_w \text{ (from IEC std)} \geq U_{rw} = K_s \times U_{cw} \quad (2)$$

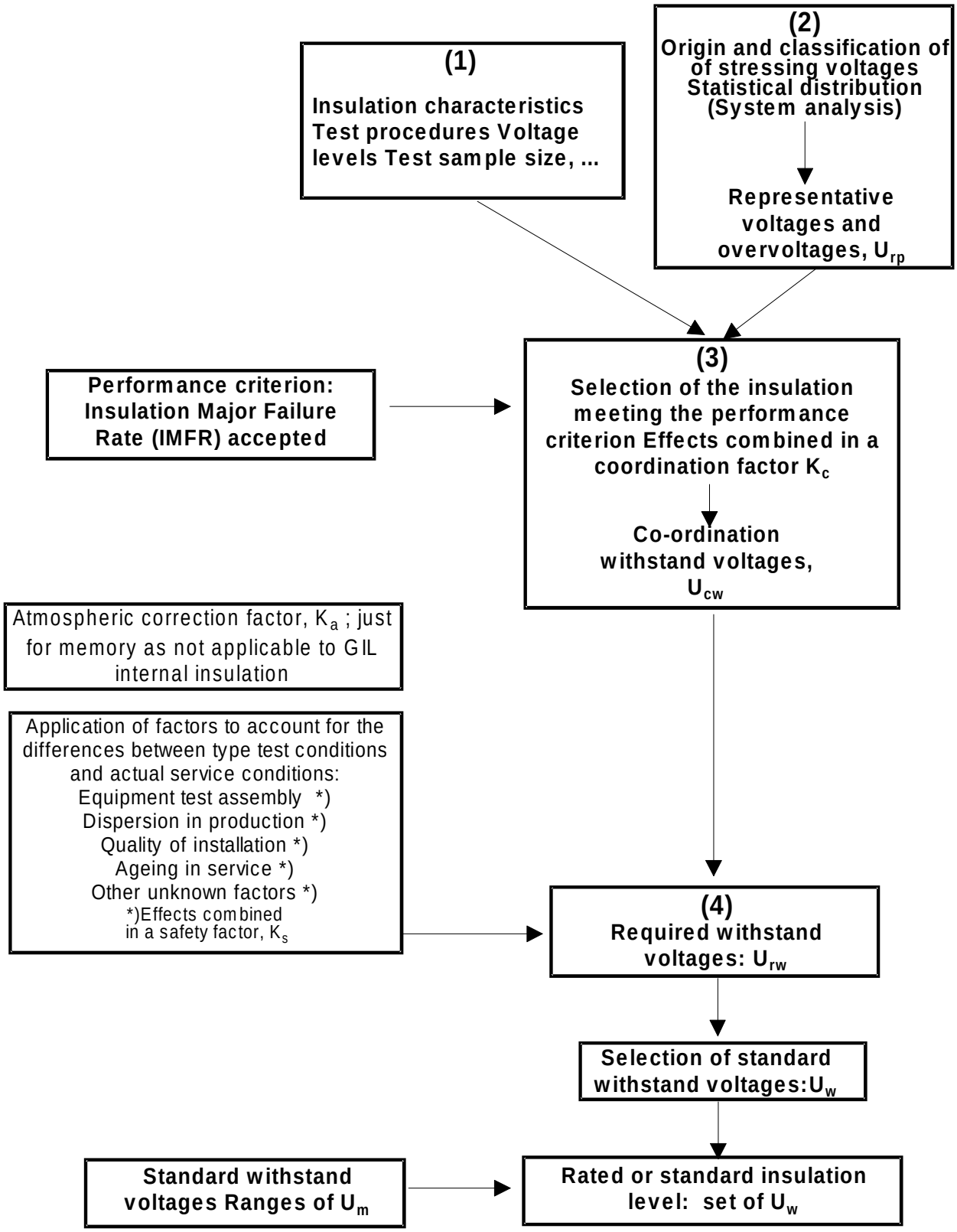

Figure 1 : Flow chart of Insulation coordination process (IEC 60071-1).

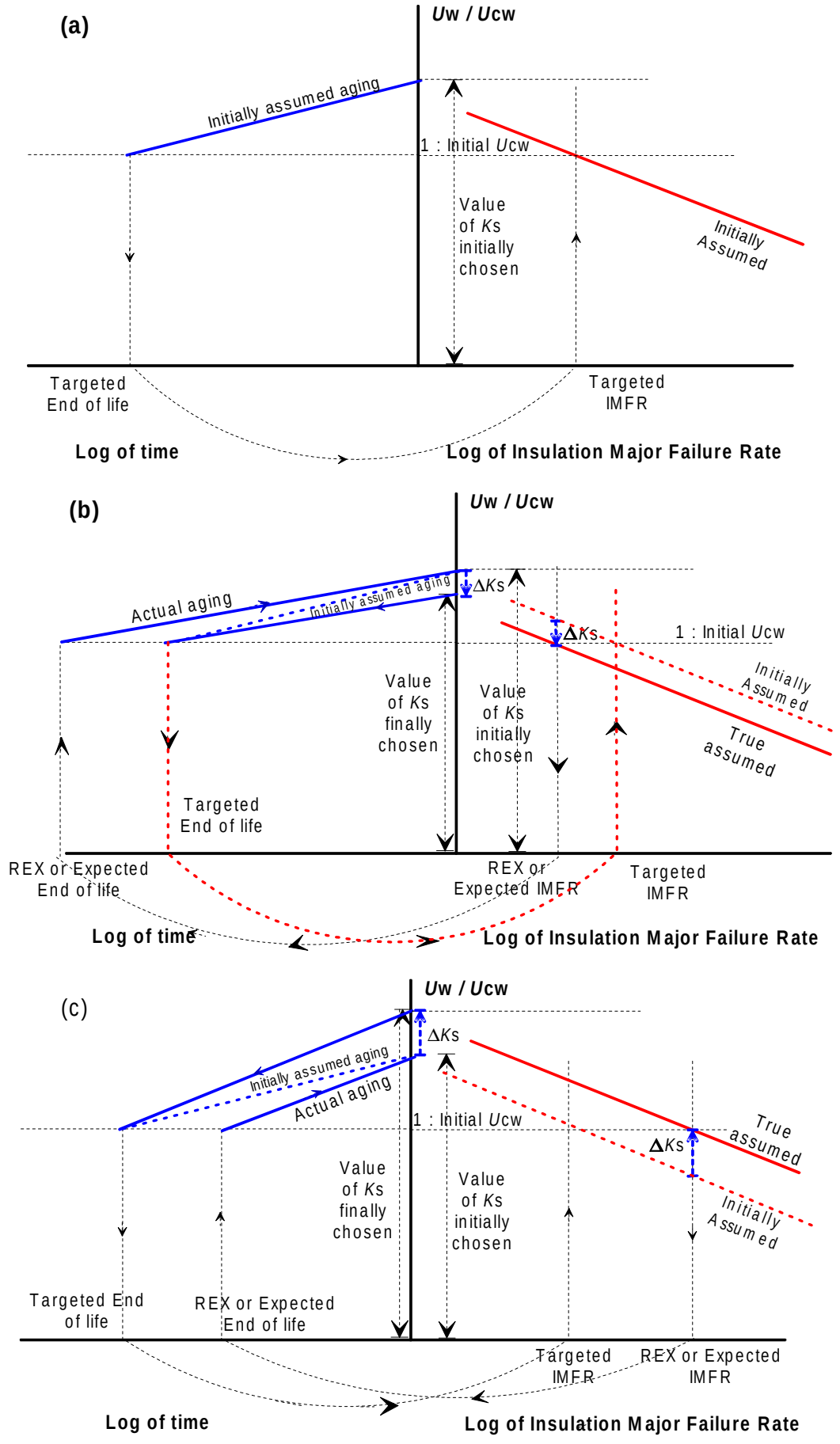

Figure 2 : Insulation coordination - Withstand voltage, insulation coordination withstand voltage, Safety Factor, aging and Major Failure Rate.

As showed in figure 2a, the co-ordination withstand voltage Ucw is the withstand voltage that an equipment should reach only at the end of its life. In that conditions, from a statistical point of view on a large population of such equipment, the Insulation Major Failure Rate ("IMFR") of the equipment population should reach the IMFR accepted by the Utility. As the actual IMFR collected by the Return of EXperience (REX) is lower figure 2b or higher figure 2c than the targeted one, the insulation coordination is correct or not. So the REX of GIL has to be analyzed and as far as possible taken into account in the Insulation Coordination process. Indeed depending on the REX, the coordination factor or the safety factors have to be adjusted compared to the ones derived from a pure probabilistic approach and a generally applied safety factor. For example, if the IMFR given by the REX or an expected IMFR derived from previous experience on similar equipment is greater than the a priori accepted IMFR, then:

- either the Utility can increase the safety factor as shown in figure 2c if the main cause of insulation failures is overvoltage,
- or the Utility can keep the same safety factor but select a new higher U_{cw} (less surge arrester or surge arrester with higher protection level) as shown in figure 3 if the main cause of insulation failures is not overvoltage but failure at the rated system voltage due to aging.

In the following, all these aspects are discussed further from the point of view of GIL equipment.

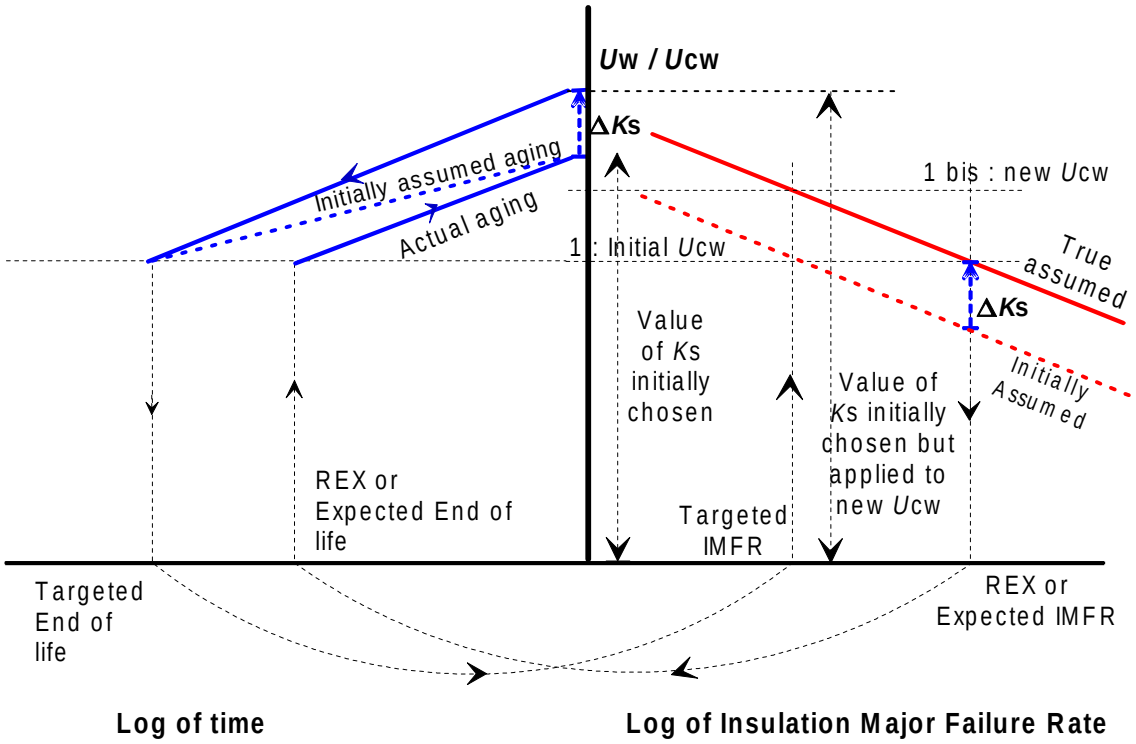

Figure 3 : Insulation coordination - Withstand voltage, insulation coordination withstand voltage, Safety Factor, aging and Major Failure Rate in case of higher IMFR.

2. Risk of failure to be accepted by utilities: Global and Insulation Major Failure Rates

In the design process of any equipment included in any system, one of the most important parameter is the target major failure rate (MFR) accepted for the equipment. This target MFR should be selected in order to achieve a given reliability and availability of the whole system.

For electric systems, this general statement is also valid but in the past and still nowadays, operating people were and are reluctant to accept the idea of equipment major failures (MF) and the accepted major failure or design target MFR of equipment is difficult to get from Utilities.

Beside when Utilities give the target MFR accepted for a given equipment, generally it is a global one: the given target MFR is intended to cover all the major failure causes. Thus, for a given equipment, generally the design target MFR accepted for each stress category should be lower than the global one given by the Utilities. So idealy, for a given equipment it is often necessary to split this global MFR accepted by Utilities in different major failure rates related to each type of stresses, taking into account the relative frequency of each type of stresses, their aging process and their influence.

Nevertheless, for HV equipment, among all the stresses which can trig major failures such as the thermo mechanical stresses, the mechanical stresses or the corrosion stresses, the voltage and overvoltage stresses are the most important. Indeed generally most of the changes in the equipment and most of the equipment component aging due to the other stresses impact the insulation characteristics of the electric equipment and thus may reduce the withstand voltages and then may lead more or less rapidly to a IMF. It is thus obvious that for HV equipment the IMFR taken for the Insulation Coordination process is the largest part of the target global failure rate.

So for a consistent approach, it is generally necessary to split the global MFR accepted by a utility for an electric equipment in *n* major failure rates: *n* being the number of independent possible causes of failure. For example, when dealing with GIS Insulation Coordination analyzing the major failure cause REX led in [6] to split in two equal parts ($n = 2$) the global target MFR accepted by Utilities: one half for the insulation major failure rate and the other half for the major failures due to all the other stresses (mainly the mechanical ones). Indeed the so large part of the global MFR taken by major failure not related to insulation is due to the moving part of circuit breakers and disconnectors.

But contrary to GIS, in the case of GIL as the switchgears will not be generally present, the global MFR accepted can be chosen as IMFR for the Insulation Co-ordination process.

2.1. Target failure rates for GIL reliability and Insulation Coordination

As previously mentionned up to now global target failure rates of equipment were not and are still not parameters which are often explicitely given by Utilities. For GIL which is rather new equipment, it is even more difficult to find common accepetd values. Nevetheless, in order to give ideas, some specific values already published in the littterature or discussed within the Working Group are given in the following.

For EDF [5], in order to be acceptable for system reliability, the availability of underground burried GIL should be as good as the availability of the EDF overhead lines; so disregarding the self restoring failures of the overhead lines (lightning, pollution,...) which do not impair the system reliability, the failure rate of overhead lines with long unavailability is in the range of 0.2 failures/100km of three phase circuit per year. For overhead lines such a failure rate is mostly due to mechanical rupture of conductors or towers. Thus for EDF, the requested global target failure rates of underground burried GIL (expected global reliability) has been requested to remain lower than 0.2 major failures/100km of three phase circuit of GIL/ year (or expressed another way 0.2 / 3=0.067 failures/100km of single phase GIL/year.

On the same aspect, for the two 3.3 km GIL circuits of Shinmeika Tokai lines built in a tunnel [7], CHUBU Elctric Power Company aims for a maximum acceptable global failure rate of 1 failure per 50 years. Such a requirement leads to 0.3 failure per 100 km per year of three phase circuit; the value is very similar to the one expressed by EDF of 0.2 failure per 100 km of three phase circuit per year.

Just for giving a rough idea of what is the meaning of such a global failure rate, one should notice that the failure rate of 0.2 failures/100km of three phase circuit per year, corresponds to an expected Mean Time Between Failures (MTBF) of:

- 5 years for a three phase GIL circuit of 100 km
- 500 years for a three phase GIL circuit of 1 km.

The 0.2-0.3 IMF/year/100km of GIL leads to $0.2\text{-}0.3 \times 10^{-5}$ IMF/year/meter of circuit.

In order to situate the afore mentionned Utilities request a comparison is needed. Depending on the repair time of an apparatus IEC 60071-2 (§3.2), as guidance, proposes acceptable IMFR ranging from 0.001/year up to 0.004/year leading to MTBF ranging from 1000 years down to 250 years for the given apparatus. Due on average to long repair times, for a GIS bay a target IMFR of 0.001/year is recommended by IEC [8]. This GIS bay target IMFR leads to 0.3×10^{-4} (10^{-4}/35) IMF/year/meter of circuit assuming for a 420 kV GIS bay 35 meters length for each phase. Converted to 100 km of GIL circuit, the target failure of GIS is equivalent for GIL to 3 IMF/year/100 kilometer of circuit, so roughly ten times (one order of magnitude) the Utilities targeted ones.

2.2. GIL Return of EXperience (REX)

As previously stated the choice of an average safety factor K_s for the insulation coordination of the GIL should be very much related to the REX of GIL. But as GIL are not broadly in service the sample size is very small and thus its statistical meaning may be questionable. Also in addition to the analyzis of the actual GIL REX, it has been valuable to analyze the GIS REX (GIS population is far larger and thus gives a better confidence for the failure rate values) in order to derive from that GIS REX a more confident value for the possible IMFR to expect for GIL. Of course, to derive an expected GIL failure rate from the average actual GIS failure rate, it is necessary to find a base of equivalence and to perform an in depth analysis of the world GIS REX as previously stated the structures of the major failure causes are different.

2.2.1. REX of GIL derived from REX of GIS

2.2.1.1. REX of GIS

Indications on the GIS REX can be find in [8] and [9]. A synthesis and correlation between GIS Global MFRs and insulation major falure rates has been done in [6] and only the main data will be again recalled here.

The table 1 shows the result of the survey on GIS insulation failures performed in [8] and limited to major (main) failures of the GIS HV insulation. Indeed, the IMFRs are rapidly increasing with the system voltage level.

Table 1 :
Insulation failures as reported by [8]

System Voltage level	cumulated bay.year	Insulation failures	Insulation failures by 100 bay.year
125-145kV	9334	24	0.26
245 kV	6133	41	0.67
420 kV	3351	61	1.8
550 kV	1109	43	3.9
All voltages	17734	165	0.9

The target of a MTBF of 1000 years (~0.1 failure/100 bay.year) as suggested for the GIS insulation coordination in IEC 60071-2 is not reached for 245 420 and 550 kV GIS; the ratio between the actual IMFR and the target one is about 7 for 245 kV system voltage and 18 for 420 kV and 39 for 550 kV system voltage. The target IMFR is approached only for the 125-145 kV system voltages.

Indeed, that IMFR excess is not due to overvoltages stresses but in 80% [8] to changes inside GIS resulting in insulation failures occurring at the service voltage (without any overvoltage). If some of these changes were large and instantaneous changes such as mechanical ruptures of rod drive of switching equipment which led to insulation failures some of them were small and progressive changes such as contact wears and shield displacements which led in the long run to the insulation failures. In both cases, these defects may be classified as due to the global aging process of the GIS that has led to the end of life of the equipment at service voltage. This global aging is produced by distinct aging factors such as mechanical stresses, thermal stresses, environmental stresses and of course electrical stresses and the interaction between one or more of them. Of course whatever is the stress at the very origin of the defect leading to an IMF, the insulation coordination procedure should take that into account as far as possible. So it is important in the failure analysis to classify the origin of the failures and to try to assess the influence of higher GIS withstand voltages on the IMFR.

2.2.1.2. Expected GIL REX derived from the GIS REX

From the previous REX of GIS, the derivation of an expected IMFR for 420 kV GIL needs some assumptions and criteria for conversion.

So in the following it is assumed that the 420 kV GIL technology will remain roughly identical to the 420 kV GIS technology: same withstand voltages of the insulating gas and spacer, same volt-time characteristics same V-n insulation characteristic of spacers and more generally of the insulation (same dielectric aging) and same erection techniques, quality control and on site tests.

The criteria for conversion of IMFR of GIS in IMFR of GIL has been the following:

- firstly, as it is clear that all the insulation failures of GIS could not be retrieved in the GIL as according to [8] most of the insulation failure are related with circuit breakers, disconnectors voltage transformers, … that will not be part of GIL. So from an in depth analysis of the IMF data is necessary to determine those which may have occurred also in GIL. From the analysis of insulation failure data bases, according to experts, it appears that:
  - roughly only 15% could have occurred in a GIL: indeed in GIS many dielectric failures are due to mechanical movement of peices which will not occur in GIL [8],
  - on that 15%, all did not occur in the vicinity of a spacer,
  - all these 15% occurred when the voltage at the instant of failure was simply the service voltage.
  - most of these 15% could have been delayed or avoided by an increase at least of the PF withstand voltage.
- secondly, for GIL very identical parts will be repeated along GIL length contrary to GIS for which the length of apparatus is a large part of the bay, so it is necessary to choose an equivalence criteria between GIS length and GIL length:
  - a rough equivalence may be based just on the length of the bay for GIS and length of the GIL (as rapidly done in § 2.1),
  - or as in GIL the spacers are expected to be the most sensitive parts a more suitable equivalence criteria may be based on the number of spacers per unit length, including for GIS bay the related part of the bus bar of the substation. It is that second equivalence spacer/length that has been adopted.

From the analyze of the 420 kV GIS bays, it appears that:

- the average bay length, including the related bus bar, is about 35 meters of three phase GIS circuit,
- the average number of spacers is 0.33 per GIS meter (one spacer each 3 meters!).

For the 420 kV GIL, it appears that a spacer or insulating supports every 8 meters is an average value.

Thus, taking into account table 1 the above assumptions leads to that the number of GIS IMFs that may occur in a 420 kV GIL is:

$$1.8 \text{ IMF/100bay.year} \times 0.15 = 0.27 \text{ IMF/100bay.year} \quad (3)$$

and thus for one GIS bay an IMFR of:

$$\text{GIS bay IMFR} = (0.27 / 100) \text{ IMF/year} \quad (4)$$

With a number of spacers inside the 420 kV GIS bay of:

$$\text{number of spacers in a GIS bay} = 35 \times 0.33 \quad (5)$$

The corresponding GIL lengh having the same number of spacers (and thus same IMF/year) is:

$$\text{GIL corresp length} = 93\text{m} = (35 \times 0.33)*8\text{m} \quad (6)$$

leading to GIL IMF/m of three phase circuit / year of:

$$\text{GIL IMFR} = (0.27/100)/93 = 2.9 \times 10^{-5}/\text{1m-3ph/year} \quad (7)$$

and then for 100 km (10^5m) of 3 phase circuit GIL, the per year insulation major failure to expect from 420 kV GIL would be:

$$\text{GIL IMFR} = (2.9 \times 10^{-5}\ /\text{1m-3ph/year}) \times 10^5\ \text{m} = 2.9\ /\text{100km-3ph/year} \quad (8)$$

Such an IMFR is roughly 10-15 times the targeted ones (§ 2.1).

2.2.2. REX of GIL in service

The table 2 and the table 3 show the result of the 2000 survey on GIL Insulation Major Failure for GIL that have circuit length longer than or equal to 500 meters. GIL producers included in this survey are ALSTOM, SIEMENS, MITSUBISHI Electric, SUMITOMO Electric Industries and The FURUKAWA Electric.

Table 2 :
Return of experience of GIL in service in terms of system voltages

System voltage (kV)	GIL Cumulated length.year (km.year)	Insulation Major Failures	IMFR Insulation failures by 100 km.year
245-275	25	0	0
420	154	3	1.95
550	30	0	0
All voltages	209	3	1.44

It should be noticed that on a so small GIL cumulated length.year very few failures occured.

As shown in table 3, the GILs in service for 10 years or shorter time (the recent ones) occupy 57 % of the total cumulated circuit length but their wheight in the GIL service experience sample is limited to 18%.

Table 3 :
Return of experience of GIL in service in terms of service period

Commercial operation (years)	GIL Cumulated circuit length (km)	GIL Cumulated length.year (km.year)
0-10	15.0 (57%)	37 (18%)
10-20	7.5 (28%)	83 (40%)
>20	4.0 (15%)	89 (42%)
Total	26.5	209

The table 4 displays the IMFR values derived from the REX of 420 kV GIS and 420 kV GIL. The 420kV GIL IMFR derived from REX of 420 kV GIS is 15 times larger than the target GIL IMFR, while the IMFR from REX of 420 kV GIL corresponds to 10 times of the target one. So the bases adopted for the derivation of GIL IMFR from GIS IMFR are consistent and beside add confidence on the GIL IMFR obtained with small GIL sample as the GIS REX data sample is larger then the GIL one.

The table 4 displays also the IMFR of surveyed GIL including all system voltages.

Table 4 :
IMFR derived from REX of GIS and REX of surveyed GIL

System voltage		REX of GIL derived from REX of GIS (A)	REX of GIL in service (B)	IMFR (A) /Target GIL IMFR	IMFR (B)/Target GIL IMFR
420 kV	Cumulated length.year (km. year)	312 (=3351 × 0.093)	154	-	-
	Insulation failures	9 (=61 × 0.15)	3	-	-
	IMFR (failures / 100 km.year)	2.9	1.95	15 times	10 times
All voltages	Cumulated length.year (km. year)	-	209	-	-
	Insulation failures	-	3	-	-
	IMFR (failures /100 km.year)	-	1.44	-	7 times

(1) 1 bay.year of GIS = 93 m.year of GIL

(2) 15 % of GIS failures = GIL failures

(3) Target GIL IMFR = 0.2 failures / 100 km.year

A previous survey by EDF [10] in 1993 reported that the cumulated installation length of GILs, of which each length was 100 m or longer, had reached 30 km.

The REX of all the CGIT GIL (CGIT formerly ABB during a certain time and including GIL from 145 kV to 1200 kV, more than 10 m) reached a cumulated circuit length of 3,000 km.year in 1995. For this larger sample of "GIL" the IMFR is of the same order of magnitude that the ones obtained in table 4 on the smaller sample of GIL with length longer than 500 meters. This again adds confidence on the actual GIL IMFR.

The figure 4 summarize the relations and gaps between the different GIS and GIL IMFR discussed in the chapter. It shows clearly that the gap between GIL IMFR targeted by Utilities and the one obtained in the the field up to now is of the same order of magnitude than for GIS. According to their GIL reliabity and availability needs, this gap has to be taken into account for the choice of the insulation level to be specified by Utilities.

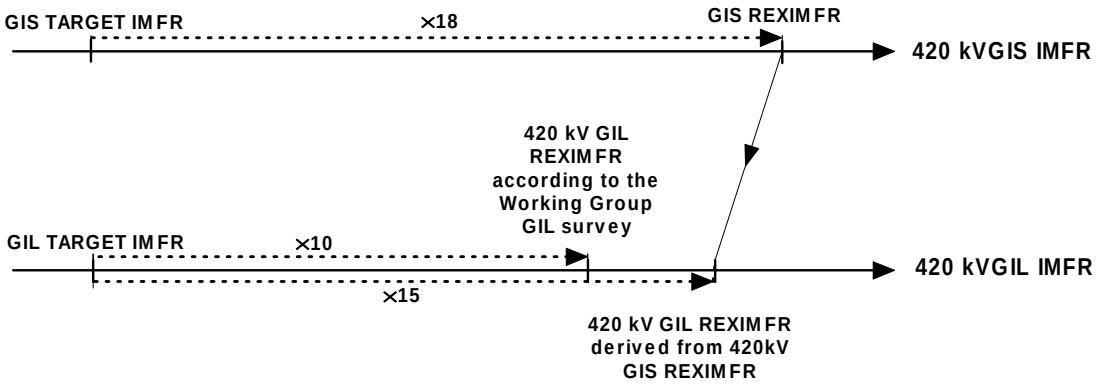

Figure 4 : Diagram showing the relations and gaps between the different GIS and GIL IMFR discussed in the chapter.

2.3. References of chapters 1 and 2

[1] IEC standard 60071-1: "Insulation Co-ordination Part 1: Definitions, principles and rules règles", seventh edition, 1993-12

[2] G. Carrara, E. Occhini, L. Paris, F. Reggiani: "Contribution to the study of insulation coordination from the probabilitic point of view", CIGRE report 421, CIGRE general session 1966.

[3] IEEE Std 1313.2-1999: "IEEE Guide for the application of Insulation Coordination".

[4] A. R. Hileman, R. W. Flugum, T. F. Garrity : "Lightning insulation coordination for a 600 kV DC gas insulated cable", IEEE transactions on Power Apparatus and Systems, Vol PAS-101, n°11November 1982, pp4399-4406.

[5] A. Sabot, D. Santos, X. Waymel, D. Feldmann, Y. Maugain., "Insulation co-ordination of 420 kV gas insulated lines" session CIGRE 1998,rapport 21-303.

[6] A. Sabot: "Insulation co-ordination and on line Insulation Monitoring & Diagnostic techniques for Gas Insulated Switchgear (GIS)" CIGRE Session 2000, Panel session on "Modern Maintenance Techniques for Efficient System Operation", report P1-09.

[7] T. Nojima, M. Shimizu, T. Araki, H. Hata, T Yamauchi: "Installation of 275 kV - 3.3 km gas-isulated transmission line for underground large capacity transmission in Japan", CIGRE 1998

[8] CIGRE WG 33/23-12 : "Insulation Coordination of GIS : return of experience, on site tests and diagnostic techniques" - Electra n° 176, February 1998.

[9] T.M. Chan, F. Heil, D. Kopejtkova, P. O'Connell, J.-P. Taillebois, I. Welch : "Report on the second International survey on high voltage gas insulated substations (GIS) service experience", Session CIGRE 1998, rapport 23-102

[10] Aucourt C., Boisseau C., Feldmann D.: "Gas insulated cables : from the state of the art to feasibility for 400 kV transmission lines ", Jicable,1995

3 Gaseous insulating medium in use

3.1 Introduction

In gas-insulated substations (GIS), sulphur hexafluoride (SF_6) gas is used for insulation purposes. SF_6 was discovered in 1900 from a reaction of fluor and sulphur [11] SF_6 became very popular as insulation gas in high-voltage equipment because of its excellent insulating properties. The first SF_6 gas-insulated substations were built in the early seventies [11]. Important properties of SF_6 are:

- SF6 is electronegative (electrons are attached to the SF6 molecules). Electron attachment results in heavy long-lived (> 10-5 s) ions, which are much slower than electrons. These ions prevent the forming of electron avalanches, leading to higher breakdown stress[12].

At atmospheric pressure the dielectric strength of SF_6 is roughly 2.3 times higher than that of air;

- At higher pressures (until liquefaction) even higher insulation levels can be obtained;
- The insulation strength recovers after breakdown;
- Pure SF6 is non-toxic, dissociation products however are toxic;
- It is non-flammable.

Because large amounts of electrical energy are transmitted in urbanised areas, alternatives for lines and high-voltage cables are desirable. Gas-insulated lines (GIL) is one of the solutions [13], [14] and [15]. Besides the fact that SF_6 is a very expensive gas, it is also a greenhouse gas. Therefore, gas mixtures of SF_6 and Nitrogen N_2 are suitable to reduce costs of the equipment and SF_6 leakage. For example, a mixture containing 10% SF6 results in 85% reduction of the used SF_6 and in 85% less SF_6 leakage [16].

N_2 is the main component of air. Properties of nitrogen are that it is cheap, inert, nontoxic, nonflammable, and of course environmentally acceptable [17] and [18]. However, the dielectric strength of nitrogen is much lower than that of SF_6.

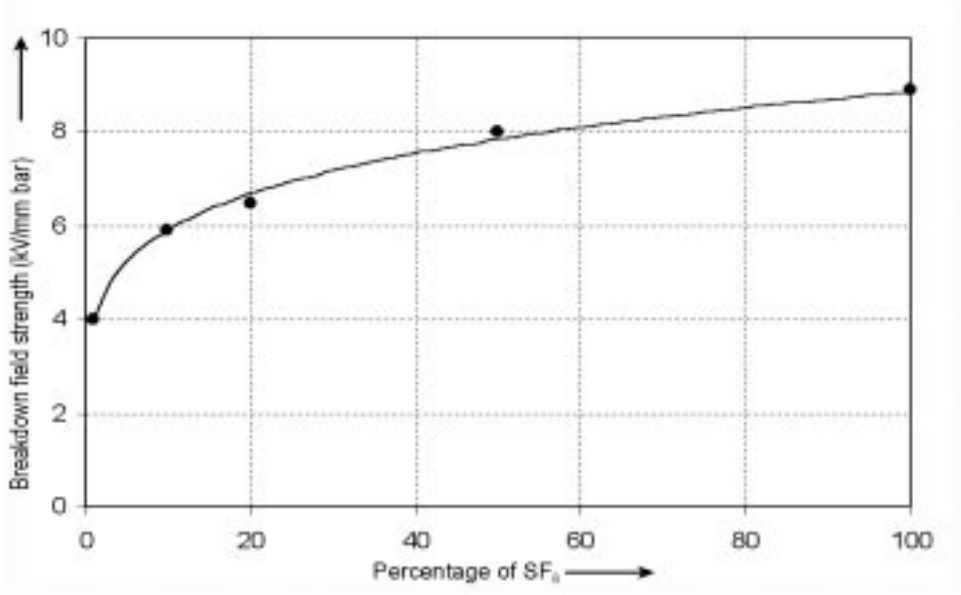

Figure 5 : Critical field strength of a SF6-N2 mixture as function of the SF6 percentage.

As is known the attachment coefficient of SF_6 is large for low-energy electrons (<0.1 eV). In case of higher energetic free electrons, i.e. high velocity, they must be slowed down to the low energy range where SF_6 possesses its most effective attachment properties. For this reason combinations of gases with properties that enable electron attachment and slow down the electron-speed are of interest. If a buffer gas like N_2 is used, the electrons are scattered into the energy region where SF_6 captures the electrons still efficiently.

It has been shown that even small amounts of SF_6 in N_2 rapidly increase the dielectric strength of the mixture; the increase in dielectric strength tends toward saturation when the amount of SF_6 is increased above 50%, see figure 5[17] and [19].

From service point of view, Gas Insulated Lines (GIL) may be considered very similar to GIS, being the main differences longer length, absence of branches and switching devices. Moreover, GIL service voltage stresses may be considered very similar to those affecting GIS.

The figure 6 taken from reference [20], reports typical shapes of voltage stresses. In addition to the typical voltage stresses reported in the figure, it is to be underlined that Very Fast Front Overvoltages (VFTO) in GIL are associated to a DC pre-stress due to the trapped charge derived by disconnectors and/or circuit breakers operations.

Class	Low Frequency		Transient		
	Permanent	Temporary	Slow front	Fast front	Very fast front
Voltage Shape	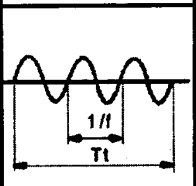	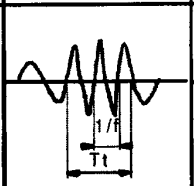	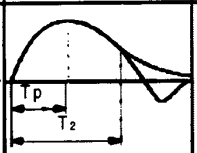	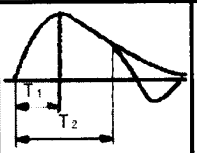	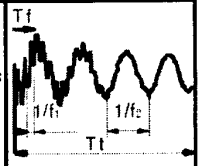
Range of voltage shapes	f = 50 or 60 Hz Tt > 3600s	10 < f < 500Hz 0.03 < Tt < 3600s	20 < Tp < 5000µs T2 < 20 ms	0.1 < T1 < 20µs T2 < 300µs	3ns < Tf < 100ns 0.3 < f1 < 100MHz 30kHz < f2 < 30MHz Tt < 3ms
Standard voltage shape	f = 50 or 60 Hz Tt *)	48 Hz < f < 62 Hz Tt = 60 s	Tp = 250µs T2 = 2500µs	T1 = 1.2µs T2 = 50µs	*)
Standard withstand test	*)	Short-duration power frequency test	Switching Impulse Test	Lightning Impulse Test	*)

*) To be specified by the relevant apparatus committees

Figure 6 : Typical voltage stresses in GIS

The figure 7 still taken from reference [20], reports typical amplitudes and time duration of possible voltage stresses. DC voltages even if reported in figure 7 are very seldom present when GILs are considered.

It may be assumed that voltage stresses present in GIL are very similar in term of shapes and amplitude to those that can affect GIS.

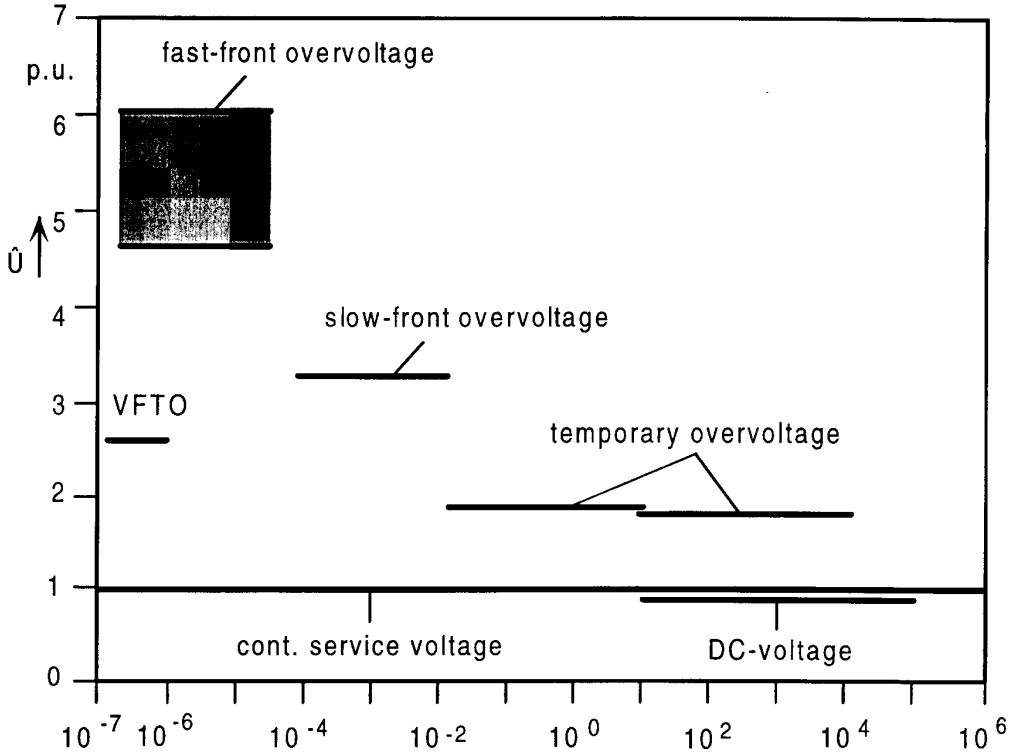

Figure 7 : Typical voltage level for voltage classes of figure 1.

As already reported, SF_6 is used in industrial applications as insulating gas since early seventies. Its dielectric characteristics were studied under different voltage stresses and different testing configurations. The results of the investigations have allowed reducing the dimension of GIS with respect to those used at the beginning of industrial applications. Moreover, the investigations have highlighted that withstand

characteristics of pure SF_6 can be reduced in industrial application for the presence of some influencing factors as for example:

- Particles
- Protrusion
- DC pre-stress associated to VFTO

Due to the larger dimensions of GILs compared with GISs and the concern of greenhouse effect caused by possible SF6 lekeage in the atmosphere, a mixture between SF_6 and N_2 is used instead of pure SF_6, in GIL, at least for the highest voltage levels, Typically, the SF_6 percentage is comprised in the range 10% to 20%.

The selection of the best SF_6 percentage in the mixture depends on many different technical and economical parameters and it is basically based on the experiences of the Manufacturer.

Several tests were performed in the past to determine the dielectric characteristics of the new insulating media. The investigations were performed on basic and industrial configurations and with different voltage stresses; aim of the present part of the paper is find a possible method to rationalize the data reported in literature relevant to industrial applications.

Considering that the diameter used presently for the enclosure of GIS application should not be changed for economical point of view, a very practical method to define withstand characteristics of SF_6/N_2 mixtures is to determine the so called pressure conversion factor k_{rp}. Where k_{rp} factor represents the increase of the pressure of the insulating mixture with respect to the pure SF_6 insulation, in order to obtain the same withstand characteristics. k_{rp} factor is defined as:

- The ratio between the pressure (of the most severe polarity, when applicable) of the mixture SF_6/N_2 and the pressure (of the most severe polarity, when applicable) of pure SF_6 in order to obtain the same dielectric performances (see figure 8).

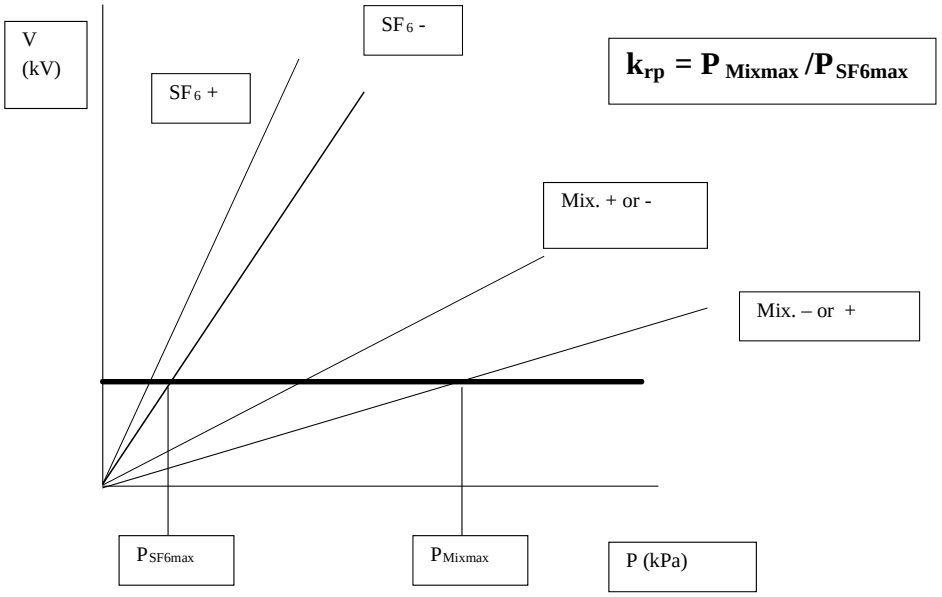

Figure 8 : k_{rp} definition

The most severe polarity is the one for which the highest pressure is necessary to obtain the required withstand characteristics.

The most severe polarity depends basically on the geometric configuration and the specified working pressure and can be either positive or negative. The figure 9 and figure 10, taken from references [33] and [32] respectively, show as the most severe polarity changes according to the working pressure; for example in figure 5 for SF_6/N_2 mixture the most severe polarity is the negative one for working pressure below 5 bars while becomes the positive for working pressure above 5 bars. In figure 10 it is shown a similar behaviour not only for SF_6/N_2 mixture but also for pure N_2 and (probably) for pure SF_6. Moreover, the two figures show the pressure value at which the withstand characteristics of positive and negative polarities cross is not constant but depends very much on the testing configuration.

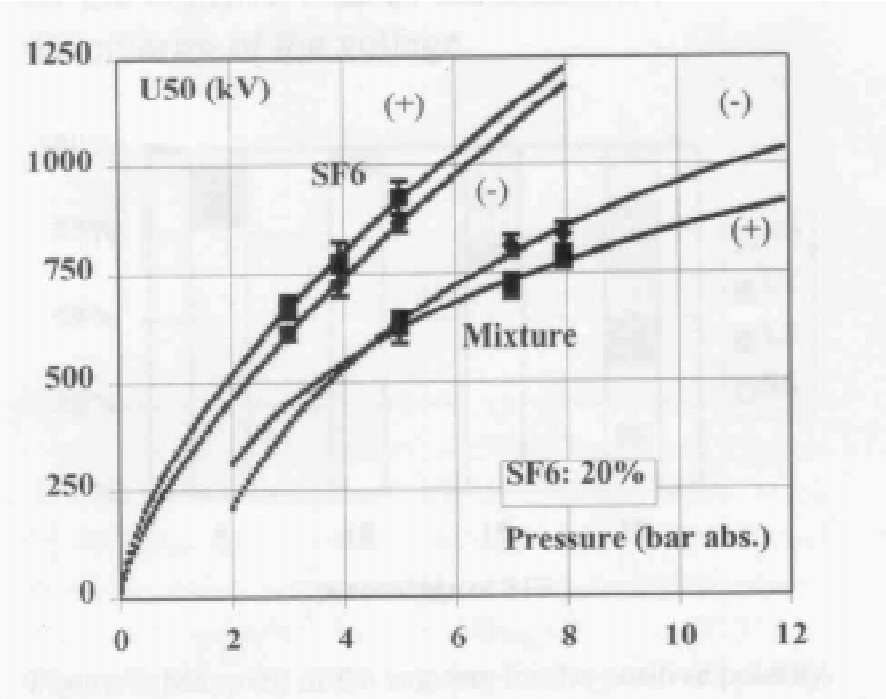

Figure 9 : Example from [33]

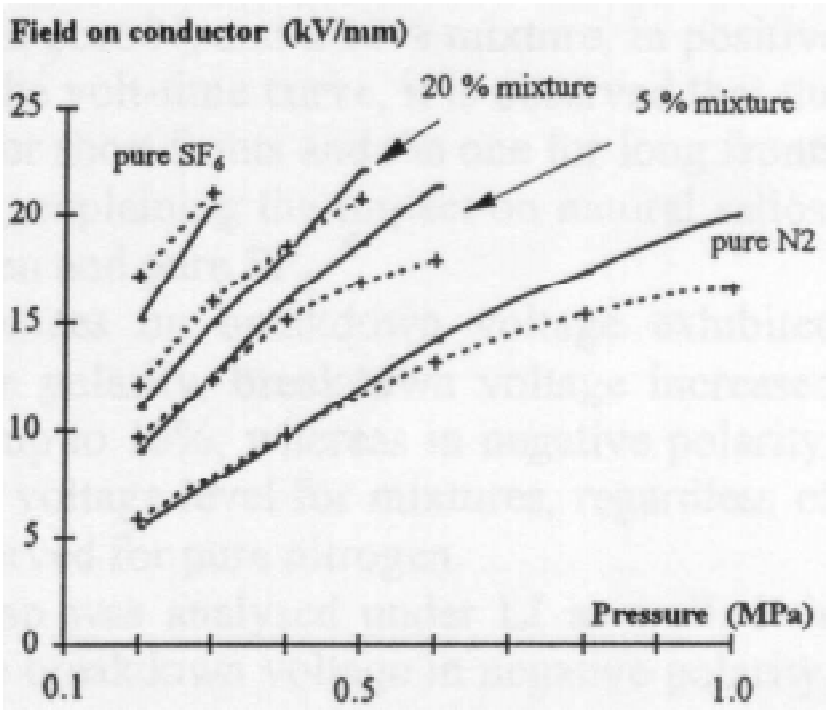

Figure 10 : Example from [32]

On the other hand, as reported in chapter 6, the definition of the voltage level to be applied during both type and on site commissioning tests requires the knowledge of the "ratio" between PF, SI and LI flashover voltages, the so called test conversion factor.

The analysis made, in the present work for the determination of k_{rp} values and test conversion factors to be applied for GIL, is based on data taken from literature and no new tests were carried out at the purpose.

The complete list of papers taken into account is reported in paragraph § 3.4, while table 5 reports, very briefly and for each of the considered paper, the main information concerning the test object, the applied voltage stresses, the gas mixtures characteristics and short comments. In table 5 papers, which data are considered for the present evaluation, are reported in **bold**, while those with data not considered are reported in *italic*

Table 5 :
List of references and relevant test performed

Ref	Configuration	Applied voltage	Mixture range SF6 content (%)	Pressure (kPa)	Comments
[13]	*Long bus duct*	*AC, SI, LI*	*18;13*		*General description of monitoring systems and possible testing equipment for commissioning. Data not considered*
[19]	*Electrode – plane*	*LI*			*The complete set of results is reported in* [16]
[20]					*Paper dealing with Insulation co-ordination of GIS: return of experience, on site tests and diagnostic technique, used only for the definition of voltage classes*
[21]	**Coaxial Φi = 89 mm; Φo = 226 mm L = 900 mm**	**AC, SI, LI**	**100, 80, 60, 40,20**	**100 – 620**	**LI and SI only for negative polarity, not considered in present report**
[22]	**Coaxial Φi = 80 mm; Φo = 230 mm + particles**	**AC**	**100; 80; 60; 50; 40; 20; 0**	**200 – 800**	**Data considered**
[23]	*Coaxial, Φi = 100 mm; Φo = 180 mm + roughness*	*VFT*	*100; 50*	*100 -200*	*Data not considered. SF_6 content out of range of interest*
[24]	**Electrode –plane Without and with particles,**	**AC – LI (mainly)**	**100; 15; 8; 3; 0**	**400 - 2000**	**Data already considered**
[25]					*Reference reports the state of the art of dielectric characteristics of different insulating media. No new data. Good list of references*
[26]	*Coaxial configuration Φi = 25.4 mm; Φo = 70 mm with and without spacer with and without particles*	*AC; LI*	*100; 75; 50; 0*	*100 – 400*	*Data refer to no industrial coaxial configuration. Moreover LI only for negative polarity. Data not considered in present report*
[27]	*Coaxial Φi = 89 mm; Φo = 226 mm L = 900 mm*	*AC, LI*	*100, 60, 40*	*100 – 450*	*The complete set of data is reported in [2]*
[28]	*Point – plane*	*VFT*	*100; 70; 50; 30; 10*	*50 – 300*	*No industrial configuration. Data not considered*
[29]	**Coaxial** +10mm needle on HV	**LI**	**100; 20; 15; 10; 5; 0**	**400 - 1100**	**Data considered**

	conductor,				
[30]	*Coaxial* *Φi = 120 mm;* *Φo = 400 mm* *L = 600 mm,*	*LI*	*100; 35; 18*	*300 - 800*	*Polarity not defined. Data not considered in present report*
[31]	**Coaxial** **Φi = 185 mm;** **Φo = 400 mm**	**AC, LI**	**100; 20; 10; 5; 0**	**200 - 1000**	**LI only with negative polarity. LI data not considered in present report**
[32]	**Coaxial** **Φi = 185mm;** **Φo = 400mm**	**LI**	**100; 20; 5; 0**	**100 - 1000**	**Data considered**
[33]	**Coaxial** **(Typical 145 kV GIS)** **+ spacers**	**LI**	**100; 20; 15; 10; 5**	**300 – 800**	**Data considered**
[34]	*Coaxial + needle,*	*Fast oscillation: 2.5 & 10 MHz*	*100; 30; 10; 5*	*100 – 300*	*Only positive polarity. Data not considered in the present report*
[35]	**Sphere gap** **(Φ = 160 mm; d = 10mm)** **Simulated earthing switch,**	**LI** **LI**	**100; 15; 10; 5** **100; 15; 10 5**	**400 – 800**	**Data considered**
[36]	**Coaxial** **Φi = 120 mm;** **Φo = 400 mm** **L = 600 mm**	**LI**	**100; 20; 10;5**	**200 – 700**	**Data considered**
[37]	*Point plane* *Φ = 1 mm; d = 20 mm*	*LI, SI*	*100; 15; 10; 5*	*100 – 1500*	*No industrial configuration. Data not considered*
[38]	**Bus bar 245 kV GITL** **Φi = 101 mm;** **Φo = 292 mm**	**AC, SI,**	**10;5**	**100 – 700**	**Data for pure SF_6 available only for SI. For AC. K_{rp} values not derived**
[39]	**Bus bar 245 kV GITL** **Φi = 101 mm;** **Φo = 292 mm**	**AC; LI**	**30; 5**	**100 – 700**	**No data available for pure SF_6. K_{rp} values not derived.** **Data used for determining voltgage shape influence**
[40]	*Homogeneous field + spacers and particles*	*AC, LI*	*100; 30; 10; 6*	*200 – 500*	*No industrial configuration. Data not considered*
[41]	*Rod-plane and plane-plane*	*LI*	*100; 50; 20; 10; 5*	*100 – 800*	*No industrial configuration. Data not considered*
[42]	*Plane – plane + particles*	*DC*	*100; 50; 20; 5*	*100 -- 500*	*No industrial configuration. Data not considered*
[43]	*Coaxial* *Φi = 100 mm; Φo = 180 mm* *+ roughness*	*VFT*	*100; 50*	*100 -200*	*Data already presented in reference [5]*
[44]	**Coaxial + spacers** **Φi = 200 mm;** **Φo = 300 mm** **l = 5200 mm**	**LI**	**100; 90; 80**	**300 – 550**	**Data considered**

3.2 Evaluation of the test results

3.2.1 Determination of k_{rp} values

As shown in figure 9 and figure 10, both referring to industrial coaxial configuration, k_{rp} values depend strongly on the geometrical configuration and on the working pressure. In order to limit the possible mixture of different physical phenomena and trying to decrease the spread of the results the analysis is limited to industrial configurations

The results are reported in table 6, table 7 and table 8 for Power Frequency (PF), Switching Impulse (SI) and Lightning Impulse (LI) voltage stresses respectively.

The three tables report a concise description of the considered configuration, the voltage level (or gradient) for which k_{rp} values are derived and, of course, the k_{rp} values. Trying to have a further reduction of the spread only the values derived for real industrial situations were considered when calculating the average values. The selection is based on the following criteria:

- Coaxial configuration, with or without spacers
- Voltage (or gradient) level giving, for pure SF_6, a pressure higher than or equal to 400 kPa.

Table 6 :
Power frequency: k_{rp} values in different test configurations

Ref.	Config.	Spacer	Stress Level (kV) **(kV/mm)**	Krp for different SF_6 percentage in the mixture SF_6/N_2 100	80	60	40	20	10	5	0
[20]	Coaxial	No	298	*1.00*	*1.05*	*1.13*	*1.23*	*1.41*			*3.23*
			510	1.00	1.10	1.16	1.26	1.45			
			549	1.00	1.10	1.18	1.26	1.48			
[22]	Coaxial	?	516	1.00	1.07	1.14	1.37	1.82			
			600	1.00	1.07	1.15	1.50				
[24]	Electrode-Plane (see figure 10)	Yes	600	1.00							*5.00*
[31]			**12**	1.00					*1.68*	*2.05*	*3.70*
			15	1.00					*1.88*	*2.37*	
Krp mean values					1.09	1.16	1.35	1.58			
Std					0.02	0.02	0.11	0.20			

Note:
1) Stress values reported in bold refer to gradient on conductor or on enclosure
2) The values not considered for the calculation of mean values are reported in *italic* in the tables.

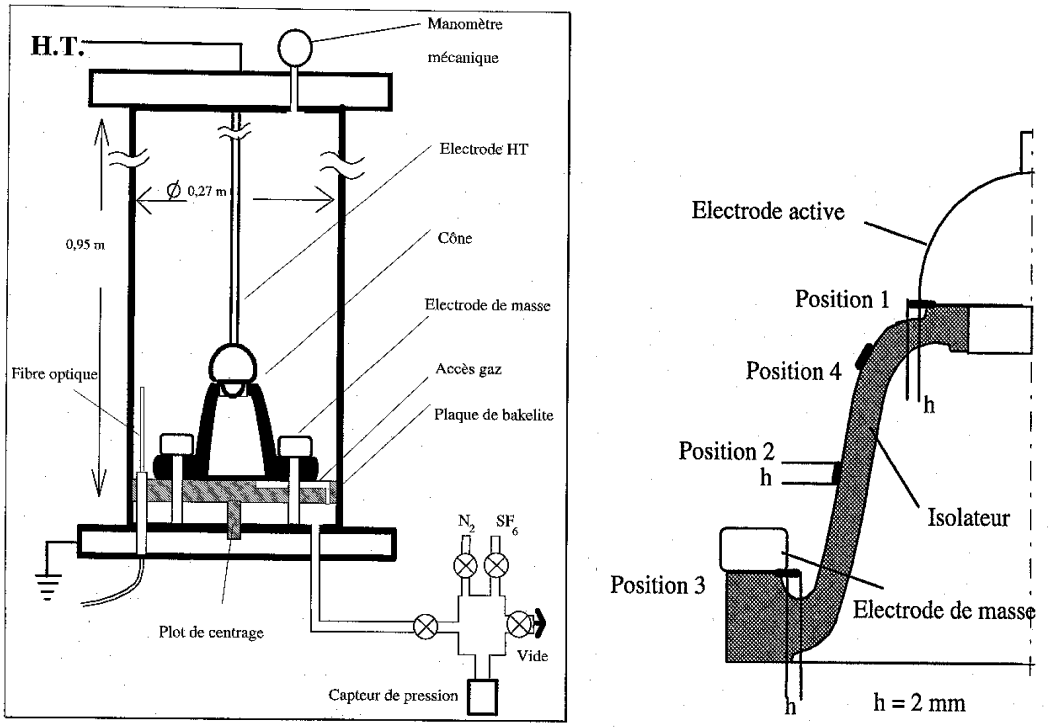

a) b)

Figure 11 : Test object of reference [24] (a) overall view, (b) positions of particles on spacers

Table 7 :
Switching impulse: k_{rp} values

Ref.	Config.	Spacer	Stress Level (kV) **(kV/mm)**	Krp for different SF_6 percentage in the mixture SF_6/N_2 100	10	5
[38]	Coaxial (figure 11	No	**92 on conductor**	1.00	*1.81*	*2.21*
			40 on enclosure	1.00	*1.98*	*2.32*
Krp mean values						
Std						

Note:
1) Stress values reported in bold refer to gradient on conductor or on enclosure
2) The values not considered for the calculation of mean values are reported in *italic* in the tables.

Table 8 :
Lightning impulse: k_{rp} values

Ref.	Config.	Spacer	Stress Level (kV) **(kV/mm)**	Krp for different SF_6 percentage in the mixture SF_6/N2 100	20	15	10	8	5	3	0
[24]	Electrode-Plane (figure 10)	Yes	400	1							*4.41*
			448	1							*4.40*
			600	1		*2.55*		*3.08*		*3.75*	*4.98*
[32]	Coaxial		**15**	1	*1.47*				*1.96*		*3.63*
			18	1	*1.56*				*2.42*		
			20	1	*1.59*						
[33]	Coaxial (figure 12)		750	1	1.74	2.15	2.51		2.71		6.72
[35]	Sphere gap (figure 13)		350	1		*1.66*	*1.88*		*2.04*		
[36]	Coaxial			1	*1.24*		*1.48*		*2.12*		
				1	*1.85*						
[44]	Coaxial (figure 14)		**20**	1	*1.47*		*1.81*				
			27	1	1.52		1.96				
Mean value					1.63	2.15	2.24	3.08	2.71		6.72
Std					0.16		0.39				

Note:
1) Stress values reported in bold refer to gradient on conductor or on enclosure
2) The values not considered for the calculation of mean values are reported in *italic* in the tables.

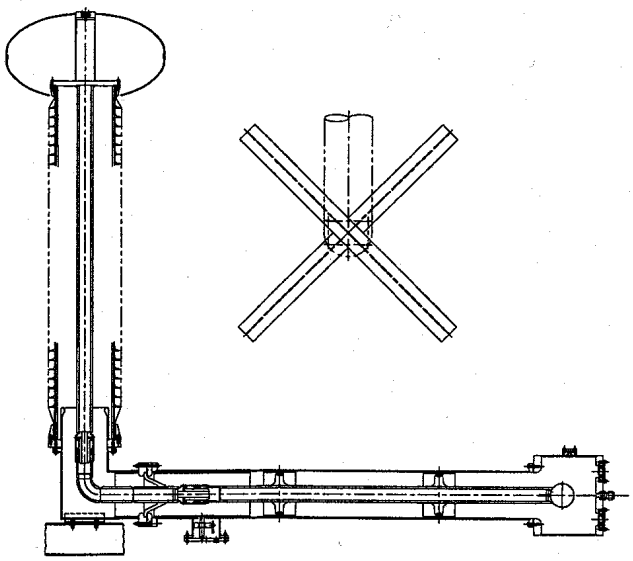

Figure 12 : Test object of reference [38]

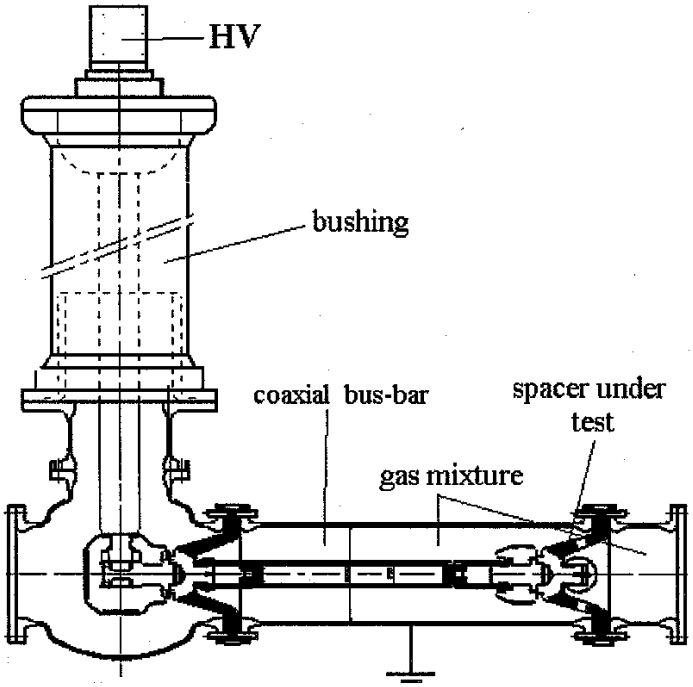

Figure 13 : Test object of reference [33]

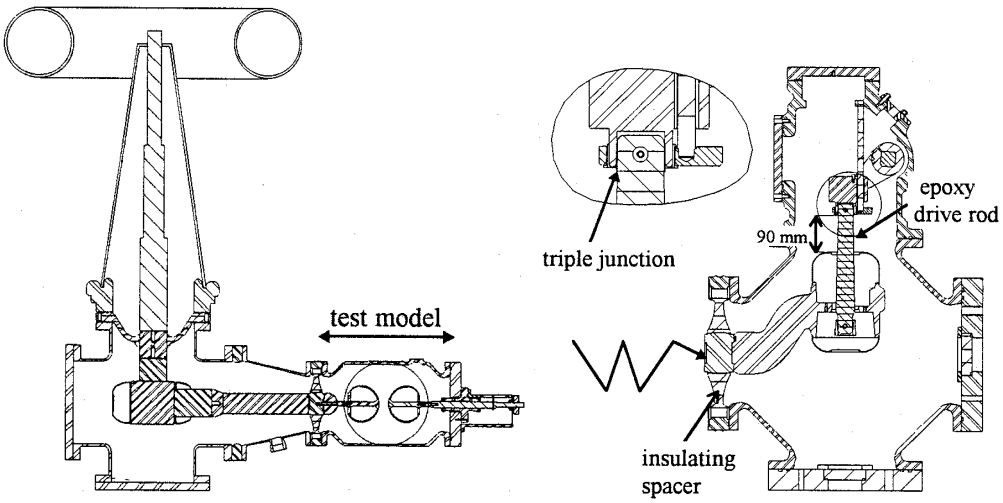

Figure 14 : Test object of reference [35]: (a) Sphere-sphere gap, (b) Simulated earthing switch

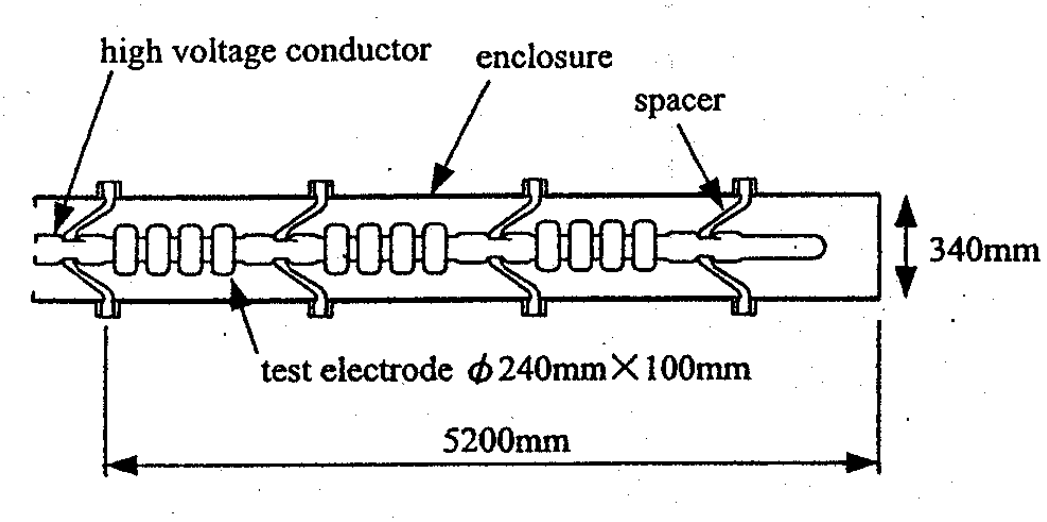

Figure 15 : Test Object of reference [44]

The figure 16 reports the k_{rp} mean values derived from table 6, table 7 and table 8 as a function of the SF_6 percentage of the mixture, the values show a clear and defined trend independently of the voltage stress. Moreover, it has to be noted that only k_{rp} mean values relevant to PF and LI voltages are available and that they concern to two not overlapping SF_6 percentage range.

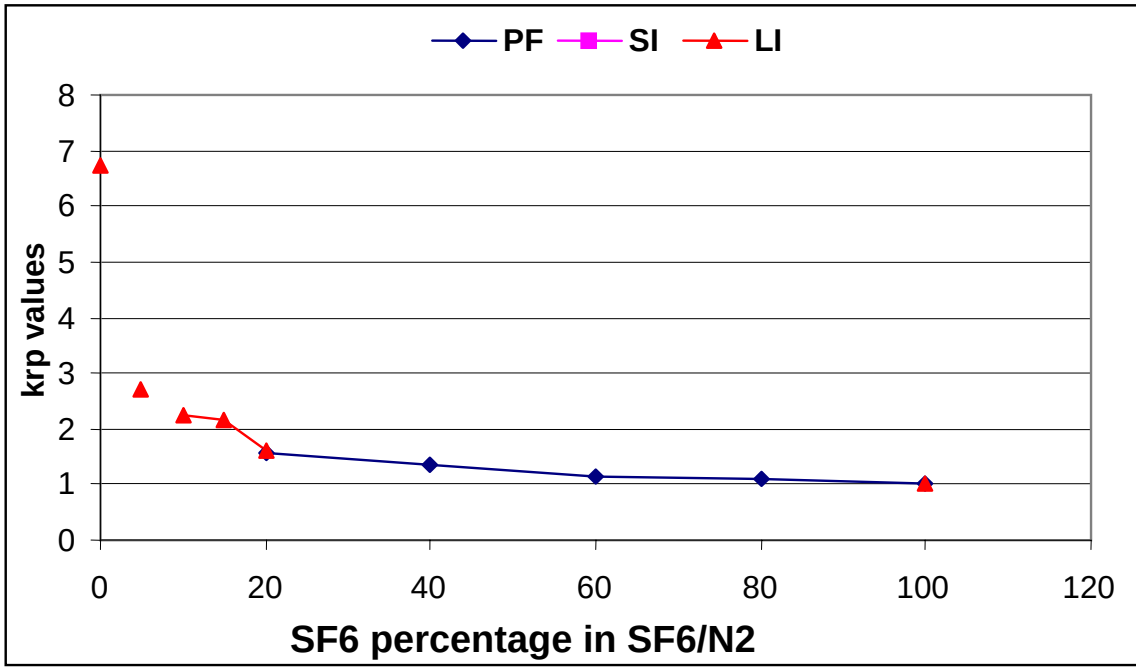

Figure 16 : k_{rp} values as a function of SF_6 percentage for different voltage classes (only data for coaxial configuration and with SF6 pressure > 0.4 Mpa)

In order trying to have a better definition of the trend, all data reported in table 6, table 7 and table 8 were considered for the calculation of k_{rp} mean values. The new set of results, reported in figure 17, shows that the basic trend of krp values versus SF_6 percentage is not changed with respect to that reported in figure 16 a part from an increased scatter.

It can be assumed that results of figure 16 are of general application independently of the voltage classes and of the SF_6 percentage considered.

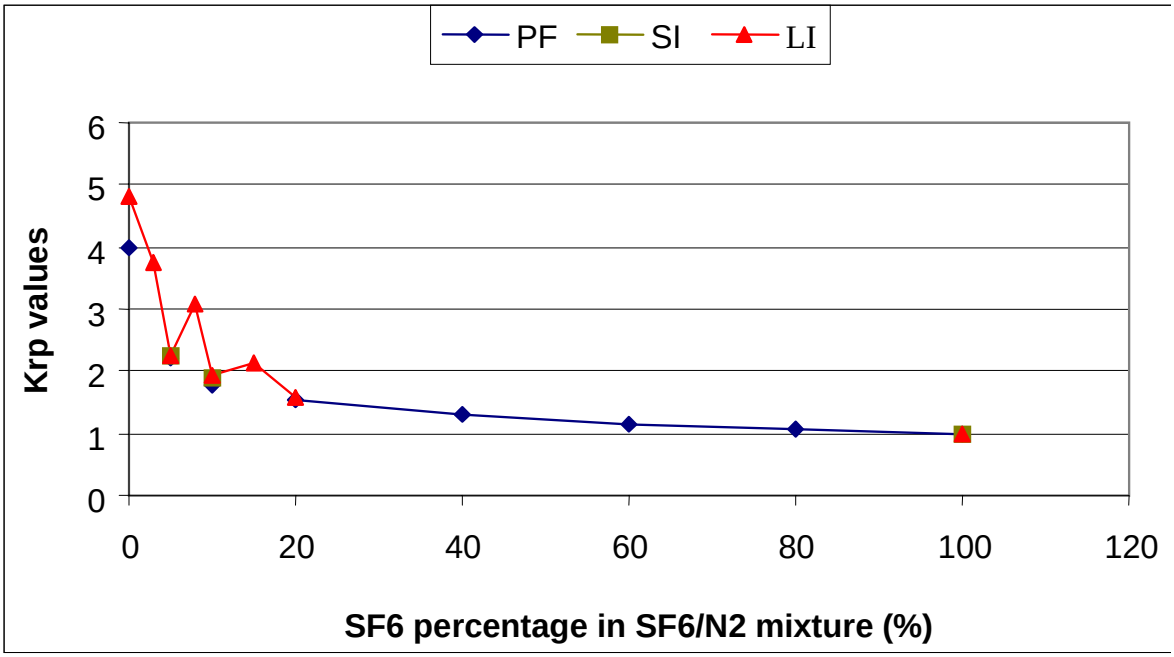

Figure 17 : k_{rp} values as a function of SF_6 percentage for different voltage classes (all available data considered)

3.2.2 Determination of the influence of the impulse shape

The available data were processed for the determination so called test conversion factors (K_t) that is the ratio between the flashover voltages with different voltage stresses and namely: power frequency and lightning impulse ($K_{tPF/LI}$) and switching impulse and between switching impulse and lightning impulse ($K_{tSI/LI}$). In order to limit the scatter of the results, the analysis was limited to industrial configuration and to practical gas pressure, that is for pure SF_6 pressure of about 400 kPa and for gas mixture a value obtained multiplying 400 kPa for k_{pr} value relevant to the considered mixture. Pressures within a range of ± 20% the calculated values are included in the evaluation.

The calculated values are reported in table 9 and table 10 for $K_{tPF/LI}$ and $K_{tSI/LI}$, respectively.

Table 9 :
Test conversion factor for AC and LI

Ref	Ratio	Pressure (kPa)	SF_6 percentage in gas mixtures								
			0%	5%	10%	15%	20%	30%	40%	60%	100 %
[20]	$K_{tPF/LI}$	400-800									0.64
[31]	$K_{tPF/LI}$	400									0.76
[21]	$K_{tPF/LI}$	450							0.73	0.72	0.72
[32]	$K_{tPF/LI}$	500									0.62
[31]	$K_{tPF/LI}$	600									0.70
[32]	$K_{tPF/LI}$	600									
[36]	$K_{tPF/LI}$	600					0.77				
[21]	$K_{tPF/LI}$	620					0.71		0.71	0.70	0.69
Mean value		$K_{tPF/LI}$					0.74		0.72	0.71	0.69
Note: In the present table peak voltages are considered for calculation, while in chapter 6 PF rms values are considered for calculation											

Table 10 :
Test conversion factor for SI and LI

Ref	Ratio	Pressure (kPa)	SF_6 percentage in gas mixtures								
			0%	5%	10%	15%	20%	30%	40%	60%	100 %
[20]	$K_{tSI/LI}$	400-800									0.75
[21]	$K_{tSI/LI}$	450							0.76	0.79	0.81
[22]	$K_{tSI/LI}$	500									0.72
[21]	$K_{tSI/LI}$	520					0.71		0.75	0.79	0.81
[36]	$K_{tSI/LI}$	600					0.77				
[32]	$K_{tSI/LI}$	600	*>0.80*			*0.75*					
[21]	$K_{tSI/LI}$	620					0.70		0.74	0.75	
Mean value		$K_{tSI/LI}$					0.73		0.75	0.77	0.77

The test conversion factors are summarized in figure 18.

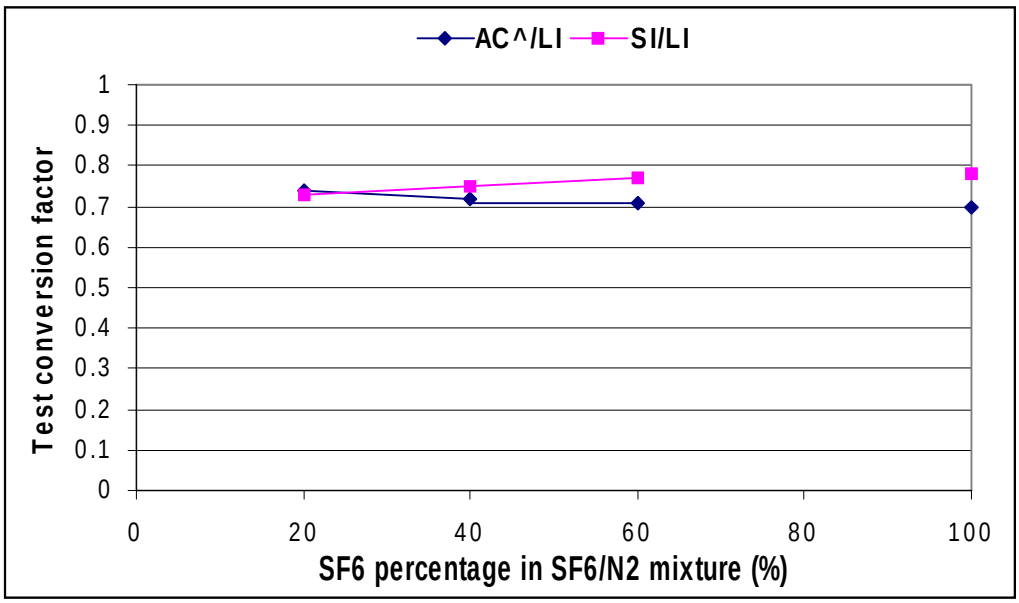

Figure 18 : Test conversion factors as a function of SF_6 percentage

3.3 General consideration and conclusions

Many results were published in the past concerning the dielectric characteristics of SF6/N2 mixtures; most of the experiments were aimed to the study of the basic mechanism of breakdown process and were carried out on basic configurations.

Several examples of tests performed on industrial configurations are reported in literature; nevertheless the comparison of the reported results, at least for the purpose of the present work, is not easy for several reasons, and among the others:

- The different pressure values used. As reported previously, pressure value places an important role for the definition of the most severe polarity
- The non uniform definition of the reported data: breakdown or withstand voltage
- The non uniform testing procedure
- The non uniform procedure used for the preparation of the gas mixture, mainly for low SF_6 contents. It was noticed that tests with pure N_2 shall be performed only with new object, in fact test objects already tested with mixtures, could retain small quantities of SF_6 that could bias significantly the results
- The influencing quantities, as for example particles and roughness, were controlled using different procedures

The available results were analyzed for the determination of both pressure and test conversion factors; for their evaluation, all the possible precaution were undertaken to have correct comparison and consequently limit the scatter on the derived quantities. The results obtained are summarized in figure 16 and figure 18 for pressure conversion factors and test conversion factors respectively.

Pressure conversion factor in the pressure range of interest, is independent of the voltage class considered and as obvious increases decreasing the SF_6 percentage.

Test conversion factors show a slight but definite trend: $K_{tSI/LI}$ increases increasing the SF_6 percentage, while $K_{tPF/LI}$ decreases increasing SF_6 percentage.

Finally, it is to be underlined that no systematic results were found on the effect of some influencing quantities (particles, moisture, roughness and so on), moreover no systematic results were found for Very Fast Transient Overvoltages, but as reported in chapter 5 paragraph 5.1 this voltage class could be disregarded for GIL.

3.4 References of chapter 3

[11] W. Mosch, W. Hauschild, Hochspannungsisolierungen mit Schwefelhexafluorid, VEB Verlag Technik, Berlin, 1979, ISBN 3-7785-0540-8.

[12] F.H. Kreuger, Industrial High Voltage, Vol. I, Delft University Press, 1991.

[13] A. Diessner, H. Koch, E. Kynast, A. Schuette, Progress in High Voltage Testing of Gas Insulated Transmission Lines, ISH 1997, Volume 4, pp. 41-44.

[14] G.P. Baer, A. Diessner, G.F. Luxa, 420 kV SF6-insulated tubular bus for the Wehr Pumped-Storage plant- electric tests, IEEE Trans. On Power App. & Systems, Vol PAS-95 (1976), pp. 469-477

[15] C. Aucourt, C. Boisseau, D. Feldmann, Gas insulated cables: from the state of the art to feasibility for 400 kV transmission lines, Proc. Of Jicable 95 conference, Versailles, France, 1995, pp. 133-138.

[16] CIGRÉ Working Group 23.02, Guide For SF6 Gas Mixtures, CIGRÉ Brochure 163, August 2000.

[17] L.G. Christophorou and R.J. Van Brunt, SF6-N2 mixtures Basic and HV insulation properties, IEEE Transactions on Dielectrics and Electrical Insulation, Vol. 2 No. 5, October 1995.

[18] L.G. Christophorou, Electron-molecule interactions and their applications, Volume 2, Academic Press inc., Orlando, 1984, ISBN 0-12-174402-7.

[19] T.B. Diarra, A. Béroual, F. Buret, E. Thuries, M. Guillen, Ph. Roussel, N2-SF6 mixtures for High Voltage Gas Insulated Lines, 10th Int. Symp. on HV Engineering, Montreal, 1997.

[20] CIGRE WG 33/23-12: “Insulation co-ordination of GIS: return of experience, on site tests and diagnostic technique”, Electra n 176

[21] A.H. Cookson, B.O. Pedersen: “Analysis of the high voltage breakdown results for mixture of SF_6 with CO_2, N_2 and air.” 3rd ISH Milan 1979, paper 31.10

[22] J. Yingshen, L. Ming, J. Yanjun, L.Hao, W. Yihua: “Breakdown characteristics of particle-contaminated SF_6 SF_6/N_2 in a large coaxial system.”, 6th ISH New Orleans 1989, paper 32.14

[23] S.D. Nielsen, D.A. Reynders, J.P. Reynders, I.R. Jandrell, R.J. Traynor: “An assessment of the sub-microsecond region of VFT V-T curves generated in pure SF_6 and 50%SF_6/N_2 gas mixture under small values of bus bar surface roughness.” 9th ISH Graz1995, paper 2282

[24] B. T. Diarra: “Etude de la tenue dielectrique dans les cables haute tensione a isolation gazeuse”. Thesis for doctor degree. Discussed on 20th December 1996 at Ecole Central de Lyon

[25] L. G. Christophorou, J. K. Olthoff and D. S. Green: “Gases for electrical insulation and arc interruption: possible present and future alternatives to pure SF_6”. NIST Technical Note 1425

[26] M. Eteiba, F.A.M. Rizk, N.G. Trinh, C. Vincent, “Influence of a conducting particle attached to an epoxy resin spacer on the breakdown voltage of compressed gas insulation”, Gaseous Discharge II. Pergamon press 1980, pp250-254

[27] A. H. Cookson, “Electrical breakdown studies of SF_6/CO_2/Fluorocarbon mixtures”, Gaseous Discharge II. Pergamon press 1980, 169-178

[28] W. Pfeiffer, V. Zimmer, P. Zipfl, “Predischarge development and dielectric strength of N_2, SF_6 and SF_6/N_2 mixtures in strong non-uniform electrical fields”, 7 ISH, Dresden August 1991. Paper 32.14

[29] S. Meijer. E. Gulski, T.S. Ramu, A. Girodet, “Performance of GIS under 5% SF_6-N_2 gas mixture insulation”, Record of the CIGRE WG 15.03 Conference “Insulating gases”. Arnhem, Netherlands, March 4-5, 1999

[30] H. Koch, “Gas mixtures as insulating gas”, CIGRE 1998 Joint session 21/23/33. Pref. Sub. 3.1 Question 1.2

[31] M.O. Pace, D.L. McCorkle, X. Waymel, “Possible high pressure nitrogen based insulation for compressed gas insulated cables”, CEIDP ’95. Virginia Beach 22-25 October 1995

[32] X. Waymel, “Low SF_6 concentration SF_6/N_2 mixtures for GIL”, VII Symposium International on Gaseous Dielectrics. Virginia Beach; June 1998

[33] M. Guillen, F. Buret, A. Beroual, “Lightning impulse withstand of a gas-insulated line filled with N_2/SF_6”, 11 ISH London 23-27 August 1999 paper 3.71.S18

[34] G. Schröder, “Discharge development in SF_6-N_2 mixtures under fast oscillating impulse conditions”, 11 ISH London 23-27 August 1999 paper 3.79.S18

[35] C. Gailac, “GIS disconnector model performance with SF_6/N_2 mixtures”, 11 ISH London 23-27 August 1999 paper 3.104.S20

[36] A. Diessner, M. Finkel, A. Grund, E. Kynast, “Dielectric properties of N_2/SF_6 mixtures for use in GIS or GIL”, 11 ISH London 23-27 August 1999 paper 3.67.S18

[37] X. Waymel, V. Delmon, T.Rees, A. Gibert, P. Domens, “Impulse breakdown in point plane gaps in SF_6/N_2 mixtures”, 10 ISH Montreal 25-27 August 1997

[38] H.I. Marsden, M. D. Hopkins, C. R. Eck, “Power frequency and SIL withstand performance of GIC with a and 10 percent SF_6/N_2 mixtures”, VII Symposium International on Gaseous Dielectrics. Virginia Beach; June 1998

[39] H.I. Marsden, S. J. Dale, M. D. Hopkins, C. R. Eck, “High voltage performance of a gas insulated cable with N_2 and SF_6/N_2 mixtures” , 10 ISH Montreal 25-27 August 1997

[40] A. Moukengué Imano, R. Schurer. K. Feser, “The influence of a conducting particles on a spacer on the insulation properties in SF_6/N_2 mixtures” , 11 ISH London 23-27 August 1999 paper 3.232.P3

[41] L. Pécastaing, T. Reess, P. Espel, J. Paillol, A. Gibert, P. Domens, “Investigation of breakdown characteristics of N_2, SF_6 and SF_6-N_2 mixtures under pressure” , 11 ISH London 23-27 August 1999 paper 3.224.P3

[42] S.A. Ward, “Influence of conducting particles on the breakdown voltages of SF_6-N_2 mixture”, 11 ISH London 23-27 August 1999

[43] D. A. Reynders, J. P. Reynders, I. R. Jandrell, "VFT V-T curves for SF_6 and SF_6:N_2 = 1:1 in a 180/110 mm coaxial duct at pressure of 1 and 2 bar with small values of surface roughness", 11 ISH London 23-27 August 1999 paper 3.264.P3

[44] H. Hama, K. Inami, M. Yoshimura, “Practical Problems in designing gas insulated bus applying N_2/SF_6 gas mixtures", Gas Discharge 2000, Glasgow.

[45] M. Yoshimura, K. Inami, H. Hana, H. Fujii: "Area Effect of Breakdown at lightning Impulse in N_2/SF_6 mixtures" Gas Discharge 2000, Glasgow.

4. GIL Representative Overvoltages between conductor and enclosure

4.1. Introduction

Due to the different applications of GIL with their parameters of the connected elements at both ends and the generation of possible voltage stresses the expected overvoltages will vary in a wide range. Calculation of the transients can show the maximum overvoltages to be expected along the GIL.

The integration of suitable overvoltage limiting devices is necessary to realize an economic and safe system. Therefore surge arresters (integrated metalclad into the system or very near to the ends of GIL) are necessary to be considered from the beginning of overvoltage stress evaluation.

4.1.1. Transient overvoltages generated by lightning phenomena

For the study of overvoltages in GIL the main focus has to be pointed onto the lightning impulse voltages, because they give the highest stresses, which has to be known for dimensioning and testing.

For each GIL application different voltage stresses can be expected due to the lot of parameters involved. A listing of the main parameters gathered under three topics is the following:

- Lightning strike:
  - location of the lightning strike (near, remote, tower)
  - lightning-current amplitude and steepness of front and tail
  - voltage amplitude and steepness of front and tail of remote strike surges
- Surrounding of GIL:
  - connection to overhead-lines, cables, GIS
  - surge-impedance's
  - grounding resistance's
  - shielding wire system
  - geometry (line length, tower height and geometry)
  - dielectric strength of the overhead line insulation
- GIL:
  - surge-impedance
  - length
  - connection to surge arresters
  - characteristic of surge arresters
  - connections at both sides
  - open end or energy transport situation
  - prestress by AC magnitude and polarity

The amount of parameters show that a general statement for the expected transient overvoltages is hard to give. General studies can only focus on some main parameters which will show the tendencies of influence. For special application of a GIL the parameters has to be checked and classified as relevant or not and the considered values or ranges of values of the parameters has to be chosen as precise as possible.

4.1.2. Continuos power-frequency voltage and temporary overvoltage

The power-frequency overvoltages are normally low in comparison to the stresses by fast and slow front overvoltages. But the combination of AC prestress with the transient phenomena resulting out of lightning activities has to be considered. The importance of considering this prestress is dependant from some parameters as shown below.

The continuous power-frequency voltage and the temporary overvoltages are the base for dimensioning the overvoltage limiting devices. The characteristic of the surge arresters is necessary to know for calculation of the transient overvoltages.

4.2. Development of surge voltages within GIL

Surge voltages within gas-insulated cables has been shown in principal by [46]. Shielding failures and back flashovers have been investigated for a GIL directly connected to an overhead line. Despite the investigations concerned a ±600 kV DC-system study their principal results can be transferred to AC systems. The investigations shows the dependency of the voltage profile, means voltage amplitude along the GIL-length, from the front- and tail-time of a surge, which travels from the entrance to the end and is reflected there.

For these investigations the DC voltage of the system (positive and negative) and the special characteristic of the used surge arresters lead to surge voltages which principal behavior will be described here. Note that the voltage amplitudes will be different from the 420 kV AC-systems-studies due to the different values of the service voltage. Also it has to be taken into account the fact that different to the DC service-voltage the AC power-frequency voltage with the maximum value in the peak of the half cycles will be met by a lightning surge with a lower probability according to the sine-wave shape. To give an idea of the probability to meet or to come near to the peak value: Only 20 % of the cycle-time reaches a value above 95 % of the power-frequency peak value or only 30 % above 90 % which has to be compared with the continuos voltage of a DC-system. This is valid for considering only one phase. Considering all three phases which is specially necessary for back flashovers the percentage of to meet near the peak value will be much higher.

For explanation of what happens at the end of a GIL when the surge is reflected equations has been developed and the voltage-wave shapes has been lined out in figure 19 and figure 20.

It can be shown that the maximum voltage for a polarity of the service voltage equal to the polarity of the incoming surge are higher than if the opposite polarity is met by the surge. The maximum voltage is largely a function of the arrester characteristics and GIL surge impedance Z_c . It can be calculated with the following equation:

$$E_M = E_i + \frac{e_{a1} - i_{a1} * Z_c \pm V_{ac}(t_0)}{2} = E_i + \Delta E \qquad (9)$$

where E_i is the surge voltage which travels toward the end of the GIL and $V_{ac}(t_0)$ is the service voltage at the time t_0, being the point on the sine wave where E_i is generated. The voltage e_{a1} and current i_{a1} are the arrester discharge voltage and current for the condition where the GIL surge impedance is equal to the derivative of the arrester voltage with respect to the arrester current

$$Z_c = \frac{de_A}{di_A} = R_A \qquad (10)$$

In [46] the development of this equation is well described. A surge voltage e is considered with a crest voltage of E_i, traveling on the cable toward the end of GIL , at which location the arrester is connected to ground. At the open end of the cable, this voltage attempts to double but the arrester decreases the voltage to e_A having a crest of E_A as shown in figure 19. The reflected voltage e´, equal to (e_a-e) having a crest of e_1´ is also shown.

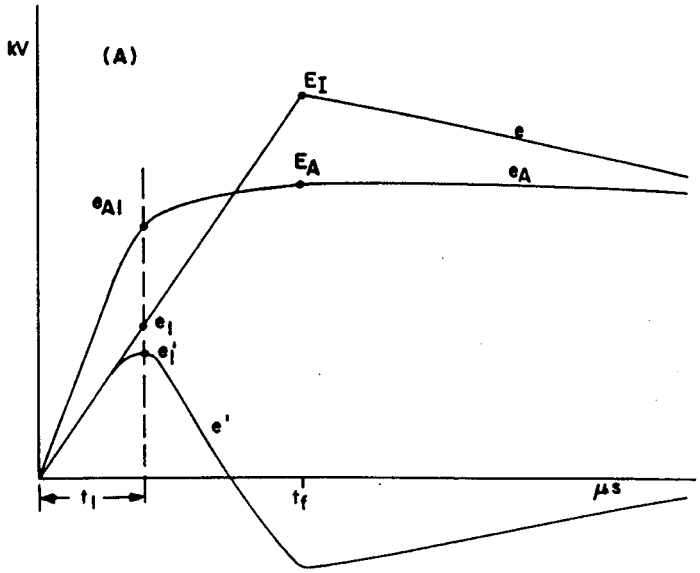

Figure 19 : Voltages at the end of GIL without service voltage

As shown in figure 20 at some location along the cable, at the time T from the end of the GIL, the crest voltage, E and e_1' results in the maximum voltage inside of GIL E_M.

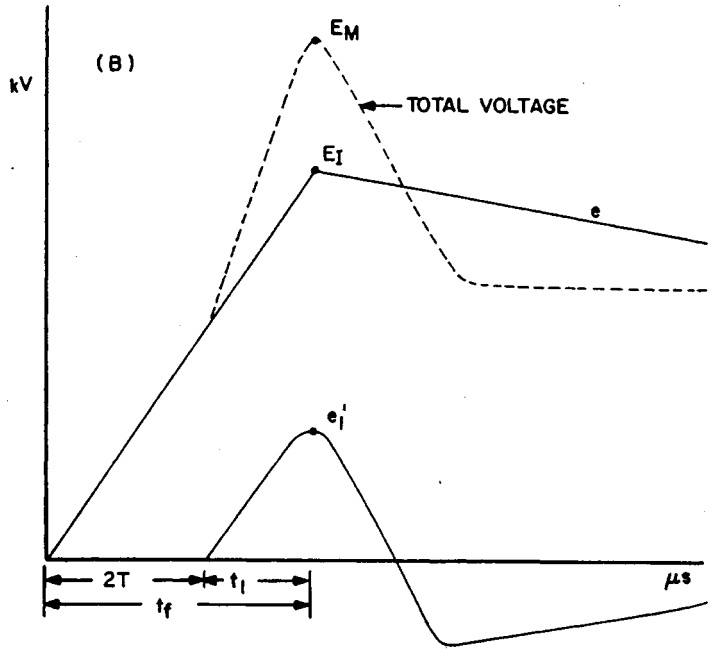

Figure 20 : Maximum voltage in GIL due to superposition of incoming and reflected surge

4.2.1. Shielding failures

The steepness of the surge currents and voltages depend on the stroke current magnitude. For the case of a 30 km GIL-length considered here, the travel time of the cable is large compared to the front of a surge voltage. Only the location along the GIL where the maximum voltage occurs and not its magnitude itself is affected by the front-time of the surge voltage. Therefore, the front of the surge voltage is arbitrarily set at the one value 10 μs. The tail of the surge voltage does also not effect the maximum voltage on the cable but the voltage profile is strongly dependant on the tail-times t_T.

For the tails of 30, 90, 160 and 250 μs and the front of 10 μs a typical surge voltage profile along the GIL is shown in figure 21 for the case when the surge voltage E_i is in the same polarity as the DC voltage. From the

calculations it can be seen that the maximum voltage and its location is independent from the tail-times always near the end of GIL, only the wave profile along the GIL varies.

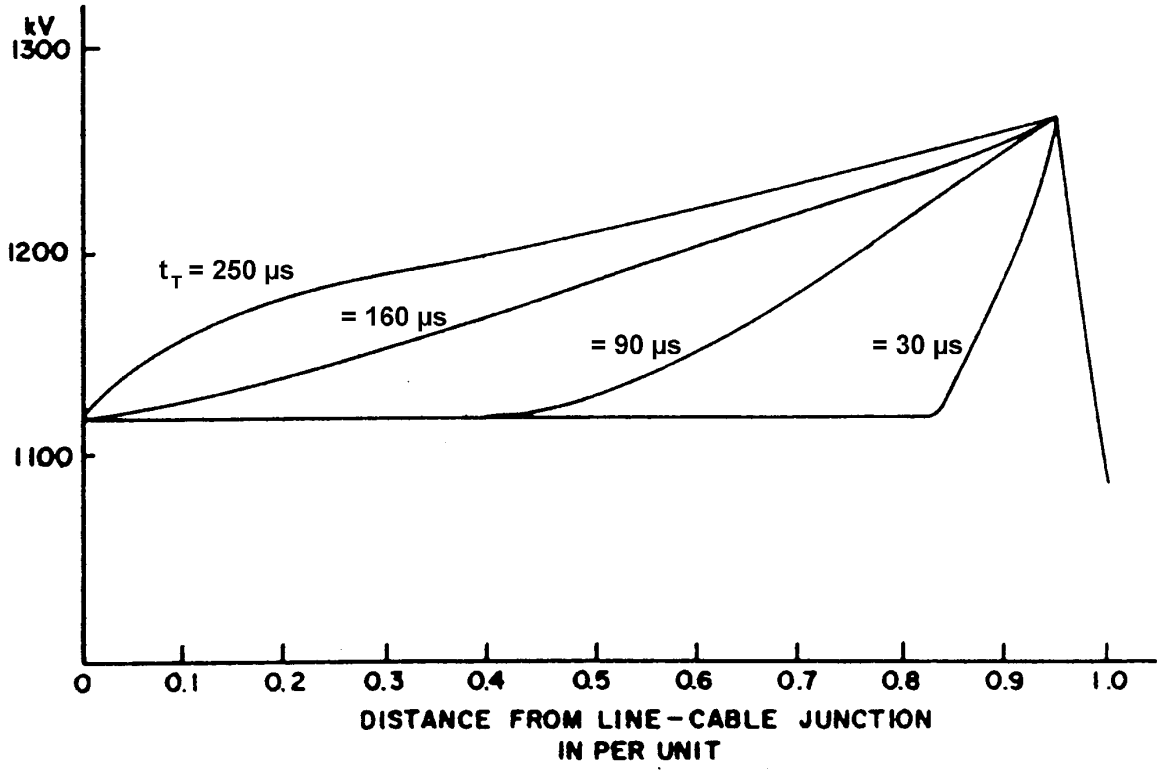

Figure 21 : Voltage profile along the 30 km GIL resulting from shielding failure. The service voltage is of the same polarity as the surge, t_T – tail-time of the surge

4.2.2. Back flashovers

For back flashovers the maximum voltage inside GIL can also be calculated by the (9). But here the profile is sharper than those obtained from shielding failures since the incoming surge caused by a back flashover has a much shorter tail.

The equivalent circuit used to calculate the surge voltages in GIL must consider the effect of reflections from the flashover point, since these reflections tend to increase the voltage inside GIL. The distance from the flashover point was investigated between the first ten towers before the GIL entrance.

The voltage profile along the GIL is shown by the solid line in figure 22 for a back flashover at the first tower from the line-GIL junction. This overvoltage will have the shortest front and tail-times due to nearly no attenuation effects. The dotted line shows the profile if reflections from the struck point are not considered. As shown, ignoring the effect of reflections decreases the entire voltage profile for a back flashover at the first tower. Beyond the fifth tower the profiles are similar and maximum voltages are identical due to attenuation between stuck point and GIL entrance.

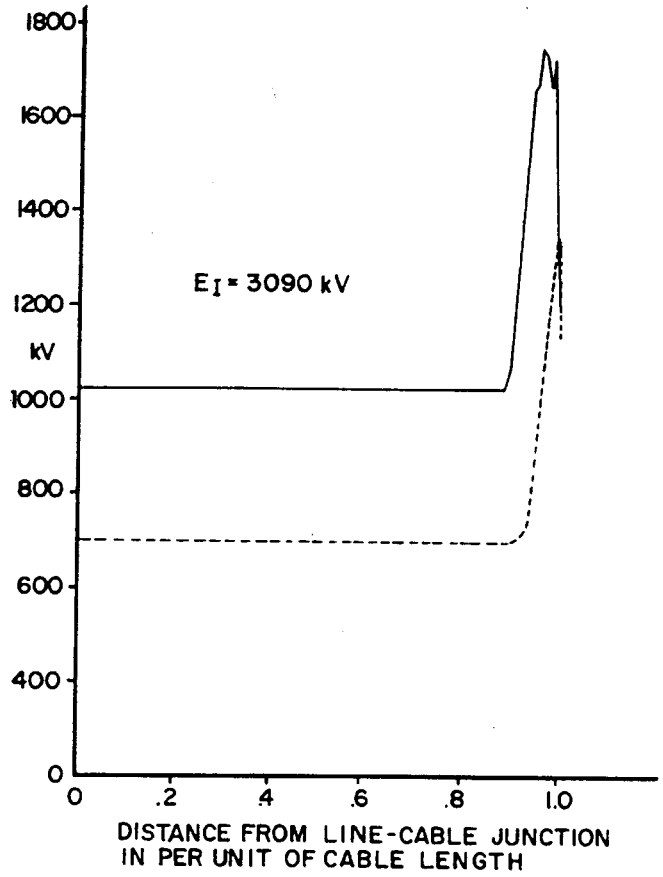

Figure 22 : Voltage profile along GIL for a surge caused by back flashover at the first tower:
solid line: actual profile considering struck point
dotted line: profile of struck point is ignored

This example shows the extreme high voltage maximum if a back flashover occurs at the first tower. The probability to reach this maximum is reduced by using line arresters, working between the line and the tower itself [49]. The main objective is to prevent arcing at the insulators. This is achieved if the residual voltage of the surge arrester is lower than the surge lightning voltage of the insulators. By means of a suitable arrester characteristic this can be below the line insulation-level.

4.3. Examples of fast front overvoltage calculations

4.3.1. EDF 420 kV system

On the base of the above described considerations the use of GIL has been investigated for the 420 kV grid of the french utility EDF [47]. The characteristics of the grid has been adapted for varies calculations which show the possible overvoltages and overvoltage distributions for the relevant parameters due to shielding failures and back flashovers.

4.3.1.1.Fast-front overvoltage stresses

For GIL, these voltage stresses arise solely from lightning stresses when the GIL is connected to one or two OVHL. On account of the 1500 kV insulation against LI for recent 420 kV lines, the frequency of faults due to lightning is of the order of:

- discharges consecutive upon shielding failures: 0.6 faults/100 km/year,
- back flashovers: 1.2 faults/100 km/year for a mean value of 15 ohms for the 420 kV tower footing resistance.
- The GIL configuration considered for the investigation has one end in an open circuit (GIL forming a siphon or GIL connected to a GIS with open circuit breaker) and one end

connected to an overhead line (figure 23). The GIL is protected by placing a lightning arrester outside the GIL at each end.

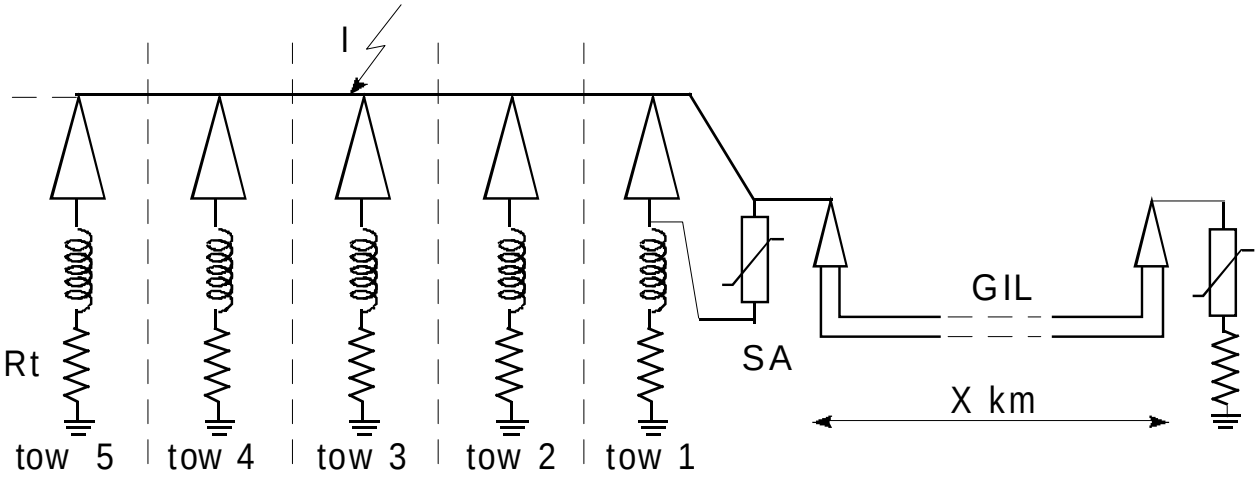

Figure 23 : Diagram of the configuration for research into fast-front voltage stresses due to lightning in a GIL.

The calculations were performed with EMTP. The towers were represented by propagation elements of 150 ohms and their tower footing resistance R_t is a parameter of the investigation; corona effect was also taken into account, as well as the length of the lightning arrester connections.

The parameters with the greatest influence on the GIL MTBF due to intrinsic insulation failures were the subject of a practically exhaustive study:

- the polarity of the AC voltage present before the discharge at the tower which simultaneously increase the overvoltage amplitudes and the frequency of such overvoltages,
- the non-linear characteristic of the lightning arresters,
- the shapes of the impinging overvoltages.
- the protection level and location of the lightning arresters,
- the surge impedance of the GIL together with the shapes of the impinging overvoltages.

With the chosen location for the surge arresters, both for back flashovers and for shielding failures, the maximum overvoltage amplitudes in the GIL are located in a reduced area at the end opposite to the point of impact of the lightning stroke. For GIL over 2-3 km long, these maximal overvoltage amplitudes are practically independent of the length of the GIL.

4.3.1.2.Back flashovers

During back flashovers, it is highly probable that the polarity of the AC voltage present on the back flashed phase will be opposite to that of the voltage generated by the lighting stroke. So, the stresses in the GIL were evaluated with this polarity condition and an AC amplitude of 1 p.u. on the back flashed phase as it is an important factor of the overvoltage amplitudes.

The voltage distribution VD(*V*) along the GIL and the maximum amplitude reached depend on the tower struck by the lightning (figure 24). Whether the GIL is 2 km or 50 km long, it is the last 2 or 3 kilometers which have the greatest influence on the probability of discharge of the whole GIL and therefore its MTBF.

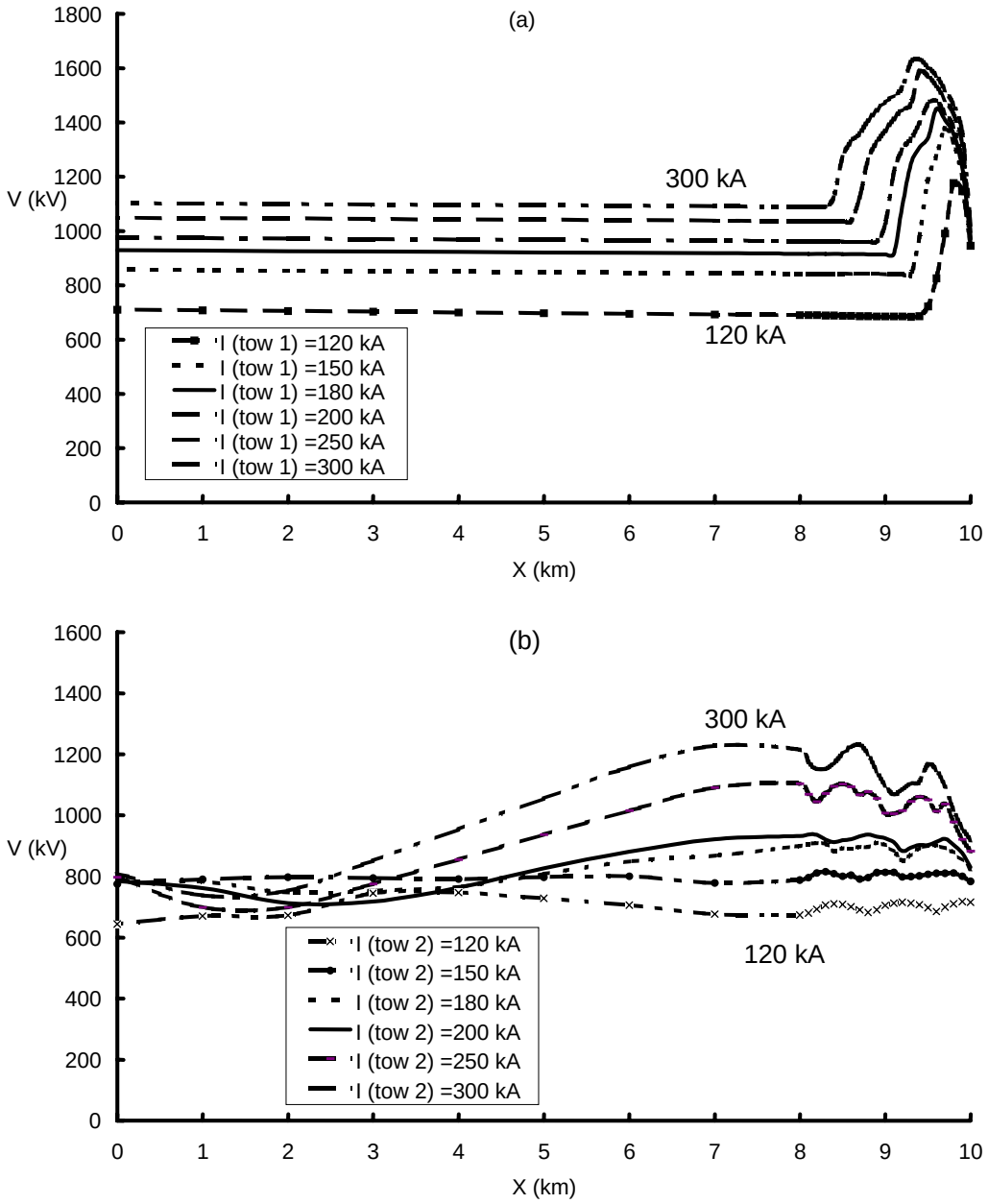

Figure 24 : Overvoltages in the case of back flashover for a GIL 10 km long (1 p.u. AC of opposite polarity voltage distribution DV(V) along the GIL as a function of the lightning current I striking tower 1 (a), tower 2 (b).

4.3.1.3.Shielding failures

On account of the insulation of the EDF 420 kV lines, as shown in figure 25, the maximum overvoltages due to shielding failures are much lower than those caused by back flashovers; only lightning strokes of 20 kA amplitude (corresponding to the maximum current likely to cause shielding failure) striking the span between tower 1 and tower 2 can reach the levels of those generated by back flashover; but their frequency will be only very low (the width of the shielding failures is very tiny for these current amplitudes) and for the EDF OVHL design their influence on the GIL MTBF is negligible compared to that of the voltage stresses caused by back flashovers.

Contrary to back flashover, for shielding failure there is no correlation between the polarity of the struck phase and the overvoltage. Indeed the maximal GIL overvoltages occur when the overvoltages and the struck phase are of the same polarity.

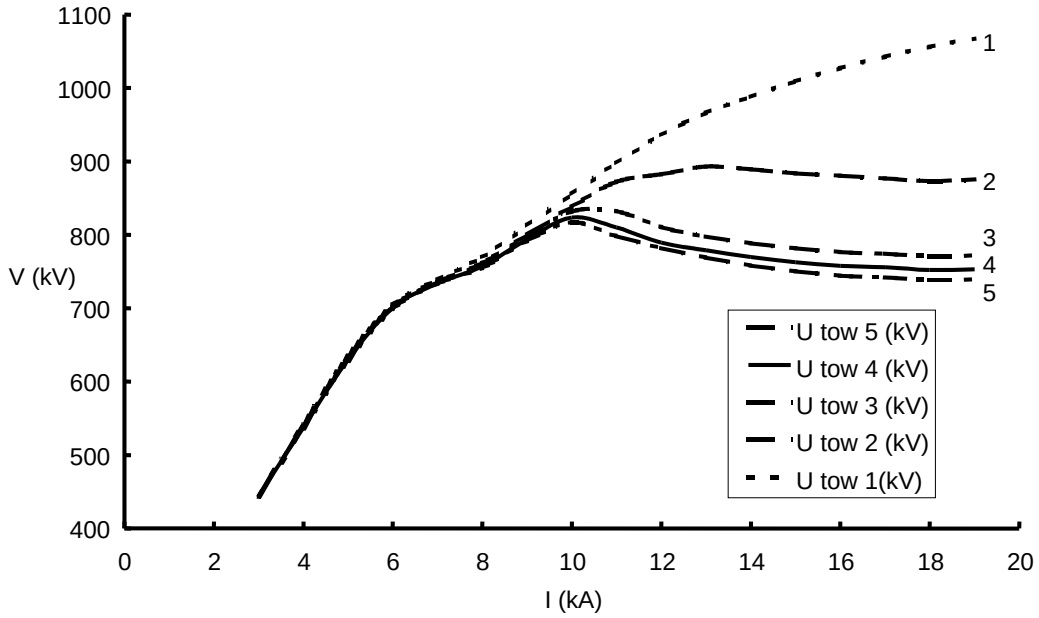

Figure 25 : Fast front overvoltage amplitudes in the case of shielding failure for a GIL 10 km long (1 p.u. AC of the same polarity) as a function of the current and striking point.

4.3.1.4.MTBF due to lightning

With the failure rates of the EDF 420 kV OVHL attributable to lightning, and the withstand level guaranteed by the on-site tests performed at 0.8 LIWL on GIL portions 300 m long, figure 26 gives the MTBF anticipated for a GIL 10 to 50 km long according to the LIWL chosen from those of standard IEC 60694 for two values of the tower footing resistance.

With a target MTBF for insulation failure of 1000 years, as for GIS, this leads to the selection of a LIWL of at least 1425 kV whilst accepting the constraint of limiting the tower footing resistance of the last five towers to less than 10 ohms. Naturally, the use of lightning arresters with a lower protection level and/or additional arresters inserted within the GIL or in parallel with the insulator strings of the tower 1 would greatly reduce the voltage stresses caused by back flashover, thus increasing the MTBF. In the EDF case these additional measures can be avoided.

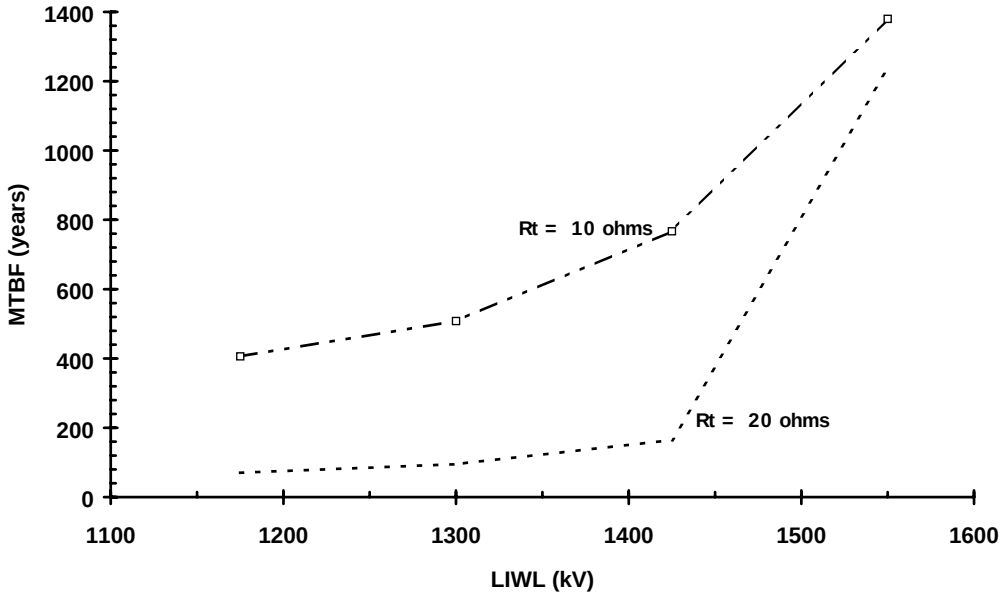

Figure 26 : MTBF due to fast front overvoltages due to lightning versus the LIWL of the 420 kV GIL for two tower footing resistance values.

4.3.2. Another 420 kV-system study for 1 km and 10 km GIL length

As examples the overvoltage stress for two projects of 420 kV GIL-application (1 and 10 km long) between overhead lines will be shown. The study has been carried out to examine the maximum overvoltages due to different lightning strikes [48]. The results show the general overvoltage behavior and can be interpreted for other system arrangements.

The GIL connection between two 420 kV-overhead lines is integrated in a typical surrounding for investigation of the voltage stresses inside of the GIL due to the conditions of lightning strikes on the overhead lines.

The figure 27 gives an overview upon the system studied. The GIL section is connected at both sides to overhead lines of different design and different overhead shielding wire systems.

4.3.2.1.Overhead lines

The line on the left side of GIL has two shielding wires and the nearest towers have heights between 45 m and 59 m (Tower No. 11 to 13). On the right side of GIL the tower height is 25 m to 34 m (Tower No. 14 to 16) with only one shielding wire. The surge impedance of the lines and the grounding resistance's of the towers are given in figure 27.

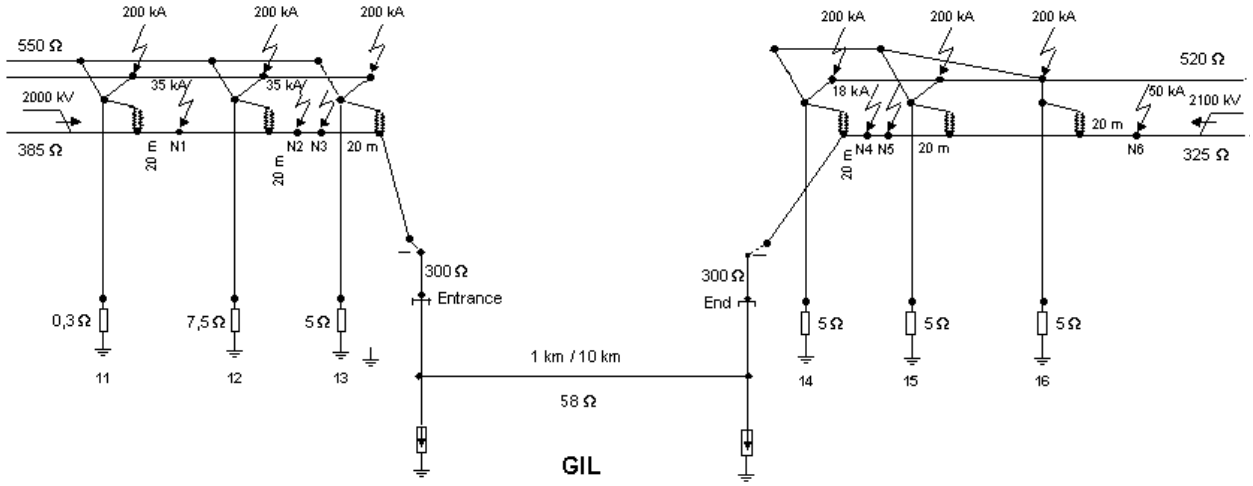

Figure 27 : Studied configuration with lightning strikes on the overhead lines

4.3.2.2.GIL with integrated surge arresters

The GIL has a length of 10 km respectively 1 km with a surge impedance of 58 Ohms. It's connection to the open air system has an impedance of 300 Ohms.

At both ends of GIL surge arresters has been integrated, that means metal-enclosed arresters are directly connected to the GIL. The surge arresters has been selected with an extreme low protective level for using the advantage that the GIL itself has no active elements which can produce overvoltages. The arresters have only to protect the GIL from surges coming from the overhead lines. The rated voltage U_r of the MO surge arresters is 322 kV. They are selected for a continuos operating voltage U_c = 255 kV. The lightning impulse residual voltage is 740 kV for a lightning impulse current (8/20 µs) of 10 kA.

4.3.2.3.Circuit conditions and lightning strike applications

Two circuit conditions has been studied. The first one is the energy transport, that means both GIL ends are connected to the overhead lines; the second condition is with one end open, that means an open disconnector between GIL and the overhead line at the opposite side of lightning strike application.

Different points of lightning strikes have been investigated for shielding failures and back flashovers. In both cases close-up strikes are of main interest because of the steepness and amplitude of the surges reaching the GIL entrance. Remote strikes cause lower voltage amplitudes inside of GIL as the calculations show

(indicated with Remote in table 11). The shape of the remote strike-surges has been assumed to be according the lightning impulse test-voltage (1,2/50 µs) without damping effect on the line.

Table 11 :
Maximum overvoltages and their location inside the 10 km GIL for different lightning strike applications during energy-transport situation

Lightning strike			Maximum voltage peak in kV			
Location		Peak	0-500 m	500-5000 m	5000-9500 m	9500-10000 m
Remote		2000 kV	530	541	709	716
Near	N1	35 kA	548	488	504	664
	N2	35 kA	572	515	665	692
	N3	35 kA	868	796	991	996
Tower	11	200 kA	no back flashover			
	12	200 kA	511	502	721	721
	13	200 kA	no back flashover			
Remote		2100 kV	795	766	596	596
Near	N4	18 kA	904	901	845	770
	N5	18 kA	880	664	676	688
	N6	50 kA	749	651	560	610
Tower	14	200 kA	no back flashover			
	15	200 kA	no back flashover			
	16	200 kA	no back flashover			

According to the different overhead line designs on both sides of the GIL shielding failures (indicated with Near N1 to N3 in table 11) with a current amplitude of 35 kA with points of strikes between the first and the third tower has been assumed for the left side line. On the right hand side of GIL lightning strikes due to shielding failures with 18 kA between the first two towers has been investigated and additionally a strike between third and fourth tower with 50 kA.

For the investigation of back flashovers strikes of 200 kA into the three towers nearest to the GIL entrances at both sides has been assumed.

4.3.2.4.Results

Due to travelling wave effects and reflections the incoming surges cause time-dependant voltage stresses inside the GIL between the conductor and the enclosure. For certain locations the voltage shape versus time have been plotted. Due to travelling wave effects the entrance and the end of GIL are of main interest, as well as the location where a superposition of the travelling waves can take place. For giving an overview upon the stresses between conductor and enclosure due to different types of surge generation the GIL has been divided into sections. The highest voltage amplitudes during the time-period of travelling wave effects per section have been pointed out. The maximum voltage amplitudes for the ”energy transport”-condition shows table 11.

The highest voltages are generated by the shielding failures N3 nearest to the GIL-entrance. The voltage versus time curves for the different locations indicated by the distance from the entrance are plotted in figure 28. The much lower overvoltages at the strike-point N5 in comparison to N4 which is only 110 m far result in the fact that here the tail of the overvoltages is chopped by flashover to ground. This leads to a less stressing superposition of the travelling waves.

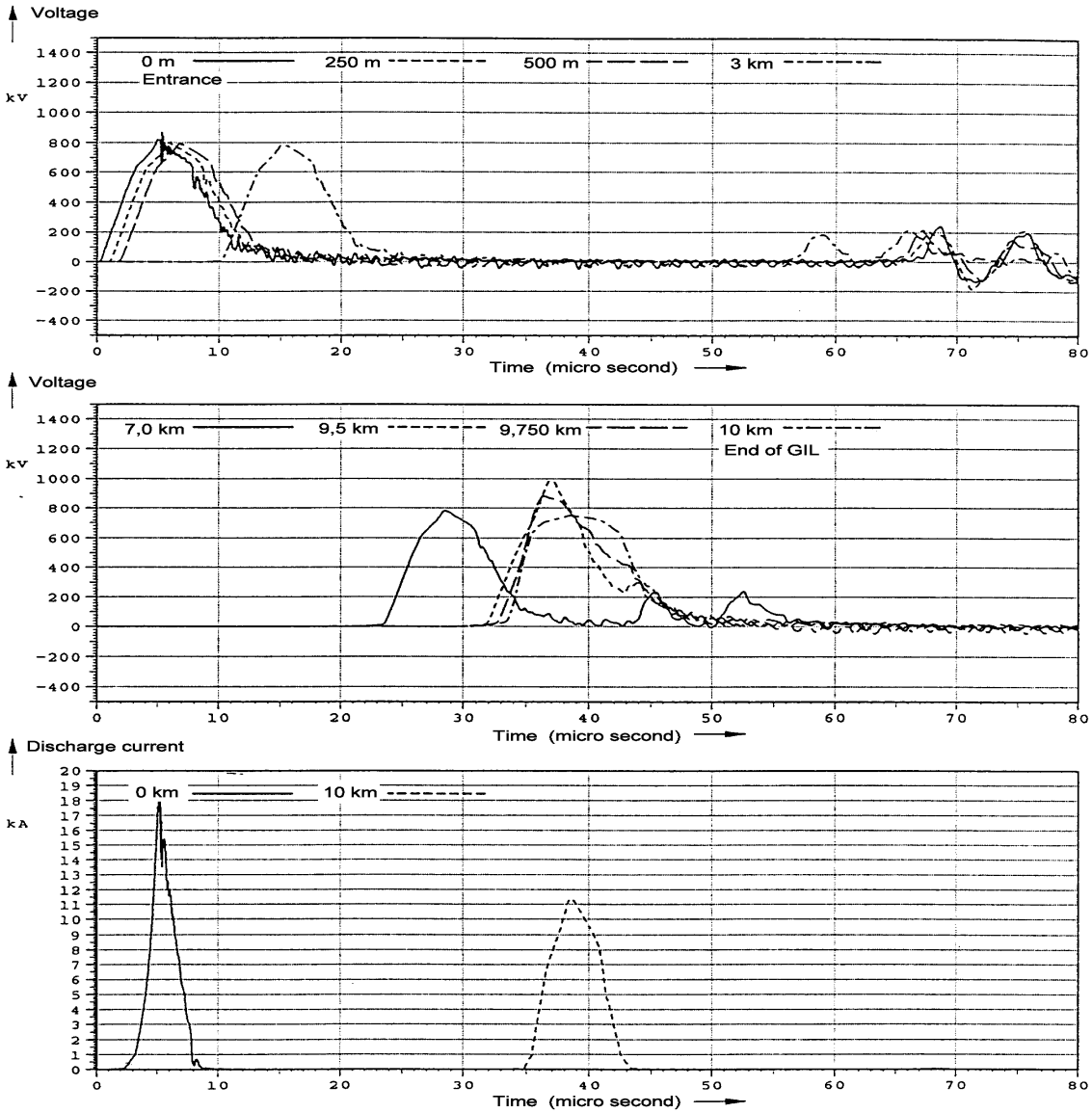

Figure 28 : Voltage distributions versus time inside of a 10 km GIL for a shielding failure of 35 kA near to the entrance (N3)

The travelling wave effect can be seen clearly be this calculation. The incoming surge at the entrance is immediately limited by the surge arrester, which is very near to the entrance. The discharge current of the surge arrester of 18 kA leads to a residual voltage of 810 kV crest (figure 28). The voltage shape has a front and also a tail time of approximately 5 µs. The surge passes the locations 250 m up to 7 km (measured from the entrance) without any disturbances. Only when it passes the area 500 m to 250 m before the end (9,5 km and 9,75 km) the shape changed due to the superposition of the passing surge and its reflected part coming back from the end. The peak value reaches nearly 1000 kV. At the end of GIL the peak value is limited by the surge arrester below 800 kV. The surge amplitude travelling back to the entrance is comparatively small, which can be seen from the voltage shape between 60 and 80 µs.

In comparison to the circuit condition ”energy transport” the voltage distribution of the condition with ”Open end” is very similar. The only difference is a slightly different reflection behavior leading to less than 5 % higher amplitudes near to the end of GIL (9,5 km).

The figure 29 shows the voltage distribution for a GIL of only 1 km length for the same shielding failure. The shape of the voltage stress versus time at the entrance and at the end is quite the same as in the 10 km GIL. Due to the shorter length the superposition takes place nearly all over the whole length. The maximum amplitude is also about 1000 kV in the center and below 800 kV at the ends.

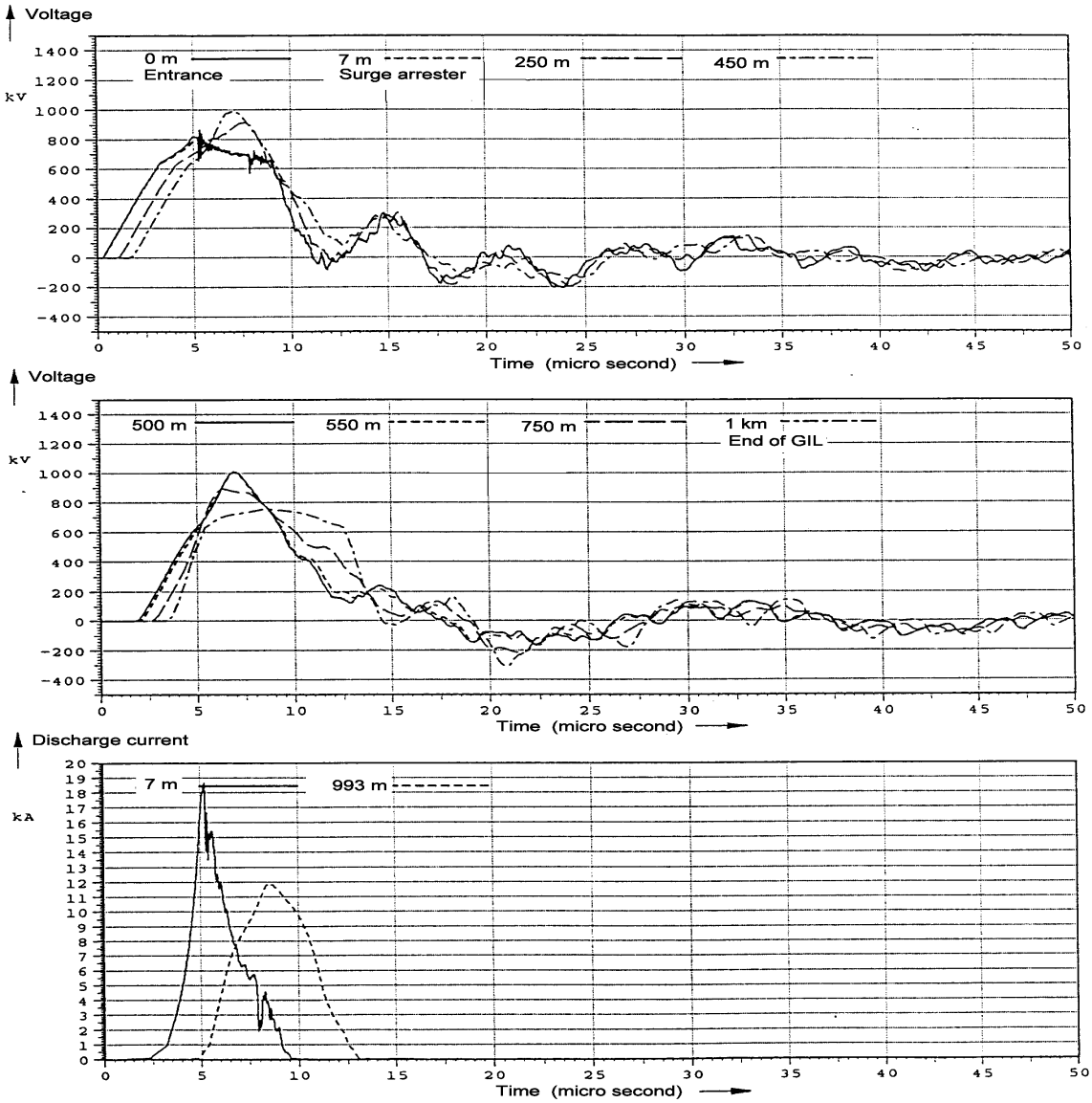

Figure 29 : Voltage distributions versus time inside of a 1 km GIL for a shielding failure of 35 kA near to the entrance (N3).

4.3.2.5.Parameters influencing the overvoltage stress

The steepness of a surge as well as the tail depend on the strike current characteristic and the distance of the struck point from the GIL entrance. Base for the calculations are the general admitted knowledge about lightning current characteristics from CIGRE WG 33.01. Variations of possible steepness of the strike currents does not effect the maximum amplitude of the voltage stress inside GIL but only the location and duration where the maximum stress occur. Only multiple strikes with largely higher steepness of the second and following strikes can effect the reflection behavior unfortunately. But because the amplitudes of this following strikes are distinctly lower than the first strike they can be excluded for the investigation of maximum stress inside of GIL.

In the study only at tower 12 back flashover occur. All 200 kA lightning strikes to all other tower did not lead to back flashovers due to the relatively low earthling resistance of the towers in the investigated surrounding of this study and the high insulation level of 2000 kV of the line.

Other configurations as cables or GIS-substations connected to the GIL will decrease the stress-income to the GIL. If they are connected to the entrance of GIL all considerations of lightning impulse stress inside of GIL can be reduced to lower levels.

For the end of GIL the connection to an open end is the worst case as the circuit-condition ”open end” in the study shows. The result is valid for open ends in GIS-technique as well as for connections to open air equipment. A connection to GIS without open end is at the lowest stress level due to the nearly same surge impedance of GIS. Nearly no reflections will take place. Closed connections to cables and open air will be in between this two extreme assumptions.

As the results of the study show (see table 11) the maximum stress occur only at certain locations inside of GIL where the superposition of the travelling wave leads to the highest amplitudes. A measure for reduction of this only locally stress enhancement is to place additional surge arresters at this locations. They will reduce the locally limited high stresses so that a dimensioning of the whole GIL according to the maximum possible voltage level can be avoided. The table 12 shows the reduction of more than 100 kV due to additional integrated surge arresters for this study.

Table 12 :
Overvoltage reduction by use of additional surge arresters at the location of highest voltage amplitudes inside GIL and on the towers.

Configuration	Surge arresters		max. fast-front overvoltages due shielding failures
	GIL	Towers	35 kA
GIL between two overhead lines	2		996 kV
	4		867 kV
	4	2	842 kV

A further reduction of the overvoltages can be achieved by using surge arresters on the first towers. The reduction in the studied configuration amounts further 25 kV (table 12). For other applications where back flashovers due to higher tower resistance’s are a problem surge arresters on the towers can extremely reduce the probability of back flashovers [49].

4.4. References of chapter 4

[46] Hileman, A.R.; Flugum, R.W.; Garrity, T.F.: "Lightning insulation Coordination for a 600 kV DC Gas insulated cable", IEEE Transactions on Power Apparatus and Systems, Vol. PAS-101, No 11 November 1982

[47] Sabot, A.: "Insulation Co-ordination Procedure for 420 kV Gas Insulated Lines (GIL)"; :ISH 1999, London

[48] Völcker, O.; Koch, H.: "Insulation Co-ordination for Gas-Insulated Transmission Lines (GIL)" IEEE Transactions on power delivery, Vol. 16, No. 1, January 2001

[49] Schnettler, A.; Balzer G.; Hudasch M.; Johnnerfelt B.: "Protection of high voltage equipment by polymer housed surge arresters", CIGRE-Session 1998, paper 33-302

5. Risk assessment method for Insulation coordination of GIL: Determination of the coordination withstand voltage and choice of the insulation level

5.1. General overview

Rigorously, as there are four different categories of overvoltage stresses, the IMFR derived in § 2. for the whole insulation coordination process should be again split in 4 according to the frequency of occurrence of the four different categories of overvoltage stresses. Thus each of the four classes may have a different acceptable failure rate for each of the 4 classes of overvoltage stresses:

- Temporary Overvoltages for the choice of the Power Frequency Withstand Level (PFWL),
- Slow Front Overvoltages for the choice of the Switching Impulse Withstand Level (SIWL),
- Fast Front Overvoltages for the choice of the Lightning Impulse Withstand Level (LIWL),
- Very Fast Front Overvoltages if needed.

The last class could be disregarded for GIL as it has been disregarded for GIS (except for disconnectors during switching). Thus the failure rate for the whole insulation coordination process should be split in only three IMFRs.

As already mentionned in the general insulation coordination process (figure 1) the determination of the GIL insulation characteristic for each of the 3 remaining overvoltage classes has to be done:

- self restoring, not self restoring or mix aspect of the GIL insulation,
- discharge probability function of the insulation,
- and the associated chosen test procedure for type, routine and on site test: this choice characterized the discharge probability associated with the test voltage levels.

So in the following before to deal with the voltage and overvoltage stressing aspect and the safety factor aspect, this important aspect of insulation characteristic for the insulation coordination of GIL will be presented.

5.2. GIL insulation characteristic

5.2.1. Discharge probability associated with test levels

IEC 60071-1 assumes that the type test or routine test or on site test withstand voltages are associated with a discharge probability (*Dpr(w)*) of the equipment insulation which depends on the self or non self restoring state of the equipment insulation:

- 0% discharge probability is associated with the PF, SI or LI test voltage in case of non self restoring insulation,
- 10% discharge probability is associated with the SI or LI test voltage in case of self restoring insulation.

As for GIS, the GIL internal insulation is mix, both self and non self restoring for test conditions and that is ambigous. Up to now for type, routine or on site tests of GIS the self restoring aspect in test conditions has been taken into account. For impulse tests, the 2/15 impulse test procedure (allowing 2 internal discharges) has been chosen for GIS and for GIL leading to associate the discharge probability of 10% with the test voltage amplitude for SI and LI.

For PF test, the situation is less clear and has never been cleared for GIS. Indeed, normally, a PF test is a 0 discharge test and thus the discharge probability associated with the test voltage would normally be 0%. If this is for sure for internal non self restoring insulation (measuring transformers, transformers) as in case of discharge the piece of equipment is definitively rejected, it is far to be true for self restoring insulation such as GIL or GIS. In fact, for GIL as for GIS, in case of discharge during a one minute PF test the test is generally immidiately repeated a second time; if during this second chance, there is no discharge the GIS or GIL piece is considered as having a 0% discharge probability at the PF test voltage. Or one should not forget that the statistical meaning of a test is different according to that the test procedure is intended to be repeated or not. Thus for internal self restoring insulation the discharge probability associated with the PF test is not 0%.

Indeed it is clear that the insulation "margins" added by the manufacturer to the insulation requested to just pass the test are different in case of non self restoring internal insulation and in case self restoring internal insulation: in the second case the additional cost of a repeated test is nothing compared to the saving. Thus the meaning of the PF test is completely different. So for the "same" test and same requested standard whistand voltage, the actual initial withstand voltage of an internal non self restoring insulated equipment will be generally higher than the actual initial withstand voltage of an internal self restoring insulated equipment.

In order to derive a discharge probability of the self restoring part of the GIL insulation to associate with the PF test voltage let us consider the probability that a self restoring insulation equipment has to pass the 2/15 impulse test procedure.

For the 2/15 impulse test, if the U_{10} of the insulation tested is equal to the test voltage, the insulation has 80% probability to pass successfully the test. Of course to derive a discharge probability associated with 80% probability to pass a PF test of one minute, one has to make assumptions:

- of the discharge probability function of the GIL insulation: here Weibull probability function truncated at $4Z$ [50]; $z_u=Z/U_{50}$ being the coefficient of variation of the discharge probability of the insulation [51], [52], [53],
- of the duration D of the temporary overvoltage stress that the PF test intends to cover: here D has been chosen to 1 second leading for a one minute PF test to a 0/60 test (no discharge for 60 applications of a 1 second voltage equal to the test voltage).

With these assumptions, the figure 30 displays the probabilities to pass different tests as a function of the $(U_{test}-U_{50})/Z$, U_{test} being the test voltage, U_{50} being the amplitude for which there is a 50% discharge probability of the insulation and Z being the standard deviation of the discharge probability function.

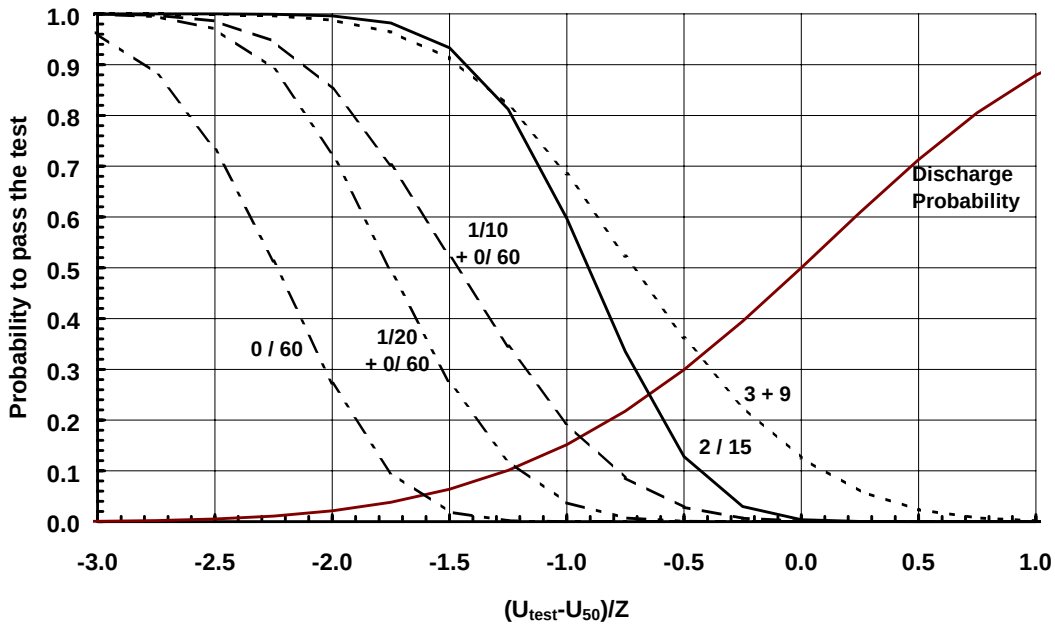

Figure 30 : Probability of an equipment sample to pass different test procedures as a function of the ratio (Utest-U50)/Z, with Utest being the applied test voltage, U50 being the amplitude for which there is a 50% discharge probability of the sample insulation and Z being the standard deviation of the discharge probability function of the sample insulation assumed to be a Weibull law truncated at 4Z.

The afore mentionned criteria of 80% probability to pass successfully a 1 minute power frequency test (0/60 test with no resuming in case of discharge) leads to a 0.5% discharge probability of the insulation to associate with the PF test voltage figure 30.

If after a discharge of the self restoring insulation of the equipment during a first 1 minute PFtest, the one minute PF test may be resumed then the accepetd PF test procedure becomes implicitely a 1/10+0/60 or 1/20+0/60 test procedure (one flashover after a 10 second PF application or 20 second PF application and then 0 flashover during 60 seconds PF application. With the later test procedure, the discharge probability of

the GIL insulation to associate with PF test voltage amplitude is thus slightly higher than for the previuos test proceudre (0/60 witout resume): roughly 2% (figure 30).

So the insulation of GIL will be treated as the insulation of GIS: self restoring for the gas part of the GIL insulation and the relations (11) and (12) will be applied :

$$\text{Impulse test:} \quad U_{10} = \text{Impulse test voltage} \tag{11}$$

$$\text{PF test:} \quad U_{2} = \text{PF test Voltage} \tag{12}$$

U_{10} and U_2 will be called in the following the withstand voltage U_x of the piece of GIL considered. In the folowing the subscript "x" will mean 10% for impulse test and 2% for PF tests ($Dpr(x)$), but as the withstand voltage associated with the piece of equipment for type test, on site test or in service is related to different length of GIL, in order to be precise, at the subscript x there will be added:

- the letter "T" for the withstand voltage associated with the x% discharge probability of the self restoring part of the insulation of GIL length T: U_{xT} for type test; nevertheless, as the name is standardized U_{xT} will continue to be written U_w,
- the letter "S" for the withstand voltage associated with the x% discharge probability of the self restoring part of the insulation of GIL length S: U_{xS} for on site test,
- the letter "L" for the withstand voltage associated with the x% discharge probability of the self restoring part of the insulation of GIL length L: U_{xL} for the whole GIL in service condition.

5.2.2. Relations between the withstand voltages U_x of the piece of GIL for type test, on site test and whole GIL link

For GIL (but also for large GIS) the lengths T of the piece of equipment tested during the type test is shorter than the length S of the piece of equipment tested on site test which in turn is generally shorter than the length L of the GIL in service. Due to the area effect or said in other words due to the fact that for a GIL length L there are M_{LS} (=L/S) identical insulations in parallel, the withstand voltage of a GIL length L, as the ones in service, will be lower than the withstand voltage of the GIL length S which have been tested on site [50].

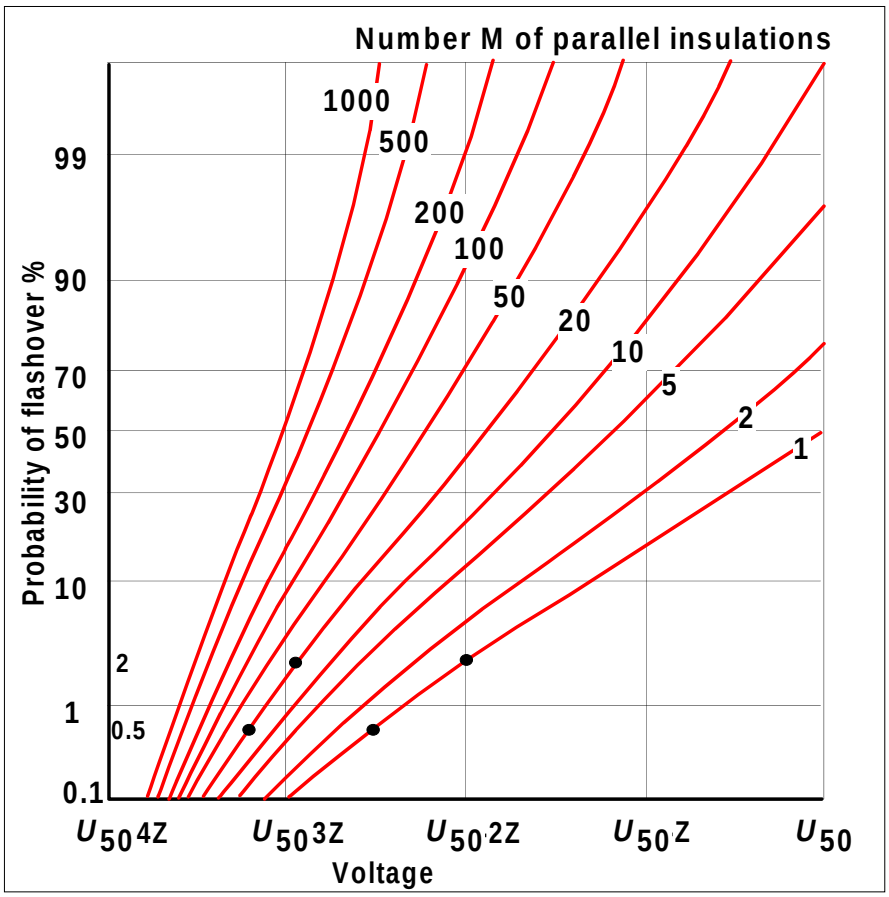

Figure 31 : Conversion chart for the reduction of the withstand voltages U_x (subscript "x" being the discharge probability associated to voltage U) versus U_{50} and Z (U_{50}: 50 % discharge voltage of one insulation and Z: standard deviation of the discharge probability of one insulation) in function of the number M of identical insulations in parallel (Weibull probability function truncated at $4Z$; $z_u=Z/U_{50}$ being the coefficient of variation of the discharge probability of one insulation) [50]

To give rough idea of the importance of the phenomena, one must remind that for the GIL, L, S and T could range according to the following:

- L : from 500 hundred meters up to tens of kilometers,
- S : between 300m up to 500m,
- T : between 25- to 30 meters.

For such lengths, the ratio M_{LS}, M_{ST}, M_{LT}: will range according to the following:

- M_{LS} ($=L/S$) : between 1 and 30 (and even more: in [53] GIL length considered are up to tens of kilometers),
- M_{ST} (S/T) : between 10 and 40
- M_{LT} (L/T) : between 10 up to 400 (and may be even more).

For typical values M_{LS} of 20 leads to the following relationships for the withstand voltages U_{10} and U_2 (10% and 2% discharge probability voltage) of L and S as shown on figure 31 derived for a **uniform voltage profile** along the GIL of length L and assuming for the discharge probability function of the self restoring insulation of GIL of length S a generalized Weibull distribution truncated at 4 times the standard deviation:

$$U_{10L} = \frac{1-2.6z_{uS}}{1-1.3z_{uS}} U_{10S} \qquad (13)$$

for z_{uS} = 0.03 or 0.08 p.u. the ratio is 0.96 or 0.88.

$$U_{2L} = \frac{1-3z_{us}}{1-2z_{uS}} U_{2S} \quad (14)$$

for z_{uS} = 0.03 or 0.08 p.u. the ratio is 0.97 or 0.9.

$$U_{0.5L} = \frac{1-3.25z_{us}}{1-2z_{uS}} U_{2S} \quad (15)$$

for z_{uS} = 0.03 or 0.08 p.u. the ratio is 0.96 or 0.88.

z_{uS} being the coefficient of variation of the discharge probability of the self restoring part of GIL insulation of length *S*.

5.2.3. Relations between withstand test voltages (on site, type test) and withstand voltage of the whole GIL link

As for GIS of highest voltage, for GIL a lot of assembling will be performed on site during the erection and there will not be any routine test performed on the whole GIL. So each piece of GIL of length S will be tested on site only before energization of the complete GIL (as for long GIS).

As for GIS, for GIL the ratio between the withstand on site test voltage (U_{xS}) of GIL lentghs *S* and the requested withstand type test voltage U_w specified for a GIL length *T* (as for GIS) will be 0.8:

$$U_{xS} = 0.8\ U_w \quad (16)$$

Due to the parallel (area) effect, if each piece of GIL length *S* is proved to withstand on site U_{xS}, it is clear that the "proved" withstand voltage U_{xL} of the GIL length *L* after the on site test of the GIL lengths *S* is lower:

$$U_{xL} = U_{xS} / K_p = 0.8\ U_w / K_p \quad (17)$$

K_p (called here the parallel factor) being larger or equal to 1 depending on the actual Voltage Profile (VD(V_2)) along the GIL of length *L* for the class of overvoltage considered; K_p depends also very much on the discharge probability x considered and on the coefficient of variation of the discharge probability of the GIL length *S* **erected in on site conditions**.

The figure 32 presents 3 typical Voltage Profiles VD(*V*) of overvoltage amplitudes along a GIL of length *L*: (a) a flat VD(*V*), (b) a ramp VD(*V*) and (c) a step or "Dirac" impulse VD(*V*); for each of these VD(*V*) and assuming a same value for the maximal amplitude of the voltage along the GIL, the parallel factor K_p is different.

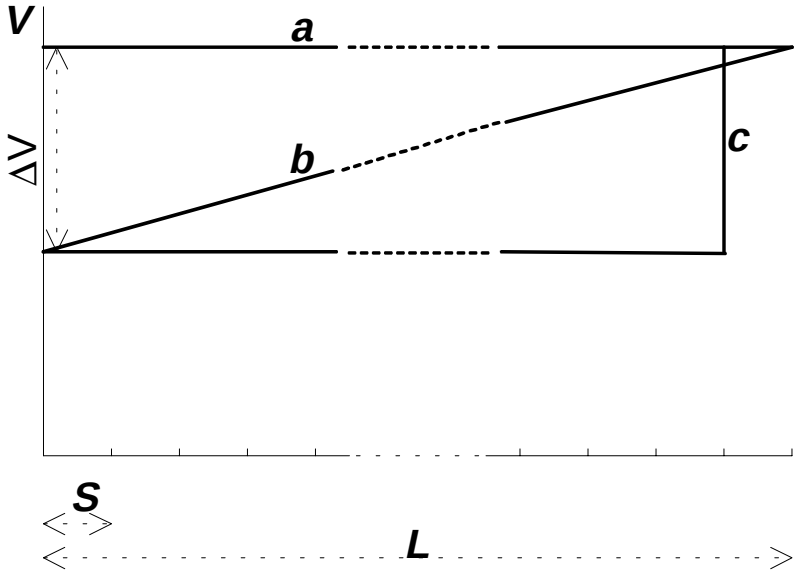

Figure 32 : The 3 typical Voltage Profiles along a GIL of length *L* ; ZuS being the standard deviation of the discharge probability function of the self restoring part of the insulation of GIL of length *S*.

In case of flat VD(*V*), each portion of length *S* of GIL in service will be stressed equally leading to equal discharge probability of each portion *S*. In that case the value of K_p(a) is maximal and can be derived direcly

from figure 31; K_p(a) depends only on the value of the coefficient of variation of the discharge probability at the standard voltage shape considered.

In case of peak VD(V), the discharge probability of the most stressed portion S is larger than the discharge probability of all the other ones and the parallel factor K_p(c) will be lower than K_p(a) and may reach 1.

In case of ramp VD(V), the discharge probability of a portion S is close to the discharge probabilities of the two adjacent ones. Thus the discharge probability of all the portions is influenced by the discharge probability of each portion. In that case the parallel factor K_p(c) willl be between the ones of flat (a) and peak (c) VD(V).

Generally speaking, the parallel factor K_p is a function of:

- the ratio L/S
- the standard deviation of the Z_{uS} of the discharge probability of length S of GIL tested on site,
- the Voltage Profile of the V_2 along the GIL: VD(V_2),
- the standard deviation Z_V of the voltage profile in each point of the GIL.

The difference in the three K_p values depends very much on the ΔV (see figure 32). If ΔV is is larger than 2.5 Z_{uS}, the following relations exist between K_p values:

$$1 = K_p(c) < K_p(b) < K_p(a) \quad \text{for } \Delta V > 2.5\ Z_{uS} \tag{18}$$

For voltage profile along the GIL of length L with ΔV lower or in the range of 2.5 Z_{uS}, the parallel factor can be calculated assuming that the voltage profile along L is the flat one (a). From an engineering point of view the inequality becomes an equality:

$$1 < K_p(c) \approx K_p(b) \approx K_p(a) \quad \text{for } \Delta V < 2.5\ Z_{uS} \tag{19}$$

5.3. Consequence for the safety factor: a minimal value

Disregarding the influence that should have the REX on the choice of a safety factor value and just for the consistence of the insulation coordination process just related to the overvoltage aspect, for the three standard voltage shapes the on site tests should prove at least that the withstand voltages U_{xL} of the self restoring part of the insulation of the GIL of length L just assembled is at least equal to the calculated coordination withstand voltage U_{cwL} needed in service for the GIL length L. So for the three standard voltage shapes, the relations (16) and (17) leads to the relation (20) linking the coordination withstand voltage of the in service GIL U_{cwL} with the withstand test voltage U_w the piece of GIL of length T on which is performed the type tests:

$$U_{xL} = \frac{U_{xS}}{K_p} = \frac{0.8U_w}{K_p} \geq U_{cwL} \tag{20}$$

This leads to the minimal value for safety factor K_s such that:

$$K_s = \frac{U_w}{U_{cwL}} \geq \frac{K_p}{0.8} = 1.25K_p \tag{21}$$

For short length L of GIL (M_{LS}<3) for which $L = S$, $K_p = 1$ and the safety factor K_s linking U_w and U_{cwL} is 1.25, value recommended for GIS in [54], [55]. This case will no longer be considered in the following.

For long GIL length L (M_{LS}<3) the safety factor K_s will be higher than 1.25 as K_p is larger generally than 1 but indeed depends on the voltage profile along the GIL for in service voltage and overvoltage stresses.

5.4. Overvoltages

This aspect has been treated in § 4.3.

5.5. Comparison of Insulation characteristic and representative overvoltage: choice of UcwL and final Ks value to adopt (associated Uw)

In the first step of the general insulation coordination process, one has to chose the coordination withstand voltage U_{cwL} of the GIL of length L in service. This process can be either deterministic (no risk supposed accepted) or probabilisic accepting a risk of failure (failure rate) when the GIL of length L is submitted to representative voltages U_{rp}. In addition one can choose a deterministic approach for a given class of overvoltages and a probabilistic approach for another class of overvoltage.

For each class of overvoltage a safety factor value will be discussed at the light of both the minimal value needed for consistence of the overvoltage aspect of the Insulation Coordination and the REX. Beside, for the final choice of the Safety Factor one must keep in mind that:

- for a given voltage stress, flatter is the voltage profile along the GIL higher is the probability that an occuring imperfections due to global aging becomes a defect decreasing the GIL withstand voltages below the coordination withstand voltages;
- lower is the Safety Factor higher, is the probability that an occurring imperfection due to global aging becomes a defect decreasing the witstand voltages below the coordination withstand voltages.

In any case, the final choice for the GIL withstand voltages U_w for the three standard test voltages should be chosen as far as possible in the **IEC 60694** (1996-05) even if the GIL is not a switchgear or at least in IEC -1.

5.5.1. Temporary Overvoltage (TOV, PFWL)

The Voltage profile of temporary overvoltages along GIL of length L in service is flat. In that conditions the risk of discharge is pratically the same all along the GIL and the parallel/area effect will be maximum leading to the maximal value for the parallel factor K_p which then depends only on:

- the coefficient of variation z_{uS} of the PF discharge probability of the self restoring part of the insulation of GIL lengths S for on site conditions of erection.
- and the ratio L/S.

For long length of GIL (M_{LS}>5), K_p is larger than 1 (14):

$$K_p = \frac{U_{2S}}{U_{2L}} = \frac{1-3z_{uS}}{1-2z_{us}} \tag{22}$$

But as M_{LS} may be larger than 20 and taking into account that for IEC the actual discharge probability intended to be proved by the PF test is $x = 0.5\%$ leads to adopt [56] in (20) the 0% discharge probability voltage U_{0L} of the self restoring part of the insulation of a GIL as conservative approximation of $U_{0.5L}$:

$$U_{0L} = \frac{1-4z_{uS}}{1-2z_{us}} U_{2S} = \frac{1-4z_{uS}}{1-2z_{us}} 0.8U_w \tag{23}$$

U_w being in this case the PFWL (figure 33).

Then the determination of U_w is done by choosing for U_0 a value higher than the maximal amplitude expected for the temporary overvoltage on the system and then to select in the corresponding IEC standard the suited PFWL.

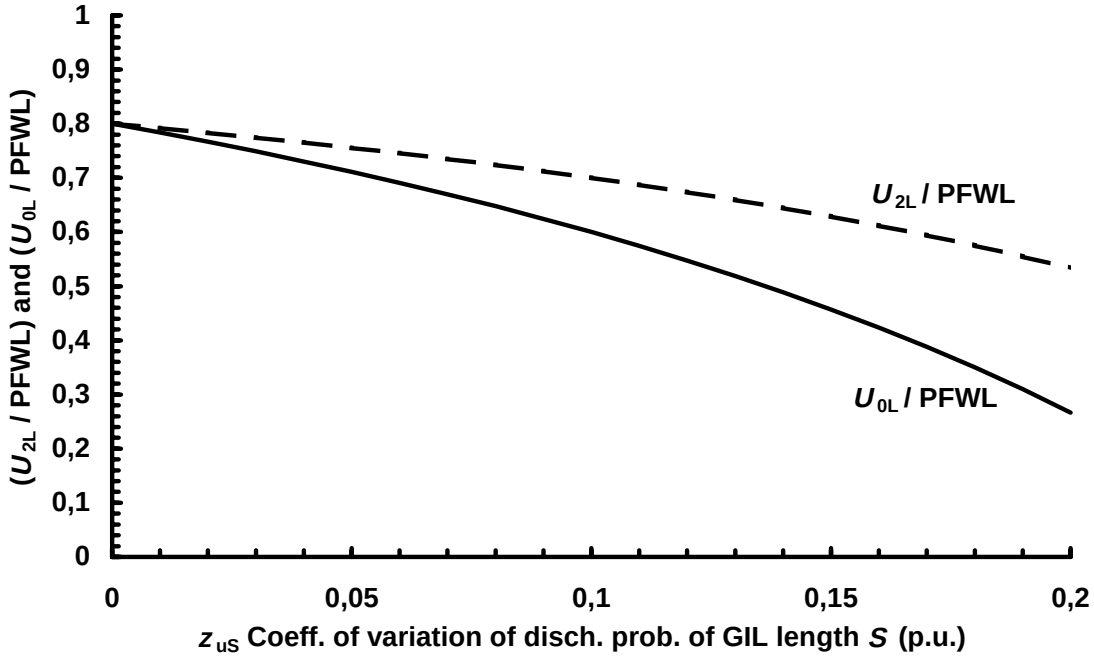

Figure 33 : Variation of the ratio U_{2L}/PFWL (=(1-3z_{uT}) / (1-2z_{uT})) and U_{0L}/PFWL (=(1-4z_{uS}) / (1-2z_{uS}) (23)) as a function of the coefficient of variation z_{uT} of the discharge probability function for on site erection conditions for lengths *S* and *L* of GIL such that M_{LS} = 20.

In order to help for the choice of an adequate z_{uT}, figure 34 displays the ratio U_{2S}/PFWL and U_{0S}/PFWL as a function of the coefficient of variation z_{uT} of the discharge probability function **for on site erection conditions for lengths *T* and *S* of GIL**. Indeed the figure 34 shows clearly that the on site test performed on GIL sections of length *S* with a test voltage of 0.8PFWL corresponds to a possible maximal z_{uT} of 0.08 p.u. for GIL sections of lentgh *T*. In fact, figure 34 shows clearly that if z_{uT} is actually lower than 0.08, the on site test PF voltage amplitude could be higher than 0.8PFWL. The choice of 0.8PFWL as on site test voltage implies that the z_{uT} of GIL sections erected on site can reach 0.08 p.u. without being rejected by the on site test. Compared to the 0.03 or 0.4 p.u. usually admitted for PF for short GIL lengths *T*, that means that pollution by free particles or defects is implicitely accepted during on site erection.

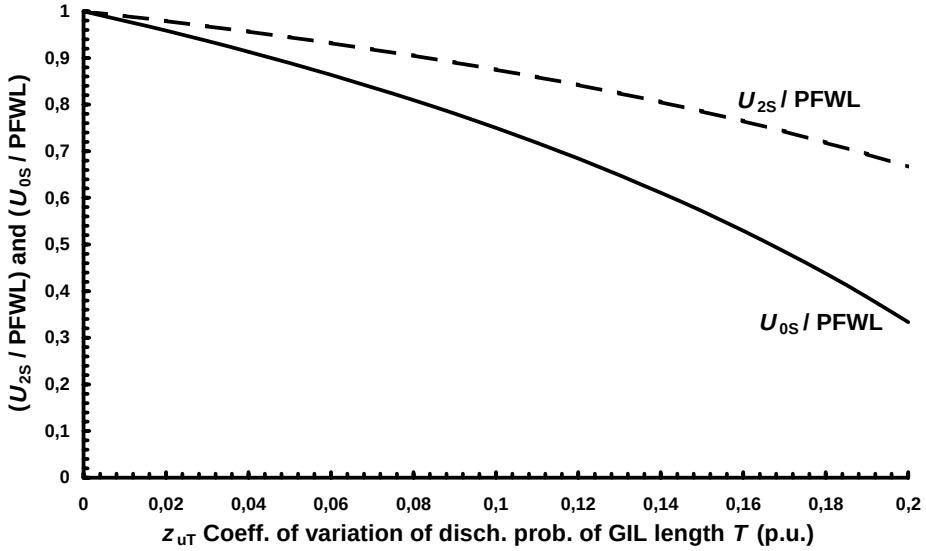

Figure 34 : Variation of the ratio U_{2S}/PFWL (=(1-3z_{uT}) / (1-2z_{uT})) and U_{0S}/PFWL (=(1-4z_{uT}) / (1-2z_{uT})) as a function of the value of z_{uT} the coefficient of variation of the discharge probability function for on site erection conditions for lengths *T* and *S* of GIL such that M_{TS} = 20.

Taking into account the gap between the targeted IMFR and the nowdays expected failure rate of 420 kV GIL, the Utilities will choose a z_{uS} value between 0.03 and 0.08 p.u. keeping in mind that most of the GIS IMF occur at the permanent voltage and are due defects resulting from global aging. So the GIL PFWL is a very important parameter for the reliability of the GIL. The table 13 shows the influence of the value of z_{uS} on the needed value of the PFWL to select and the associated U_m for a 420 kV GIL for two TOV levels.

Table 13 :
Influence of the value of z_{uS} on the needed value of the PFWL to select for a 420 kV GIL for two TOV levels according to IEC 60517 Ed.3 1990-10

TOV	z_{uS}	K_p	K_s	U_{rwPF}	PFWL	U_m
1.25 p.u. = 303 kV	0.03	1,07	1.25	404	520 kV	420 kV
	0.055	1.15	1.25	433	520 kV	420 kV
	0.08	1.24	1.25	468	520 kV	420 kV
1.45 p.u. = 352 kV	0.03	1,07	1.25	470	520 kV	420 kV
	0.055	1.15	1.25	502	520 kV	420 kV
	0.08	1.24	1.25	543	620 kV	550 kV

5.5.2. Slow Front Overvoltage (SIWL)

As for temporary overvoltage, the Voltage Profile of slow front overvoltages along GIL in service is rather flat even for tens kilometer GIL. In that conditions the area effect will be maximum leading to the maximal value for K_p which then depends only on the coefficient of variation z_{uS} of the Switching Impulse (SI) discharge probability function of the self restoring part of the insulation of GIL of length S for on site conditions of erection.

For SI the discharge probability associated with the withstand voltage of tests is 10% leading between the withstand voltage of the on site test GIL lentgth S, U_{10S} and the withstand voltage of the GIL lentgth L, U_{10L}, to a parallel factor K_p of (13):

$$K_p = \frac{U_{10S}}{U_{10L}} = \frac{1-2.6z_{uS}}{1-1.3z_{us}} \tag{24}$$

For the z_{us}, a value of 3% is proposed in [53] derived from [57]. In that case K_p will be 1.04 leading to a minimal safety factor value of 1.3 (1.25*1.04). As according to the expected REX, the insulation failures due to slow front overvoltages are rare, the minimal value should be sufficient.

5.5.2.1. Deterministic approach

As the on site test would be performed at 80% of the specified withstand voltage U_{10S} = 0.8SIWL, the deterministic approach leads to the following general relation:

$$U_{10L} = \frac{0.8SIWL}{K_p} \geq K_{cd}V_2 \Rightarrow SIWL \geq 1.25K_pK_{cd}V_2 \tag{25}$$

V_2 being the amplitude of the slow front overvoltage having a 2% probability to be exceeded and K_{cd} being chosen according to the figure 35.

Applying this method to the data provided in [53] for a 10 km long 420 kV GIL: V_2 = 718 kV, U_{ps} = 710 kV (SI protective level of the surges arresters) and S = 500 m leads to a withstand voltage U_w for the type test of:

$$SIWL \geq 1.25 \times 1.04 \times 1.04 \times 718kV = 970kV \tag{26}$$

which, according to IEC 694, gives a SIWL of 1050 kV. Of course a lower value of U_{ps} may lead to lower SIWL.

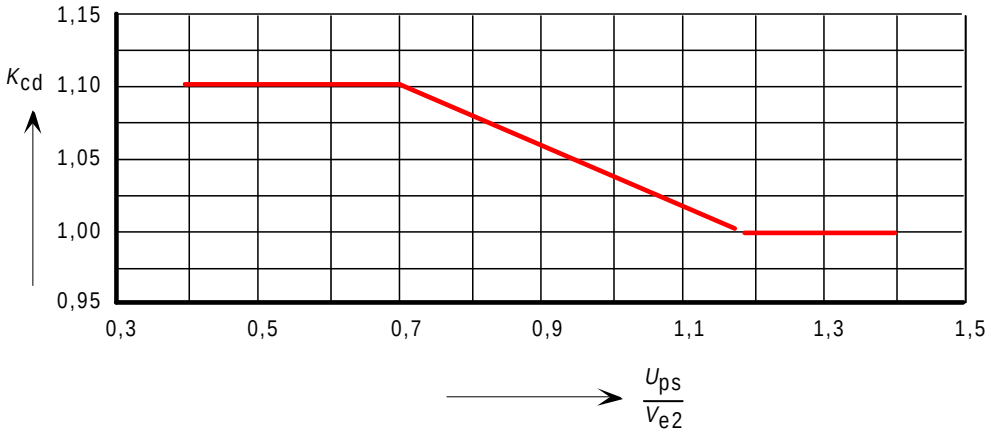

Figure 35 : Evaluation of the deterministic coordination factor K_{cd} for the phase to earth insulation: U_{ps} being the SI protective level of the surge arresters and V_{e2} the 2% slow front overvoltage amplitude [50]

5.5.2.2. Satistical approach

For the statistical approach, the withstand of the GIL length will be the same. For the risk, the IEC 71 suggests for the overhead lines a failure rate of 0.01 down to 0.001 per operation, as the GIL insulation is not self restoring (in service) it suggested to chose 0.0001 per operation as done in [53]. Such a figure leads for the 10 km 420 kV GIL discussed in the deterministic approach § 5.5.2.1 to the same SIWL of 1050 kV, but again a lower value of U_{ps} may lead to lower SIWL.

5.5.3. Fast Front Overvoltage (LIWL)

Contrary to temporary Ovevoltage and slow front overvoltages, for fast front overvoltagse due to lightning the Voltage Profile along GIL shape can be flat, ramp or peak depending on how far from the GIL impinging end the lightning flash strikes the overhead line (*Reference to Ede part to be put later*). Beside for a given distance the voltage profile along the GIL may be different according to the number of arresters used: only at both end or at both end and on both side at one kilometer from the entrance (*Reference to Ede part to be put later*). Thus the resulting minimal K_p value to take will be different.

Nevertheless there is a constant, the highest amplitudes of the voltage profile are roughly located around one kilometer from the GIL end opposed to the end where the overvoltages impinge the GIL.

In case of peak Voltage Profile along the GIL (case where there is only one arrester at each end of the GIL), most of the risk of failure will be due to one kilometer and thus as the length S of the GIL on site tested is of the same order of magnitude than the stressed portion in service, the K_p factor is:

$$K_p = \frac{U_{10S}}{U_{10L}} = 1 \qquad (27)$$

In case of flat Voltage profile along the GIL (case where there are more than one arrester at each end of the GIL - some along the GIL), the risk of discharge is pratically the same all along the GIL and the parallel effect is maximum leading to the maximal value for the parallel factor K_p which depends only on the ratio L/S and on the coefficient of variation z_{uS} of the discharge probability of the self restoring part of the insulation of the GIL of length S.

For LI, the discharge probability x associated with the test voltage is 10%. For a flat voltage profile along the GIL of length L, the 10% value leads to a parallel factor K_p between the withstand voltage of the on site test GIL lentgth S, U_{10S} and the withstand voltage of the GIL lentgth L, U_{10L}, of:

$$K_p = \frac{U_{10S}}{U_{10L}} = \frac{1 - 2.6 z_{uS}}{1 - 1.3 z_{us}} \qquad (28)$$

For the z_{us}, a value of 3% is proposed in [53] derived from [57] and thus K_p will be 1.04. The choice of 3% has been made because in [53] most of the contribution to the risk of failure is due to a peak voltage distribution along the GIL and thus the risk of failure of the whole GIL is pratically determined by the risk of failure of a single S legth section. In case of ramp or even more flat voltage distribution higher z_{us} values should be chosen to take into account that in that cases the risk of failure of the whole GIL depends not only

on a unique S length section but on all the S legth sections of the GIL and in that case the probability of a defect left after on site test or due to aging is indeed higher for all the S length section than for a unique S length section.

In case of a ramp voltage profile along the GIL, the K_p value is between the two former ones and thus the following can be adopted:

$$K_p = \frac{U_{10S}}{U_{10L}} = 1.02 \tag{29}$$

Then, whatever method is chosen (deterministic or statistical) it must be emphasized that the reduction to expect on the needed requested LI withstand voltage for example of the installation of an additional set of surge arrester at one kiometers of the entrances and flatening the voltage profile will be indeed reduced because of the increase of the K_p factor.

6. On site test procedure and associated voltage levels

As already stated, the on site should prove that for the three standard voltage shape, PF, SI and LI the withstand voltage U_{xS} of the self restoring part of the insulation each GIL length S is at least the one needed to assess that the withstand volatge U_{xL} of the GIL length L is at least equal to the coordination withstand voltage of the GIL. Beside, as for GIS, the on site test voltage applied will be of 80% of the standard withstand voltage chosen for the GIL. So as in the coordination process, the parallel effect has been taken into account for each standard voltage shape, the following relation should be verified:

$$U_{xS} \geq 0.8\ U_w \qquad (30)$$

But generally on site, only the PF voltage will be applied. In this case, and as recommended in [54], the on site power frequency voltage UPF_{ost} should not be related only to the PFWL of the GIL but through the test conversion factors K_t of the GIL insulation it should be related to the withstand voltage which most influences the GIL design. That is to say, that the power frequency on site voltage UPF_{ost} may be higher than 80% of the PFWL according to the respective values of the the conversion factors K_t and the chosen withstand voltages:

$$UPF_{ost}=0.8\text{Max}(\text{PFWL},\ \text{LIWL}\ K_{tPF/LI},\ \text{SIWL}\ K_{tPF/SI}) \qquad (31)$$

In this respect, depending on the rated voltage of the GIL, the UPF_{ost} may be higher (table 14) in case of N_2/SF_6 gas mixture insulation than in case of SF_6 insulation as the test conversion factor $K_{tPF/LI}$ of the N_2/SF_6 gas mixtures is higher than that of the pure SF_6 (Ref to Giuseppe Rizzi part).

Table 14 :
Examples of on site Power frequency voltage amplitude UPF_{ost} according to the GIL insulationg medium and the chosen standard withstand voltages

	Withstand voltages	Test Conversion factor: $K_{tPF/LI}$		on site test voltage (UPF_{ost})
GIL 420 kV SF_6 0.5MPa	PFWL=620kV LIWL=1425 kV	⇨ 0.45 ⇨	0.8×620=496 0.45×0.8×1425=513	UPF_{ost} = 513 kV
420 kV GIL N_2/SF_6 1 MPa	PFWL=620 kV LIWL=1425 kV	⇨ 0.50 ⇨	0.8×620=496 0.5×0.8×1425= 570	UPF_{ost} = 570 kV

Of course as the test conversion factors K_t are evaluated for defect free GIL, this approach disregard the fact that the behavior of the insulating medium may be different in presence of defects like the well known sharp protrusions on the HV side which decrease the LIW but not the PFW for GIS insulated with pure SF_6; to account to some extent for that phenomena, the one minute on site power frequency test should be complemented by measurements of partial discharges (see chapter 8) performed during the decrease of the test voltage at least at 80% of UPF_{ost} during 1 minute but, still during the decrease of the test voltage, also at a phase to ground voltage equal to the rated voltage of the GIL during 20 minutes.

6.1. References of chapter 5 and 6

[50] IEC standard 60071-2: " Insulation Co-ordination Part 2: Application guide", third edition, 1996-12

[51] W. Hauschild, W. Mosch: "Statistical techniques for high voltage engineering", IEE Power series 13, Peter Peregrinus, ISBN 0 86341 205 X

[52] G.W. Brown, R. Samm, J. Cronin: "AC analysis and testing of realistically contaminated gas-insulated systems", IEEE transactions on PAS, Vol. PAS-97, JAn/Feb 1978, pp59-67

[53] A. Sabot, D. Santos, X. Waymel, D. Feldmann, Y. Maugain., "Insulation co-ordination of 420 kV gas insulated lines" session CIGRE 1998,rapport 21-303.

[54] CIGRE WG 33/23-12 : "Insulation Coordination of GIS : return of experience, on site tests and diagnostic techniques" - Electra n° 176, February 1998.

[55] CIGRE WG 23.10/TF 03: "User guide for the application of gas-insulated switchgear (GIS) for rated voltages of 72.5 kV and above", CIGRE brochure 125, April 1998

[56] A. Sabot: " Insulation Co-ordination Procedure for 420 kV Gas Insulated Lines", Eleventh Symposium on High-Voltage Engineering ISH 99, London, 23-27 August 1999, IEE conference publication N°467, volume 3, topic D, report 3.1.S18.

[57] P. Hoegg, W. Schmidt, H. Stasser : "Conception de l'appareillage blindé, isolé au SF_6 pour atteindre une haute sûreté de service", Session Gigré de 1972, rapport 23-10.

7. Long duration test to proof the GIL reliability

To prove the reliability of GIL for its whole lifetime a long-duration test has been proposed. This test has to be done on a prototype setup which includes all relevant elements of the GIL design with a total length of the test setup in the range of 100 m. The proposed test program includes mainly a long duration stressing of the GIL by application of power-frequency high voltage and rated current. The current is applied in several cycles for stressing the test object by continuous temperature rise and cooling down. The high voltage can be applied during the current-zero periods or during the whole test cycles, which depends on the test facilities because of the insulation of the current source. This test is proposed to be carried out one time to qualify the general design of a GIL.

The main subjects of such a test are the following:

- Handling and erection under on-site conditions (Preparation of welding, welding of the tubes, cleanliness, handling of tools and material on small or otherwise uncomfortable on-site areas)
- Investigation of the thermal behaviour of the whole system (max. temperature of conductor and enclosure, environmental temperature, movement of compensating elements and sliding contacts)
- Prove of the lifetime reliability of the insulation materials(power-frequency high voltage application with a value and duration high enough, to prove the stability for the GIL lifetime; twice the service voltage for 2000 h are proposed)

After erection and after long duration testing: prove of the insulation withstand capability (with impulse and power-frequency voltage of suitable values).

Is there a real need of the long duration test? For handling and erection there is a need, if new technologies are used, which cannot be tested under other realistic conditions at smaller sections. A short duration test for quality control after that is sufficient.

The thermal behaviour cannot be tested on single elements in the laboratory in any case. Thinking of buried GIL, they will show a quite different behaviour than in a test setup without covering with concrete or sand; but a lot can be done by calculations in that case. In any case for investigation of the thermal behaviour a short duration test of several hours will be sufficient. The relative movement of parts by several times of temperature rise can be simulated by special test equipment like mechanical oscillators. They can show the reliability of moving parts, like for example sliding contacts.
Concerning the life expectancy of the insulation materials a comparison to GIS has to be drawn. For the gas insulation, neither for SF_6 nor for mixtures any ageing effects are known in a sound system. For the solid insulation like spacers and gas-barriers the quality is dependent on the material and the manufacturing process. Because insulators have been used in GIS for long time now with in general good experience the established technique of manufacturing on that field should be large enough to cast insulators for GIL. The stress during lifetime will be quite the same. If manufacturing processes and quality control are the same as for GIS there is no need of carrying out long duration tests specially for GIL.
If GIL is a new technique for a manufacturer the erection of a suitable long test setup and carry out of a quality control tests can be helpful. In the beginning of the GIS technique also large test set-ups like complete bays or even substations has been investigated in laboratories as a design study. Meanwhile this is not necessary du to the manufacturers experiences. The same can be transferred to GIL technology.
The new item to use a gas mixture instead of pure SF6 is no reason for long duration testing, the solid insulation can be treated like new GIS insulators. Experience concerning erection and handling on-site can be drawn from experiences from GIL with pure SF6 which have been a well known technique for more than twenty years [58] or less with recent technologies [59].

About recent developments and GIL designs and tests has been reported during the CIGRE Session 2000. The main features and tested parameters has been gathered in table 15 (see Session reports: A [60]; B [61]; C1 [62]; C2 [62]).

Furthermore it has been reported about several special measurements during the long duration tests:

- check of mechanical stress of enclosure
- record of soil-temperature
- record of movement due to current-cycles
- observation of corrosion protection

One type is a study on a 145 kV prototype with a polymere enclosure. The other four presented types of GIL are types with an aluminum enclosure for rated voltage 400/420 kV. All are single phase designs with N2/SF6 gas mixture (80 –90 % N2) as insulating medium. Except one the GIL-types are designed for direct burying, one is for installing in a tunnel. The table 15 1 gives an overview about the parameters of the long duration tests for the different GIL designs.

Beside the GIL designs with gas mixture insulation the 275 kV GIL for Shinmeika-Tokai Line (Japan) with pure SF6-insulation has been included in the table [63]. This GIL is already in service since 1998 (ref [7] of paragraph 1&2).

Test set-ups of all types in the range of hundred meter has been investigated in long-term tests with the intention to test the erection on site (all are welded on site) and to show the mechanical, thermal and electrical long-term behaviour. The voltage and current application has been chosen depending on the test facilities and specified ratings with the aim to prove a lifetime of 50 years in service.

Table 15 :
Parameters of long duration tested GIL designs

Type	A [60]	B [61]	C1 [62]	C2 [62]	D [59], [63]
Ratings					
Rated voltage	145 kV	400 kV	420 kV	420 kV	275 kV
Nominal power	670 MVA	2000 MVA	2250 MVA	2250 MVA	2850 MVA
PF-withstand voltage	275 kV	620 kV			460 kV
LIWV	650 kV	1425 kV	1300 kV	1425 kV	1050 kV
SIWV	---	1050 kV	1050 kV	1050 kV	
Nominal current	2800 A	3150 A	3150 A	3150 A	6300 A
Short time current		63 kA	63 kA	63 kA	50 kA/2 s
Pressure	0.6 MPa	0.8 MPa	0.7 MPa	0.7 MPa	0.4 MPa
Gas mixture SF6/N2	10/90 %	10/90 %	20/80 %	20/80 %	100 % SF6
Design					
Application	buried	buried	tunnel	buried	tunnel
Phase/enclosure	Single phase in Polymer enclosure	Single phase in aluminum alloy enclosure	Single phase in aluminum alloy enclosure	Single phase in aluminum alloy enclosure	Single phase in aluminum alloy enclosure
Long duration and other tests					
equivalent with time in service	50 years		50 years	50 years	50 years
Length	31 m 3-phase	300 m 1-phase	70 m 1-phase	100 m 1-phase	140 m 1-phase
Gas mixture SF6/N2	10/90 %	10/90 %	20/80 %	20/80 %	100 % SF6
Pressure		8 bar			0.4 MPa
Voltage duration	145 kV 3120 hours continously	400 kV 6000 hours continously	480 kV	480 kV	235 kV 2575 hours continously
Current	2900 A/3700 A	4000 A 22 hours per	3200 A	3200 A	6300 A daily cycles

	daily cycles	day 3 – 4 weeks			
Application	AC continously Current separete in cycles	AC continously Current separete in cycles	voltage and current in cycles total 2500 hours	voltage and current in cycles total 2880 hours	AC continously current in cycles
Commissioning test	AC: 275 kV; PD LI: 650 kV	AC: 570 kV	AC: 630 kV; PD LI: 1300 kV SI: 1050 kV	AC: 504 kV; PD LI: 1140 kV	AC: 460 kV PD LI: 1050 (for each unit)
Final test	not jet	- - -	AC: 630 kV; PD LI: 1300 kV SI: 1050 kV	AC: 504 kV; PD LI: 1140 kV	
Intermediate testing	- - -	- - -	SI: 1050 kV every 480 h	LI: 1140 kV every 480 h	
Repair test	- - -	Cut out a section with again commissioning test	Cut out a section with again commissioning test	Cut out a section with again commissioning test	
Special measurements		Check of mechanical stress of enclosure: record of soil-temperature			Properties of SF_6 PD; Acoustic emission; mechanical stress of enclosure

7.1. References of chapter 7

[58] Baer, G.; Dießner, A.; Luxa, G.: "420 kV SF6 insulated tubular bus for the Wehr pumped-storage plant; electric tests", IEEE Transactions on Power Apparatus and Systems, Vol. PAS-95, no. 2, March/April 1976

[59] Miyazaki, A.; Hiroyuki, H.; Hideaki, N.: "275 kV Shinmeika-Tokai GIL for long distance bulk-power transmission in a tunnel", IEEE PES Summer Meeting, Montreal, 1997

[60] Meinecke, H. ...: "Dimensioning criteria and test results for a polymer enclosed gas insulated line", CIGRE Session 2000, Report 21/23/33-01

[61] Feldmann, D....: "Development of a directly buried 400 kV Gas Insulated Line technology", CIGRE Session 2000, Report 21/23/33-02

[62] Koch, H. ...: "Electrical and mechanical long-time behavior of gas-insulated transmission lines" CIGRE Session 2000, Report 21/23/33-03

[63] Murasawa, I.; Ichihara, M.; Kawai, T.; Miyazaki, A.; Takinami, N.: Development of long-distance 275 kV gas insulated transmission line (GIL), The Eleventh International Conference on Gas Discharges and their Applications, Chou University Tokyo September 11-15, 1995

8. Monitoring and Diagnostics of PD in GIS and GIL

Small defects in SF6 gas-insulated substations (GIS) like fixed particles (fixed to conductors or on spacer surfaces) or free particles can influence the insulation strength of the insulation system. The analysis of this influence is often divided into four steps: detection, identification, location and risk assessment of the defect, which are dealt with in the following.

8.1. Assessment of the insulation condition

Small defects in SF6 gas-insulated substations like fixed protrusions on the conductors or spacers or free particles can influence the insulation strength of the insulation system. The assessment of the influence of such defects on the insulation condition in GIS is often divided into four steps: detection, identification, location and risk assessment of the defect. A similar procedure can be followed to assess the insulation condition of gas-insulated lines.

8.1.1. Detection

To detect PD in GIS the following measuring systems are used:

- conventional measuring systems based on the IEC 270 recommendations [64];
- acoustic measurements using externally mounted acoustic sensors which detect the acoustic signals emitted by a PD source [65];
- modern VHF/UHF measuring systems which use narrowband or wideband filters: detection in a frequency range up to several GHz, which system has been introduced over the last decade during on-site tests [66], [67], [68] and [69];
- other methods for example based on chemical or optical properties of PD processes [70].

8.1.1.1. The IEC 270 measuring system

During routine tests and tests after installation of high-voltage equipment, only a PD measuring circuit that complies with one of the world-wide used standards (for example according to the IEC 270 recommendations [64]) is acceptable. Most commercially available narrowband and wideband PD detectors measure the PD signals using frequency ranges up to a few hundreds of kHz. The measurement of discharge levels is in pC according to the IEC 270 recommendations. Such PD detection circuit is composed of a coupling capacitor, a coupling device and a PD detector, Figure 36.

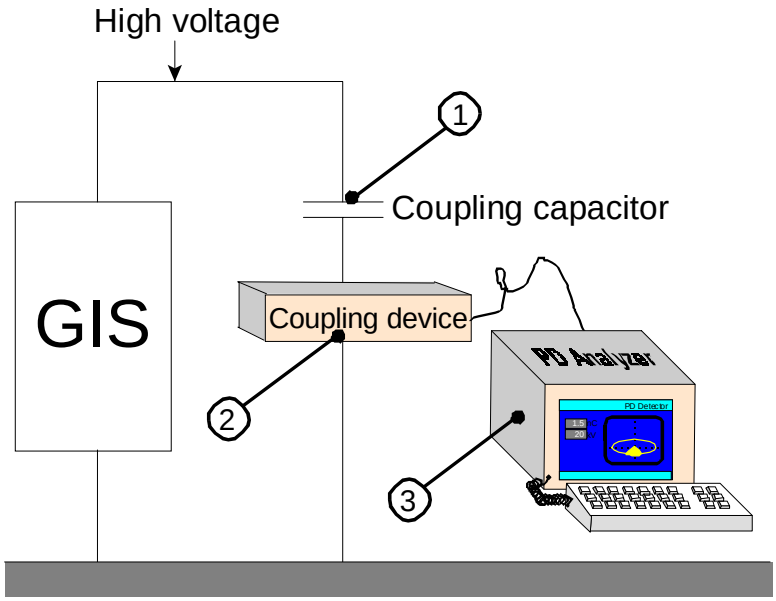

Figure 36: PD measuring circuit according to the IEC 270 recommendations [64].

In testing practice, the evaluation is restricted to measuring the inception voltage and largest PD magnitude, which are both compared to the test specifications. Although these are the only standardized PD parameters for acceptance of high-voltage equipment, more information can be obtained by an analysis of the PD pulses with respect to the phase angle of the sine wave: the

phase-resolved PD pattern. Phase-resolved PD analysis can enforce the diagnosis. Statistical analysis and cluster analysis, in particular fractal analysis and tree analysis [71] and [72], have shown to be successful evaluation processes, which have been adapted to the UHF range [82].

8.1.1.2. The VHF/UHF system

As shown in [69], the lowest frequency components of the PD signal (up to several hundreds of kHz) have to be measured to get geometry independent information of the apparent charge of the PD. Unfortunately, due to external noise, which is frequently present in the field (on-site/on-line) in these low frequencies, the use of the conventional test circuit, as recommended by the IEC 270 [64], is quite difficult. To solve this problem and to achieve a sensitive measuring circuit for on-line testing of GIS, a VHF/UHF detection system has been introduced [67], [69]. It has been shown that this detection system has about the same sensitivity as the IEC 270 system [73], [74].

8.1.1.2.1.The VHF System

The VHF detection system is based on the detection of travelling electromagnetic waves (em-waves) in the VHF frequency range of 100-300 MHz. In this frequency range, there is only little damping of the em-waves in the GIS. The principles of the wide-band VHF PD measurement system are shown in Figure 37. A sensor (3) with a coupling capacitance C_1 and a stray capacitance to ground C_2 (~10-100C_1) is connected to a signal conditioning unit (4). The filtered PD signals are fed into a PD detector (5).

The advantages of this wide-band technique are [69]:

- less influence of disturbances than a conventional PD detection system;
- the measurement system can be calibrated;
- independent of the layout of the GIS (to the first order).

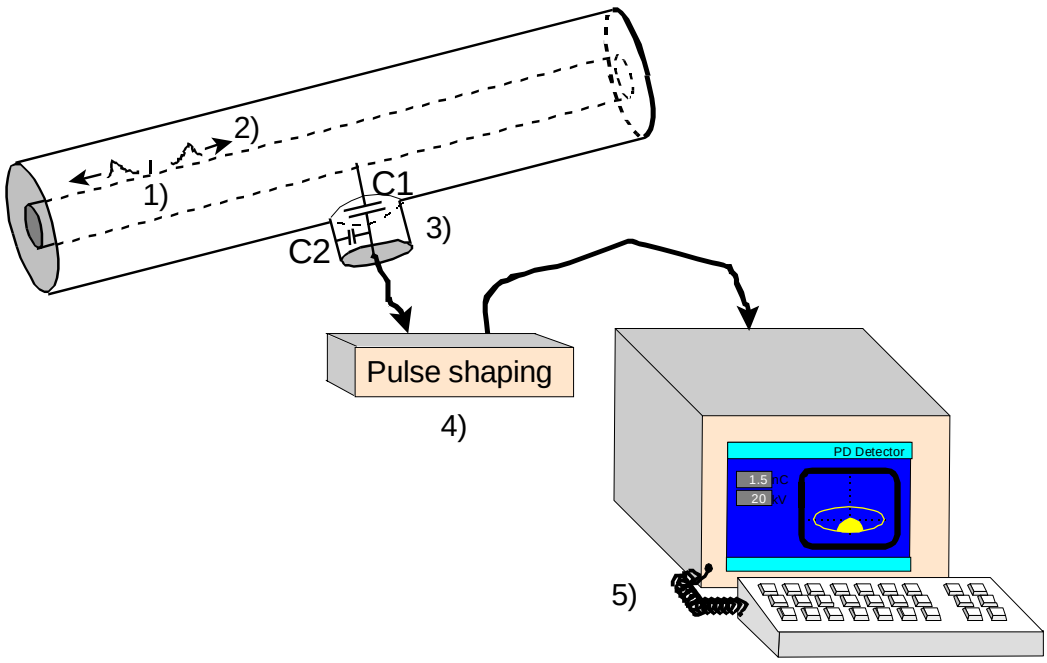

Figure 37: Five important parts for the VHF PD measuring technique:

1) the discharging defect
2) excitation of travelling waves
3) transfer function of the sensor
4) Pulse shaping
5) Data processing.

8.1.1.2.2.The narrow band UHF system

The narrow band UHF detection circuit operates in the frequency range between 300 and 1800 MHz. It is composed of a UHF coupler (which can be fitted either internal or external), a spectrum analyzer (SA) and a computer for data processing. The UHF coupler picks up the electromagnetic waves as produced inside the GIS enclosure by each PD pulse, see Figure 38.

The main advantage of the narrow band VHF/UHF system is the possibility to suppress external noise and disturbances by selecting a frequency range with a sufficient signal-to-noise ratio and lowest influence of disturbances, see Figure 39a [67].

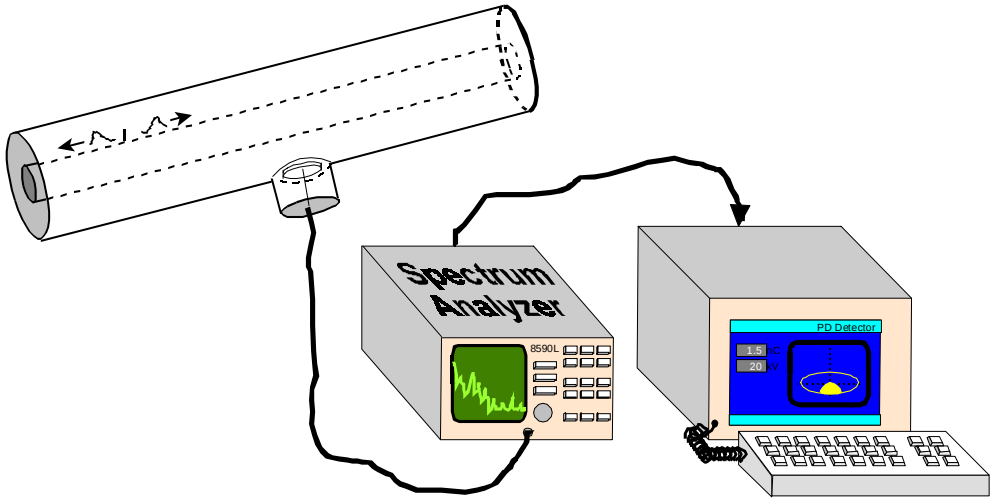

Figure 38: Four important parts for the UHF PD measuring technique:
1) the discharging defect
2) excitation of travelling waves
3) transfer function of the sensor
4) data processing.

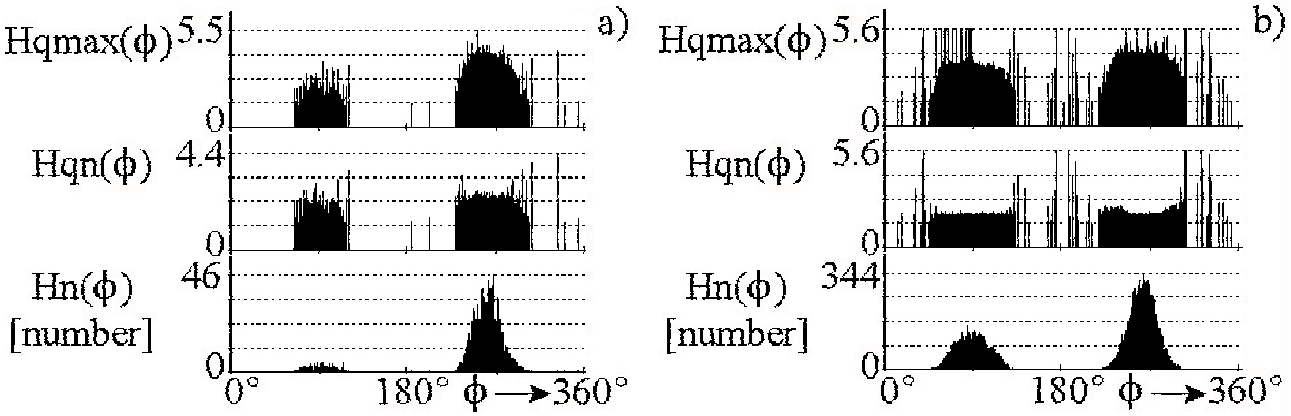

Figure 39: PD patterns measured for a protrusion fixed to the high-voltage conductor:

1) with the narrow band UHF system;
2) with the wide band UHF system.

8.1.1.2.3.The wide band uhf system

In addition, a wide band UHF system has been introduced [75]. This system measures the time domain signal in a frequency range from 500 MHz up to 1500 MHz. Using wide band amplification of the signal, an increase of the signal-to-noise ratio can be expected. On the other hand however, more influence of disturbances cannot be excluded, see Figure 39b.

8.1.1.3. The acoustic system

As the name suggests the method is only able to detect defects, those in some way emit sound. Sound is emitted from defects that have been activated by the applied voltage, e.g. protrusions with discharges and impacts from moving particles. The signals propagate from the source to the sensor located at the outside of the enclosure.

Two basic ways of signal excitation exist: pressure waves or “explosions” in the gas from discharges, and mechanical impacts of particles on the enclosure or movement of metal structures (e.g. conductor, bolts).

8.1.1.3.1.Mechanical impacts

A *particle* hitting the inner surface of a GIS generates a wide band acoustic signal (i.e. > 1 MHz). In the enclosure several wave types and –modes can be excited [65], [76]. The resulting wave will in principle depend on the frequencies generated and the thickness and material of the enclosure.

8.1.1.3.2.Pressure waves

A *discharge* acts as a local “explosion” due to current pulses creating and heating gas plasma. As the current pulse lasts only tens of nanoseconds the source will be wide band. The sound waves are generated in the gas and have to propagate to the enclosure before the excitation of the enclosure follows. When the pressure wave hits the enclosure there has to be coincidence between the wavelengths in the gas and in the enclosure along the interface to get sound transmitted into the enclosure. The phase velocities determine this interference [65].

The gas acts as a low pass filter depending on the gas pressure as shown in Figure 40 [77].

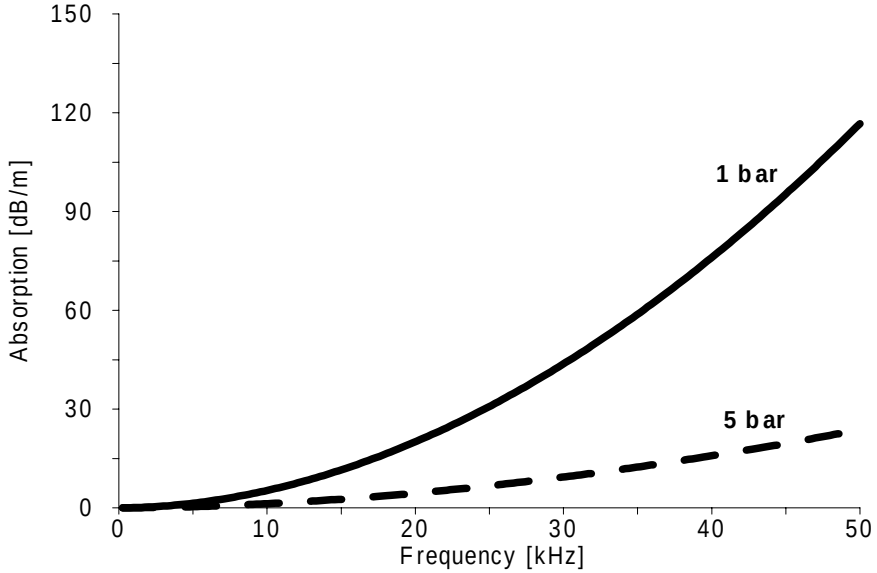

Figure 40: Sound absorption in SF6.

For detection accelerometers or acoustic emission (AE) sensors can be used. There is good experience with AE sensors with a resonance in the 30-40 kHz regime [78]. Compared to the conventional discharge detection method, the relevant AE sensors have characteristics with lower pulse resolution capabilities.

8.1.1.4. Other detection methods

8.1.1.4.1.Optical detection

In principle, the photon emission of partial discharges can be used for PD detection. Light measuring instruments like photodiodes or photo-multiplier tubes of extremely high sensitivity are available. The application of such a system is restricted because of the high light absorption in SF6, which increases with the gas density. The resulting high number of sensors which have to be installed necessarily in a real GIS for an effective PD detection system does not permit an application in practice [79].

8.1.1.4.2.Chemical detection

Under the action of arcs and discharges SF6 gas decomposes. The initial arc-decomposition products are metal fluorides, sulfur tetrafluoride and lower fluorides of sulfur. Specific information about gas decomposition by-products can be obtained by gaschromatography. As described in [79] the chemical method can also be used successfully to detect PD, provided that PDs develop for a relatively long time interval and with a high repetition rate. It may be effective with fixed-type defects while the sensitivity may be less for free particles. The sensitivity may be low in long ducts, depending on the by-product diffusion down a long chamber, which often includes impediments (spacers). In addition, when using detector tubes, interpretation problems may arise when different electrical phenomena are present in the same compartment (e.g. PD and arcing by disconnector operations). Other problems may arise when using the chemical method because of desiccants and absorbers in the GIS chambers in service, with consequent drastic reduction in by-products [79].

8.1.1.5. Suitability for practical use in GIL

For in-service monitoring, all diagnostic techniques are applicable. For monitoring during commissioning, the chemical method is not suitable because time is needed to produce by-products in a concentration high enough to be detectable [79]. In case the GIL is buried, it will be rather difficult to apply acoustic detection. In the case of the UHF method, couplers can be permanently mounted. However, a coupler is necessary after approximately every 7th conical spacer to obtain enough sensitivity. The resulting high number of UHF couplers which have to be installed in a real GIL for an effective PD detection system can make the application of continuous UHF monitoring less practical. The em-waves in the VHF range have less attenuation, and therefore the VHF measuring technique offers a more practical solution for sensitive PD detection in long GIL.

In the following tables, overviews of the sensitivity of different detection methods to find critical defects are given [80].

From Table 16 can be concluded, that it is possible to detect critical defects in a 420 kV GIS, using a PD detection circuit according to the IEC 270 recommendations.

Table 16:
Detection of critical particles according to IEC 270 in a laboratory setup [80].

Defect	Critical length	Detection in 420 kV GIS
Free particle	2-5 mm	3 mm
Protrusion	1-2 mm	1 mm
Particle fixed on spacer	2-3 mm	3 mm
Floating electrode	-	Yes
Void in spacer	-	Yes

Table 17 gives an overview of the possibility to detect critical defects on-site with different detection methods. From the table can be concluded that most critical free particles can be detected. Protrusions are very difficult to detect and critical particles fixed to a spacer cannot be detected at all.

Table 17:
On-site commissioning testing on 420 kV GIS with a sensitivity of 5 pC at an AC test voltage of 0.36xLIWL[80].

Defect	Critical length	IEC	UHF	Acoustic
Free particle	2-5 mm	5 mm	5 mm	1 mm
Protrusion	1-2 mm	2 mm	no	no
Particle fixed on spacer	2-3 mm	no	no	no
Floating electrode	-	yes	yes	yes

Table 18 shows the sensitivity of on-line monitoring of a 420 kV GIS using the UHF technique. From the table can be concluded that it is possible to detect free particles, electrically floating electrodes and voids in solid material. It is not possible to detect critical particles fixed to conductors or spacers. However, such defects are removed during commissioning testin

Table 18:
On-line monitoring of 420 kV GIS using the UHF technique [80].

Defect	Critical length	Detection in 420 kV GIS with UHF
Free particle	2-5 mm	5 mm
Protrusion*	1-2 mm	8 mm
Particle fixed on spacer*	2-3 mm	12 mm
Floating electrode		yes
Voids in solid material		yes

*These defects are removed during commissioning

Similar sensitivities can be expected in GIL. Moreover, it has been shown that free particles can effectively be removed in GIL using particle traps [81].

8.1.2. PD identification

Until recently the industrial standard technique for diagnostic screening for defects in the insulation system was detection of partial discharges (PD). Sensitivities in the 5-10 pC regime are

required. However, discharge levels have little relevance to the risk of breakdown. For example, floating shields produces discharges in the nanocoulomb range while discharges from protrusions, which are more harmful, are in the picocoulomb range. Pattern recognition has therefore been developed to compensate for this shortcoming of the conventional PD detection method. In the following different methods to evaluate PD measurements are described.

8.1.2.1. Electrical measurements

Identification of defects is often based on phase-resolved pattern analysis, see Figure 41 [82], [83]. However, also the frequency spectra generated by different defects look rather different, see Figure 44 [84].

8.1.2.1.1.Phase-resolved pd patterns

Correlating the PD signals to the 50 Hz waveform of the applied voltage results in phase-resolved PD patterns, see Figure 41. It is known that a relationship exists between the shape of phase-resolved PD patterns and the discharge source (type of defect) [85]. Each discharging defect with its geometry, location in insulation, dielectric properties and local field is characterized by a specific PD sequence. Analysis of these sequences has shown a good means to distinguish the different discharge sources [85]. To automate this process, several digital tools are in use to analyze the phase-resolved patterns: statistical analysis and cluster analysis [71].

We have to distinguish between signals emitted from fixed and moving particles. Fixed particles can produce corona discharges, whereas moving particles can produce both corona discharges during flight and contact discharges when striking a surface [86]. In addition to physically related conditions, several parameters like the measuring frequency in the case of the narrow band UHF system, the choice of PD quantities as well as the statistical tools for discrimination are of importance.

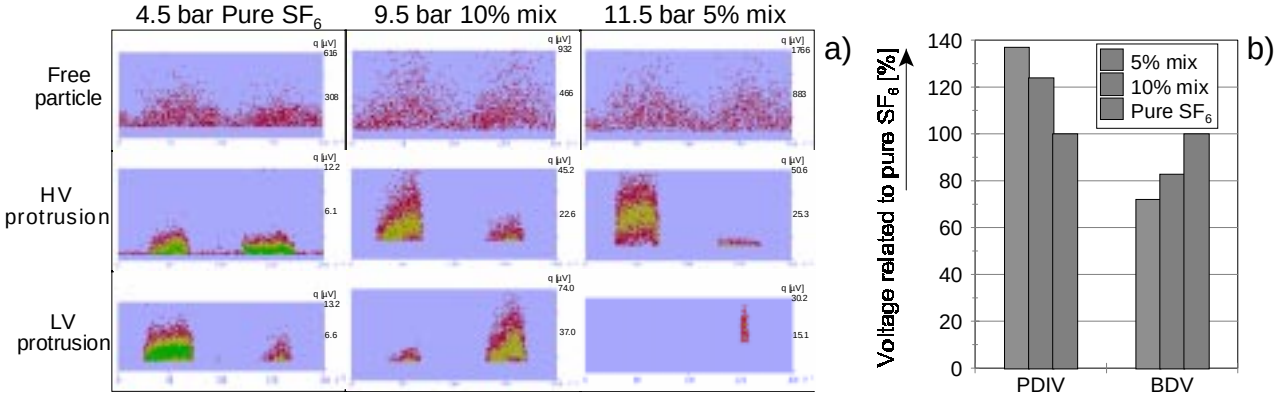

Figure 41: a) Typical PD patterns of a 10 mm free particle, a 10 mm protrusion fixed to the conductor and a 30 mm protrusion fixed to the enclosure, obtained in 4.5 bar pure SF_6 and SF_6-N_2 mixtures with comparable lightning withstand voltages.
b) PD inception voltage (PDIV) and breakdown voltage (BDV) in case of a protrusion fixed to the high-voltage conductor relative to the values in pure SF_6

In general, after a PD measurement is finished, three steps have to be taken for PD identification:

- Step 1: Feature extraction
- Step 2: Classification
- Step 3: Confidence interval

An overview of different methods, which are commonly used, is given in Table 19. More methods are in use, such as artificial neural networks [88] or others which cannot be described due to lack of information, e.g. [89].

Table 19:
Overview of some PD identification methods.

Feature extraction (step 1)	Classification (step 2)	Confidence interval (step 3)	Reference
Statistical analysis	Centour score	Centour score	[71]
Fourier-transformation	L2-distance	Dynamic boundary	[87]
Haar-transformation	ANN	>50%	[87]
Walsh Hadamard	Fuzzy	Dynamic boundary	[87]

An example of the statistical analysis method is given in the following.

Step 1: The feature extraction aims to reduce the dimensionality of the PD patterns by processing characteristic properties from the PD pattern [71]. Statistical operators, such as skewness and kurtosis, have been used to derive a so-called ‘fingerprint’ [72].

Step 2: For classification of PD measurements the centour score method has been used [71]. This method uses fingerprint populations of known discharge defects in a database. It compares the fingerprint of the new PD measurement with the centre of each population.

Step 3: The centour score is defined as the percentile rank of the fingerprints that are further away from the centre of the known discharge population than the fingerprint of the new PD measurement. This has been illustrated in Figure 42.

An example of the outcome of the PD pattern classification of an on-site measured PD pattern with a database developed in the laboratory, is shown in Figure 42.

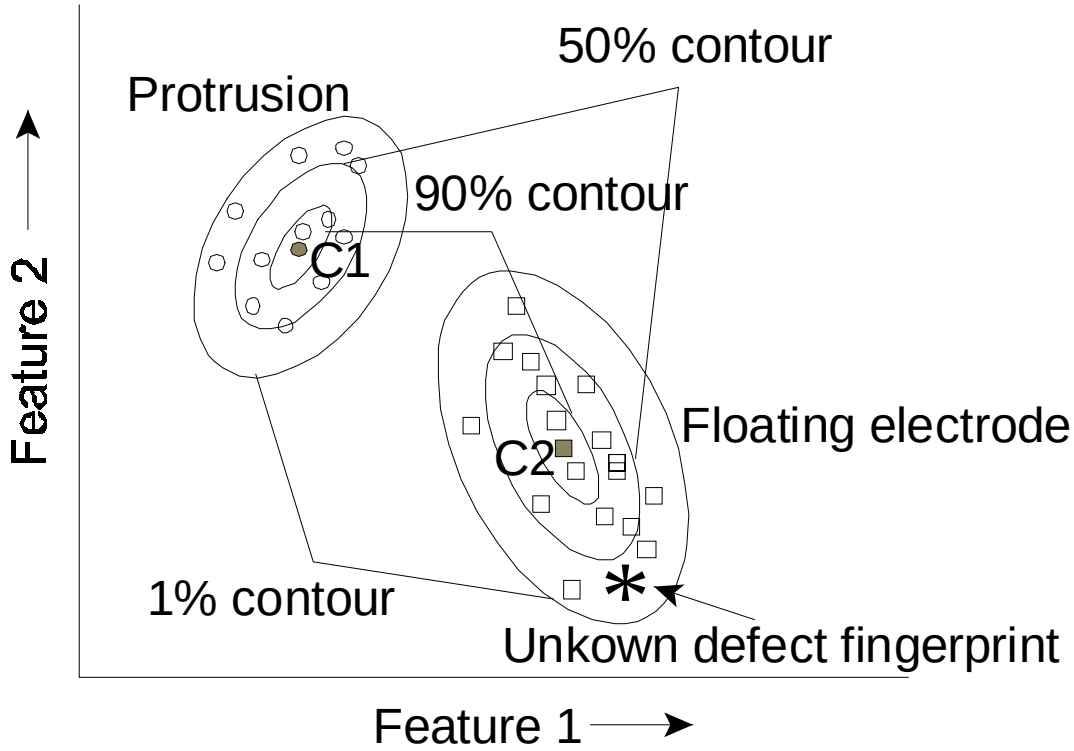

Figure 42: Contours of the centour score method. Circles: fingerprints of a protrusion fixed to the enclosure; squares: fingerprints of a floating electrode [71].

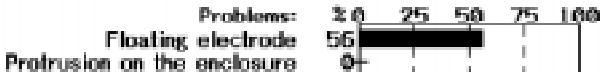

Figure 43: Outcome of the PD pattern classification using the centour score method of an on-site obtained PD pattern with a laboratory developed database.

8.1.2.1.2.Analysis of frequency spectra

With the UHF PD measuring method, a frequency spectrum is measured at one of the couplers inside the GIS. The shape of this spectrum looks rather arbitrary and highly depends on the type of radiating source (discharging defect), location of this defect, type of coupler and structure of the GIS. For example, Figure 44 shows spectra measured for different defects. In this respect, frequency spectra have to be analyzed for automatic defect recognition [84].

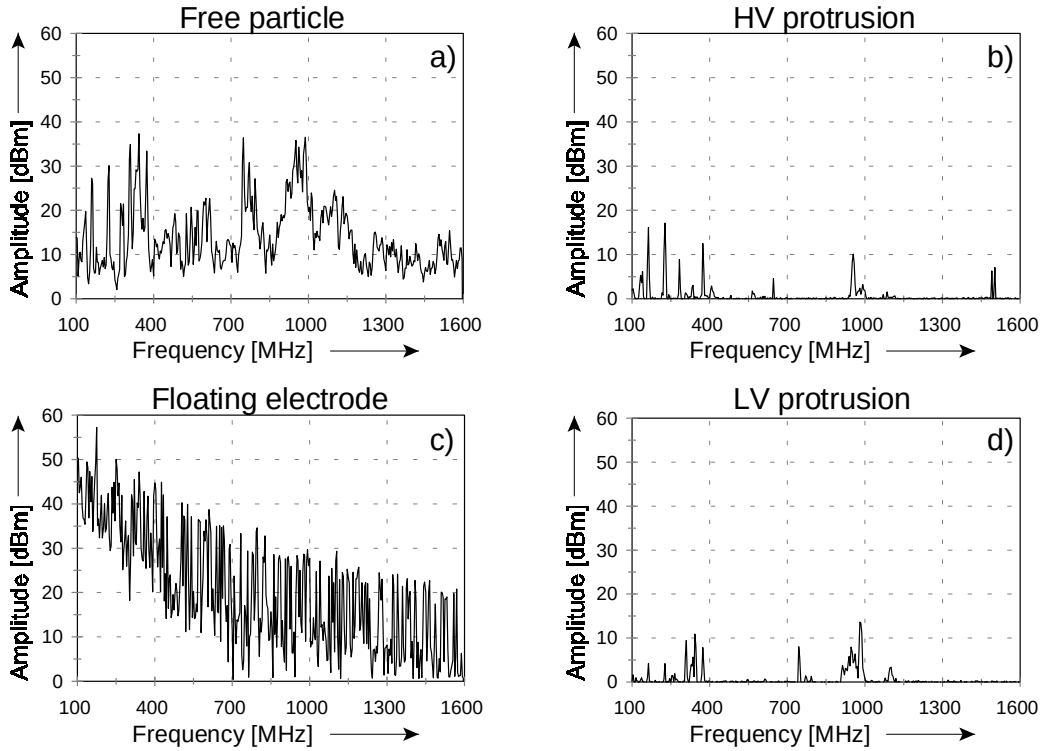

Figure 44: Different frequency spectra measured for different defects:

a) Free moving particle;
b) Protrusion fixed to the high-voltage conductor;
c) Electrically floating electrode;
d) Protrusion fixed to the enclosure.

Statistical analysis of frequency spectra results in a feature vector of spectra, consisting of 13 features. These characterizations can be further analyzed using clustering techniques [71]. The result of such analysis can be visualized in a tree structure, as shown in Figure 45. The purpose of this analysis is to find groups of similar fingerprints. A detailed description of clustering techniques can be found in [71].

Figure 45 shows a simplified example how cluster analysis works. Here five feature vectors consisting of one feature are analysed. First, the two vectors which have the smallest distance (i.e. which are the most similar) are connected, see Figure 45a. They are replaced by one new feature vector, for instance by taking the average. In this way, the number of vectors is decreased by one. These steps are repeated until the last vectors are connected, see Figure 45b-d.

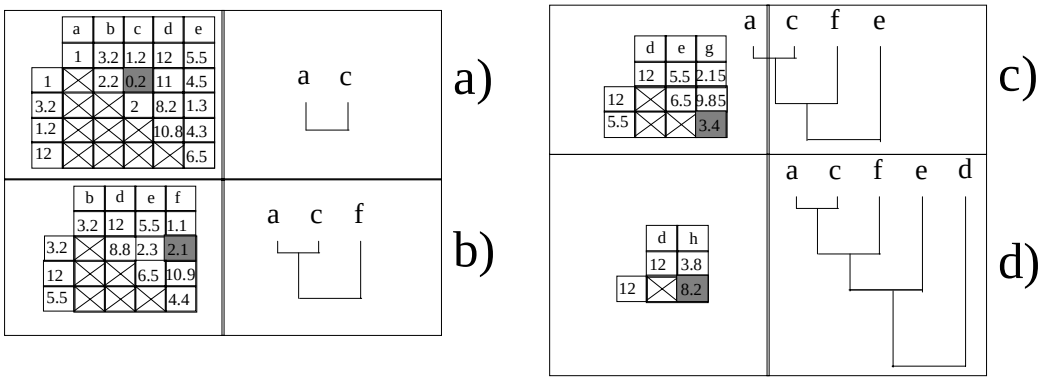

Figure 45: Example of cluster analysis of fingerprints using the tree-structure.

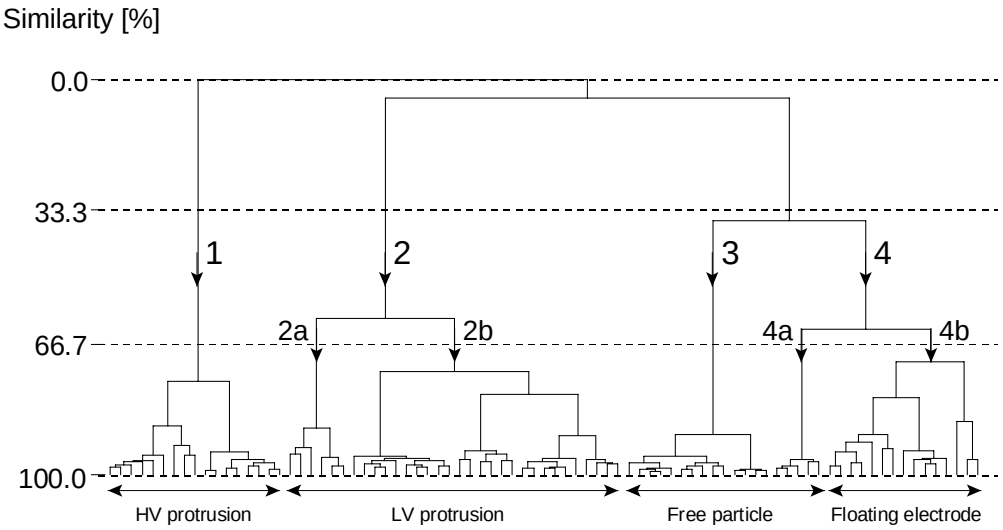

Figure 46: Cluster analysis applied to the characterizations calculated from the frequency spectra for four different defects: protrusion fixed to the high-voltage conductor, protrusion fixed to the enclosure, free moving particle and electrically floating electrode.

Cutting the tree at a certain level results in four main clusters. Analysis of these clusters shows that measurements of one type of defect are grouped in each cluster, except for cluster 4. Cluster 1 contains measurements of a protrusion fixed to the high-voltage conductor; cluster 2 contains measurements of a protrusion fixed to the grounded enclosure and cluster 3 measurements of a free moving particle.

As indicated in Figure 46, two clusters inside clusters 2 and 4 can be distinguished. Comparison of the spectra grouped in cluster 2a and 2b did not provide any significant differences to explain the reason for both clusters. Both clusters found in cluster 4 can be explained: cluster 4b represents the measurements obtained from an electrically floating electrode while cluster 4a contains measurements obtained from a free moving particle. Further analysis of the measurements in cluster 4a showed that these were obtained at the very beginning of the PD activity coming from a free particle. In this case, very small contact noise-like PD activity was observed. The PD pattern is rather similar to the pattern of an electrically floating electrode.

8.1.2.2. Acoustical measurements

As with the UHF method, the amplitude of the detected acoustic signals can be plotted against the phase-angle of the applied voltage. This results in typical acoustic phase-resolved PD patterns as shown in Figure 47.

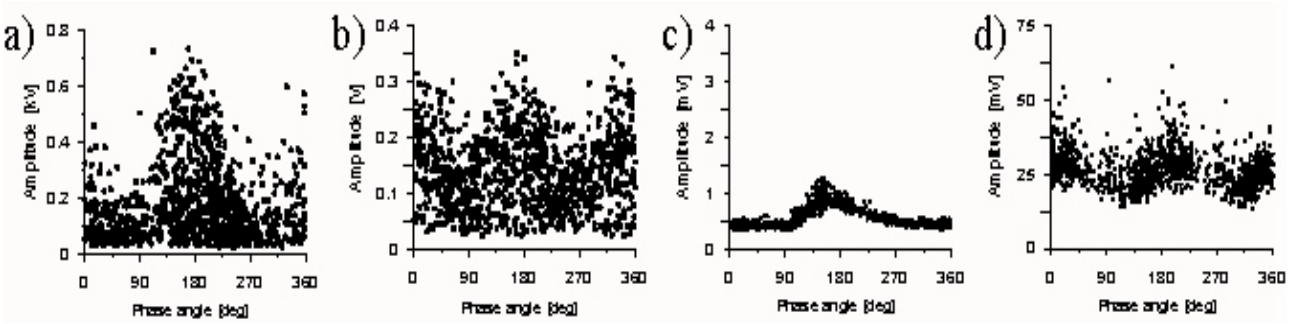

Figure 47: Typical acoustic phase-resolved PD patterns from [78]:
a) a short thick particle;
b) a long thin particle;
c) a protrusion fixed to the high-voltage conductor;
d) an electrically floating electrode.

For defect recognition, the scheme shown in Figure 48 has been proposed in [78].

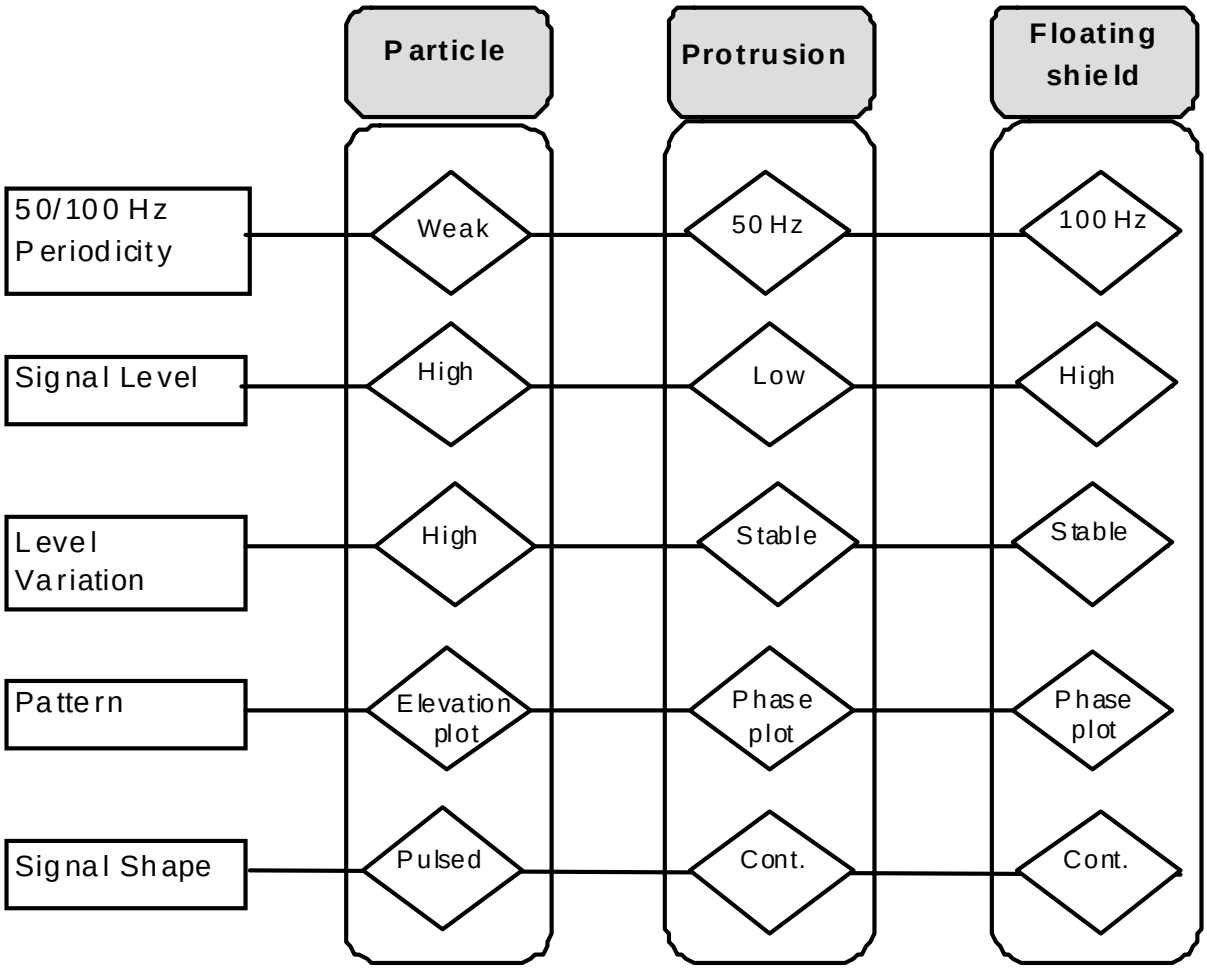

Figure 48: Scheme for source recognition [78]. Discrimination between the most common sources can easily be done based on some basic parameters as illustrated in Figure 48. The acoustic analyzer evaluates the 50/100 Hz periodicity, the signal level, the variation in the signal level, the PD patterns and the signal shape.

8.1.3. Location

The (electric or acoustic) pulse emitted by a PD source propagates in both directions along the GIS, see Figure 49. As a result, the source may be located by measuring the time difference between the wave fronts arriving at couplers on either side of the PD source: the time-of-flight technique [67]. For this technique, two sensors (either acoustic or UHF) are used to pick up PD

signals. To measure electrical PD pulses in SF6 that have rise times as short as a few hundreds of picoseconds and time differences of a few hundreds of nanoseconds a fast digitizing oscilloscope is necessary.

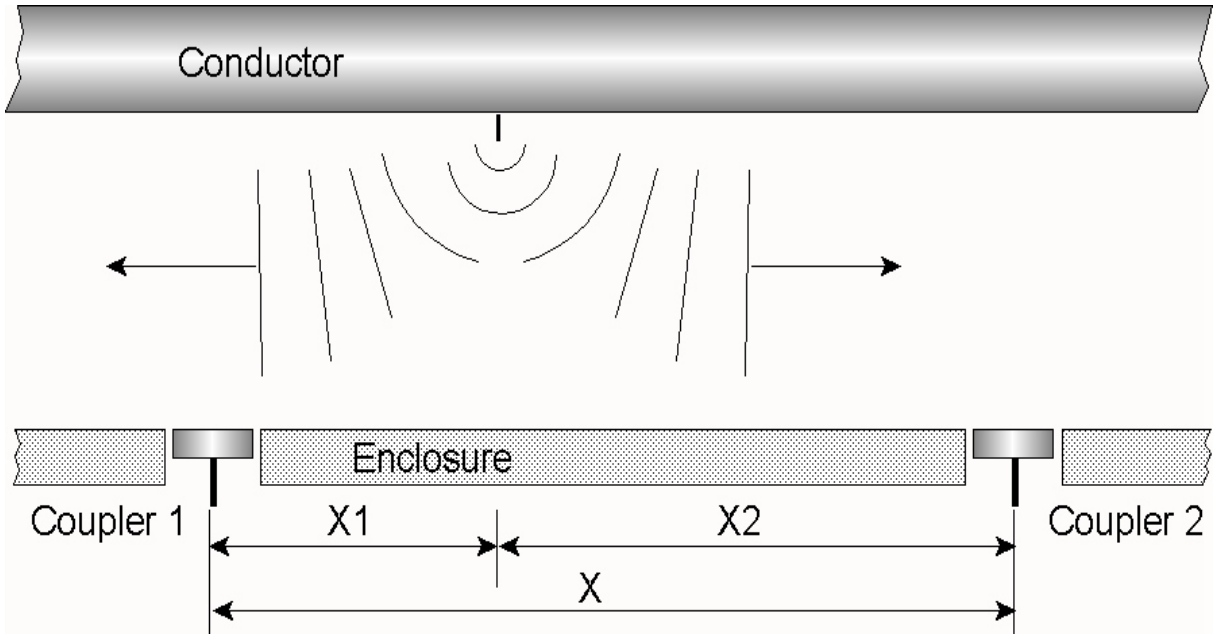

Figure 49: The principles of defect location using time-of-flight measurements. Sensors 1 and 2 pick up the pulses emitted by the PD source. From the difference in arrival time between both sensors at the detection equipment, the location of the defect can be calculated.

The distance X_1 between coupler 1 and the PD source can be calculated with equation:

$$X_1 = \frac{X - (X_2 - X_1)}{2} = \frac{X - dX}{2} = \frac{X - v \cdot dt}{2} \qquad (32)$$

where X is the distance between both couplers, dX is the difference in the distance between coupler 2 and the PD source and coupler 1 and the PD source, dt is the difference in the arrival time of the signal at coupler 2 and coupler 1 and v is the propagation velocity of the signal, described by:

$$v = \frac{1}{\sqrt{\mu_r \cdot \mu_0 \cdot \varepsilon_r \cdot \varepsilon_0}} \qquad (33)$$

In case of a gas, the propagation velocity approaches the speed of light. However, in a medium of permittivity εr, such as spacers, the propagation velocity is decreased by a factor proportional to the square root of εr.

Besides above described method is based on electrical measurements, results that are even more accurate can be obtained by acoustic measurements.

8.1.4. Risk assessment under power-frequency voltage

For assessing the risk of a defect it is necessary to have knowledge about the design of the GIS, the physical properties of the defect and experience of similar defects from the past. Risk assessment is the process of establishing information regarding acceptable levels of a risk of a defect to the insulation system [90]. Critical defects are those defects, which are at the threshold of being harmful to the dielectric integrity of the GIS under normal operating conditions [79]. Cigre working group 15.03 is dealing in more detail regarding this topic. Below some of the ideas discussed in this working group are described.

Here only two examples are shown: free particles and fixed protrusions (either fixed to the high-voltage conductor or to the enclosure). Work in this field is still going in one of the task forces of working group 15.03.

8.1.4.1. Criticality of free particles

The defect in GIS that occurs most often and is most dangerous is the free moving particle [79]. Especially when a particle approaches the high-voltage conductor, breakdown can occur. In the behavior of a free moving particle, three different stages have been observed [84]:

1. *shuffling particle*: the particle just starts to move really slowly and a very small contact-noise-like PD activity is measured;
2. *moving particle*: the particle starts dancing;
3. *jumping particle*: the particle starts to jump and sometimes stays airborne for a few cycles.

It is clear that the third stage, the jumping particle, is the most critical one because it can reach the high voltage conductor.

Risk assessment of free particles has to be such that jumping particles can be distinguished of moving particles. In the following paragraphs, analysis of acoustic and UHF measurements is described to determine the risk of free particles.

As stated in [91], risk assessment of moving particles in GIS requires the estimation of a particle's mass and length. For this purpose, four methods are described in [91] based on combinations of acoustic and electric measurements, see Figure 50.

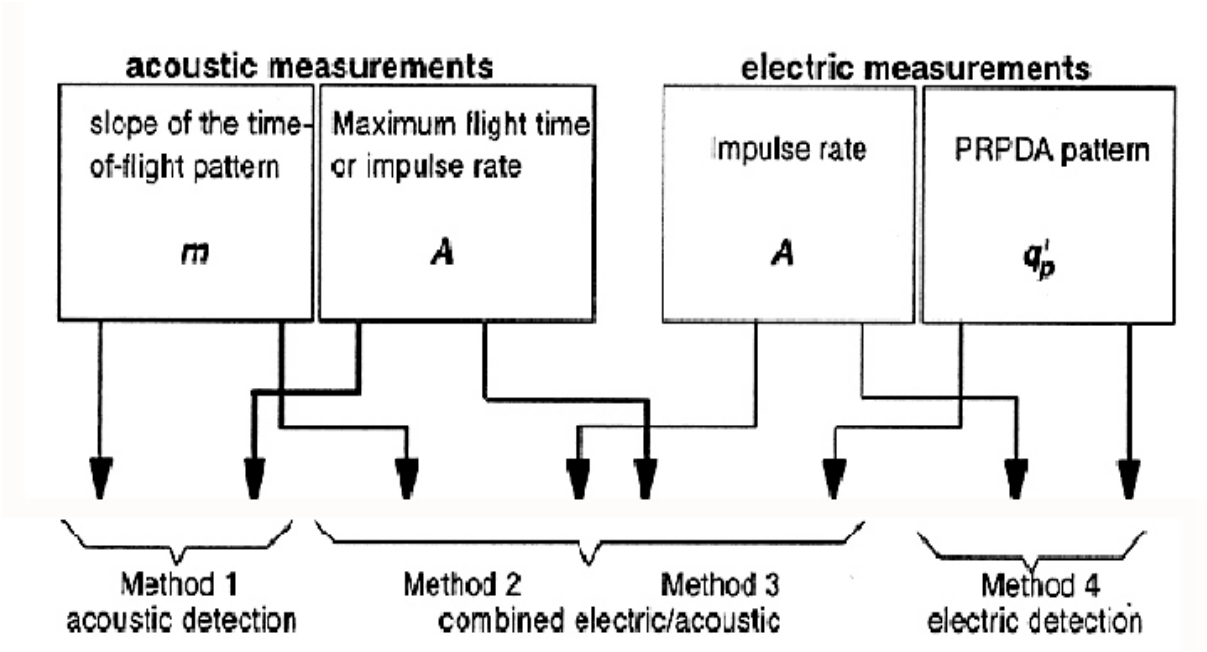

Figure 50: Different methods to calculate the mass and length of free particles based on acoustic and electric measurements (taken from [91]).

Typical frequency spectra measured for each stage in the movement of a free particle is shown in Figure 51. It shows processed frequency spectra using an averaging or max-hold technique over the 20 measured sweeps [84]. In all three situations, it is clear that the hold-max frequency spectrum is larger than the averaged frequency spectrum. To compare the spectra, a key value [84] has been calculated, see Table 20.

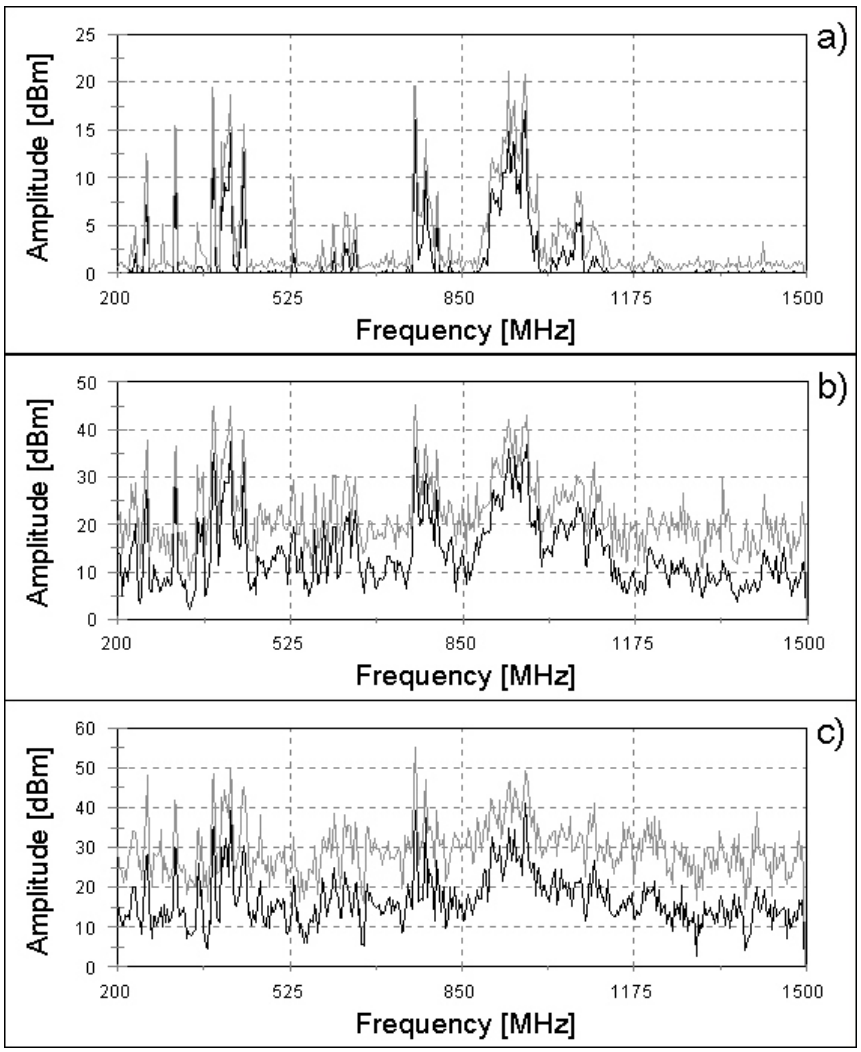

Figure 51: Max-hold (gray line) and averaged (black line) frequency spectra measured for a free particle when it is a) shuffling, b) moving and c) jumping [84].

Table 20:
Key value calculated from the post-processed frequency spectra of a shuffling, moving and jumping particle,
using an averaging or hold-max processing technique [84].

Defect	Averaged spectrum	Hold-max spectrum
Shuffling	0.18 mV	0.94 mV
Moving	6.3 mV	22.6 mV
Jumping	5.8 mV	28.8 mV

Table 20 confirms that the amplitudes in the max-hold frequency spectrum exceed the averaged amplitudes. However, once the particle starts jumping, the amplitude of the averaged spectrum decreases, whereas the amplitude of the max-hold spectrum increases. We will explain this by analysing three individual sweeps as shown in:

Stage 1: shuffling particle:

Compared to the dancing and jumping particle, the peaks in the frequency spectra of the shuffling particle have very low amplitude and all measured sweeps are almost similar.

Stage 2 moving particle:

When the particle starts moving, but not jumping, the amplitude of the peaks in the frequency spectrum increases significantly and, again, all measured sweeps are almost similar.

Stage 3: jumping particle:

When the particle starts jumping, the frequency spectra are again different: the maximum amplitude of the peaks in the frequency spectra has increased again, but ‘empty’ parts are also observed in the spectra, which are indicated by arrows. These empty parts imply that no

detectable PD activity occurs. This means that the particle does not hit the enclosure and is somewhere in the gap between the enclosure and conductor. This was confirmed by visual observation during the measuring period. If we post-process the spectrum by averaging the measured sweeps, the result will be reduced due to these empty parts.

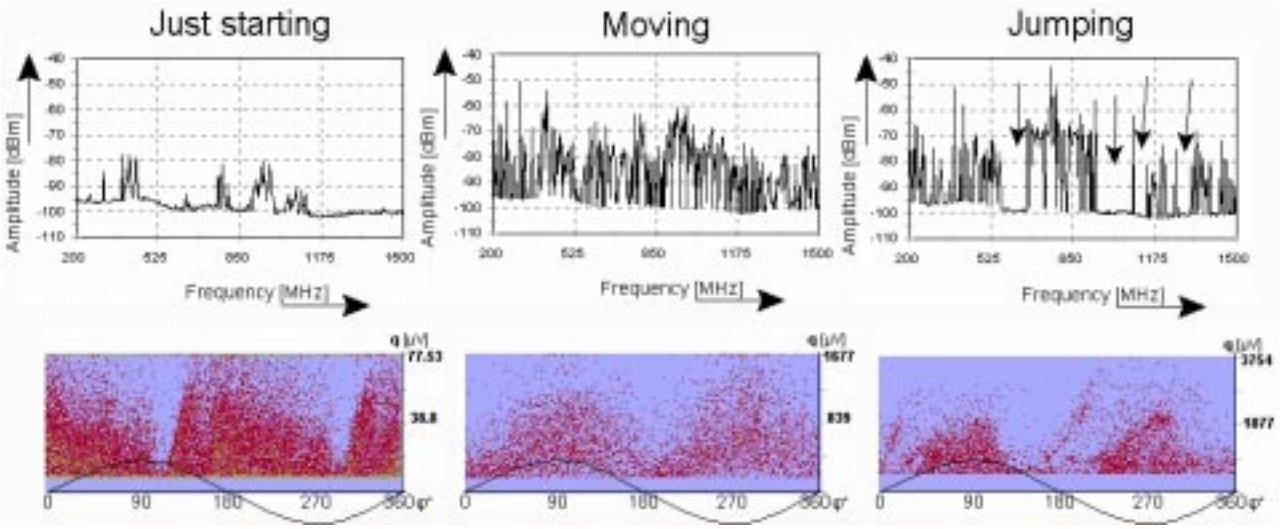

Figure 52: Frequency spectra and PD patterns measured for each stage in the particle movement [84].

These empty parts can be explained by the way that the spectrum analyser captures a frequency spectrum. A spectrum analyser effectively performs a Fourier analysis of the input signal. Like a radio receiver it tunes at consecutive frequencies and captures the amplitude of the spectral content of the input signal at the tuned frequency. It takes a certain amount of time for the SA to tune at all frequencies in the frequency spectrum, called sweep time. As shown in figure 7.11, during the sweep time, the discharging signal at the input of the SA changes with each discharge. Therefore, the final captured frequency spectrum is build from several discharges signals. Moreover, if the particle is jumping, for example at t_3 as indicated in Figure 53, there is no discharge activity and therefore there is also no input signal. This results in the empty part of the frequency spectrum.

So the empty parts occurring in a frequency spectra has nothing to do with no spectral content of the discharging signal as can be seen in the Fourier spectra at times t_1, t_2 and t_4 which have no empty parts. Only due to the minimal amount of time required to capture a frequency spectrum, these empty parts appear as soon as the particle is jumping and for some time, no discharge activity occurs. Because the particle movement is a random process, the empty parts in the spectra can change from sweep to sweep, as shown in the three sweeps of jumping particles in Figure 52.

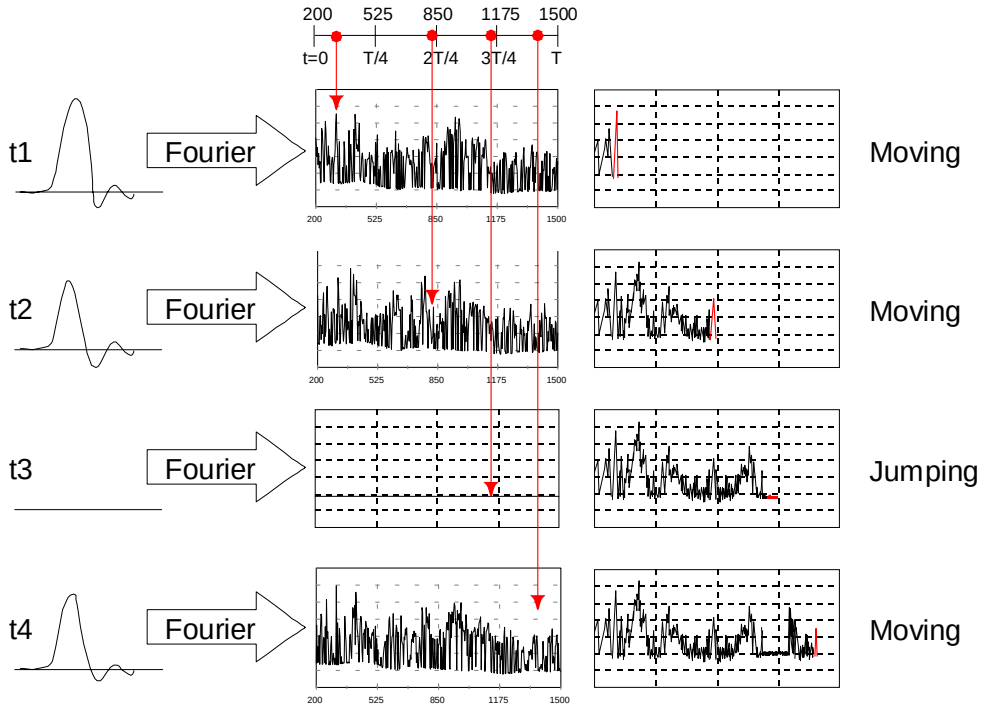

Figure 53: The method to capture the frequency spectrum of a discharging defect using a spectrum analyser (SA):
- the discharge signal at the input of the SA has a certain Fourier spectrum; at t_3 the particle is jumping so there is no input signal and consequently there is no Fourier spectrum;
- during the sweep-time T, the SA continuously tunes at successive frequencies and captures the corresponding spectral contribution of the (Fourier spectrum of the) input signal; in the case the particle is jumping, there is no input signal and the SA only measures the noise level.

In case of free particles, criticality risk assessment means that jumping particles and not-jumping particles can be distinguished. From Table 20 can be concluded that the ratio of the key-value processed from the averaged spectra and hold-max spectra is different for moving and jumping particles. Therefore probability distributions have been processed for both moving stages, see Figure 54. It is clear that the ratio of moving and jumping particles are differently distributed. As can be seen, the significance of the difference between both distributions is σ. These distributions have been used to calculate the probability of particles jumping or not.

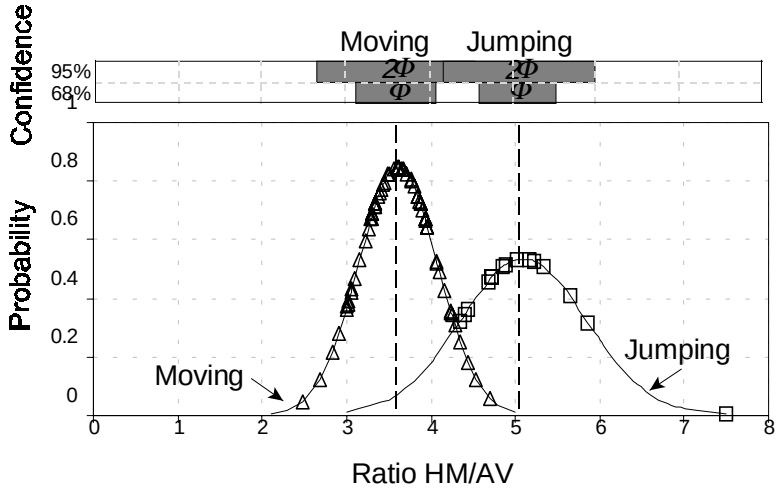

Figure 54: Probability density distribution for moving (triangles) and jumping particles (squares).

8.1.4.2. Fixed protrusions

Protrusions fixed to a conductor can lead to corona-like PD activity. Corona stabilization can occur by fixed protrusions at the operating voltage level, but does not lead to a breakdown. However, an over-voltage such as a fast lightning stroke can immediately trigger a breakdown in GIS [79]. Therefore, the measuring results have to be analyzed thoroughly to determine the risk of a defect.

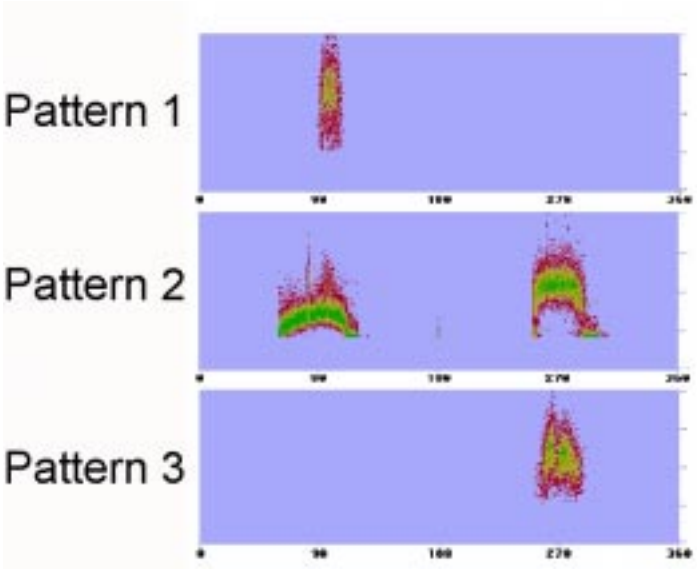

Figure 55: Different types of patterns measured for protrusions fixed to the high-voltage conductor or to the enclosure [84].

In case of protrusions, three stages can be determined based on the patterns shown in Figure 55. Table 21 gives an overview of these stages. Risk assessment of fixed protrusions has to be such that stage 3 can be distinguished from stages 1 and 2.

Table 21:
Different stages for protrusions fixed to the high-voltage conductor (HV-side) or fixed to the enclosure (LV-side), defined from inception (stage 1) to close to breakdown (stage 3).

Defect	Stage 1: Inception	Stage 2	Stage 3: Close to breakdown
High-voltage protrusion	Pattern 3	Pattern 2	Pattern 1
Low-voltage protrusion	Pattern 1	Pattern 2	Pattern 3

For example, the phase-resolved PD pattern shown in Figure 56a was analysed. The defect causing this PD pattern was identified as a fixed protrusion as shown in Figure 56b. For this purpose the measured PD pattern was compared with the PD patterns stored in a reference database. In this database, different types of protrusions are stored, represented by several types of PD patterns. However, nothing can be concluded about the position of this protrusion: 90% similarity with the cluster of protrusions fixed to the enclosure and 76% similarity with the cluster of protrusions fixed to the high-voltage conductor. This can be explained by the large overlap of the clusters of fixed protrusions because of the similar patterns observed for both protrusions. Moreover, the 14% difference in the similarity is smaller than the standard deviation of each cluster and therefore nothing can be concluded about the position of this protrusion: fixed to the high-voltage conductor or enclosure.

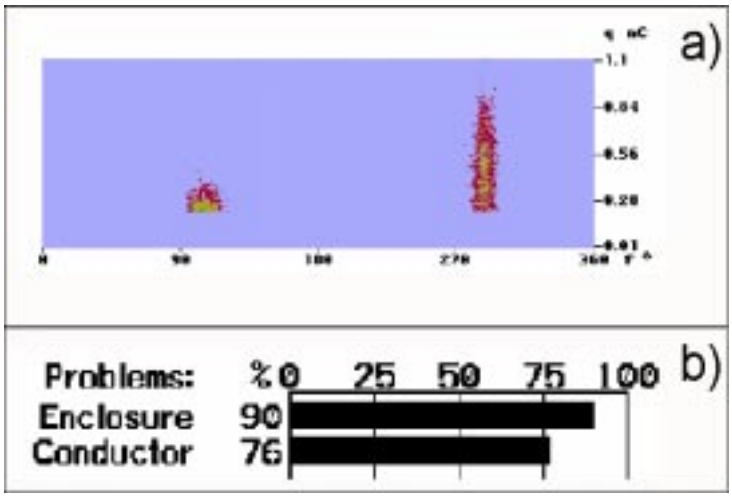

Figure 56: a) Phase-resolved PD pattern from a fixed protrusion
b) the statistical defect recognition based on phase-resolved PD pattern analysis.

Above-mentioned defect was therefore further analysed by combined PD pattern analysis and spectral analysis, see Figure 57. From the PD pattern analysis can be concluded that the pattern is originating from a fixed protrusion, giving partial discharge activity with pattern type 3. From spectral analysis can be concluded that the protrusion is fixed to the enclosure. Comparing this with knowledge stored in an expert system, a high-risk protrusion fixed to the enclosure has been concluded.

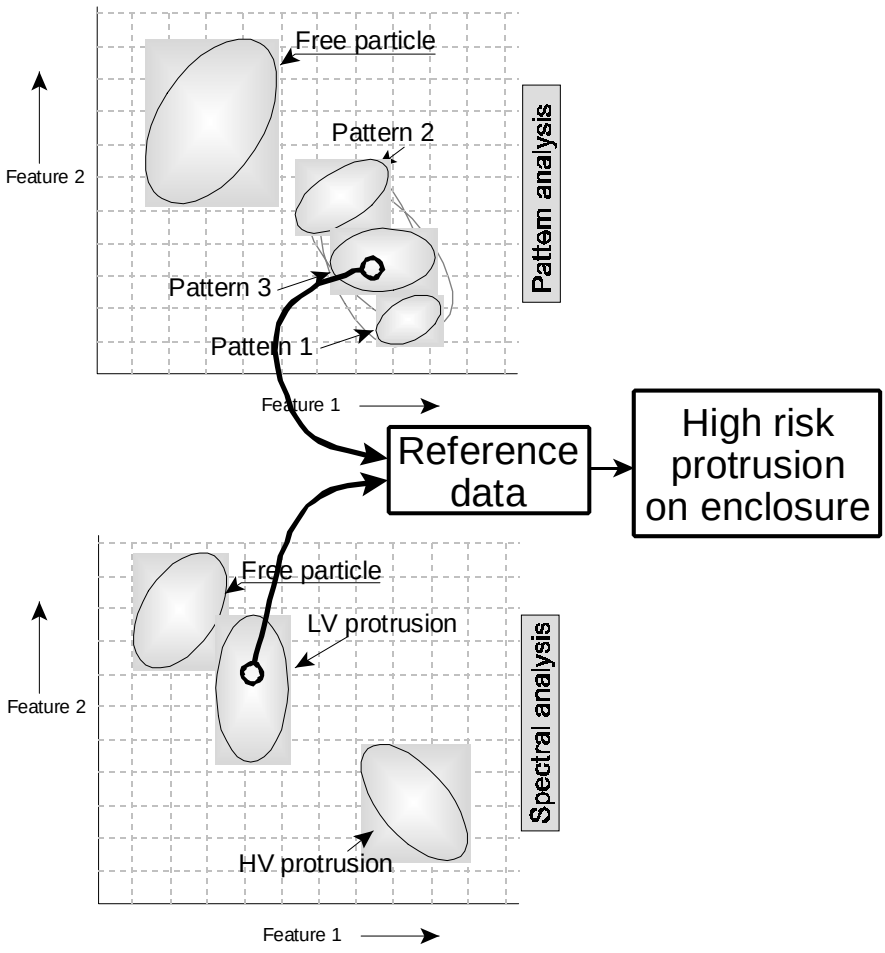

Figure 57: Risk assessment of a fixed protrusion for the insulation condition under AC conditions.

8.2. Conclusions

Similar types of defects occurring in GIS can be expected in GIL.

In contrast to GIS where pure SF_6 is used as an insulating gas, SF_6-N_2 gas mixtures will be used in gas-insulated lines. The difference in the influence of defects on the gaseous insulation are:

- Free particles show the same behavior in the investigated gases. The gas has no significant influence on the PD quantities from free particles;
- PD activity from protrusions fixed to the conductor strongly depends on the type of gas. In gaseous insulation with the same dielectric strength, the margin between inception of the PD activity and the actual breakdown of the gas decreases with decreasing SF_6 content for the same protrusion.

Critical defects:

For GIS critical fixed protrusions and particles fixed to insulator surfaces are difficult to detect on-line. However, such defects are often removed during commissioning.

Part of the free particles of critical length can be detected by on-line monitoring. Therefore, particle traps provide a good means to remove critical particles during service life.

The same PD detection methods can be used. However, due to the long lengths UHF or VHF PD monitoring are the most suitable ones. Acoustical detection is not possible in case of buried GIL.

The same methods to recognize defects in GIS are applicable in GIL.

Same procedures to assess the risk of defects on the insulation condition of the GIS are applicable in GIL.

8.3. References of chapter 8

[64] IEC Publication 270, *Partial Discharge Measurements*, 2nd Edition, 1981.

[65] L.E. Lundgaard, M. Runde, B. Skyberg, *Acoustic diagnosis of SF_6 gas insulated substations: a theoretical and experimental basis*, IEEE Transactions on Power Delivery, Vol. 5, No. 4, pp. 1751-1759, Oktober 1990.

[66] H.D. Schlemper, R. Kurrer and K. Feser, *Sensitivity of on-site partial discharge detection in GIS*, Proc. 8th Int. Symp. On HV Engineering, Yokohama, Vol. 3, 157-160, 1993.

[67] B.F. Hampton, R.J. Meats, *Diagnostic measurements at UHF in gas insulated substations*, IEE Proceedings, Vol. 135, Pt. C, No. 2, pp. 137-144, 1988.

[68] J.S. Pearson, B.F. Hampton, A.G. Sellars, *A continuous UHF monitor for gas- insulated substations*, IEEE Transactions on Electrical Insulation, Vol. 26, No.3, pp. 469-478, 1991.

[69] I. Herbst, *PD-measurement in GIS – A theoretical and experimental comparison of different electrical measurement techniques*, CIGRÈ symposium Berlin 1993, paper 130-02.

[70] A. Bargigia, W. Koltunowicz, A. Pigini, *Detection of Partial Discharges in Gas Insulated Substations*, IEEE Trans. on Power Delivery, Vol. 7, No. 3, pp. 1239-1249, July 1992.

[71] A. Krivda, *Automated Recognition of Partial Discharges*, IEEE Trans. on Dielectrics and Elec. Insulation, Vol. 2 No. 5, pp. 796-821, 1995.

[72] E. Gulski, Computer-aided Recognition of PD Using Statistical Tools, Delft University Press, 1991.

[73] R. Kurrer, K. Klunzinger, K. Feser, N. de Kock, D. Sologuren, *Sensitivity of the UHF-method for Defects in GIS with Regard to On-line Partial Discharge Detection*, IEEE International Symp. On Electr. Insulation, pp. 95-98, Montreal, 1996.

[74] N. de Kock, B. Coric, R. Pietsch, UHF PD Detection in Gas-Insulated Switchgear - Suitability and Sensitivity of the UHF method in Comparison with the IEC 270 method, IEEE Electrical Insulation Magazine Vol. 12, No. 6.

[75] J.S. Pearson, O. Farish, B.F. Hampton, M.D. Judd, D. Templeton, B.M. Pryor, I.M. Welch, *Partial Discharge Diagnostics for Gas Insulated Substations*, IEEE Trans. on Dielectrics and Elec. Insulation, Vol. 2 No. 5, pp. 893-905, 1995.

[76] L.Cremer, M.Heckel, E.E.Ungar: “Structure borne sound”, Springer Verlag, Berlin, 1988, ISBN 0-387-1241-1 (US).

[77] L.Lundgaard, B.Skyberg: "Acoustic signals from corona discharges in GIS", Published CEIDP, Knoxville 1991, pp 449-456.

[78] L.E. Lundgaard, B. Skyberg, A. Schei, A. Diessner, *Method and Instrumentation for Acoustic Diagnoses of GIS*, CIGRE-report 15-309, Paris, 2000

[79] Working Group 15.03, *Diagnostic Methods for GIS Insulating Systems*, CIGRE session 1992, paper 15/23-01.

[80] K. Feser, R. Kurrer, *Insulation Monitoring of Gas-Insulated Substations with Respect to Life Cycle*, Tutorial In-Service Diagnostics of High Voltage Power Apparatus, ISH 1997.

[81] M.M. Morcos, S.A. Ward, H. Anis, K.D. Srivastava, S.M. Gubanski, *Insulation integrity of GIS/GITL System and Management of Particle Contamination*, IEEE Electrical insulation magazine, Vol. 16, No. 5, pp. 25-37, September/October 2000.

[82] S. Meijer, E. Gulski, J.J. Smit, *Pattern Analysis of Partial Discharges in SF_6*, IEEE Trans. on Dielectrics and Electrical Insulation, Vol. 5, No. 6, pp. 830-842, December 1998.

[83] S. Meijer, E. Gulski, J.J. Smit, R. Brooks, *Comparison of Conventional and VHF/UHF Partial Discharge Detection Methods for SF_6 Gas Insulated Systems*, 10th Int. Symp. on HV Engineering, Montreal, Vol. 4, pp. 187-190, 1997.

[84] S. Meijer, *PD diagnosis of high-voltage gas-insulation systems*, Thesis to be printed.

[85] E. Gulski, *Digital analysis of partial discharges*, IEEE Trans. on Dielectrics and Elec. Insulation, Vol. 2 No. 5, pp. 822-837, 1995.

[86] Cigre working group 15.03, Effects of Particles on GIS insulation and the Evaluation of Relevant Diagnostic Tools, CIGRE, Vol. I, paper 15-103, 1994.

[87] T. Huecker, J. Gorablenkow, *UHF partial discharge monitoring and expert system diagnosis* IEEE Trans. on Power Delivery, Vol. 13 No. 4, pp. 1162-1167, 1998.

[88] J. Pearson, B.F. Hampton, M.D. Judd, B. Pryor and P.F. Coventry, *Experience with Advanced In-service Condition Monitoring Techniques for GIS and Transformers*, IEE Colloquium on Condition Monitoring and Associated Database Handling Strategies (Ref. No. 1998/448), 1998.

[89] T. Irwin, J. Lopez-Roldan, C. Charlson, *Partial discharge detection of free moving particles in GIS by the UHF method: recognition pattern depending on the particle movement and location*, Power Engineering Society Winter Meeting, Volume: 3, 2000, pp. 2135 –2140

[90] Society for Risk Analysis, *Glossary of Risk Analysis Terms*, www.sra.org, September 26, 2000.

[91] H.-D. Schlemper, K. Feser, *Characterization of moving particles in GIS by acoustic and electric partial discharge detection*, 10th ISH 1997, Montreal

9. Bonding and Grounding for permanent and transient voltage

The grounding of Gas Insulated Line must be adapted to the different service conditions represented by normal service, short circuit and over-voltage conditions. The disposition of the GIL (buried, in a tunnel, in a trench) and the possibility to have low voltage equipment as densimeters, temperature sensors or partial discharge monitoring systems connected on the enclosure has to be considered when the grounding mesh is studied. The design of the grounding system must provide all the safety regarding the persons and the equipment in case of potential rise.

9.1. General definitions:

The definition referred to the figure 58

9.1.1. Step voltage

The 'step voltage' e_s is the greatest potential difference liable to appear between two points which are a step's length apart.

9.1.2. Touch voltage

The 'touch voltage' e_t is the greatest potential difference which is liable to appear between the surface of the ground and any conducting structure connected to the electrode.

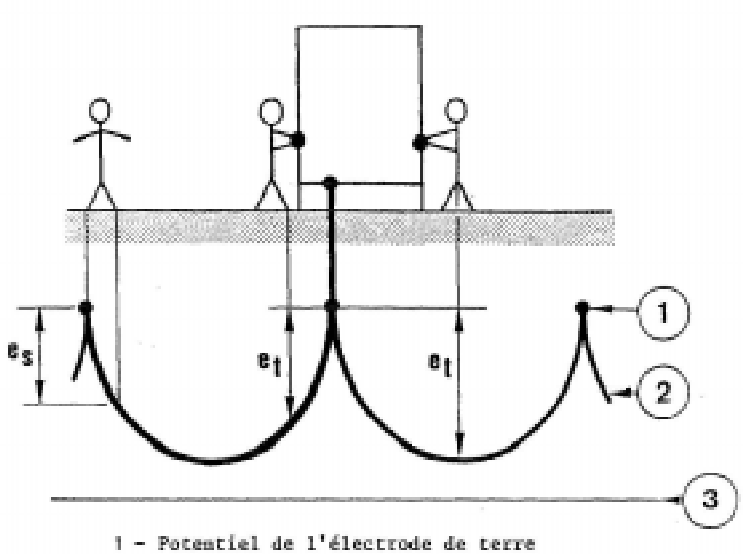

1 - Potentiel de l'électrode de terre
Potential of earth electrode
2 - Variation du potentiel à la surface du sol pendant un défaut phase-terre
Variation in potential at the surface of the ground during a phase-earth fault
3 - Potentiel du sol lointain
Potential of the remote earth

Figure 58 : definition of step and touch voltage

9.2. Maximum admissible voltage

The duration of the current and the weigh of the person are parameters which influence the maximum allowable body current. Based on the ANSI/IEEE Standard 80 [92] the following rules can be taken into account for the calculation of the body current.

$$I_{ballowable} = \frac{0.116}{\sqrt{t}} \text{ amperes for a 50 kg body} \quad I_{ballowable} = \frac{0.157}{\sqrt{t}} \text{ amperes for a 70 kg body} \qquad (34)$$

$t = \text{duration (s) of the current}$

The touch voltage and the step voltage depend on the resistance of the human body (Rb) and the foot resistance (Rf). In ANSI/IEEE Standard the resistance of human body is assumed to be 1000Ω and the foot resistance equal respectively to 6ρ and 1.5ρ for the step and the touch voltage.

Thus for a 50kg body:

$$V_{touch,allowable} = (1.5\rho + 1000)\frac{0.116}{\sqrt{t}}\ volts$$
$$V_{step,allowable} = (6\rho + 1000)\frac{0.116}{\sqrt{t}}\ volts \qquad (35)$$
$$\rho = resistivity\ of\ the\ soil\ (\Omega.m)$$

The step and the touch voltage should not exceed the foregoing values for a safe grounding system. As a general rule the touch voltage has to be maintained around 50V in case of short circuit condition The computation of the voltage can be done by dedicate software modelling the substation and its grounding system.

9.3. Calculation of touch voltage and circulating current

The calculation of step voltage or touch voltage for short circuit conditions can be performed using several PI model in series for the representation of the GIL. The matrix of resistance, inductance and capacitance has to be evaluated taking into account:

- The geometry of the problem(diameter of conductors, position in or above the ground),
- The skin effect,
- The effect of mutual if more than two conductors are modelized,
- The resistivity and the distribution of the current in the soil,
- The inductance and resistance of grounding and bonding connections

A particular problem lies in the calculation of the impedance term taking into account correctly the return current in the soil. Carson and Pollaczeck have developed a theory to study the current distribution based on the fact that they are concentrated on particular fictive surfaces [93], [94]. Considering a single layer the depth of the current return can be approximated with the formula

$$p = \sqrt{\frac{\rho}{\omega\mu_0}}$$
with (36)
$$\rho = earth\ resistivity\ \Omega.m$$

EMTP program [95] provides some facilities to determine the coefficients of the inductance and capacitance matrixof a GIL burried or above the ground.

In case of a single line GIL located above the ground, the following formula can be used for an approximation of the inductance and capacitance of the GIL taking into account its geometrical characteristics and the effect of the soil (figure 59).

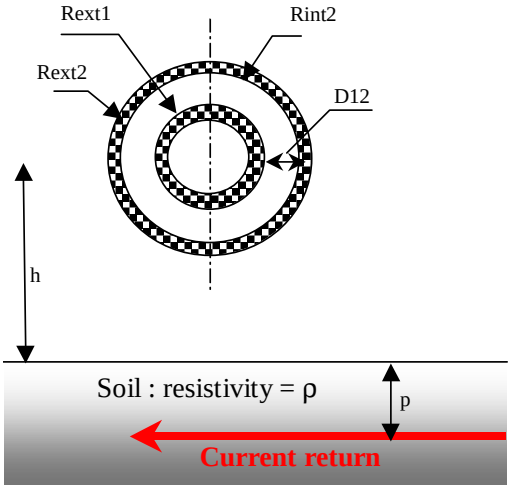

Figure 59 : Geometrical parameters of the GIL

$$Inductance\ matrix = \begin{bmatrix} L_{11} & L_{12} \\ L_{21} & L_{22} \end{bmatrix}$$

Where

$$L_{11} = \frac{\mu_0}{2 * \pi} ln\left(\frac{2(h+p))}{Re\,xt_1}\right) \qquad L_{22} = \frac{\mu_0}{2 * \pi} ln\left(\frac{2(h+p)}{Re\,xt_2}\right) \tag{37}$$

$$L_{12} = \frac{\mu_0}{2 * \pi} ln\left(\frac{2(h+p))}{D_{12}}\right) = L_{21}$$

L_{ii} = self inductance, per unit length, of the loop formed by the conductor i and the ground return

L_{ij} = mutual inductance, per unit length, between conductor i and j.

$$Capacitance\ matrix = \begin{bmatrix} C_{11} & -C_{12} \\ -C_{21} & C_{22} \end{bmatrix}$$

Where

$$C_{ii} = C_{i\,/\,earth} + \sum_j C_{ij} \tag{38}$$

$$C_{ij} = 2\pi\varepsilon_0\varepsilon_r \frac{1}{ln\left(\frac{R\,int_i}{Re\,xt_j}\right)} \qquad C_{i\,/\,earth} = 2\pi\varepsilon_0\varepsilon_r \frac{1}{ln\left(\frac{Re\,xti}{h}\right)}$$

C_{ii} = sum of the capacitances, per unit length, between conductor i and all other conductors as well as ground.

C_{ij} = mutual capacitance, per unit length, between conductor i and j.

9.3.1. Touch voltage in short circuit conditions

The touch voltage depends on the location and the number of grounding wires as well as the location of the fault. The following chapter presents the calculation based on different cases to estimate a reasonable rule for the earthing circuit. The calculations are performed in the most critical case corresponding to a short circuit fault.

The touch voltage is calculated on a 500m, single phase GIL, formed with five sections of 100 m (figure 60). The GIL is considered to be located above the soil at a distance of one meter. The enclosure and the internal conductor are made of aluminum. The fault current is limited by an inductance to 50 kA. The soil resistivity is fixed to 20 Ohm.m. The results are presented in table 22.

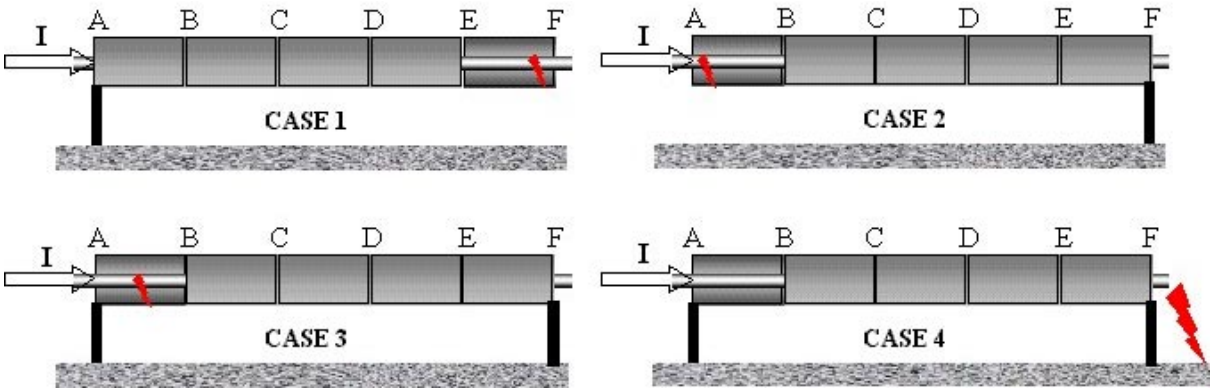

Figure 60 : définition of fault cases and grounding system

The touch voltage can largely overtakes the maximum allowable touch voltage when the enclosure is grounded on only one side. The drop of voltage along the enclosure is the sum of a resistive term corresponding to the electrical resistance of the enclosure (equal in case 1 and 2) and an inductive term depending on the path of the return current. The high inductance of the loop, due to the complete return of current by the soil, explains the high values of the touch voltage in case n°2. The current return, in case n°1, is done by the external enclosure providing a lower inductance. The benefic effect is a reduction of the touch voltages.

In case of a fault located outside the GIL with a grounding at each side of the GIL, the mutual coupling effect between the internal conductor and the enclosure leads to create a circulating current in the enclosure equal to the one in the conductor. Nevertheless the touch voltage does not exceed the maximum allowable values

In case of a grounding on both side, the distance between the two grounding paths can reach more than 500m without risk to exceed the maximum allowable touch voltage define in the § 9.2. The protection of low voltage equipment and persons is insured in such conditions.

Table 22 : Touch voltage at different sections of a GIL

		Touch voltage [V]					
	Fault position	A	B	C	D	E	F
Case 1	F	2.7	13	23.5	34	44.5	55
Case 2	A	11130	8900	6680	4450	2220	0.42
Case 3	A	2.8	2.2	1.7	1.1	0.56	6.6E-4
	B	2.7	10.6	7.9	5.3	2.65	3E-4
	C	2.7	8.4	14	9.5	4.7	5.6E-4
	D	2.7	6.4	10	13.7	6.8	1.2E-3
	E	2.7	4.2	5.8	7.4	8.9	1E-2
	F	2.7	2.2	1.7	1.1	0.6	1.2E-2
Case 4	outside	2.7	1.7	0.57	0.52	1.6	2.7

9.3.2. Circulating currents

The circulating currents are calculated on a 500 m long GIL (figure 61) formed by three independent phases comprising five portions of 100 m for each one. For the purpose of the study both ends are connected to the ground by a resistance and an inductance of respectively 5Ω and 2μH representing the resistance and the inductance of the wire and of the grounding point. The intermediate points of the enclosure section can be bounded. The GIL is considered to be located above the soil at a distance of one meter with a distance between phases of 1.5 meters.

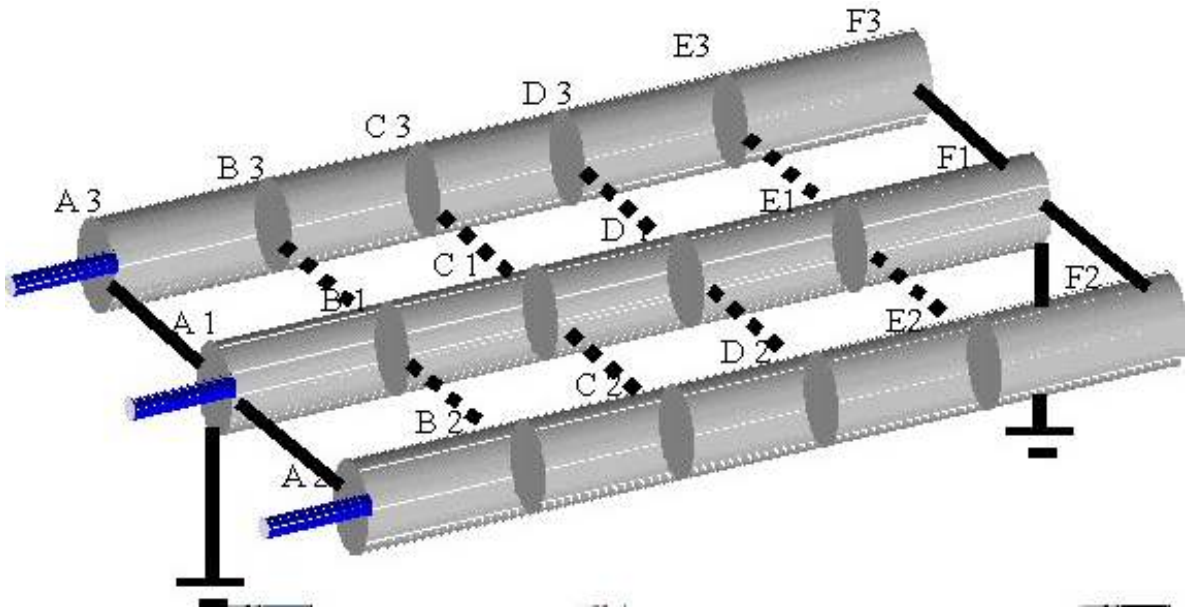

Figure 61 : Scheme of the GIL configuration

9.3.2.1. Normal service conditions

The current distribution (figure 62) in each enclosure is calculated with two configurations of earthing and bonding system.

The bounds between the three phases provide a return current in the enclosure which partially balance the current in the conductor. The resulting magnetic field is reduced by more than 90% by the current circulation in the enclosure.

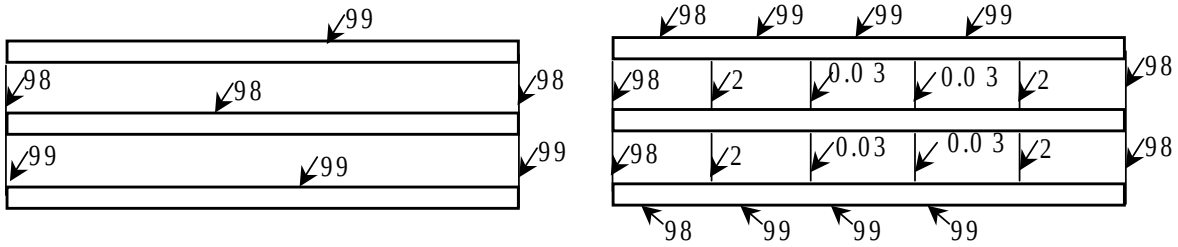

Figure 62 : Current distribution [%] bounded at each end (left) bounded at each section (right)

9.3.2.2. Short circuit conditions

The GIL is considered to be earthed at each ends. A single phase and a three phase faults on the overhead line connected to the GIL is taken into account in this study. The short circuit and the rated current is limited respectively to 50kA and 2000A. The figure 63 and figure 64 display the current distribution as a percentage of the short circuit current.

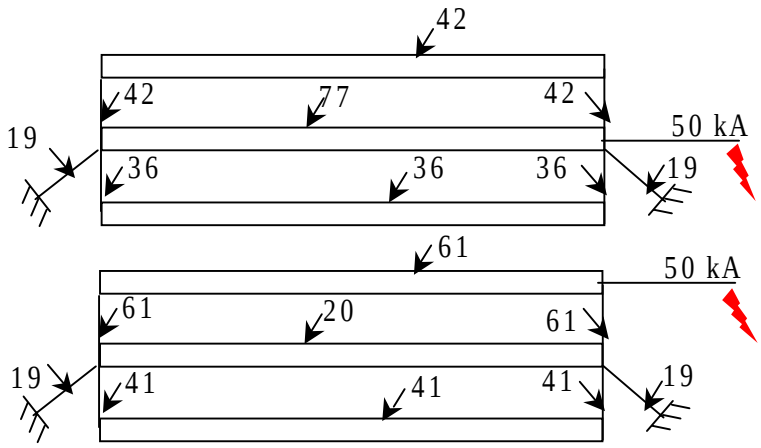

Figure 63 : Current distribution in case of single phase fault

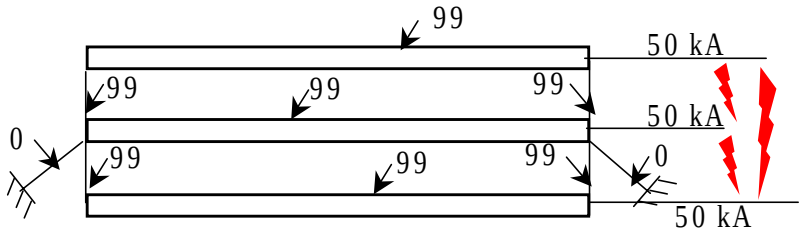

Figure 64 : Current distribution in case of a three phase faults

The single phase fault contributes to an non homogeneous distribution of current in the enclosures. The phase on which the fault occurs carries more than 60 % of the short circuit current, where as the two others take part for 20 to 45%. The current in the grounding wire is limited by the resistance of the earthing foot.

The three phase faults is similar to the normal conditions of service. The circuit can be represented by a balanced system and the current in the grounding wire becomes negligible.

9.4. General recommendations for bonding and grounding GIL

In addition to the optimization of the grounding system by calculation with dedicated program some basic recommendations can be formulated to avoid major troubles during operation of the GIL.

For short length GIL (less than 500 m), the GIS design rules are applicable [97]. For longer ones , the design must be done taking into account the Technical Report IEC 61640 [98].

Table 23 : Touch voltage at different sections of a GIL

Service conditions	Dispositions	Reasons
normal service conditions	• solid bonding at both ends • low impedance grounding connection at both ends	• induced sheath current circulation to avoid magnetic induction on the neighborhood • reduction of induced e.m.f along the enclosure • enclosure at or near ground potential
short circuit current (internal or external fault)	• multiple grounding connections • multiple solid bonds	• reduction of enclosure phase to ground touch voltage • reduction of enclosure phase to phase touch voltage
over-voltages (lightning, switching, very fast transient)	• electrical connections between each section of the enclosure • electrical connection of each metallic support to the enclosure • Protection with non linear resistors	• prevention of flash-over between the different sections of the enclosure, protection of electronic equipment • prevention of flash-over between metallic support and enclosure • limitation of transient enclosure voltages

9.5. Examples of application

9.5.1. GIL as outdoor application :

Tepco has installed in 1988 a 138m and 158m GIL in Shin Noda substation [99]. The enclosures are solidly bonded at both ends and three time along the line. The calculations performed on this configuration (figure 65) pointed out that the current flowing in the enclosure balance the conductor current. The magnetic field is decreased and the induced voltage is consequently eliminated.

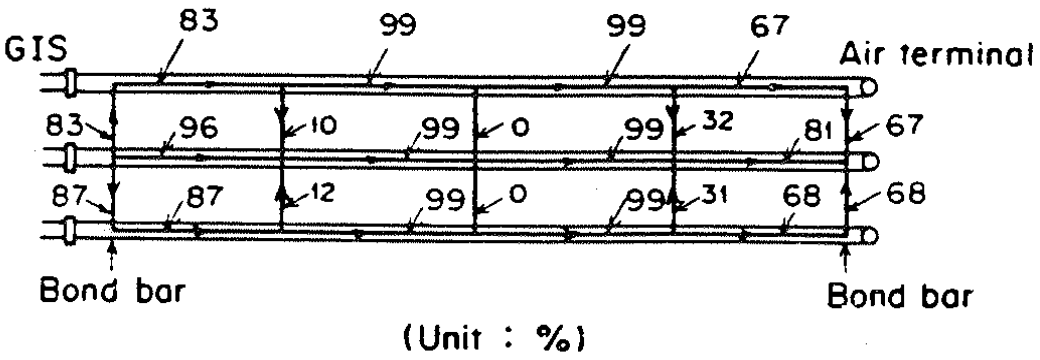

Figure 65 : Calculated circulating current in enclosure

Earthing conductors are buried parallely to the GIS to reduce the induced voltage between the enclosure and the ground (figure 66). They are connected to the earthing mesh of the substation and the earthing of the tower The effect of the earthing mesh regarding the transient voltage of the enclosure is improved by grounding points at both ends and at each bonding system.

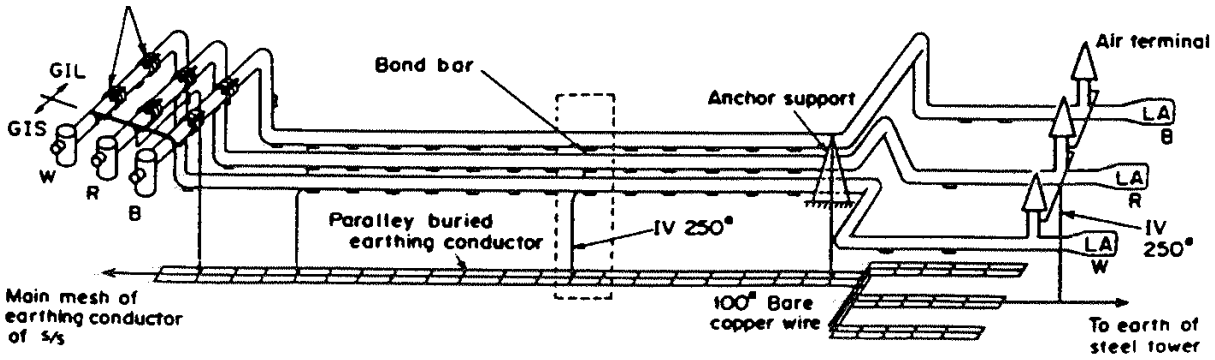

Figure 66 : Grounding system diagram

9.5.2. GIL installed in a tunnel :

Chubu electric has installed a 3.25 km length GIL double circuit between two GIS substations. The grounding system adopted for the Shinmeika Tokai line project is presented in figure 67. The following conditions are applied. The enclosure are solidly bounded and earthed at both ends. Earthing conductors, embedded in the concrete of the tunnel are connected to the mesh of the substation. The supports located along the line are connected to the earthing conductors and to the enclosure.

Transient enclosure voltage measurement has been performed during circuit-breaker and disconnector operations. The maximum voltage is observed at the insulated flange separating the GIL from the GIS. This high frequency voltage is limited by the use of surge arresters at about 20kV. The maximum voltage measured on the enclosure, close to the support, are below 7 kV and they correspond to high frequency waveforms which will not be critical for the persons.

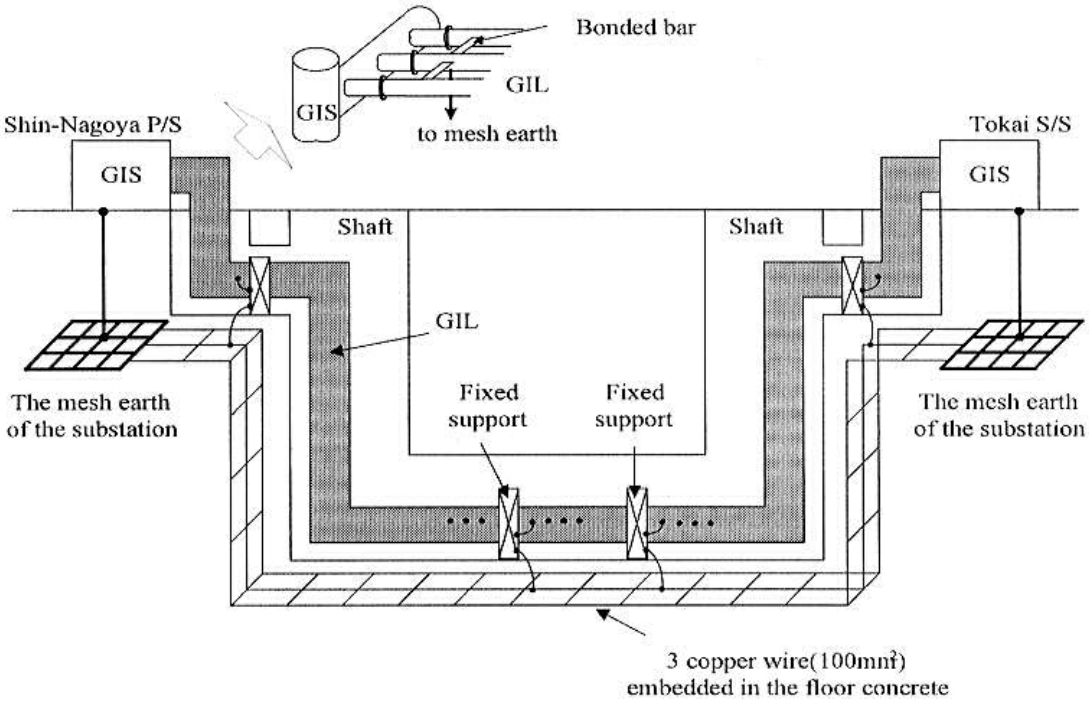

Figure 67 : Earthing circuit

9.6. References of chapter 9

[92] ANSI/IEEE Standard 80, IEEE Guide for the safety in AC substation grounding, 1986

[93] Carson "Wave propagation in overhead wires with earth return", Bell System technical journal Oct 1926 n°5 p 539-554

[94] Pollaczek, "Sur le champ produit par un conducteur simple infiniment long parcouru par un courant alternatif", traduit par Pomey , Revue générale d'electricité 30 mai 1931, p 851-867

[95] Electro-magnetic Transients Program : Theory book , Bonneville Power Administration, Portland Oregon

[96] P. Clarenne, G. Ebersohl, J. Vigreux, G. Voisin : " The effect of high frequency transient voltage on the secondary equipement in gas-insulated substations », Electra N°126, pp 94-116

[97] John Lewis WG 23.10 " Earthing of GIS – an application guide" , Electra N°151, pp 31 –51

[98] Technical report IEC 61640 First edition 1998-07

[99] Y. Kuroyanagi, A. Toya, T. Hayashi, T. Araki: " Construction of a 8000A class 275kV insulated transmission line", IEEE Power delivery Vol 5, n°1 January 1990.

[100] A. Miyazaki and Al "Line constant measurements and loading current test in long distance 275kV GIL",IEEE Transaction on Power Delivery, Vol 16, No 2, pp165-170, 2001

10. References

10.1. References of chapters 1 and 2

[1] IEC standard 60071-1: "Insulation Co-ordination Part 1: Definitions, principles and rules règles", seventh edition, 1993-12

[2] G. Carrara, E. Occhini, L. Paris, F. Reggiani: "Contribution to the study of insulation coordination from the probabilitic point of view", CIGRE report 421, CIGRE general session 1966.

[3] IEEE Std 1313.2-1999: "IEEE Guide for the application of Insulation Coordination".

[4] A. R. Hileman, R. W. Flugum, T. F. Garrity : "Lightning insulation coordination for a 600 kV DC gas insulated cable", IEEE transactions on Power Apparatus and Systems, Vol PAS-101, n°11November 1982, pp4399-4406.

[5] A. Sabot, D. Santos, X. Waymel, D. Feldmann, Y. Maugain., "Insulation co-ordination of 420 kV gas insulated lines" session CIGRE 1998,rapport 21-303.

[6] A. Sabot: "Insulation co-ordination and on line Insulation Monitoring & Diagnostic techniques for Gas Insulated Switchgear (GIS)" CIGRE Session 2000, Panel session on "Modern Maintenance Techniques for Efficient System Operation", report P1-09.

[7] Nojima, T, Shimizu, M, Araki, T, Hata, H, Yamauchi, T „Installation of 275 kV - 3.3 km gas-isulated transmission line for underground large capacity transmission in Japan“, CIGRE 1998

[8] CIGRE WG 33/23-12 : "Insulation Coordination of GIS : return of experience, on site tests and diagnostic techniques" - Electra n° 176, February 1998.

[9] T.M. Chan, F. Heil, D. Kopejtkova, P. O'Connell, J.-P. Taillebois, I. Welch : "Report on the second International survey on high voltage gas insulated substations (GIS) service experience", Session CIGRE 1998, rapport 23-102

[10] Aucourt C., Boisseau C., Feldmann D.: "Gas insulated cables : from the state of the art to feasibility for 400 kV transmission lines ", Jicable,1995

10.2. References of chapter 3

[11] W. Mosch, W. Hauschild, Hochspannungsisolierungen mit Schwefelhexafluorid, VEB Verlag Technik, Berlin, 1979, ISBN 3-7785-0540-8.

[12] F.H. Kreuger, Industrial High Voltage, Vol. I, Delft University Press, 1991.

[13] A. Diessner, H. Koch, E. Kynast, A. Schuette, Progress in High Voltage Testing of Gas Insulated Transmission Lines, ISH 1997, Volume 4, pp. 41-44.

[14] G.P. Baer, A. Diessner, G.F. Luxa, 420 kV SF6-insulated tubular bus for the Wehr Pumped-Storage plant- electric tests, IEEE Trans. On Power App. & Systems, Vol PAS-95 (1976), pp. 469-477

[15] C. Aucourt, C. Boisseau, D. Feldmann, Gas insulated cables: from the state of the art to feasibility for 400 kV transmission lines, Proc. Of Jicable 95 conference, Versailles, France, 1995, pp. 133-138.

[16] CIGRÉ Working Group 23.02, Guide For SF6 Gas Mixtures, CIGRÉ Brochure 163, August 2000.

[17] L.G. Christophorou and R.J. Van Brunt, SF6-N2 mixtures Basic and HV insulation properties, IEEE Transactions on Dielectrics and Electrical Insulation, Vol. 2 No. 5, October 1995.

[18] L.G. Christophorou, Electron-molecule interactions and their applications, Volume 2, Academic Press inc., Orlando, 1984, ISBN 0-12-174402-7.

[19] T.B. Diarra, A. Béroual, F. Buret, E. Thuries, M. Guillen, Ph. Roussel, N2-SF6 mixtures for High Voltage Gas Insulated Lines, 10th Int. Symp. on HV Engineering, Montreal, 1997.

[20] CIGRE WG 33/23-12: “Insulation co-ordination of GIS: return of experience, on site tests and diagnostic technique”, Electra n 176

[21] A.H. Cookson, B.O. Pedersen: “Analysis of the high voltage breakdown results for mixture of SF_6 with CO_2, N_2 and air.” 3rd ISH Milan 1979, paper 31.10

[22] J. Yingshen, L. Ming, J. Yanjun, L.Hao, W. Yihua: “Breakdown characteristics of particle-contaminated SF_6 SF_6/N_2 in a large coaxial system.”, 6th ISH New Orleans 1989, paper 32.14

[23] S.D. Nielsen, D.A. Reynders, J.P. Reynders, I.R. Jandrell, R.J. Traynor: “An assessment of the sub-microsecond region of VFT V-T curves generated in pure SF_6 and 50%SF_6/N_2 gas mixture under small values of bus bar surface roughness.” 9th ISH Graz1995, paper 2282

[24] B. T. Diarra: “Etude de la tenue dielectrique dans les cables haute tensione a isolation gazeuse”. Thesis for doctor degree. Discussed on 20th December 1996 at Ecole Central de Lyon

[25] L. G. Christophorou, J. K. Olthoff and D. S. Green: “Gases for electrical insulation and arc interruption: possible present and future alternatives to pure SF_6”. NIST Technical Note 1425

[26] M. Eteiba, F.A.M. Rizk, N.G. Trinh, C. Vincent, “Influence of a conducting particle attached to an epoxy resin spacer on the breakdown voltage of compressed gas insulation”, Gaseous Discharge II. Pergamon press 1980, pp250-254

[27] A. H. Cookson, “Electrical breakdown studies of SF_6/CO_2/Fluorocarbon mixtures”, Gaseous Discharge II. Pergamon press 1980, 169-178

[28] W. Pfeiffer, V. Zimmer, P. Zipfl, “Predischarge development and dielectric strength of N_2, SF_6 and SF_6/N_2 mixtures in strong non-uniform electrical fields”, 7 ISH, Dresden August 1991. Paper 32.14

[29] S. Meijer. E. Gulski, T.S. Ramu, A. Girodet, “Performance of GIS under 5% SF_6-N_2 gas mixture insulation”, Record of the CIGRE WG 15.03 Conference “Insulating gases”. Arnhem, Netherlands, March 4-5, 1999

[30] H. Koch, “Gas mixtures as insulating gas”, CIGRE 1998 Joint session 21/23/33. Pref. Sub. 3.1 Question 1.2

[31] M.O. Pace, D.L. McCorkle, X. Waymel, “Possible high pressure nitrogen based insulation for compressed gas insulated cables”, CEIDP ’95. Virginia Beach 22-25 October 1995

[32] X. Waymel, “Low SF_6 concentration SF_6/N_2 mixtures for GIL”, VII Symposium International on Gaseous Dielectrics. Virginia Beach; June 1998

[33] M. Guillen, F. Buret, A. Beroual, “Lightning impulse withstand of a gas-insulated line filled with N_2/SF_6”, 11 ISH London 23-27 August 1999 paper 3.71.S18

[34] G. Schröder, “Discharge development in SF_6-N_2 mixtures under fast oscillating impulse conditions”, 11 ISH London 23-27 August 1999 paper 3.79.S18

[35] C. Gailac, “GIS disconnector model performance with SF_6/N_2 mixtures”, 11 ISH London 23-27 August 1999 paper 3.104.S20

[36] A. Diessner, M. Finkel, A. Grund, E. Kynast, “Dielectric properties of N_2/SF_6 mixtures for use in GIS or GIL”, 11 ISH London 23-27 August 1999 paper 3.67.S18

[37] X. Waymel, V. Delmon, T.Rees, A. Gibert, P. Domens, “Impulse breakdown in point plane gaps in SF_6/N_2 mixtures”, 10 ISH Montreal 25-27 August 1997

[38] H.I. Marsden, M. D. Hopkins, C. R. Eck, “Power frequency and SIL withstand performance of GIC with a and 10 percent SF_6/N_2 mixtures”, VII Symposium International on Gaseous Dielectrics. Virginia Beach; June 1998

[39] H.I. Marsden, S. J. Dale, M. D. Hopkins, C. R. Eck, “High voltage performance of a gas insulated cable with N_2 and SF_6/N_2 mixtures” , 10 ISH Montreal 25-27 August 1997

[40] A. Moukengué Imano, R. Schurer. K. Feser, “The influence of a conducting particles on a spacer on the insulation properties in SF_6/N_2 mixtures” , 11 ISH London 23-27 August 1999 paper 3.232.P3

[41] L. Pécastaing, T. Reess, P. Espel, J. Paillol, A. Gibert, P. Domens, “Investigation of breakdown characteristics of N_2, SF_6 and SF_6-N_2 mixtures under pressure” , 11 ISH London 23-27 August 1999 paper 3.224.P3

[42] S.A. Ward, “Influence of conducting particles on the breakdown voltages of SF_6-N_2 mixture”, 11 ISH London 23-27 August 1999

[43] D. A. Reynders, J. P. Reynders, I. R. Jandrell, “ VFT V-T curves for SF_6 and SF_6:N_2 = 1:1 in a 180/110 mm coaxial duct at pressure of 1 and 2 bar with small values of surface roughness” , 11 ISH London 23-27 August 1999 paper 3.264.P3

[44] H. Hama, K. Inami, M. Yoshimura, “Practical Problems in applying N_2/SF_6 gas mixtures to gas insulated bus”,TF2 IWD64

[45] M. Yoshimura, K. Inami, H. Hana, H. Fujii: "Area Effect of Breakdown at lightning Impulse in N_2/SF_6 mixtures" Gas Discharge 2000, Glasgow.

10.3. References of chapter 4

[46] Hileman, A.R.; Flugum, R.W.; Garrity, T.F.: "Lightning insulation Coordination for a 600 kV DC Gas insulated cable", IEEE Transactions on Power Apparatus and Systems, Vol. PAS-101, No 11 November 1982

[47] Sabot, A.: "Insulation Co-ordination Procedure for 420 kV Gas Insulated Lines (GIL)"; :ISH 1999, London

[48] Völcker, O.; Koch, H.: "Insulation Co-ordination for Gas-Insulated Transmission Lines (GIL)" IEEE Transactions on power delivery, Vol. 16, No. 1, January 2001

[49] Schnettler, A.; Balzer G.; Hudasch M.; Johnnerfelt B.: "Protection of high voltage equipment by polymer housed surge arresters", CIGRE-Session 1998, paper 33-302

10.4. References of chapter 5 and 6

[50] IEC standard 60071-2: " Insulation Co-ordination Part 2: Application guide", third edition, 1996-12

[51] W. Hauschild, W. Mosch: "Statistical techniques for high voltage engineering", IEE Power series 13, Peter Peregrinus, ISBN 0 86341 205 X

[52] G.W. Brown, R. Samm, J. Cronin: "AC analysis and testing of realistically contaminated gas-insulated systems", IEEE transactions on PAS, Vol. PAS-97, JAn/Feb 1978, pp59-67

[53] A. Sabot, D. Santos, X. Waymel, D. Feldmann, Y. Maugain., "Insulation co-ordination of 420 kV gas insulated lines" session CIGRE 1998,rapport 21-303.

[54] CIGRE WG 33/23-12 : "Insulation Coordination of GIS : return of experience, on site tests and diagnostic techniques" - Electra n° 176, February 1998.

[55] CIGRE WG 23.10/TF 03: "User guide for the application of gas-insulated switchgear (GIS) for rated voltages of 72.5 kV and above", CIGRE brochure 125, April 1998

[56] A. Sabot: " Insulation Co-ordination Procedure for 420 kV Gas Insulated Lines", Eleventh Symposium on High-Voltage Engineering ISH 99, London, 23-27 August 1999, IEE conference publication N°467, volume 3, topic D, report 3.1.S18.

[57] P. Hoegg, W. Schmidt, H. Stasser : "Conception de l'appareillage blindé, isolé au SF_6 pour atteindre une haute sûreté de service", Session Gigré de 1972, rapport 23-10.

10.5. References of chapter 7

[58] Baer, G.; Dießner, A.; Luxa, G.: "420 kV SF6 insulated tubular bus for the Wehr pumped-storage plant; electric tests", IEEE Transactions on Power Apparatus and Systems, Vol. PAS-95, no. 2, March/April 1976

[59] Miyazaki, A.; Hiroyuki, H.; Hideaki, N.: "275 kV Shinmeika-Tokai GIL for long distance bulk-power transmission in a tunnel", IEEE PES Summer Meeting, Montreal, 1997

[60] Meinecke, H....: "Dimensioning criteria and test results for a polymer enclosed gas insulated line", CIGRE Session 2000, Report 21/23/33-01

[61] Feldmann, D....: "Development of a directly buried 400 kV Gas Insulated Line technology", CIGRE Session 2000, Report 21/23/33-02

[62] Koch, H. ...: "Electrical and mechanical long-time behavior of gas-insulated transmission lines"
CIGRE Session 2000, Report 21/23/33-03

[63] Murasawa, I.; Ichihara, M.; Kawai, T.; Miyazaki, A.; Takinami, N.: Development of long-distance 275 kV gas insulated transmission line (GIL), The Eleventh International Conference on Gas Discharges and their Applications, Chou University Tokyo September 11-15, 1995

10.6. References of chapter 8

[64] IEC Publication 270: Partial Discharge Measurements", 2nd Edition, 1981.

[65] L.E. Lundgaard, M. Runde, B. Skyberg: "Acoustic diagnosis of SF_6 gas insulated substations: a theoretical and experimental basis", IEEE Transactions on Power Delivery, Vol. 5, No. 4, pp. 1751-1759, Oktober 1990.

[66] H.D. Schlemper, R. Kurrer and K. Feser: "Sensitivity of on-site partial discharge detection in GIS", Proc. 8th Int. Symp. On HV Engineering, Yokohama, Vol. 3, 157-160, 1993.

[67] B.F. Hampton, R.J. Meats: Diagnostic measurements at UHF in gas insulated substations", IEE Proceedings, Vol. 135, Pt. C, No. 2, pp. 137-144, 1988.

[68] J.S. Pearson, B.F. Hampton, A.G. Sellars: A continuous UHF monitor for gas- insulated substations", IEEE Transactions on Electrical Insulation, Vol. 26, No.3, pp. 469-478, 1991.

[69] I. Herbst: "PD-measurement in GIS – A theoretical and experimental comparison of different electrical measurement techniques", CIGRÈ symposium Berlin 1993, paper 130-02.

[70] A. Bargigia, W. Koltunowicz, A. Pigini: Detection of Partial Discharges in Gas Insulated Substations", IEEE Trans. on Power Delivery, Vol. 7, No. 3, pp. 1239-1249, July 1992.

[71] A. Krivda: "Automated Recognition of Partial Discharges", IEEE Trans. on Dielectrics and Elec. Insulation, Vol. 2 No. 5, pp. 796-821, 1995.

[72] E. Gulski, Computer-aided Recognition of PD Using Statistical Tools, Delft University Press, 1991.

[73] R. Kurrer, K. Klunzinger, K. Feser, N. de Kock, D. Sologuren: "Sensitivity of the UHF-method for Defects in GIS with Regard to On-line Partial Discharge Detection", IEEE International Symp. On Electr. Insulation, pp. 95-98, Montreal, 1996.

[74] N. de Kock, B. Coric, R. Pietsch: "UHF PD Detection in Gas-Insulated Switchgear - Suitability and Sensitivity of the UHF method in Comparison with the IEC 270 method", IEEE Electrical Insulation Magazine Vol. 12, No. 6.

[75] J.S. Pearson, O. Farish, B.F. Hampton, M.D. Judd, D. Templeton, B.M. Pryor, I.M. Welch, *Partial Discharge Diagnostics for Gas Insulated Substations*, IEEE Trans. on Dielectrics and Elec. Insulation, Vol. 2 No. 5, pp. 893-905, 1995.

[76] L.Cremer, M.Heckel, E.E.Ungar: “Structure borne sound”, Springer Verlag, Berlin, 1988, ISBN 0-387-1241-1 (US).

[77] L.Lundgaard, B.Skyberg: "Acoustic signals from corona discharges in GIS", Published CEIDP, Knoxville 1991, pp 449-456.

[78] L.E. Lundgaard, B. Skyberg, A. Schei, A. Diessner, *Method and Instrumentation for Acoustic Diagnoses of GIS*, CIGRE-report 15-309, Paris, 2000

[79] Working Group 15.03, *Diagnostic Methods for GIS Insulating Systems*, CIGRE session 1992, paper 15/23-01.

[80] K. Feser, R. Kurrer, *Insulation Monitoring of Gas-Insulated Substations with Respect to Life Cycle*, Tutorial In-Service Diagnostics of High Voltage Power Apparatus, ISH 1997.

[81] M.M. Morcos, S.A. Ward, H. Anis, K.D. Srivastava, S.M. Gubanski, *Insulation integrity of GIS/GITL System and Management of Particle Contamination*, IEEE Electrical insulation magazine, Vol. 16, No. 5, pp. 25-37, September/October 2000.

[82] S. Meijer, E. Gulski, J.J. Smit, *Pattern Analysis of Partial Discharges in SF_6*, IEEE Trans. on Dielectrics and Electrical Insulation, Vol. 5, No. 6, pp. 830-842, December 1998.

[83] S. Meijer, E. Gulski, J.J. Smit, R. Brooks, *Comparison of Conventional and VHF/UHF Partial Discharge Detection Methods for SF_6 Gas Insulated Systems*, 10th Int. Symp. on HV Engineering, Montreal, Vol. 4, pp. 187-190, 1997.

[84] S. Meijer, *PD diagnosis of high-voltage gas-insulation systems*, Thesis to be printed.

[85] E. Gulski, *Digital analysis of partial discharges*, IEEE Trans. on Dielectrics and Elec. Insulation, Vol. 2 No. 5, pp. 822-837, 1995.

[86] Cigre working group 15.03, Effects of Particles on GIS insulation and the Evaluation of Relevant Diagnostic Tools, CIGRE, Vol. I, paper 15-103, 1994.

[87] T. Huecker, J. Gorablenkow, "UHF partial discharge monitoring and expert system diagnosis", IEEE Trans. on Power Delivery, Vol. 13 No. 4, pp. 1162-1167, 1998.

[88] J. Pearson, B.F. Hampton, M.D. Judd: B. Pryor and P.F. Coventry: "Experience with Advanced In-service Condition Monitoring Techniques for GIS and Transformers", IEE Colloquium on Condition Monitoring and Associated Database Handling Strategies (Ref. No. 1998/448), 1998.

[89] T. Irwin, J. Lopez-Roldan, C. Charlson: "Partial discharge detection of free moving particles in GIS by the UHF method: recognition pattern depending on the particle movement and location"*é*, Power Engineering Society Winter Meeting, Volume: 3, 2000, pp. 2135 –2140

[90] Society for Risk Analysis: "Glossary of Risk Analysis Terms", www.sra.org, September 26, 2000.

[91] H.-D. Schlemper, K. Feser: "Characterization of moving particles in GIS by acoustic and electric partial discharge detection", 10th ISH 1997, Montreal

10.7. References of chapter 9

[92] ANSI/IEEE Standard 80, IEEE Guide for the safety in AC substation grounding, 1986

[93] Carson “Wave propagation in overhead wires with earth return“, Bell System technical journal Oct 1926 n°5 p 539-554

[94] Pollaczek, "Sur le champ produit par un conducteur simple infiniment long parcouru par un courant alternatif", traduit par Pomey , Revue générale d'electricité 30 mai 1931, p 851-867

[95] Electro-magnetic Transients Program : Theory book , Bonneville Power Administration, Portland Oregon

[96] P. Clarenne, G. Ebersohl, J. Vigreux, G. Voisin : “ The effect of high frequency transient voltage on the secondary equipement in gas-insulated substations », Electra N°126, pp 94-116

[97] John Lewis WG 23.10 “ Earthing of GIS – an application guide” , Electra N°151, pp 31 –51

[98] Technical report IEC 61640 First edition 1998-07

[99] Y. Kuroyanagi, A. Toya, T. Hayashi, T. Araki: “ Construction of a 8000A class 275kV insulated transmission line”, IEEE Power delivery Vol 5, n°1 January 1990.

[100] A. Miyazaki and Al “Line constant measurements and loading current test in long distance 275kV GIL”,IEEE Transaction on Power Delivery, Vol 16, No 2, pp165-170, 2001